STRUCTURAL AND PHYSICAL INVESTIGATIONS OF NOVEL GERMANIUM COMPOUNDS: ARYLOXIDES, NANOMATERIALS, AND PHOTOLYSIS OF OLIGOGERMANES

By

AARON C. SCHRICK

Bachelor of Science in Chemistry
Midwestern State University
Wichita Falls, Texas
2009

Submitted to the Faculty of the
Graduate College of the
Oklahoma State University
in partial fulfillment of
the requirements for
the Degree of
DOCTOR OF PHILOSOPHY
May, 2014

STRUCTURAL AND PHYSICAL

INVESTIGATIONS OF NOVEL GERMANIUM

COMPOUNDS: ARYLOXIDES, NANOMATERIALS,

AND PHOTOLYSIS OF OLIGOGERMANES

Dissertation Approved:

Dr. Charles S. Weinert

Dissertation Adviser

Dr. Allen Apblett

Dr. Nicholas Materer

Dr. Richard A. Bunce

Dr. John Veenstra

Name: AARON C. SCHRICK

Date of Degree: MAY, 2014

Title of Study: STRUCTURAL AND PHYSICAL INVESTIGATIONS OF NOVEL GERMANIUM COMPOUNDS: ARYLOXIDES, NANOMATERIALS, AND PHOTOLYSIS OF OLIGOGERMANES

Major Field: CHEMISTRY

Abstract: The work described in this dissertation will explore the synthesis and characterization of novel germanium containing compounds in order to gain a better understanding of the organometallic chemistry of germanium. These compounds include germanium bisamides, aryloxogermylenes, polyfunctional aryloxides such as calix[*n*]arenes and binaphthoxogermanium compounds, and oligogermanes containing up to four germanium atoms.

We have found that the germanium bisamides can be trapped using the germylene trapping agent benzil and we have fully characterized those products. The germanium bisamides can also be used as starting materials to synthesize germanium aryloxides via protonolysis of a phenol that contains one or more phenolic groups. Using this method we have prepared the germanium(IV) aryloxides $[Ge(OC_6H_3Ph_2\text{-}2,6)_2(R)(I)]$ (R = Bu^t or Me) where the R = Me derivative was then converted to the triaryloxo species $[Ge(OC_6H_3Ph_2\text{-}2,6)_3(Me)]$ upon reaction of the iodine containing compound with an extra equivalent of 2,6-diphenylphenol. Using polyfunctional phenols, we prepared and characterized the germanium(II) calix[5]arene complex $\{calix[5]arene\}_2Ge_2(OSiMe_3)_4(OH)_2$, the calix[6]arene complex $[(C_6H_3)_6(CH_2)_6(OSiMe_2Ph)_6]$, and the binaphthoxogermanium(II) complex (*S,S*)-$[Ge\{OC_{20}H_{10}(OSiMe_2Ph)\text{-}2'\text{-}(SiMe_3)_2\text{-}3,3'\}_2]$.

Chapter five describes the synthesis of a series of three oligogermanes including a digermane, a trigermane, and a branched neopentyl germane. We have found that these oligogermanes can be used as precursors for the preparation of germanium(0) nanomaterials, and that the size of the resulting nanoparticles correlates with the number of catenated germanium atoms in the precursor compounds. These nanoparticles are fluorescent and the position of the emission maximum is red shifted as the size of the particles increases.

Lastly, the sixth chapter will discuss the synthesis, characterization, and photochemistry of a series of six linear oligogermanes. The optical and electronic properties of these compounds were probed using UV/visible spectroscopy and differential pulse voltammetry. The photochemistry of these compounds will be analyzed by photolyzing each compound using UV-C light (280-100 nm) in the presence of acetic acid as a germylene trapping agent. If germylenes $:GeR_2$ are formed, they should be trapped to yield $R_2Ge(H)OAc$. The photolysis products will be characterized by NMR (^1H and ^{13}C) spectroscopy, infrared spectroscopy (FTIR), and gas-chromatography mass spectroscopy (GC/MS).

TABLE OF CONTENTS

Chapter Page

LIST OF TABLES

Table Page

Table Page

LIST OF FIGURES

Figure Page

Figure Page

Figure Page

Figure Page

LIST OF SCHEMES

Scheme Page

Scheme Page

Scheme Page

CHAPTER I

INTRODUCTION

Germanium was discovered in 1886 by Clemens Winkler in Freiberg, Saxony from the ore argyrodite, which has the formula Ag_8GeS_6.[1-2] Germanium is a group 14 metalloid that is an indirect band gap semiconductor. The major uses of germanium are for fiber-optic systems, infrared optics, polymerization catalysts, and electronics.[3] The most common oxidation states for germanium are +4 and +2, and germanium exists as five naturally occurring isotopes ^{70}Ge, ^{72}Ge, ^{73}Ge, ^{74}Ge, and ^{76}Ge with the most abundant isotope being ^{74}Ge with a natural abundance of 36 %.[4] The first organogermanium compound prepared was tetraethylgermane $GeEt_4$ synthesized by the element's discoverer, Winkler, by reacting germanium tetrachloride with diethylzinc in 1887.[2] However, the organometallic chemistry of germanium has not been as extensively investigated relative to that of organosilicon or organotin compounds.

The research described in this dissertation will explore the synthesis and characterization of novel germanium containing compounds in order to gain a better understanding of the inorganic and organometallic chemistry of germanium. Each chapter will focus on a specific area of germanium chemistry.

Chapters II through IV describe the synthesis and reactivity of germanium(II)-containing compounds including germanium bisamides, aryloxogermylenes, and polyfunctional aryloxides including calix[*n*]arenes and binaphthoxogermanium compounds. Germanium(II) is not the most

stable oxidation state and thus germylenes must be stabilized by utilizing large bulky ligands such as bistrimethylsilylamido -$[N(SiMe_3)_2]_2$ or –$[N(SiMe_2Ph)_2]_2$ groups in the germanium bisamides. These germylenes can be trapped using benzil to form $Ph_2C_2O_2Ge[N(SiR_3)_2]_2$ in an oxidative addition reaction. The germanium bisamides can also be used as starting materials to synthesize germanium aryloxides via the protonolysis reaction with a phenol that contains one or more phenolic -OH group. Chapter III describes how we have prepared and structurally characterized the germanium(IV) aryloxide $[Ge(OC_6H_3Ph_2\text{-}2,6)_2(Bu^t)(I)]$[5]. We have also prepared $[Ge(OC_6H_3Ph_2\text{-}2,6)_2(Me)(I)]$ which was then converted to the triaryloxo species $[Ge(OC_6H_3Ph_2\text{-}2,6)_3(Me)]$ upon reaction of the iodine containing compound with an extra equivalent of 2,6-diphenylphenol. The aryloxide species $[Ge(OC_6H_3Ph_2\text{-}2,6)_2(R)(I)]$ (R = Bu^t or Me) exhibit different reactivity toward 2,6-diphenylphenol due to the steric attributes of the organic substituent bound to the germanium atom. Chapter IV describes how the germanium(II) calix[5]arene complex $\{calix[5]arene\}_2Ge_2(OSiMe_3)_4(OH)_2$, the calix[6]arene complex $[(C_6H_3)_6(CH_2)_6(OSiMe_2Ph)_6]$, and the binaphthoxogermanium(II) complex (*S,S*)-$[Ge\{OC_{20}H_{10}(OSiMe_2Ph)\text{-}2'\text{-}(SiMe_3)_2\text{-}3,3'\}_2]$ were prepared in order to determine the effects of having an odd number of phenolic groups in the calixarene, and the effects of having a more bulky amido group on the germanium(II) precursor on the reactivity of these systems. It was found that changing these factors has a significant impact on the nature of the products obtained.

Chapter V will discuss our first endeavor into the materials chemistry of germanium, which involves the preparation of germanium(0) nanoparticles. We have prepared a series of three oligogermanes including a digermane, a trigermane, and a branched neopentyl germane where the formal oxidation states at germanium vary from +3 to +2 and zero depending on the number of germanium-germanium single bonds present at a given germanium atom. We have found that these oligogermanes can be used as precursors for the preparation of germanium(0) nanomaterials, and that the size of the resulting nanoparticles correlates with the number of catenated germanium atoms in the

precursor compounds. These nanoparticles are fluorescent and the position of the emission maximum undergoes a red shift as the size of the particles increases.

Lastly, the sixth chapter will discuss the synthesis, characterization, and photochemistry of a series of six oligogermanes. These oligogermanes include two previously known digermanes $Et_3GeGePh_3$ and $Bu^n_3GeGePh_3$, two trigermanes $Et_3GeGePh_2GeEt_3$ and $Bu^n_3GeGePh_2GeBu^n_3$, and two new tetragermanes $Et_3Ge(GePh_2)_2GeEt_3$ and $Bu^n_3Ge(GePh_2)_2GeBu^n_3$. The optical and electronic properties of these compounds were probed using UV/visible spectroscopy and differential pulse voltammetry. The photochemistry of these compounds was investigated by photolyzing each compound using UV-C light (280-100 nm) in the presence of acetic acid as a germylene trapping agent. Germylenes R_2Ge: were formed and they were trapped to yield $R_2Ge(H)OAc$.[6] The species formed were characterized by NMR spectroscopy (^1H and ^{13}C), infrared spectroscopy (FTIR), and gas-chromatography mass spectroscopy (GC/MS).

References

1. Winkler, C., *Chem. Ber.* **1886,** (19), 210-211.

2. Winkler, C., *J. Prakt. Chem.* **1887,** *36* (1), 177-209.

3. In *U.S. Geological Survey, Mineral Commodity Summaries*, 2013.

4. Greenwood, N. N.; Earnshaw, A.; NetLibrary Inc., Chemistry of the elements. 2nd ed.; Butterworth-Heinemann,: Boston, Mass., 1997; p. 1344 p.

5. Wetherby, A. E.; Samanamu, C. R.; Schrick, A. C.; DiPasquale, A.; Golen, J. A.; Rheingold, A. L.; Weinert, C. S., *Inor.g Chim. Acta* **2010,** *364* (1), 89-95.

6. Billone, P. S.; Beleznay, K.; Harrington, C. R.; Huck, L. A.; Leigh, W. J., *J.Am. Chem. Soc.* **2011,** *133* (27), 10523-10534.

CHAPTER II

SYNTHESIS OF $Ge[N(SiMe_2Ph)_2]_2$ AND CRYSTAL STRUCTURES OF THE BENZIL ADDUCTS $Ph_2C_2O_2Ge[N(SiMe_3)_2]_2$ AND $Ph_2C_2O_2Ge[N(SiMe_2Ph)_2]_2$

2.1 Introduction

Germylenes are the heavy analogues of carbenes[1], and when compared to their tin-containing congeners, are highly reactive species. Germanium prefers to be in the +4 oxidation state, and germylenes, which contain germanium in the +2 oxidation state, often require the use of sterically encumbering or electron donating ligands to enable their isolation and characterization. In 1948, M. Lesbre and J. Satgé at the University of Toulouse, France pioneered the chemistry of germylenes, and since then, it has developed a considerable amount.[2] The synthesis and characterization of germylenes has advanced mainly due to advances in spectroscopic methods.[1] Germylenes have been shown to exhibit a variety of structural motifs including monomers, dimers, clusters, polymers, and there have been some polyfunctional germylenes prepared. The structure of the compound is highly dependent on the type of ligands attached to the germanium center. The formation of monomeric germylenes has been stabilized by the utilization of large, bulky, electron withdrawing ligands. Germylene monomers have a diverse range of chemistry because the germanium(II) center contains both a lone pair of electrons and a vacant p-orbital (**Figure 2.1**). The vacant p-orbital allows the germylene to act as a Lewis acid and accept electron density into the orbital. However, the germylene can also act as

a Lewis base and donate its lone pair of electrons located in a sp^2 hybridized orbital.[3]

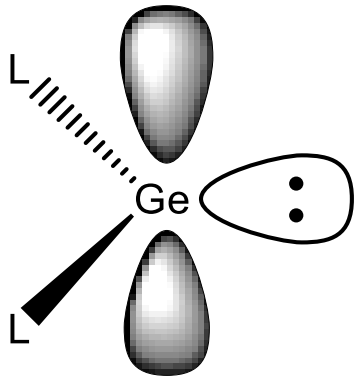

Figure 2.1: General structure for germanium(II) monomer.

Even though germylenes are much more reactive than their tin counterparts, there are some examples where they have a similar reactivity. One such example is the reaction of $Ge(NR_2)_2$ or $Sn(NR_2)_2$ (R=$SiMe_3$) with $M(CO)_6$ (M= Cr, Mo, or W).[4] In both cases, the reaction results in ligand substitution where the germylene or stannylene has replaced a CO ligand (**Scheme 2.1**).

a) $Sn[N(SiMe_3)_2]_2 \xrightarrow[\text{M = Cr, Mo, or W}\\ \text{- CO}]{M(CO)_6} M(CO)_5[Sn[N(SiMe_3)_2]_2$

b) $Ge[N(SiMe_3)_2]_2 \xrightarrow[\text{M = Cr, Mo, or W}\\ \text{- CO}]{M(CO)_6} M(CO)_5[Ge[N(SiMe_3)_2]_2$

Scheme 2.1: a) Reaction of $Sn[N(SiMe_3)_2]_2$ with $M(CO)_6$ (M = Cr, Mo, or W).[4]

b) Reaction of $Ge[N(SiMe_3)_2]_2$ with $M(CO)_6$ (M = Cr, Mo, or W).[4]

Several methods exist for the preparation of germylene compounds. Common methods include the reaction between tetraphenylgermoles and benzyne which leads to the formation of a 7,7-disubstituted-7-germabenzonorbornadiene intermediate that can then afford a dialkylgermylene upon heating or UV irradiation (**Scheme 2.2**), UV irradiation of diaryl(bissilyl)germanium compounds (**Scheme 2.3**), photochemical deazotination of dimethyldiazidogermane ($Me_2Ge(N_3)_2$) (**Scheme 2.4**), and photolytical cleavage of strained cyclogermanes containing germanium-germanium bonds (**Scheme 2.5**).[1]

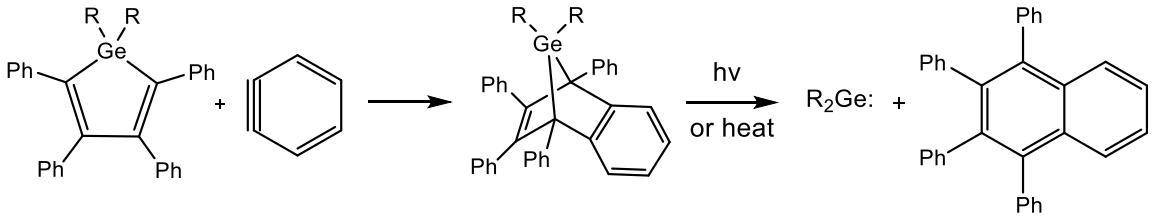

Scheme 2.2: Germylene extrusion from the product of the reaction between tetraphenylgermoles and benzyne.[1]

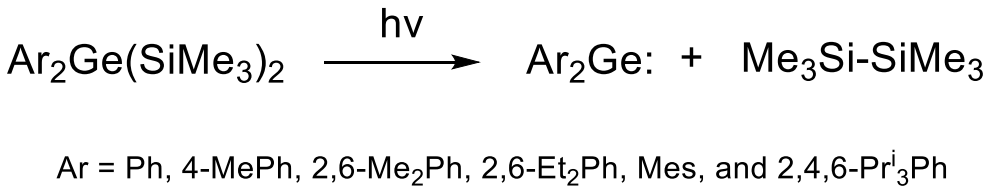

Scheme 2.3: Germylene extrusion via UV irradiation of diaryl bissilylgermanium compounds.[1]

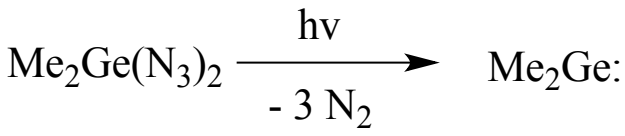

Scheme 2.4: Germylene extrusion via photochemical deazotination of dimethyldiazidogermane.[1]

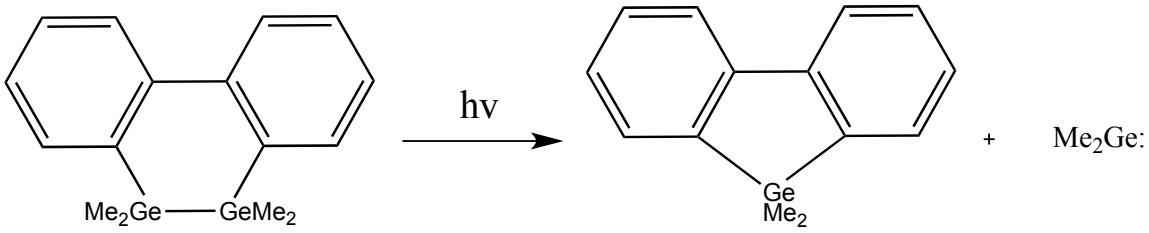

Scheme 2.5: Germylene extrusion via photolytical splitting of strained cyclogermanes.[1]

Despite these various synthetic routes to prepare germylenes, the isolation and characterization of these molecules has been complicated by the fact that most of the germylenes formed are highly reactive species that undergo rapid polymerization. The characterization of these compounds has been achieved through isolation via a hydrocarbon matrix at 77 K or using germylene trapping agents such as 1,3-dienes or benzil.[1]

While most germylenes are not stable, there are some germylenes that are resistant toward polymerization that have been prepared utilizing large bulky ligands at the germanium(II) center. The ligands used are of a wide variety and include aryl, alkyl, amido, aryloxo, and arylthiolato groups, which have been shown to kinetically and thermodynamically stabilize germylenes in a manner that leads to the formation of monomers and dimers.[5] The two most commonly used ligands of this type are the disyl ($CH(SiMe_3)_2$) and trimethylsilylamido ($[N(SiMe_3)_2]$) groups, which afford the bis[bis(trimethylsilyl)methyl] germanium(II)

($Ge[CH(SiMe_3)_2]_2$) and bis[bis(trimethylsilyl)amido] germanium(II) ($Ge[N(SiMe_3)_2]_2$) germylenes respectively. The monomeric nature of these germylenes is due to the steric bulk of their ligands which contributes to their stability in two main ways. First, the lack of any β-hydrogens and the presence of a β-silicon prevents metal-ligand decomposition through a β-elimination pathway. Second, the reactivity is limited further due to the presence of the bulky ligands themselves, which impede access to the germanium center through steric effects. Both of these germylenes also contain a large number of methyl groups. Along with contributing to the steric bulk, the large number of methyl groups also enhances the solubility of these germylenes in hydrocarbon solvents. This allows for much easier manipulation of these compounds.

Although the structure of these germylenes appear similar from their formula, they are prepared by different methods, and have different solid state structures. The bis[bis(trimethylsilyl)methyl] germanium(II) ($Ge[CH(SiMe_3)_2]_2$) is typically prepared by the reaction of bis(trimethylsilyl)methyl lithium and germanium(II) amide (**Scheme 2.6**).[6]

$$2\ Li[CH(SiMe_3)_2] + Ge[N(SiMe_3)_2]_2 \xrightarrow[0\text{ to }-20\ ^oC]{Et_2O} Ge[CH(SiMe_3)_2]_2 + 2\ Li[N(SiMe_3)_2]$$

Scheme 2.6: Synthesis of bis[bis(trimethylsilyl)methyl] germanium(II) via reaction of bis(trimethylsilyl)methyl lithium and germanium(II) amide.[6]

The germylene $Ge[CH(SiMe_3)_2]_2$ is dimeric in the solid state (**Figure 2.2**)[7], but behaves as a monomer in solution. This behavior in solution can be attributed to the weak nature of the germanium-germanium bond. The germanium-germanium bond measures 2.347(2)Å, which is

indicative of a Ge=Ge double bond, and the average germanium-carbon bond distance measures 2.011(3)Å and the Ge-Ge-C bond angles are 113.7(3)^{o} and 122.3(2)^{o}.[7]

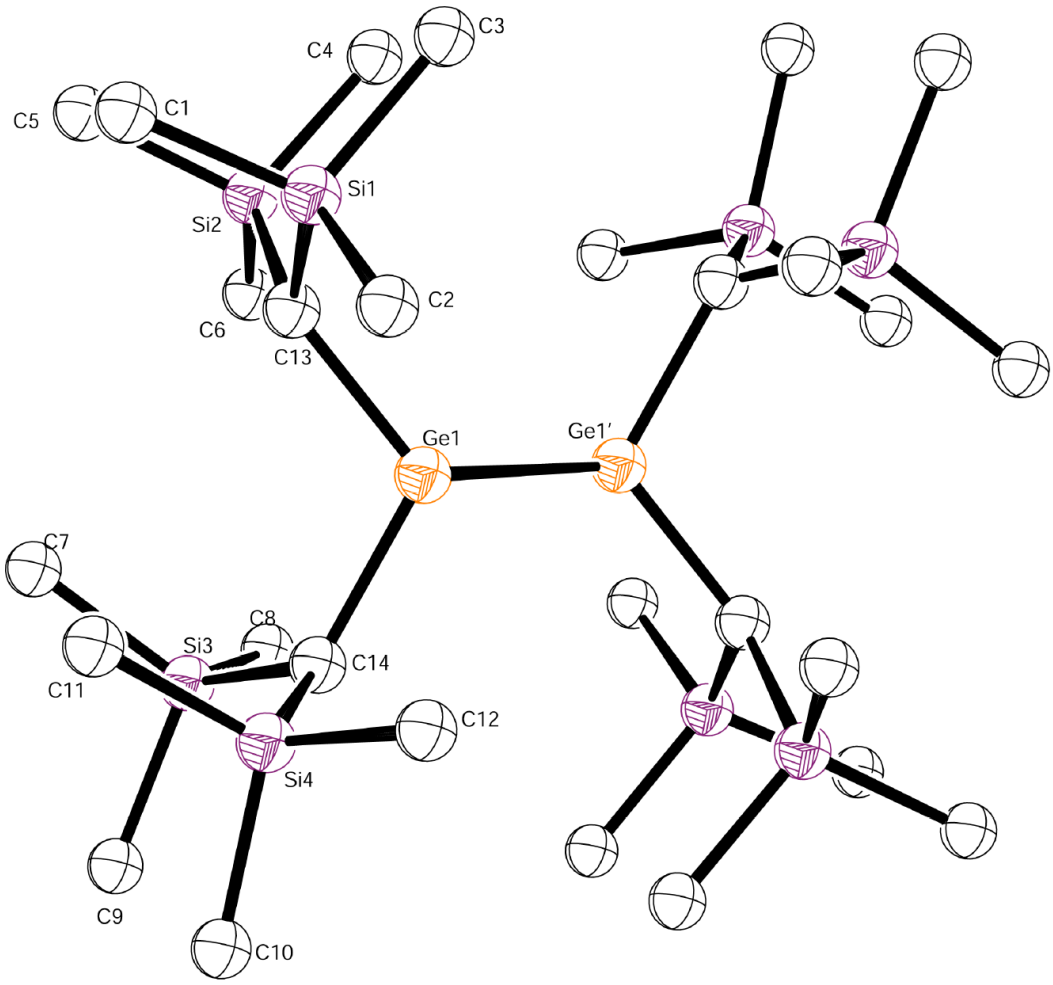

Figure 2.2: X-ray crystal structure of :Ge[CH(SiMe$_3$)$_2$]$_2$.[7]

Table 2.1: Selected bond distances and angles for :Ge[CH(SiMe$_3$)$_2$]$_2$.[7]

Bond Lengths	(Å)	Bond Angles	(°)
Ge(1)-Ge(1')	2.347(2)	Ge(1')-Ge(1)-C(14)	122.3(2)
Ge(1)-C(14)	1.979(9)	Ge(1)-C(13)-Si(1)	119.1(4)
Ge(1)-C(13)	2.042(8)	Ge(1)-C(13)-Si(2)	110.0(4)
		Ge(1)-C(14)-Si(3)	113.9(4)
		Ge(1)-C(14)-Si(4)	121.8(4)

The germylene Ge[CH(SiMe$_3$)$_2$]$_2$ has been used in CH activation of a variety of compounds including alkanes[8], ethers[8], cyanides[9], amines[10], and ketones.[11] CH activation with this germylene typically requires the use of $MgCl_2$ or PhI. Several examples of these reactions are shown below (**Schemes 2.7-2.10**).[8-11]

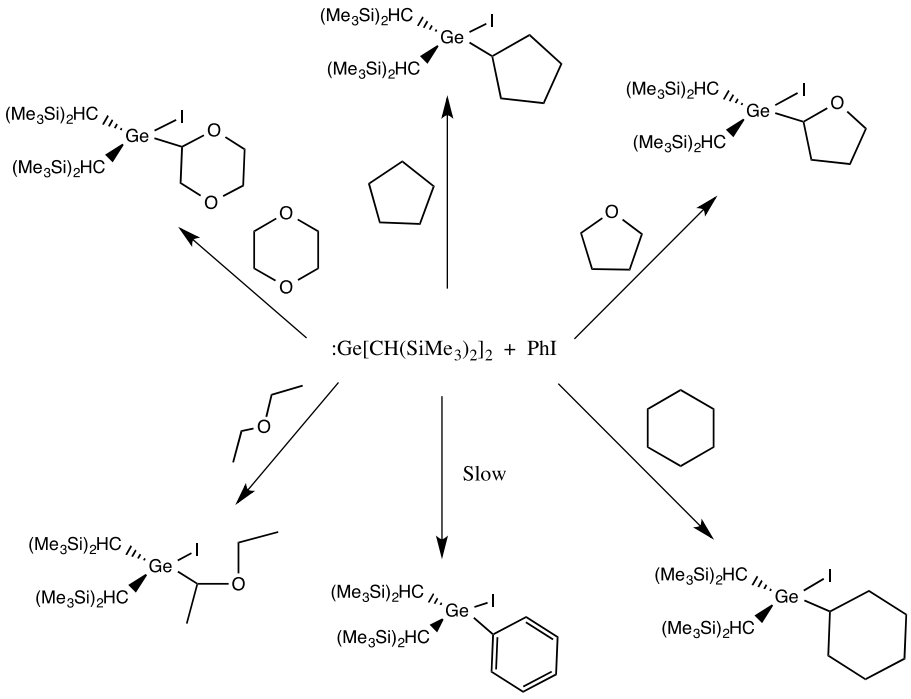

Scheme 2.7: CH activation of alkanes and ethers with Ge[CH(SiMe$_3$)$_2$]$_2$ and PhI.[8]

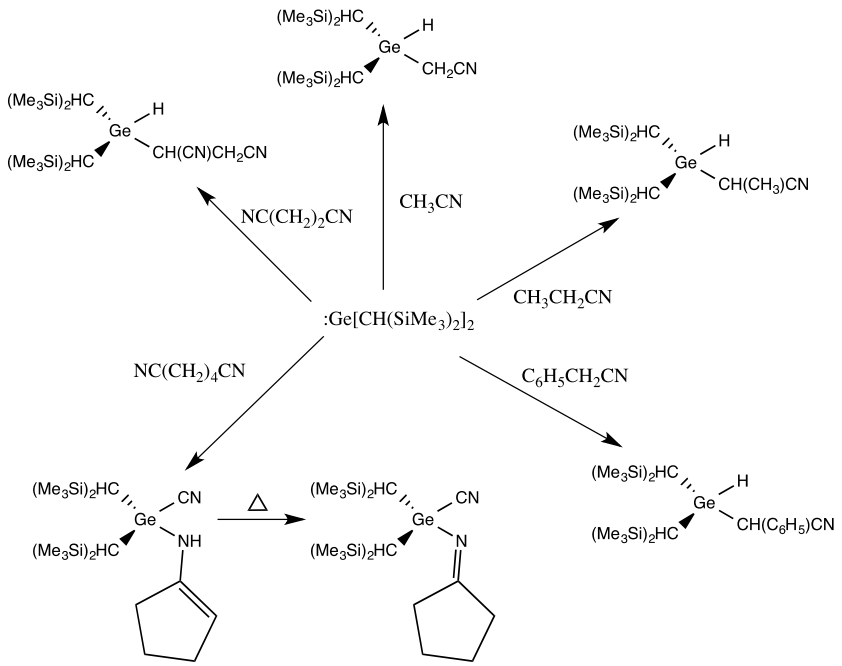

Scheme 2.8: CH activation of CN containing compounds with $Ge[CH(SiMe_3)_2]_2$. Reactions were performed using $MgCl_2$ or LiCl in THF.[9]

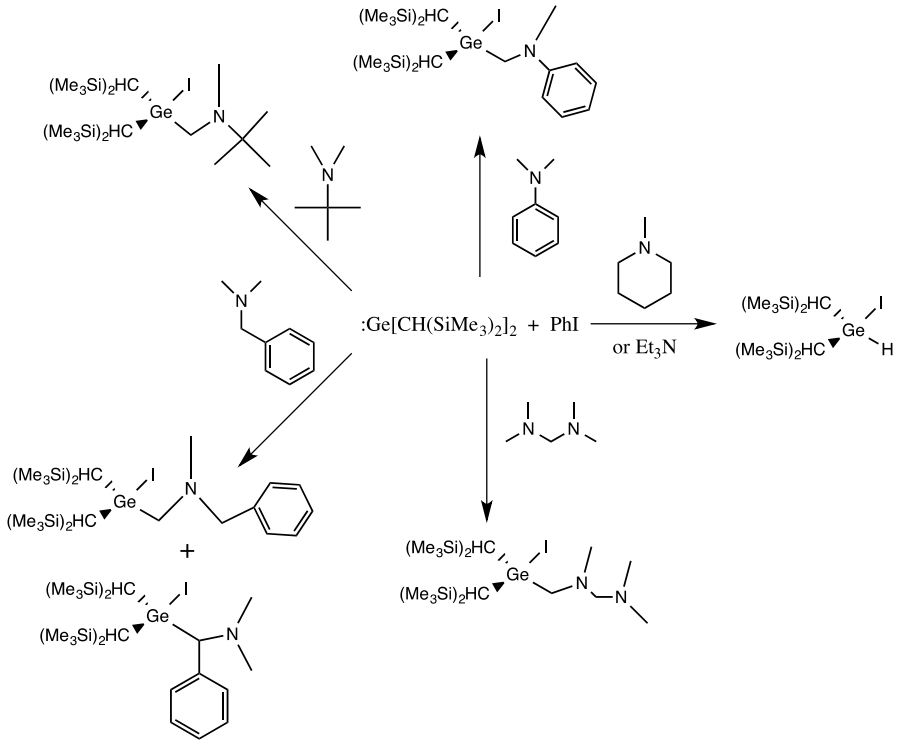

Scheme 2.9: CH activation of amine containing compounds with $Ge[CH(SiMe_3)_2]_2$ and PhI.[10]

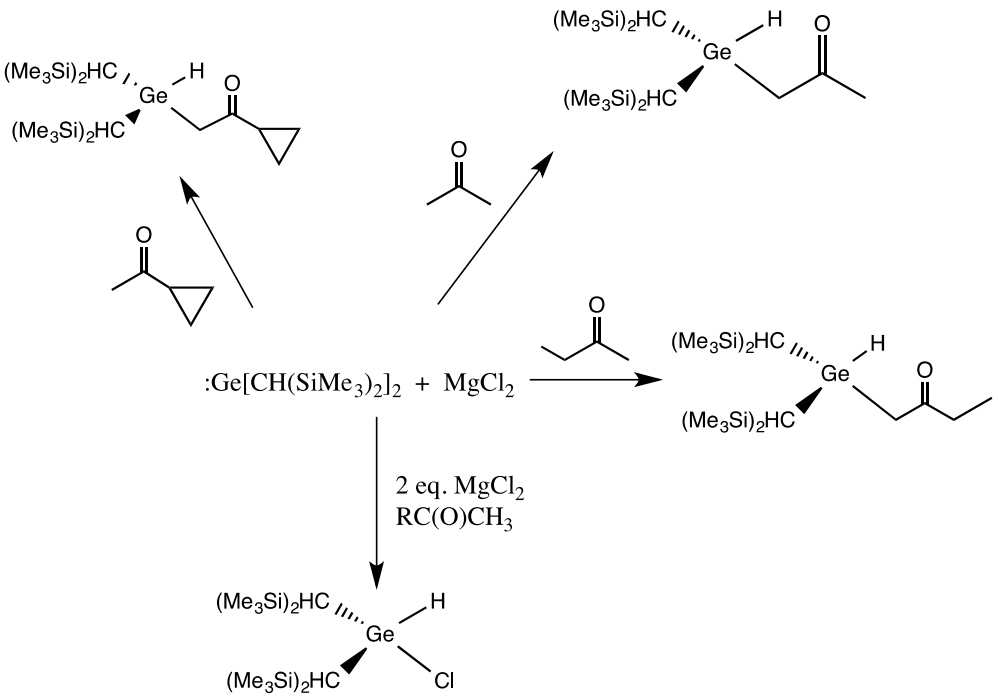

Scheme 2.10: Reaction of $Ge[CH(SiMe_3)_2]_2$ with ketones in the presence of $MgCl_2$ resulting in insertion into CH bonds.[11]

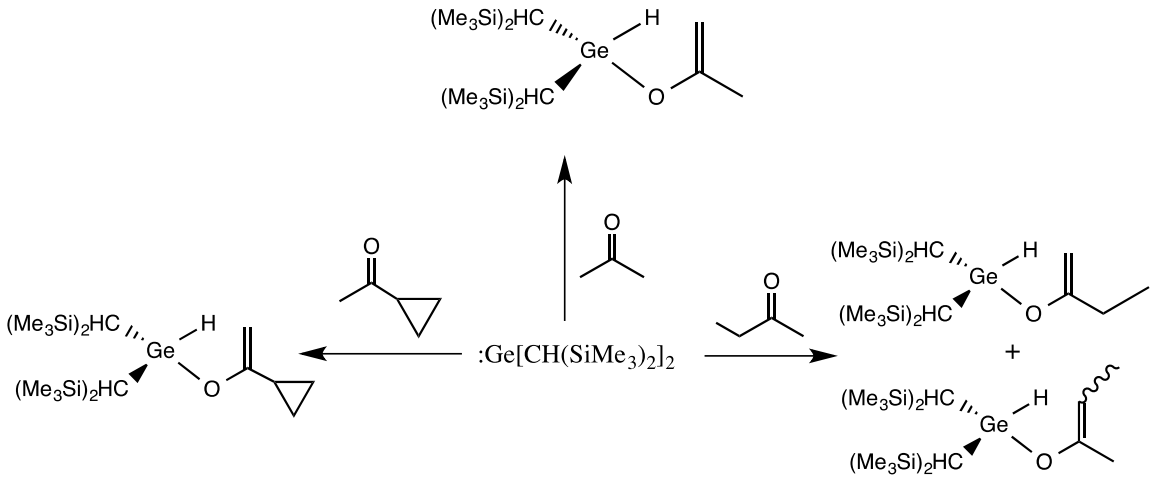

Scheme 2.11: Reaction of $Ge[CH(SiMe_3)_2]_2$ with ketones in the absence of $MgCl_2$ resulting in insertion into OH bonds.[11]

The germanium(II) amide, $Ge[N(SiMe_3)_2]_2$, was first reported by Lappert *et al.* in 1974.[12] The germylene contains sterically encumbering bis(trimethylsilyl)amido ligands that kinetically stabilize the germanium(II) center. The nitrogen atoms attached directly to the germanium atom have some electron withdrawing ability as well, which renders the lone pair of electrons at germanium unavailable with respect to dimerization to form digermenes.[5-6, 12-16]

The germylene $Ge[N(SiMe_3)_2]_2$ is a thermochromic yellow/orange liquid at room temperature and it becomes colorless upon cooling to -196 ^oC. This germylene was first synthesized by reacting two equivalents of lithium hexamethyldisilazide with germanium dichloride (1,4-dioxane). This reaction resulted in the formation of the desired germylene with two equivalents of LiCl and 1,4-dioxane as side products (**Scheme 2.12**).[12]

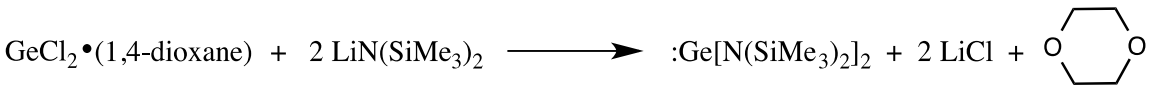

Scheme 2.12: Original synthesis of $Ge[N(SiMe_3)_2]_2$.[12]

The germanium bisamide $Ge[N(SiMe_3)_2]_2$ is monomeric in the solid state and the X-ray crystal structure of the germanium bisamide (**Figure 2.3**)[5] features a bent singlet state geometry rather than a linear triplet state (**Figure 2.4**)[17] where the germanium-nitrogen bond distances are 1.873(5) and 1.878(5)Å, and the N-Ge-N bond angle is 107.1(2)^O (**Table 2.2**).[5]

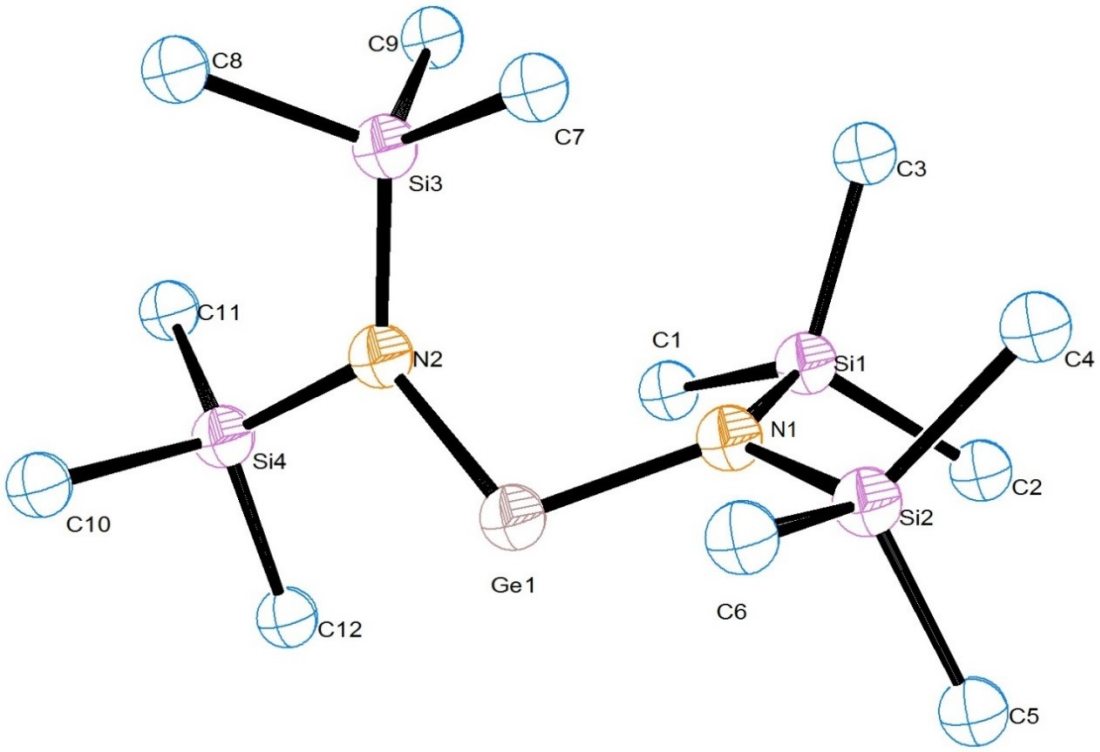

Figure 2.3: X-ray crystal structure of $Ge[N(SiMe_3)_2]_2$.[5]

Table 2.2: Selected bond distances and angles for $Ge[N(SiMe_3)_2]_2$.[5]

Bond Lengths	(Å)	Bond Angles	(^{O})
Ge – N(1)	1.878(5)	N(1) – Ge – N(2)	107.1(2)
Ge – N(2)	1.873(5)	Si(1) – N(1) – Si(2)	120.7(3)
N(1) – Si(1)	1.751(5)	Si(3) – N(2) – Si(4)	120.5(3)
N(1) – Si(2)	1.749(5)	Ge – N(1) – Si(1)	124.4(3)
N(2) – Si(3)	1.757(5)	Ge – N(1) – Si(2)	113.0(3)
N(2) – Si(4)	1.749(6)	Ge – N(2) – Si(3)	125.3(3)
		Ge – N(2) – Si(4)	112.2(3)

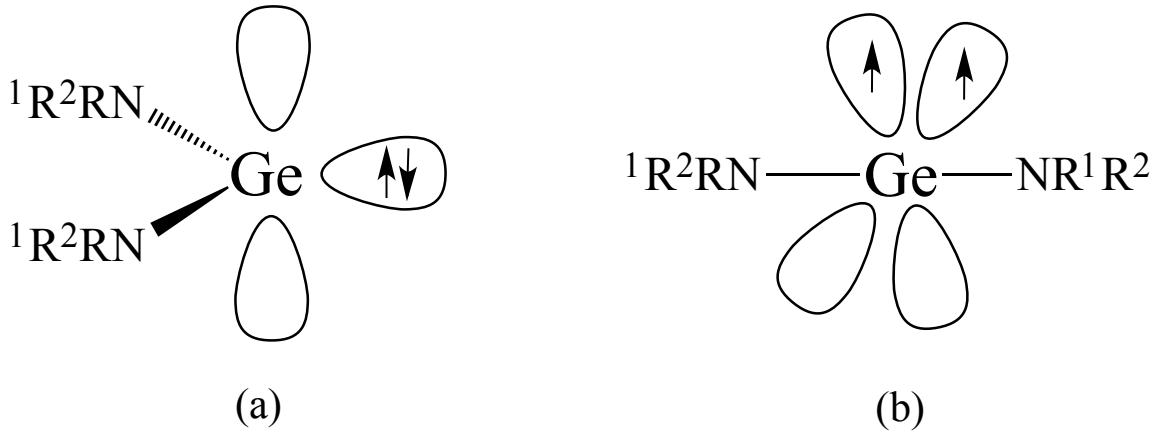

Figure 2.4: Expected structures for monomeric $M(NR^1R^2)_2$. (a) singlet and (b) triplet ground state.[17]

The original synthetic route (**Scheme 2.12** above) for the preparation of $Ge[N(SiMe_3)_2]_2$ was via the reaction of two equivalents of lithium hexamethyldisilazide with germanium dichloride(1,4-dioxane), and resulted in only moderate yields. Roskamp and coworkers improved the synthesis of $Ge[N(SiMe_3)_2]_2$ by utilizing a stable triphenylphosphonium trichlorogermanate intermediate in 1992.[18] Their synthetic method involved a multistep synthesis beginning with the reaction of triphenylphosphine with germanium tetrachloride and tributyltinhydride in diethyl ether at room temperature to yield the triphenylphosphonium trichlorogermanate and tributyltinchloride (**Scheme 2.13**).[18] Triethylamine was then added to the triphenylphosphonium trichlorogermanate to yield triethylammonium trichlorogermanate and free triphenylphosphine (**Scheme 2.14**).[18] Finally, the triethylammonium trichlorogermanate was reacted with three equivalents of lithium hexamethyldisilazide to give $Ge[N(SiMe_3)_2]_2$ in 70-77% yield, with triethylamine, lithium chloride, and hexamethyldisilazane as side products which can easily be removed from the reaction mixture (**Scheme 2.15**).[18]

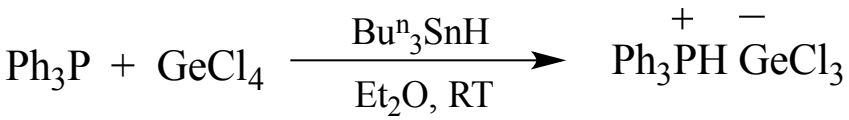

Scheme 2.13: Synthesis of triphenylphosphonium trichlorogermanate from triphenylphosphine and tetrachlorogermane.[18]

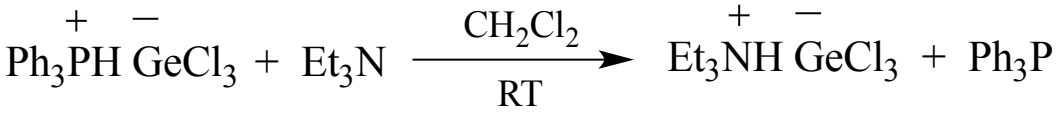

Scheme 2.14: Reaction of triphenylphosphonium trichlorogermanate with triethylamine.[18]

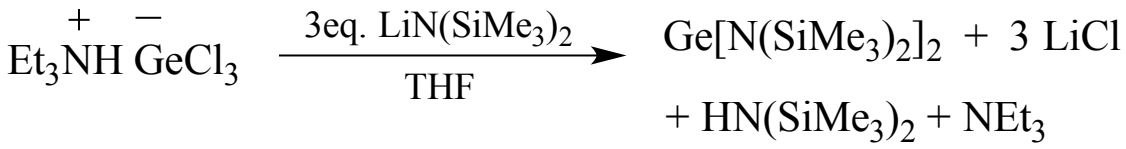

Scheme 2.15: Reaction of triethylammonium trichlorogermanate with three equivalents of lithium hexamethyldisilazide.[18]

The reactivity of $Ge[N(SiMe_3)_2]_2$ has been shown to be quite versatile. Some reactions similar to the CH insertion reactions of $Ge[CH(SiMe_3)_2]_2$ have been reported as well as several different reactions where $Ge[N(SiMe_3)_2]_2$ has been used as a ligand for transition metal elements including copper,[19] ruthenium,[20] nickel,[21] chromium, molybdenum, tungsten, platinum, and palladium.[4] A few examples of these reactions are given below (**Scheme 2.16**).[4, 21]

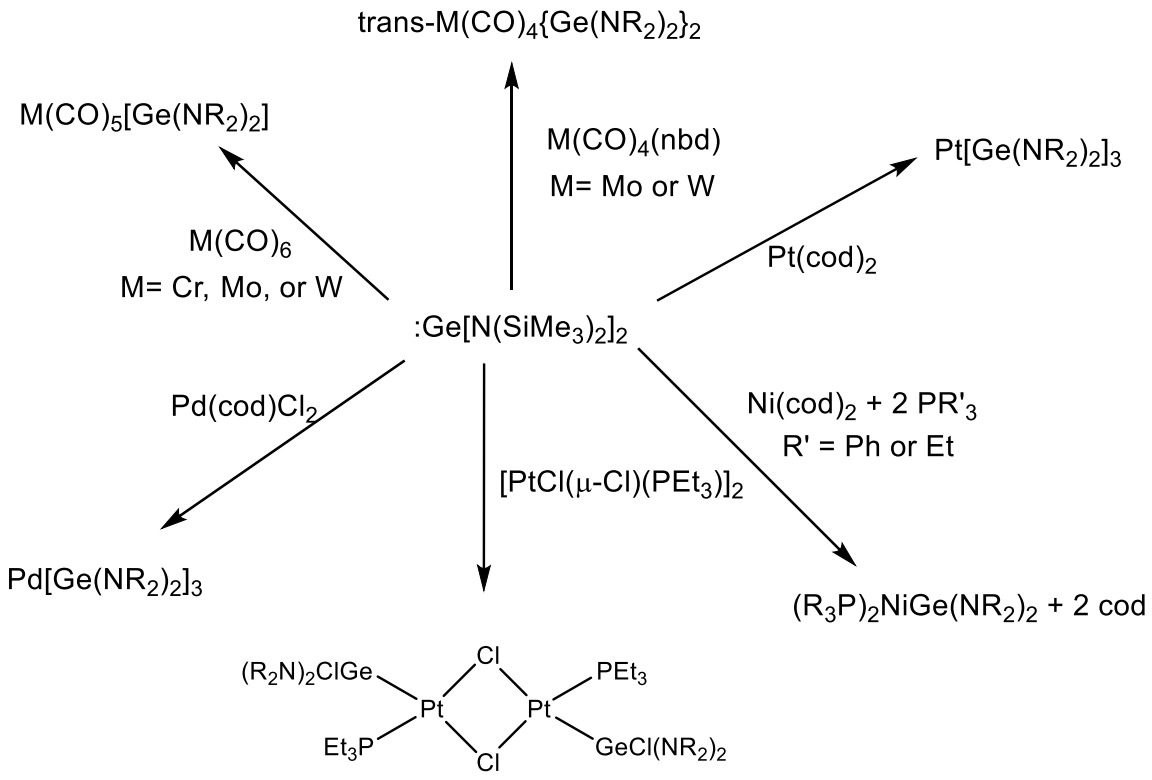

Scheme 2.16: Example reactions of $Ge[N(SiMe_3)_2]_2$ (R = $SiMe_3$) with transition metal complexes.[4, 21]

The binding strength of $Ge[N(SiMe_3)_2]_2$ to the copper complex $[(o\text{-xy})_2N_2C_2HMe_2]Cu\text{-}Ge[N(SiMe_3)_2]_2$ as well as to the palladium and platinum complexes $(Et_3P)_2M\text{-}Ge[N(SiMe_3)_2]_2$ (M = Ni,[22] Pt,[22-23] or Pd[22]) was examined utilizing the germylene trapping agent benzil (1,2-phenylethane-1,2-dione). The binding strength of the germylene to the group 10 complexes was found to decrease in the order Ni<Pd<Pt,[22] while the binding of the germanium bisamide to the copper complex was shown to be more labile than the platinum complex but less labile that the nickel congener.[19] In addition to benzil there are several common germylene and divalent group 14 compound trapping agents which include 2,3-dimethyl-1,3-butadiene, and diphenylacetylene.[1]

The preparation of the benzil trapping product of $Ge[N(SiMe_3)_2]_2$ **(1)** has been reported (**Scheme 2.17**),[23] however, the structures of this complex and other benzil trapped germylenes are not known.

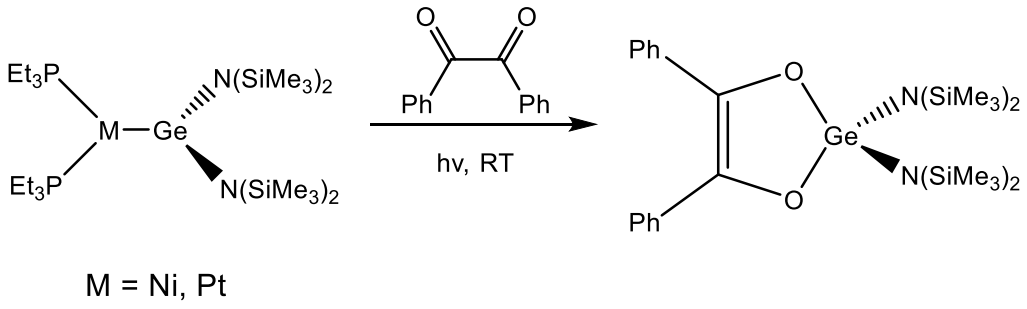

Scheme 2.17: Trapping of **1** using benzil via photolysis of $(Et_3P)_2M\text{-}Ge[N(SiMe_3)_2]_2$.[23]

The following section will present the synthesis of the previously unknown germylene $Ge[N(SiMe_2Ph)_2]_2$ (**2**) and the X-ray crystal structures of the benzil trapping products $Ph_2C_2O_2Ge[N(SiMe_3)_2]_2$ (**3**) and $Ph_2C_2O_2Ge[N(SiMe_2Ph)_2]_2$ (**4**) of **1** and **2** respectively.

2.2 Results and Discussion

The germylene $Ge[N(SiMe_2Ph)_2]_2$ (**2**) was synthesized in 81% yield starting by lithiating $HN(SiMe_2Ph)_2$ with Bu^nLi in THF and subsequently cannulating that solution into a solution of 0.5 equivalents of $GeCl_2$(dioxane) as shown below in **Scheme 2.18**. Compound **2** appears orange in color and is a liquid similar to $Ge[N(SiMe_3)_2]_2$ (**1**). The ^1H NMR in benzene-d_6 of **2** (**Figure 2.5**) exhibits a singlet at δ 0.42 ppm corresponding to the two methyl groups of the bis(dimethylphenyl)amido ligands. The ^1H NMR of **2** also exhibits two multiplets centered at

δ 7.48 and 7.17 ppm corresponding to the *meta*-, *ortho*-, and *para*- protons of the phenyl group respectively. The resonance for the methyl groups of **2** is shifted downfield from the signal at δ 0.35 ppm for the six methyl groups of **1** due to the presence of the phenyl substituent bound to silicon in **2**.

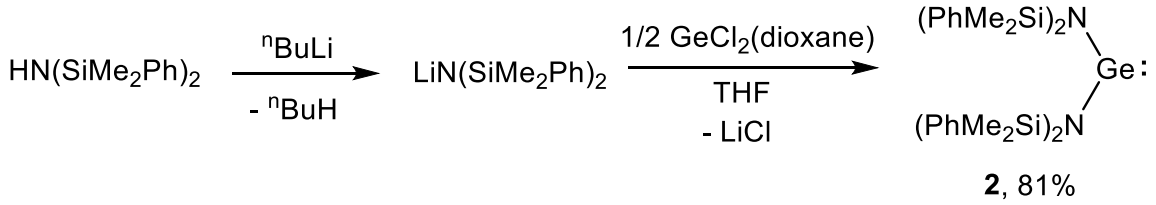

Scheme 2.18: Synthesis of germylene $Ge[N(SiMe_2Ph)_2]_2$ (**2**).

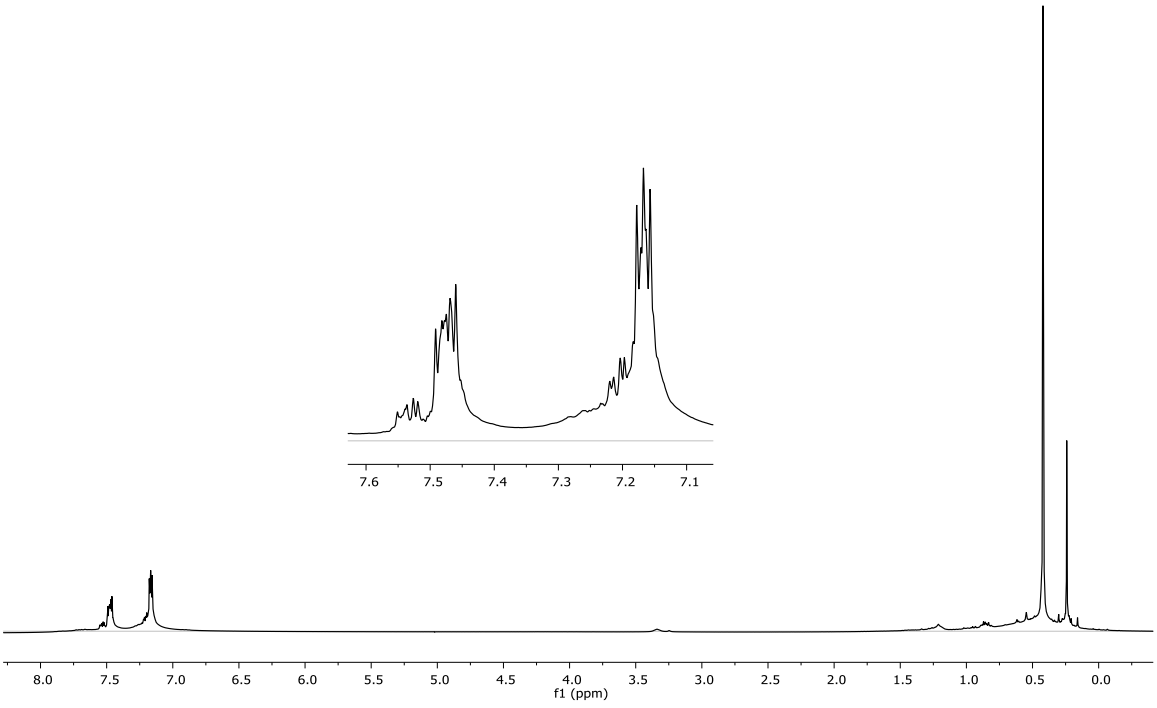

Figure 2.5: ^1H NMR spectrum of $Ge[N(SiMe_2Ph)_2]_2$ (**2**).

The reaction of both **1** and **2** with benzil yielded the corresponding oxidative addition complexes **3** and **4** respectively (**Scheme 2.19**), both of which formally contain germanium in the tetravalent oxidation state. During the reaction, the carbonyl groups of benzil are expected to convert to alkoxy groups with the corresponding conversion of the single bond between the two α-carbons to a double bond.

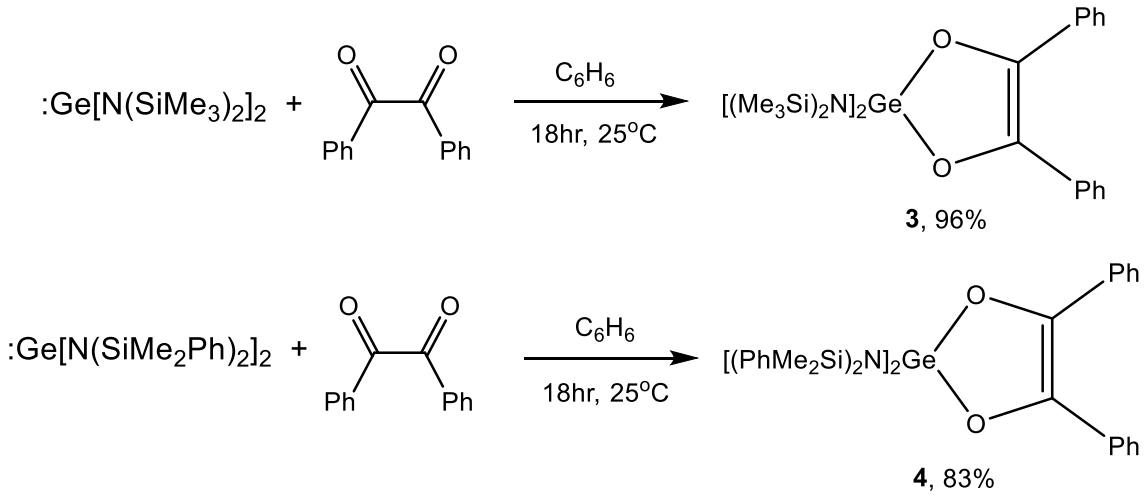

Scheme 2.19: Oxidative addition reactions of germylenes **1** and **2** with benzil to yield benzil trapping products **3** and **4.**

Both of the products were thick maroon liquids upon removal of the solvent where the maroon substance is presumably a polymeric side product of benzil itself. Colorless crystals slowly crystallized out of the product mixture and were isolated in yields of 96% (**3**) and 83% (**4**).

The ^{1}H NMR spectrum of **3** (**Figure 2.6**) contains a singlet at δ 0.37 ppm corresponding to the 36 methyl protons present in the two –$N(SiMe_3)_2$ ligands that is shifted downfield slightly from the resonances for the same protons in $Ge[N(SiMe_3)_2]_2$ (**1**) at δ 0.32 ppm due to the increase

in the formal oxidation state of germanium from +2 to +4. Similarly, the ^{1}H NMR spectrum of **4** (**Figure 2.7**) contains a singlet at δ 0.59 ppm for the methyl groups of the two –N(SiMe$_2$Ph)$_2$ ligands that is also shifted downfield from that of the Ge[N(SiMe$_2$Ph)$_2$]$_2$ (**2**), although the downfield shift is larger for **4** than that for **3**. The ^{13}C NMR spectrum of Ge[N(SiMe$_2$Ph)$_2$]$_2$ contains a resonance at δ 3.9 ppm corresponding to the methyl carbons of the –N(SiMe$_2$Ph)$_2$ groups which are essentially unchanged upon oxidative addition with benzil to yield **4** (δ 3.7 ppm).

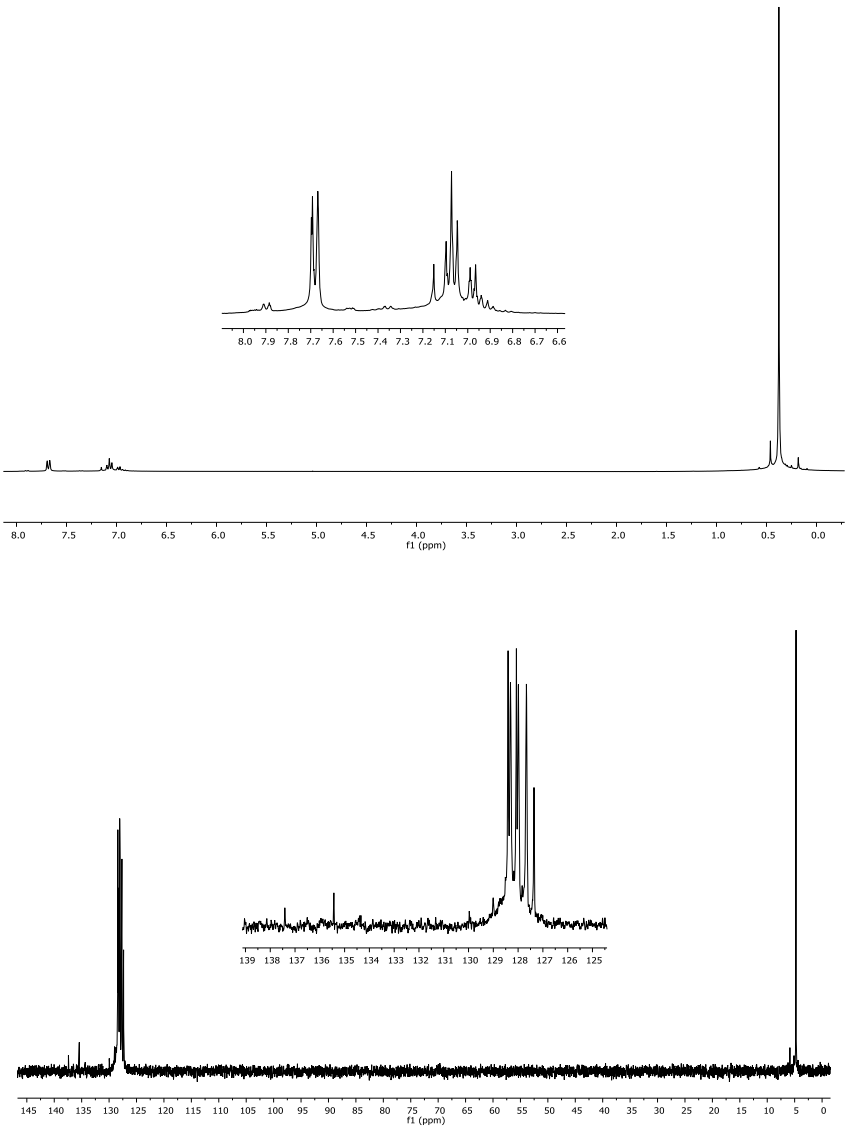

Figure 2.6: ^{1}H (top) and ^{13}C (bottom) NMR spectra of $Ph_2C_2O_2Ge[N(SiMe_3)_2]_2$ (**3**) in C_6D_6.

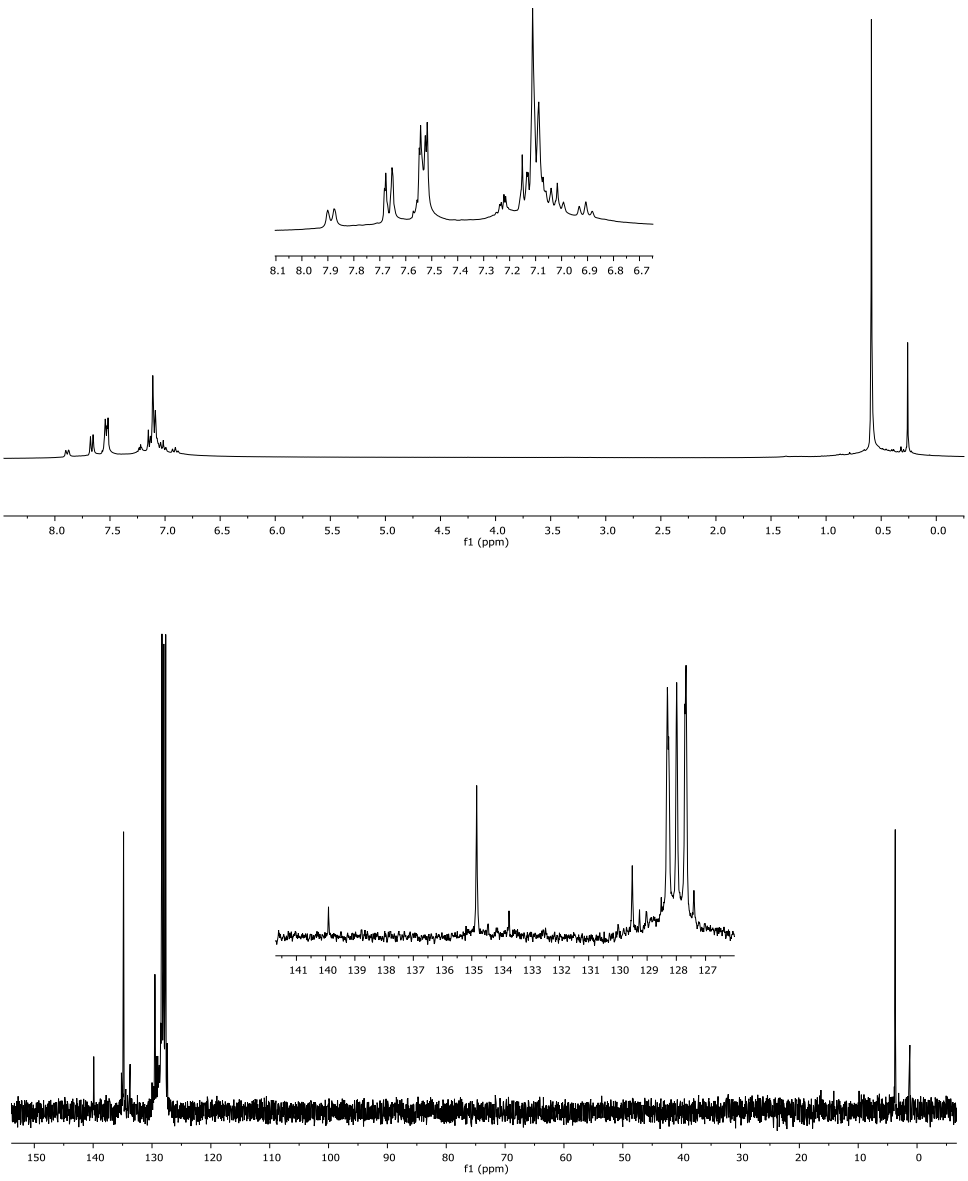

Figure 2.7: ^{1}H (top) and ^{13}C (bottom) NMR spectra of $Ph_2C_2O_2Ge[N(SiMe_2Ph)_2]_2$ (**4**) in C_6D_6.

The X-ray crystal structure of $Ph_2C_2O_2Ge[N(SiMe_3)_2]_2$ (**3**) is shown below as an ORTEP diagram in **Figure 2.8** and selected bond distances and angles for the structure are collected in **Table 2.3**.

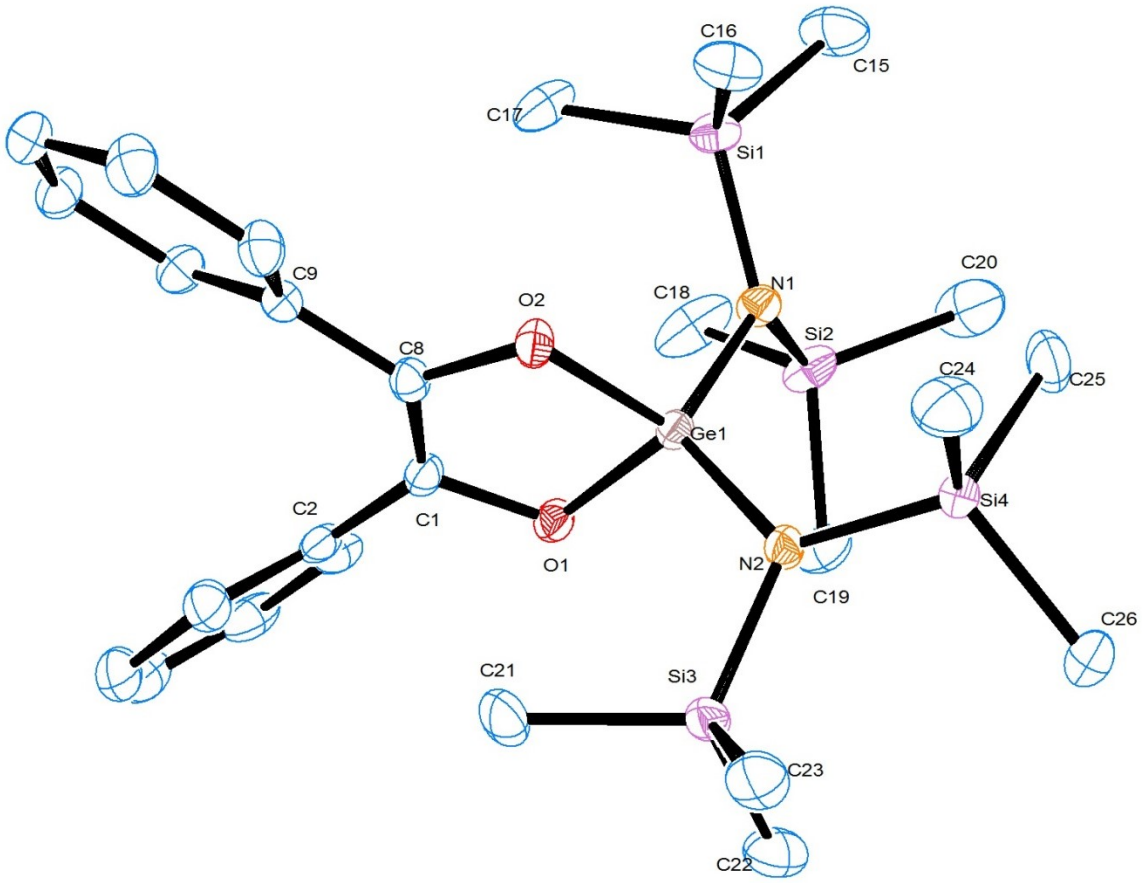

Figure 2.8: X-ray crystal structure of the benzil adduct $Ph_2C_2O_2Ge[N(SiMe_3)_2]_2$ (**3**)

Table 2.3: Selected bond distances (Å) and angles (deg) for $Ph_2C_2O_2Ge[N(SiMe_3)_2]_2$ (**3**).

Bond Lengths	(Å)	Bond Angles	(deg)
Ge(1) - O(1)	1.805(1)	O(1) - Ge(1) - O(2)	91.87(5)
Ge(1) - O(2)	1.801(1)	O(1) - Ge(1) - N(1)	108.55(5)
Ge(1) - N(1)	1.817(1)	O(1) - Ge(1) - N(2)	112.77(5)
Ge(1) - N(2)	1.803(1)	O(2) - Ge(1) - N(1)	109.52(5)
N(1) - Si(1)	1.767(1)	O(2) - Ge(1) - N(2)	112.36(5)
N(1) - Si(2)	1.756(1)	N(1) - Ge(1) - N(2)	118.55(6)
N(2) - Si(3)	1.783(1)	Si(1) - N(1) - Si(2)	122.54(8)
N(2) - Si(4)	1.762(1)	Si(3) - N(2) - Si(4)	119.06(8)
O(1) - C(1)	1.395(2)	Si(1) - N(1) - Ge(1)	116.53(7)
O(2) - C(8)	1.393(2)	Si(2) - N(1) - Ge(1)	115.50(8)
C(1) - C(8)	1.346(2)	Si(3) - N(2) - Ge(1)	117.65(7)
C(1) - C(2)	1.474(2)	Si(4) - N(2) - Ge(1)	122.76(8)
C(8) - C(9)	1.473(2)	Ge(1) - O(1) - C(1)	107.14(9)
		Ge(1) - O(2) - C(8)	107.42(9)
		O(1) - C(1) - C(2)	113.3(1)
		O(1) - C(1) - C(8)	116.7(1)
		O(2) - C(8) - C(9)	114.1(1)
		O(2) - C(8) - C(1)	116.4(1)

The average Ge-O bond distance in $Ph_2C_2O_2Ge[N(SiMe_3)_2]_2$ (**3**) is 1.803(1) Å which is consistent with that expected for Ge(+4)-O single bonds. The Ge-O bond distance in **3** is shorter than the Ge-O bond distance typically seen for germanium(II) aryloxide complexes (1.8 to 2.0 Å).[24-30] This observation is expected since the germanium atom in **3** has a higher formal oxidation state, and therefore a smaller covalent radius, than aryloxygermylenes which contain germanium in the +2 oxidation state. Similarly, the average Ge-N bond distance in **3** is 1.810(1) Å which is shorter than the average Ge-N bond distance in $Ge[N(SiMe_3)_2]_2$ (**1**) ($dGe\text{-}N_{avg}$ = 1.876(5) Å). The N-Si bond distances in **3** range from 1.756(1) – 1.783(1) Å ($dN\text{-}Si_{avg}$ = 1.767(1) Å) which are slightly longer than the N-Si bond distances in **1** which average 1.752(5) Å.

The N-Ge-N bond angle in $Ph_2C_2O_2Ge[N(SiMe_3)_2]_2$ (**3**) is 118.55(6)° which is significantly more obtuse than the corresponding bond angle in $Ge[N(SiMe_3)_2]_2$ (**1**) which is 107.1(2)°. This expansion can be attributed to the to the smaller radius of Ge(IV) in **3**. Because the molecule has to accommodate the two bulky $–SiMe_3$ groups bound to each of the nitrogen atoms, the N-Ge-N bond angle is significantly distorted from the expected normal tetrahedral angle of 109.5°. However, the O-Ge-O bond angle of 91.88(5)° is the most distorted of the six bond angles at germanium in **3**. This is not only due to the steric bulk of the $–N(SiMe_3)_2$ ligands and the phenyl groups attached to the GeO_2C_2 ring, but this distorted angle can also be attributed to the need to incorporate the germanium atom into a five-membered ring itself. The four O-Ge-N bond angles approach the expected tetrahedral value with an average bond angle of 110.80(6)°. Contained in the GeO_2C_2 ring, the two C-O bonds average 1.395(2) Å which is typical for C-O single bonds, while the C(1)-C(8) bond distance of 1.364(2) Å corresponds to a C=C double bond. Therefore, the expected structure of this complex is confirmed by the X-ray crystal structure shown in **Figure 2.8**.

One interesting structural feature in $Ge[N(SiMe_3)_2]_2$ (**1**) is that the nitrogen atoms exhibit a planar environment even though they are sp^3 hybridized. The sum of the Si-N-Si and two Ge-N-Si bond angles is very close to 360°. This feature is due to π-type interactions between both nitrogen and silicon as well as nitrogen and germanium. Typically a planar geometry is observed at nitrogen in metal silylamides rather than the expected trigonal pyramidal geometry due to the lone pair of electrons on the nitrogen atom. In the structure of $Ph_2C_2O_2Ge[N(SiMe_3)_2]_2$ (**3**), the sum of the two Ge(1)-N(2)-Si(3 or 4) and the Si(3)-N(2)-Si(4) bond angles sum to 359.47(8)° indicating that this planar geometry is maintained at N(2). The three relevant angles at N(1) sum to 354.57(8)° indicating that it still approaches planarity but is very slightly pyramidalized when compared to N(2). This showns that the π-type interactions present in **1** are maintained in the tetravalent compound **3**. This was also observed in the tetravalent germanium species

$BrGe[N(SiMe_3)_2]_3$, which exhibits a planar geometry at the nitrogen atoms where the sum of the three corresponding bond angles equals 359.5°.[31]

The benzil trapped germylene $Ph_2C_2O_2Ge[N(SiMe_2Ph)_2]_2$ (**4**) crystallizes with two independent molecules in the unit cell, and the crystal structures of both molecules are given below in **Figure 2.9** with selected bond distances and angles provided in **Table 2.4**. Compound **4** is essentially isostructural with $Ph_2C_2O_2Ge[N(SiMe_3)_2]_2$ (**3**), in that the average Ge-O, Ge-N, and N-Si bond distances are 18.05(2), 1.815(2), and 1.771(2) Å respectively, and the bond lengths in the GeO_2C_2 ring are very similar as well. The environment at germanium is also nearly identical, and the O-Ge-N and N-Ge-N bond angles in **4** are 110.92(8) and 118.43(9)°. However, there are two slight structural variations in $Ph_2C_2O_2Ge[N(SiMe_2Ph)_2]_2$ (**4**) when compared to those of $Ph_2C_2O_2Ge[N(SiMe_3)_2]_2$ (**3**). The first is that the O-Ge-O bond angle in **4** measures 91.58(7)°, which is 0.30° more acute than the same angle of **3**. The other variation is that the sum of the two Si-N-Ge angles and the single Si-N-Si bond angle at each nitrogen atom deviate from the sum of 360° at all four nitrogen atoms. The sum of these angles at each nitrogen atom are as follows: ΣN(1) = 356.3(1)°, ΣN(2) = 355.5(1)°, ΣN(3) = 354.2(1)°, and ΣN(4) = 356.5(1)°. Each of the four nitrogen atoms is bent out of the plane defined by the two silicon atoms and the germanium atom to which the nitrogen atom is attached, whereas in **3** one of the nitrogen atoms is co-planar with the corresponding silicon and germanium atoms. Thus, all of the nitrogen atoms in **4** are very slightly pyramidalized which can be attributed to the steric demand of the larger phenyl group of the $–SiMe_2Ph$ ligands in **4** when compared to the three methyl groups of the $–SiMe_3$ ligands in **3**.

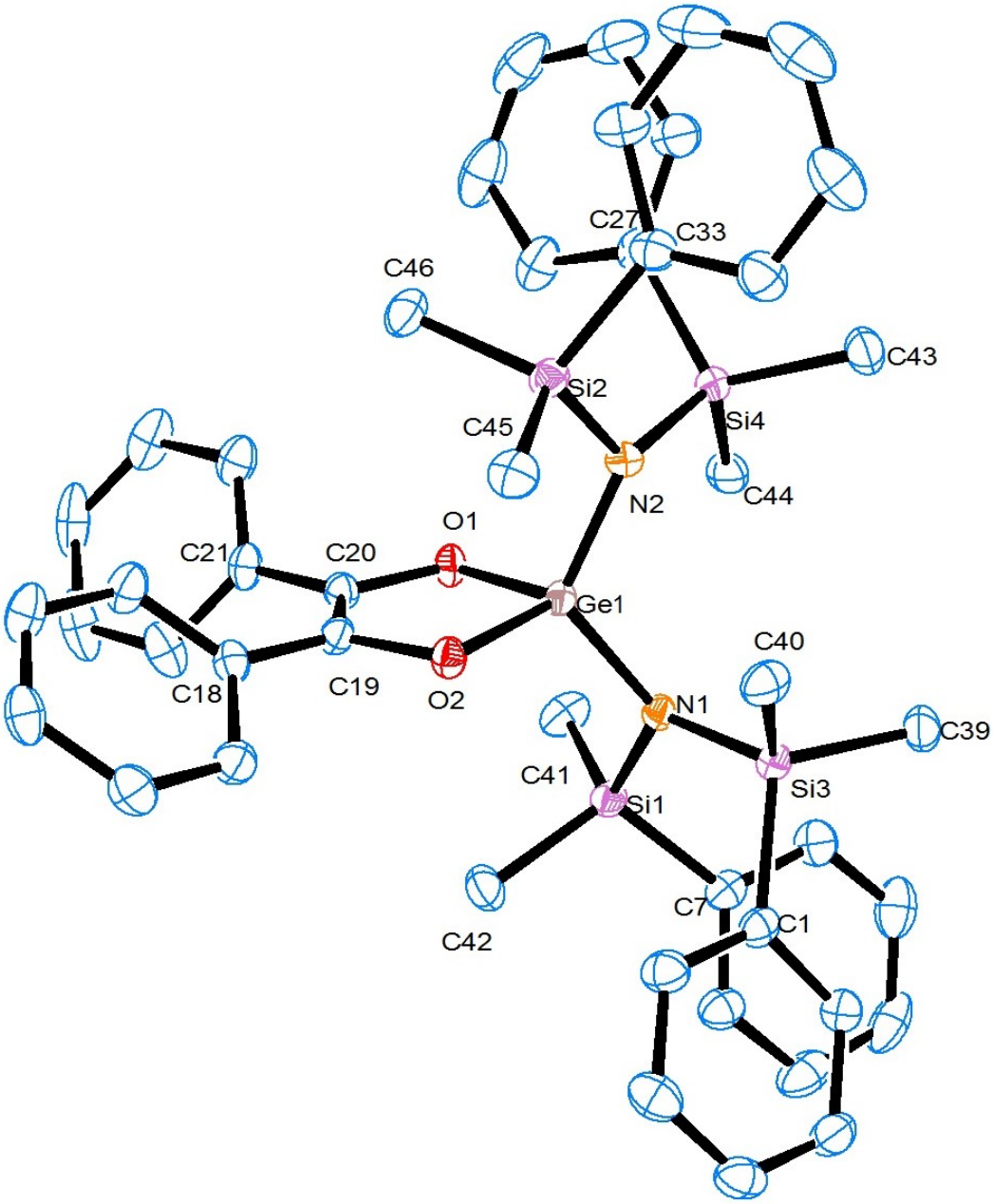

X-ray structure of 4: Molecule 1

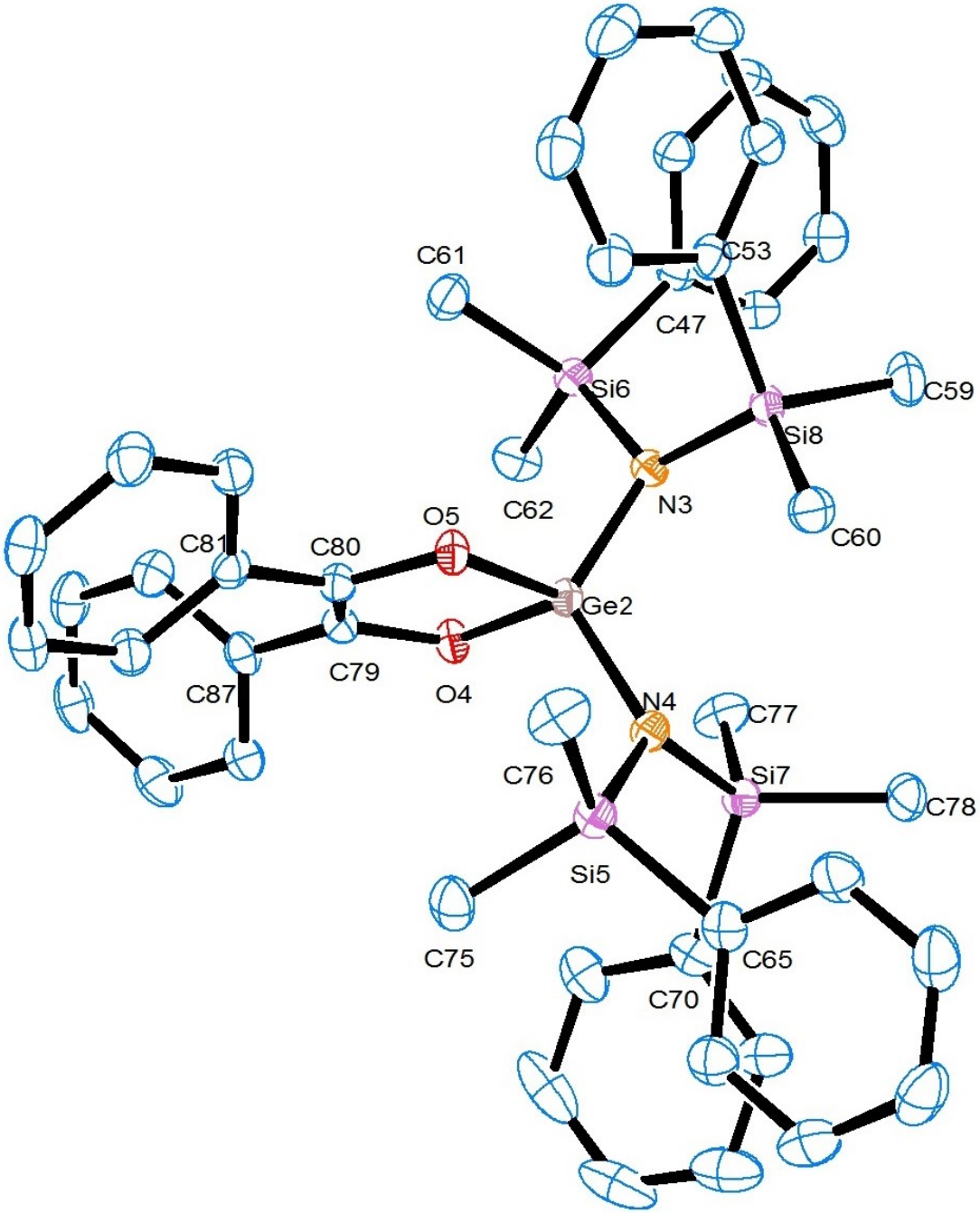

X-ray structure of 4: Molecule 2

Figure 2.9: X-ray crystal structure of the benzil adduct $Ph_2C_2O_2Ge[N(SiMe_2Ph)_2]_2$ (**4**) which contains two unique molecules in the unit cell.

Table 2.4: Selected bond distances (Å) and angles (deg) of the benzil adduct $Ph_2C_2O_2Ge[N(SiMe_2Ph)_2]_2$ (**4**)

Molecule 1		Molecule 2		Average
Ge(1) - O(1)	1.811(2)	Ge(2) - O(4)	1.805(2)	1.808(2)
Ge(1) - O(2)	1.802(2)	Ge(2) - O(5)	1.801(2)	1.802(2)
Ge(1) - N(1)	1.812(2)	Ge(2) - N(3)	1.814(2)	1.813(2)
Ge(1) - N(2)	1.817(2)	Ge(2) - N(4)	1.814(2)	1.816(2)
N(1) - Si(1)	1.771(2)	N(3) - Si(6)	1.778(2)	1.775(2)
N(1) - Si(3)	1.772(2)	N(3) - Si(8)	1.770(2)	1.771(2)
N(2) - Si(2)	1.772(2)	N(4) - Si(5)	1.768(2)	1.770(2)
N(2) - Si(4)	1.769(2)	N(4) - Si(7)	1.766(2)	1.768(2)
O(1) - C(20)	1.392(3)	O(4) - C(79)	1.397(3)	1.395(3)
O(2) - C(19)	1.399(3)	O(5) - C(80)	1.394(3)	1.397(3)
C(19) - C(20)	1.345(4)	C(79) - C(80)	1.349(4)	1.347(3)
C(19) - C(18)	1.466(3)	C(79) - C(87)	1.474(3)	1.470(3)
C(20) - C(21)	1.480(3)	C(80) - C(81)	1.468(3)	1.474(3)
O(1) - Ge(1) - O(2)	91.53(7)	O(4) - Ge(2) - O(5)	91.62(7)	91.58(7)
O(1) - Ge(1) - N(1)	112.55(8)	O(4) - Ge(2) - N(3)	112.28(8)	112.42(8)
O(1) - Ge(1) - N(2)	109.30(8)	O(4) - Ge(2) - N(4)	109.91(8)	109.61(8)
O(2) - Ge(1) - N(1)	110.72(8)	O(5) - Ge(2) - N(3)	110.53(8)	110.63(8)
O(2) - Ge(1) - N(2)	111.50(8)	O(5) - Ge(2) - N(4)	110.50(8)	111.00(8)
N(1) - Ge(1) - N(2)	118.13(9)	N(3) - Ge(2) - N(4)	118.72(9)	118.43(8)
Si(1) - N(1) - Si(3)	121.6(1)	Si(6) - N(3) - Si(8)	119.8(1)	120.7(1)
Si(2) - N(2) - Si(4)	120.3(1)	Si(5) - N(4) - Si(7)	122.2(1)	121.3(1)
Si(1) - N(1) - Ge(1)	117.1(1)	Si(6) - N(3) - Ge(2)	115.9(1)	116.5(1)
Si(3) - N(1) - Ge(1)	117.6(1)	Si(8) - N(3) - Ge(2)	118.5(1)	118.1(1)
Si(2) - N(2) - Ge(1)	118.2(1)	Si(5) - N(4) - Ge(2)	117.7(1)	118.0(1)
Si(4) - N(2) - Ge(1)	116.4(1)	Si(7) - N(4) - Ge(2)	116.6(1)	116.5(1)
Ge(1) - O(1) - C(20)	107.3(1)	Ge(2) - O(4) - C(79)	107.6(1)	107.5(1)
Ge(1) - O(2) - C(19)	107.8(1)	Ge(2) - O(5) - C(80)	108.0(1)	107.9(1)
O(1) - C(20) - C(19)	117.1(2)	O(4) - C(79) - C(80)	116.5(2)	116.8(2)
O(1) - C(20) - C(21)	114.4(2)	O(4) - C(79) - C(87)	113.6(2)	114.0(2)
O(2) - C(19) - C(20)	115.7(2)	O(5) - C(80) - C(79)	116.0(2)	115.9(2)
O(2) - C(19) - C(18)	114.0(2)	O(5) - C(80) - C(81)	113.9(2)	114.0(2)

Table 2.5: Crystallographic data for **3** and **4**.

Compound	$Ph_2C_2O_2Ge[N(SiMe_3)_2]_2$ (**3**)	$Ph_2C_2O_2Ge[N(SiMe_2Ph)_2]_2$ (**4**)
Empirical Formula	$C_{26}H_{46}GeN_2O_2Si_4$	$C_{46}H_{54}GeN_2O_2Si_4$
Formula Weight	603.6	851.86
Temperature (K)	273(2)	100(2)
Wavelength (Å)	1.54178	0.71073
Crystal System	Monoclinic	Monoclinic
Space Group	$P2_1/n$	$P2_1/c$
a, Å	9.1920(8)	11.5993(7)
b, Å	33.146(3)	21.747(1)
c, Å	10.6316(9)	35.338(2)
α, °	90	90
β, °	92.705(3)	90.324(1)
γ, °	90	90
V, $Å^3$	3235.6(5)	8964.2(9)
Z	4	8
ρ (g cm^{-3})	1.239	1.262
Absorption coefficient (mm)	2.892	0.829
F(000)	1280	3584
Crystal Size (mm^{-1})	0.34 x 0.30 x 0.26	0.40 x 0.20 x 0.15
Theta range for data collection	4.95 to 68.26°	1.48 to 25.46°
Index ranges		
	$-8 \le h \le 10$	$-13 \le h \le 11$
	$-38 \le k \le 39$	$-26 \le k \le 26$
	$-12 \le l \le 12$	$-42 \le l \le 42$
Reflections collected	23459	70031
Independent reflections	5639	16527
	(R_{int} = 0.0224)	(R_{int} = 0.0496)
Completeness to θ	θ = 65.00 (97.9%)	θ = 25.46 (99.6%)
Absorption correction	Multi-scan	Semi-empirical from equivalents
Max. and Min. transmission	0.5202 and 0.4397	0.8858 and 0.7328
Refinement method	Full-matrix least -squares on F^2	Full-matrix least -squares on F^2
Data/restraints/parameters	5639/0/328	16527/0/991
Goodness-of-fit on F^2	1.088	1.024
Final *R* indices ($I < 2\sigma(I)$)		
R_1	0.0256	0.0387
wR_2	0.0661	0.0912
Final R indices (all data)		
R_1	0.0256	0.0515
wR_2	0.0661	0.0973
Largest diff. peak and hole (e $Å^{-3}$)	0.406 and -0.351	0.713 and -0.384
CCDC deposition number	859459	859460

2.3 Experimental

General remarks

All manipulations were carried out under an inert atmosphere of nitrogen using standard Schlenk, syringe, and glovebox techniques.[32] Solvents were dried using a Glass Contour solvent purification system. The compound $Ge[N(SiMe_3)_2]_2$ (**1**) was prepared following the literature procedure.[18] The reagents $HN(SiMe_2Ph)_2$, $GeCl_2$(dioxane), and benzil were purchased from Aldrich and used as received. ^1H and ^{13}C NMR were recorded on a Inova Gemini 2000 spectrometer at 300.0 and 75.5 MHz respectively and were referenced to the solvent. Elemental analyses were conducted by Galbraith Laboratories (Knoxville, TN).

*Synthesis of $Ge[N(SiMe_2Ph)_2]_2$ (**2**)*

To a solution of $HN(SiMe_2Ph)_2$ (2.013 g, 7.05 mmol) in THF (25 mL) was added to a solution of Bu^nLi (3.05 mL, 2.54 M, 7.75 mmol) in hexanes dropwise at 0 °C. The reaction mixture was allowed to come to room tempertature and was stirred for 3 h. The resulting solution was added via cannula at 0 °C to a solution of $GeCl_2$(dioxane) (0.817 g, 3.53 mmol) in THF (20 mL). The reaction mixture was allowed to come to room temperature and then stirred for 18 h, after which time, the volatiles were removed *in vacuo*. The resulting material was suspended in hexane and filtered through Celite and the hexane was removed from the filtrate *in vacuo* to yield **2** (1.842 g, 81%) as a viscous orange liquid. ^1H NMR (C_6D_6, 23 °C) δ 7.48 (m, 8H, *m*-H), 7.17 (m, 12H, *o*-H and *p*-H), 0.43 (s, 24H, -CH_3) ppm. ^{13}C NMR (C_6D_6, 23 °C) δ 141.3 (*o*-C), 134.5 (*p*-C), 129.3 (*ipso*-C), 128.3 (*m*-C), 3.9 (-Si(*C*H_3)$_2$) ppm. *Anal*. Calcd. For $C_{32}H_{44}GeN_2Si_4$: C, 59.95; H, 6.92. Found: C, 60.09; H, 6.88.

*Synthesis of $Ph_2C_2O_2Ge[N(SiMe_3)_2]_2$ (**3**)*

Compound **3** was synthesized by a slight modification of the literature procedure.[23] To a solution of benzil (0.176 g, 0.837 mmol) in benzene (15 mL) was added a solution of $Ge[N(SiMe_3)_2]_2$ (**1**) (0.300 g, 0.763 mmol) in benzene (10 mL). The reaction mixture was stirred for 18 h at room temperature after which time, the solution was dark red in color. The volatiles were removed *in vacuo* to yield a thick maroon oil from which crystals slowly formed over a period of two days to yield **3** (0.442 g, 96%) as colorless crystals. ^{1}H NMR (C_6D_6, 23 °C) δ 7.67 (d, J = 7.2Hz, 4H, *o*-H), 7.07 (t, J = 7.5Hz, 4H, *m*-H), 6.96 (t, J = 7.2Hz, 2H, *p*-H), 0.37 (s, 36H, -CH_3) ppm. ^{13}C NMR (C_6D_6, 23 °C) δ137.4 (*C*=*C*), 135.5 (*ipso*-C), 128.4 (*o*-C), 128.0 (*p*-C), 127.4 (*m*-C), 4.7 (-*C*H_3) ppm. *Anal.* Calcd. For $C_{26}H_{46}GeN_2O_2Si_4$: C, 51.75; H, 7.69. Found: C, 51.91; H, 7.57.

*Synthesis of $Ph_2C_2O_2Ge[N(SiMe_2Ph)_2]_2$ (**4**)*

To a solution of benzil (0.108 g, 0.514 mmol) in benzene (10 mL) was added a solution of $Ge[N(SiMe_2Ph)_2]_2$ **(2)**, (0.300 g, 0.468 mmol) in benzene (10 mL). The solution was stirred at room temperature for 18 h and the volatiles were then removed *in vacuo* to yield a purple-red oil from which crystals slowly formed over a period of three days to yield **4** (0.331 g, 83%) as colorless crystals. ^{1}H NMR (C_6D_6, 23 °C) δ 7.66 (d, J = 7.5 Hz, 4H, *o*-(C_6H_5)$_2C_2O_2$), 7.53 (d, J = 7.8 Hz, 8H, *o*-Si(C_6H_5)Me_2), 7.15 – 7.07 (m, 18H, *m*-H and *p*-H), 0.59 (s, 24H, -CH_3) ppm. ^{13}C NMR (C_6D_6, 23 °C) δ 139.9 (*C*=*C*), 134.8 (*ipso*-(C_6H_5)$_2$C=C), 133.7 (*ipso*-(C_6H_5)Si), 129.5 (*o*-C), 129.3 (*o*-C), 128.5 (*p*-C), 128.2 (*p*-C), 127.7 (*m*-C), 127.4 (*m*-C), 3.7 (-*C*H_3) ppm. *Anal.* Calcd. For $C_{46}H_{54}GeN_2O_2Si_4$: C, 64.87; H, 6.40. Found: C, 64.74; H, 6.32.

X-ray crystal structure analysis

X-ray crystallographic measurements for **3** and **4** were made using a Bruker APEX CCD system under a stream of nitrogen gas. Data were corrected for absorption using SADABS and the structures were solved using direct methods (SIR-2004). All non-hydrogen atoms were refined anisotropically by full-matrix least squares (SHELXL-2008). Crystallographic data for **3** and **4** are collected in **Table 2.5**. The CCDC deposition numbers shown in **Table 2.5** contain the supplementary crystallographic data for this chapter. These data can be obtained free of charge from the Cambridge Crystallographic Data Centre via www.ccdc.ac.uk/data_request/cif.

2.4 References

1. Neumann, W. P., *Chem. Rev.* **1991,** *91* (3), 311-334.

2. Lesbre, M.; Mazerolles, P.; Satgé, J., *The organic compounds of germanium*. Interscience Publishers: London, New York,, 1971; p xii, 701 p.

3. Cotton, J. D. D., P.J.; Lappert, M.F., *Dalton Trans.* **1976,** (21), 2275-2286.

4. Lappert, M. F.; Rowe, R. S., *Coordin. Chem. Rev.* **1990,** *100*, 267-292.

5. Chorley, R. W.; Hitchcock, P. B.; Lappert, M. F.; Leung, W. P.; Power, P. P.; Olmstead, M. M., *Inorg. Chim. Acta.* **1992,** *198*, 203-209.

6. Davidson, P. J.; Harris, D. H.; Lappert, M. F., *J. Chem. Soc. Dalton* **1976,** (21), 2268-2274.

7. Hitchcock, P. B.; Lappert, M. F.; Miles, S. J.; Thorne, A. J., *J. Chem. Soc., Chem. Commun.* **1984,** (7), 480.

8. Miller, K. A.; Bartolin, J. M.; O'Neill, R. M.; Sweeder, R. D.; Owens, T. M.; Kampf, J. W.; Holl, M. M. B.; Wells, N. J., *J. Am. Chem. Soc.* **2003,** *125* (30), 8986-8987.

9. Miller, K. A. W., T. W.; John E. Bender, I.; Holl, M. M. B.; Kampf, J. W. , *J. Am. Chem. Soc.* **2001,** (123), 982-983.

10. Walker, R. H.; Miller, K. A.; Scott, S. L.; Cygan, Z. T.; Bartolin, J. M.; Kampf, J. W.; Holl, M. M. B., *Organometallics* **2009,** *28* (9), 2744-2755.

11. Sweeder, R. D.; Miller, K. A.; Edwards, F. A.; Wang, J.; Holl, M. M. B.; Kampf, J. W., *Organometallics* **2003,** *22* (24), 5054-5062.

12. Harris, D. H. L., M. F., *J.C.S., Chem. Comm.* **1974**, 895-896.

13. Al-Ktaifani, M. M.; Hitchcock, P. B.; Lappert, M. F.; Nixon, J. F.; Uiterweerd, P., *Dalton Trans.* **2008,** (21), 2825-2831.

14. Ellis, D.; Hitchcock, P. B.; Lappert, M. F., *J Chem Soc Dalton* **1992,** (23), 3397-3398.

15. Lappert, M. F.; Misra, M. C.; Onyszchuk, M.; Rowe, R. S.; Power, P. P.; Slade, M. J., *J. Organomet. Chem.* **1987,** *330* (1-2), 31-46.

16. Lappert, M. F.; Power, P. P., *J. Chem. Soc. Dalton* **1985,** (1), 51-57.

17. Gynane, M. J. S.; Harris, D. H.; Lappert, M. F.; Power, P. P.; Riviere, P.; Rivierebaudet, M., *J. Chem. Soc. Dalton* **1977,** (20), 2004-2009.

18. Zhu, Q. F., K. L.; Roskamp, E. J., *Heteroatom Chemistry* **1992,** *3*, 647-649.

19. York, J. T.; Young, V. G.; Tolman, W. B., *Inorg. Chem.* **2006,** *45* (10), 4191-4198.

20. Cabeza, J. A.; Garcia-Alvarez, P.; Polo, D., *Inorg. Chem.* **2011,** *50* (13), 6195-6199.

21. Litz, K. E.; Bender, J. E.; Kampf, J. W.; Holl, M. M. B., *Angew. Chem. Int. Edit.* **1997,** *36* (5), 496-498.

22. Cygn, Z. T.; Bender, J. E.; Litz, K. E.; Kampf, J. W.; Holl, M. M. B., *Organometallics* **2002,** *21* (24), 5373-5381.

23. Litz, K. E.; Bender, J. E.; Sweeder, R. D.; Holl, M. M. B.; Kampf, J. W., *Organometallics* **2000,** *19* (6), 1186-1189.

24. Boyle, T. J.; Tribby, L. J.; Ottley, L. A. M.; Han, S. M., *Eur. J. Inorg. Chem.* **2009,** (36), 5550-5560.

25. Weinert, C. S.; Fenwick, A. E.; Fanwick, P. E.; Rothwell, I. P., *Dalton Trans.* **2003,** (4), 532-539.

26. Weinert, C. S.; Fanwick, P. E.; Rothwell, I. P., *J. Chem. Soc. Dalton* **2002,** (15), 2948-2950.

27. Wetherby, A. E.; Goeller, L. R.; DiPasquale, A. G.; Rheingold, A. L.; Weinert, C. S., *Inorg. Chem.* **2007,** *46* (18), 7579-7586.

28. Wetherby, A. E.; Goeller, L. R.; DiPasquale, A. G.; Rheingold, A. L.; Weinert, C. S., *Inorg. Chem.* **2008,** *47* (6), 2162-2170.

29. Wetherby, A. E.; Rheingold, A. L.; Feasley, C. L.; Weinert, C. S., *Polyhedron* **2008,** *27* (7), 1841-1847.

30. Weinert, C. S., *Main Group Metal Chemistry* **2007,** *30* (2-3), 93-100.

31. Walding, J. L.; Fanwick, P. E.; Weinert, C. S., *Inorg. Chim. Acta* **2005,** *358* (4), 1186-1192.

32. D. F. Shriver, M. A. Drezdzon, *The Manipulation of Air Sensitive Compounds*. John Wiley and Sons, New York: 1986.

.

CHAPTER III

SYNTHESIS AND STRUCTURES OF ARYLOXOGERMANIUM(IV) ALKYL IODIDE COMPLEXES AND A TRI(ARYLOXO)GERMANIUM COMPLEX

3.1 Introduction

The bulky germanium(II) amide, $Ge[N(SiMe_3)_2]_2$, which was discussed in greater detail in the previous chapter of this dissertation, has also been shown to react with organic molecules and other main group metals to give a wide range of products, including the formation of Ge-Si,[1] Ge-O,[2] Ge-N,[3] Ge-S,[4] Ge-Se,[4] and Ge-Te[4] bonds. Examples of some of these reactions are given below (**Schemes 3.1-3.3**).[1-2, 4]

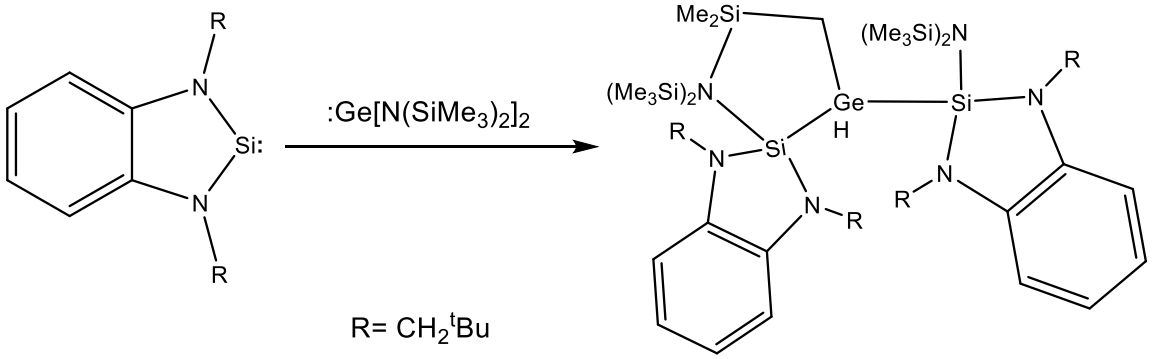

Scheme 3.1: Reaction of $Ge[N(SiMe_3)_2]_2$ to yield Ge-Si bond formation.[1]

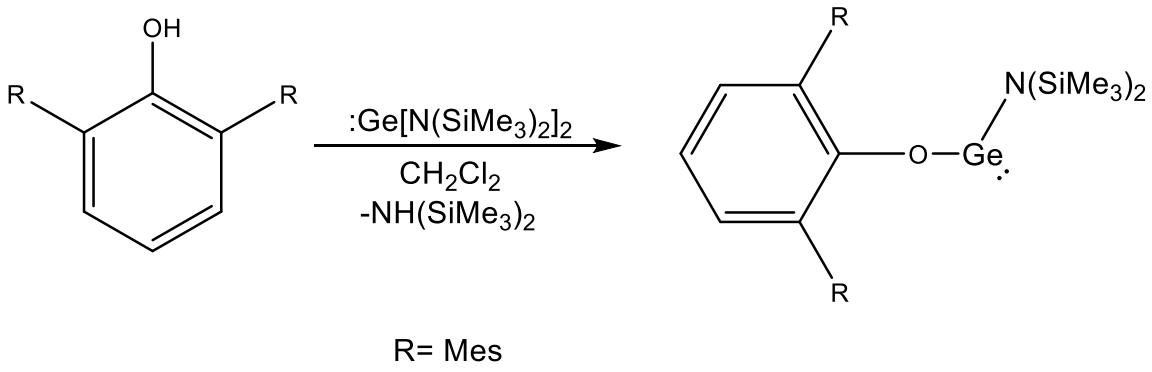

Scheme 3.2: Reaction of $Ge[N(SiMe_3)_2]_2$ to yield Ge-O bond formation.[2]

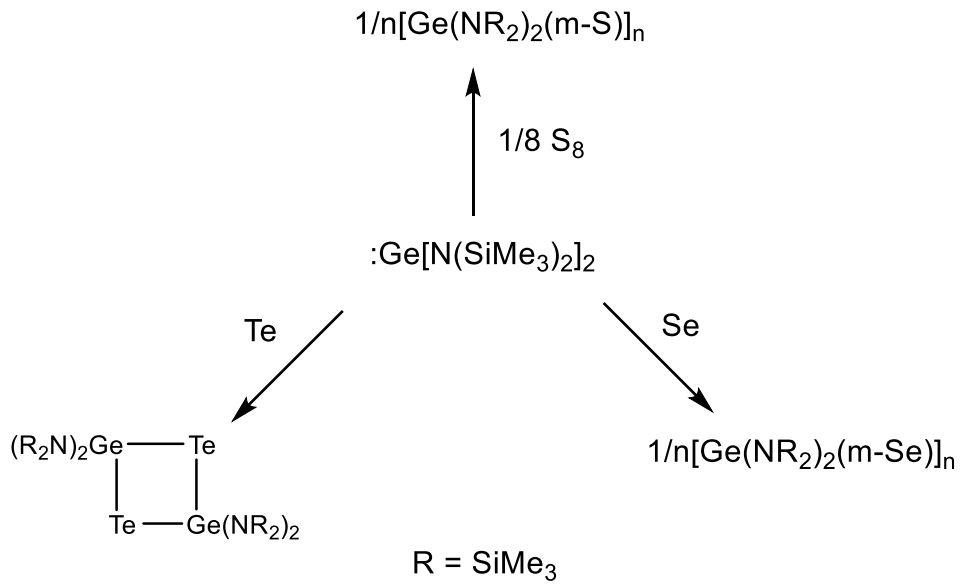

Scheme 3.3: Reaction of $Ge[N(SiMe_3)_2]_2$ to yield Ge-S, Ge-Se, and Ge-Te bond formation.[4]

In addition to the reactions of $Ge[N(SiMe_3)_2]_2$ with the transition and main group metals, $Ge[N(SiMe_3)_2]_2$ has been utilized for the preparation of numerous germanium(II) aryloxides (aryloxygermylenes). Germanium aryloxides contain germanium attached to one or more phenolic oxygen atoms and the aromatic rings can have a varying substitution pattern at the

ortho-, meta-, and/or *para-* positions. The germanium(II) aryloxides are typically synthesized via a protonolysis reaction using $Ge[N(SiMe_3)_2]_2$ and two equivalents of phenol. These aryloxides can have a variety of different structures including monomers, dimers, or clusters. The structure of these aryloxides is typically dictated by the steric bulk of the aryloxo ligands. The formation of monomeric germanium(II) aryloxides has been observed when the aryl groups are ($OC_6H_3Mes_2$-2,6),[2] (OC_6H_2Me-4-Bu^t_2-2,6),[5] ($OC_6H_3Ph_2$-2,6),[6] and (OC_6HPh_4-2,3,5,6).[6] Dimeric species have been observed when the aryl groups are ($OC_6H_2Me_3$-2,4,6)[6] or ($OC_6H_3{}^iPr_2$-2,6).[6] Cluster formation has been observed when the starting phenol lacks a substituent at one of its *ortho-* positions, this has been observed when the aryl group is ($OC_6H_3Bu^t$-2-Me-6).[7] The synthetic schemes for these compounds are given below (**Schemes 3.4-3.8**).[2, 5-7]

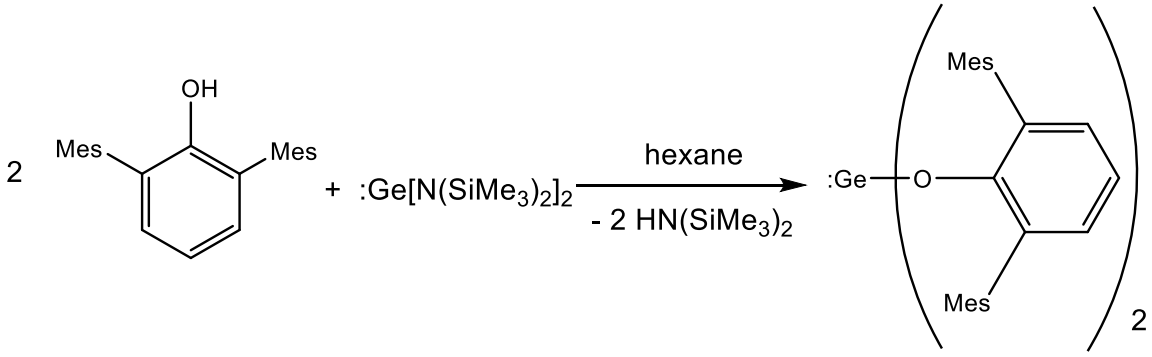

Scheme 3.4: Synthesis of $Ge(OAr)_2$ monomer (OAr = $OC_6H_3Mes_2$-2,6) (Mes = 2,4,6-trimethylphenyl).[2]

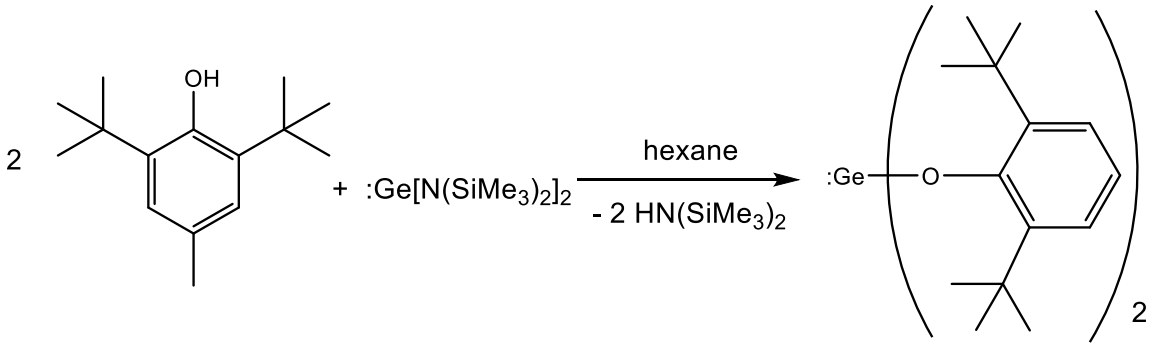

Scheme 3.5: Synthesis of $Ge(OAr)_2$ monomer (OAr = OC_6H_2Me-4-Bu^t_2-2,6).[5]

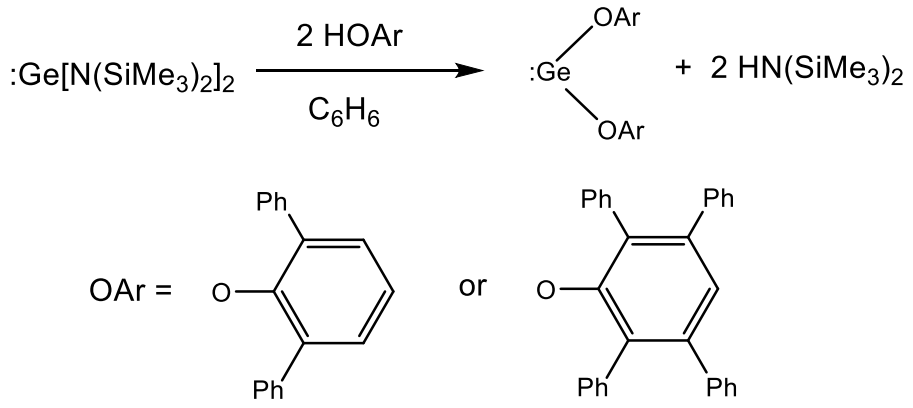

Scheme 3.6: Synthesis of $Ge(OAr)_2$ monomers (OAr = $OC_6H_3Ph_2$-2,6 or OC_6HPh_4-2,3,5,6).[6]

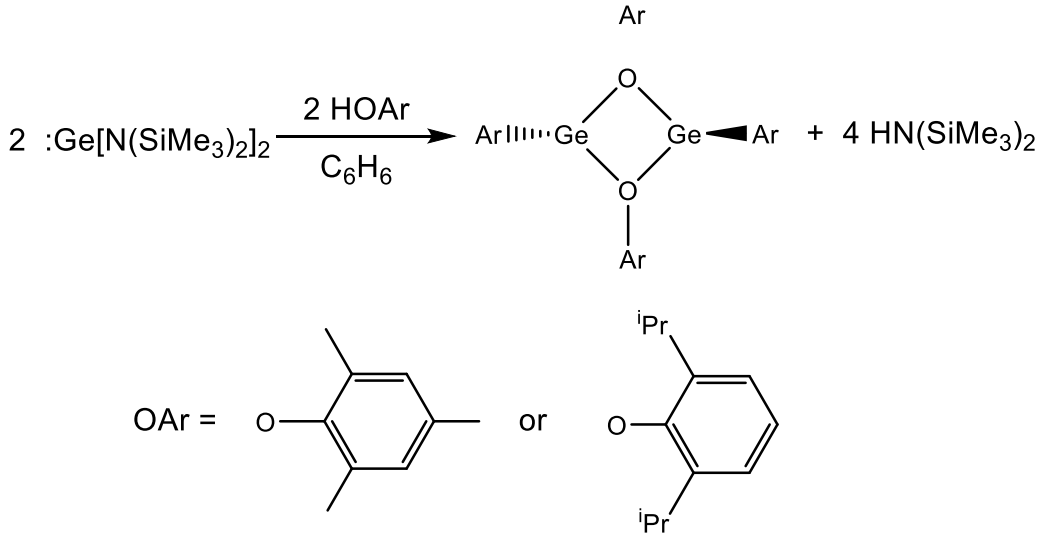

Scheme 3.7: Synthesis of $[Ge(OAr)_2]_n$ dimers (n = 2 and OAr = $OC_6H_2Me_3$-2,4,6 or $OC_6H_3{}^iPr_2$-2,6).[6]

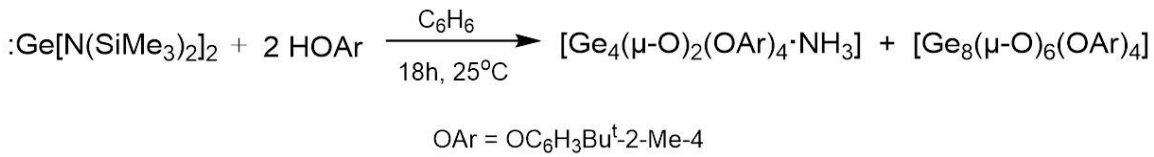

Scheme 3.8: Synthesis of germanium(II) aryloxide clusters.[7]

Germanium aryloxides are an interesting class of compounds that have been shown to exhibit a diverse array of possible structures. Some examples of which are shown in the schemes above. Aryloxygermylenes have also been shown to be useful as well-defined precursors for the preparation of germanium(0) nanomaterials. Specifically, the morphology of the germanium nanomaterial obtained was shown to be dependent on the germanium containing precursor. The germanium(II) or germanium(IV) precursors contained different substituent patterns, and depending on the substituents present, there was formation of different morphologies of germanium(0) nanomaterials.[8-9]

The monomeric germanium(II) aryloxide [$Ge(OC_6H_3Ph_4\text{-}2,3,5,6)_2$] has been shown to yield the germanium(IV) aryloxide complex [$Ge(OC_6H_3Ph_4\text{-}2,3,5,6)_2(Me)(I)$] via the oxidative addition of the germanium(II) center into the C-I bond of methyl iodide (**Scheme 3.9**).[6]

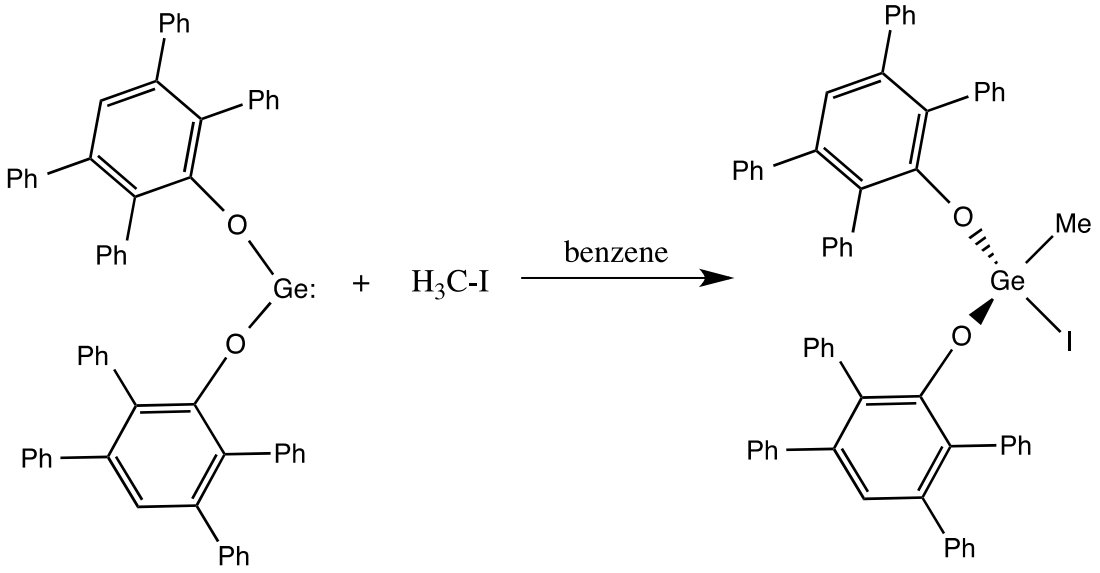

Scheme 3.9: Oxidative addition reaction of [$Ge(OC_6H_3Ph_4\text{-}2,3,5,6)_2$] with methyl iodide.[6]

The X-ray crystal structure of [Ge($OC_6H_3Ph_4$-2,3,5,6)$_2$(Me)(I)] has not been obtained, and crystallographically characterized compounds that contain a germanium-iodine bond are rare. Furthermore, as of April 2010, the only structurally characterized compound that contained germanium bound to both oxygen and iodine was the acetylacetonate complex (acac)GeI and the X-ray crystal structure is shown below in **Figure 3.1**.[10] The Ge-I bond distance in this structure is 2.736(1) Å, the two Ge-O bond distances are 1.931(5) and 1.914(5)Å, the O-Ge-O bond angle is rather acute at 91.38(22)°, and the two I-Ge-O bond angles are 91.60(16)° and 93.92(16)°. At the time, there were also no examples of any structurally characterized germanium(IV)-containing species where germanium was bound both to oxygen and iodine as found via a search of the CCDC database.

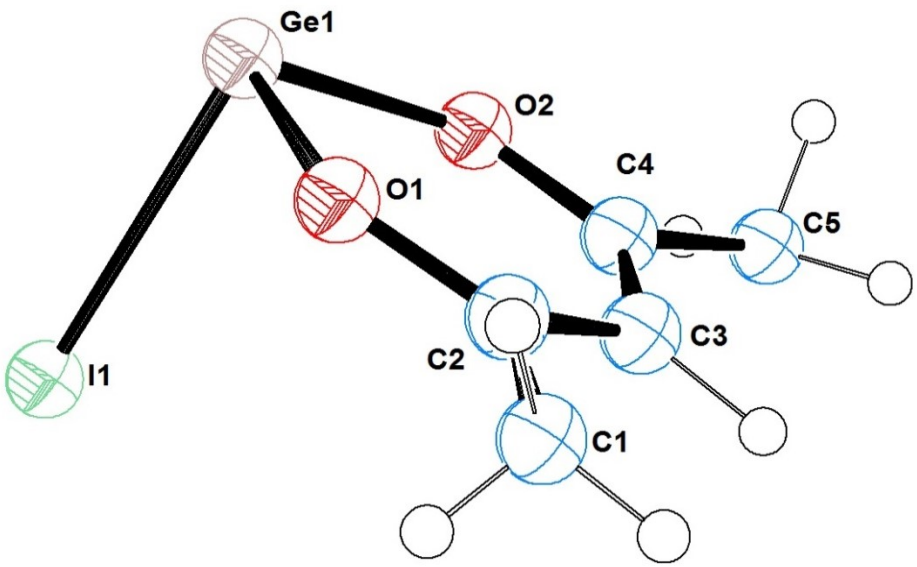

Figure 3.1: X-ray crystal structure of (acac)GeI.[10]

We have prepared and structurally characterized the germanium(IV) aryloxide $[Ge(OC_6H_3Ph_2\text{-}2,6)_2(Bu^t)(I)]$.[11] We have also prepared $[Ge(OC_6H_3Ph_2\text{-}2,6)_2(Me)(I)]$ which was then converted to the triaryloxo species $[Ge(OC_6H_3Ph_2\text{-}2,6)_3(Me)]$ upon reaction of the iodine containing compound with an extra equivalent of 2,6-diphenylphenol. The aryloxide species $[Ge(OC_6H_3Ph_2\text{-}2,6)_2(R)(I)]$ (R = Bu^t or Me) exhibit different reactivity toward 2,6-diphenylphenol due to the steric attributes of the organic substituent bound to the germanium atom.

3.2 Results and Discussion

The germanium(II) aryloxide $[Ge(OC_6H_3Ph_2\text{-}2,6)_2]$[6] (**1**) was synthesized using $Ge[N(SiMe_3)_2]_2$ and $HOC_6H_3Ph_2$-2,6 (2,6-diphenylphenol) according to **Scheme 3.6**[6] above. The X-ray crystal structure of **1** is known and is shown below as an ORTEP diagram in **Figure 3.2**.[6] Some selected bond distances and angles for the structure of **1** are provided below in **Table 3.1**.[6] The two Ge-O bond lengths average 1.820(1) Å and this bond distance is typical for monomeric germanium species that contain germanium(II) bound to oxygen. This bond length is longer than the Ge-O bond distance typically seen in species containing germanium(IV) which is expected due to the smaller radius of germanium(IV).[11] The O-Ge-O bond angle in **1** measures 92.10(5)° and is slightly more obtuse than the O-Ge-O bond angle in the germanium(II) aryloxide $[Ge(OC_6HPh_4\text{-}2,3,5,6)_2]$ which measures 91.09(7)°.[6]

Table 3.1: Selected bond distances (Å) and angles (deg) for [Ge($OC_6H_3Ph_2$-2,6)$_2$] (**1**).[6]

Bond Lengths	Å	Bond Angles	°
Ge - O(1)	1.822(1)	O(1) - Ge - O(2)	92.10(5)
Ge - O(2)	1.817(1)	Ge - O(1) - C(11)	117.2(1)
O(1) - C(11)	1.376(2)	Ge - O(2) - C(21)	117.1(1)
O(2) - C(21)	1.376(2)		

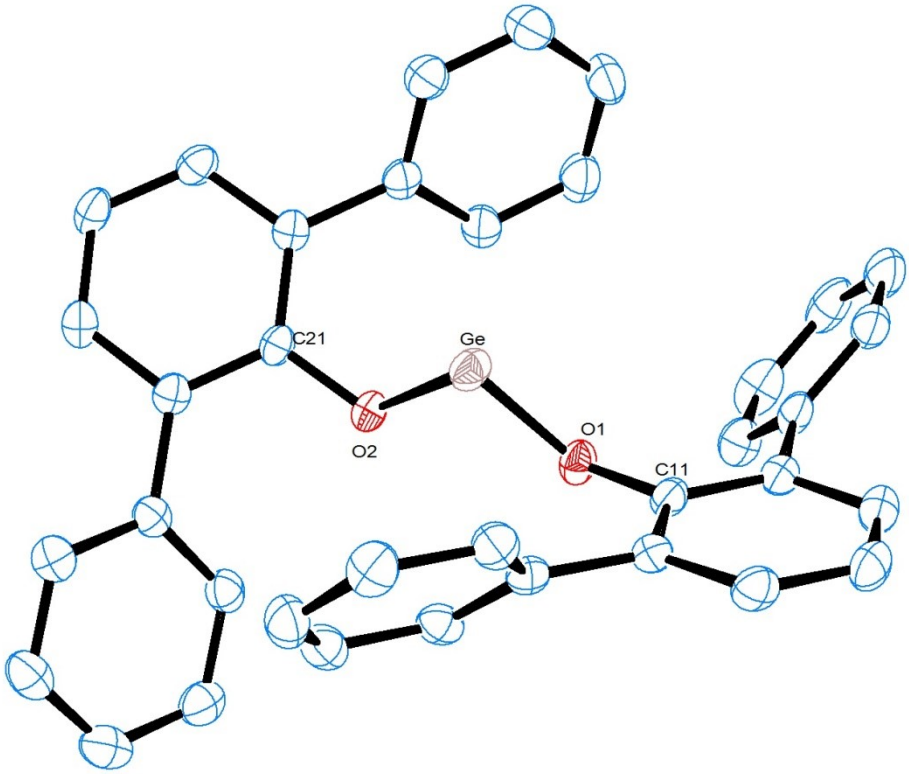

Figure 3.2: X-ray crystal structure of [Ge($OC_6H_3Ph_2$-2,6)$_2$] (**1**).[6]

The reaction of the 2,6-diphenylphenoxy-substituted germylene [Ge($OC_6H_3Ph_2$-2,6)$_2$] (**1**) with *tert*-butyliodide yields the germanium(IV) species [Ge($OC_6H_3Ph_2$-2,6)$_2$(Bu^t)(I)][11] (**2**) (**Scheme 3.10**). The ^{1}H NMR spectrum of **2** contains a resonance at δ 0.32 ppm corresponding to the nine

methyl protons of the *tert*-butyl group bound to the germanium atom. Crystals of [Ge($OC_6H_3Ph_2$-2,6)$_2$(Bu^t)(I)] (**2**) suitable for X-ray diffraction were obtained by slow evaporation of a benzene solution of the compound. The X-ray crystal structure of **2** is provided below as an ORTEP diagram, and a space-filling model included in **Figure 3.3**[11] and selected bond distances and angles for the structure are given below in **Table 3.2**.[11]

The iodine atom and the central carbon atom of the *tert*-butyl group are disordered with one another and were refined with occupancies of 0.5. Consequently, there is a crystallographic C_2-axis in **2** that renders both oxygen atoms equivalent.

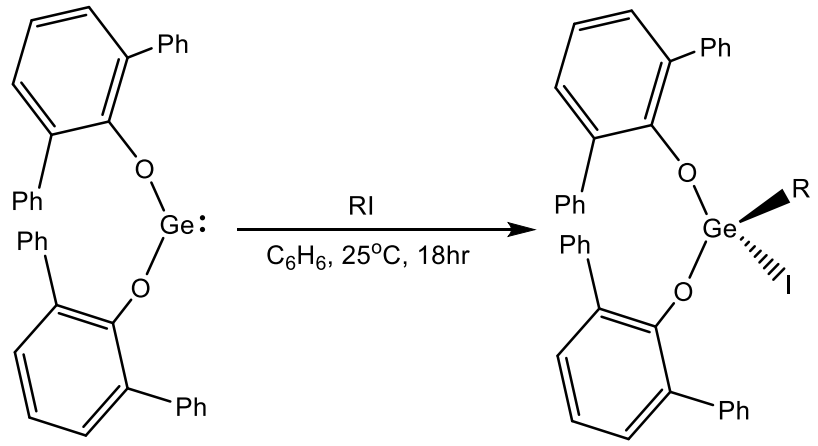

Scheme 3.10: Reaction of [Ge($OC_6H_3Ph_2$-2,6)$_2$] (**1**) with alkyl iodide compounds Bu^tI to yield [Ge($OC_6H_3Ph_2$-2,6)$_2$(Bu^t)(I)][11] (**2**) and MeI to yield [Ge($OC_6H_3Ph_2$-2,6)$_2$(Me)(I)] (**3**).

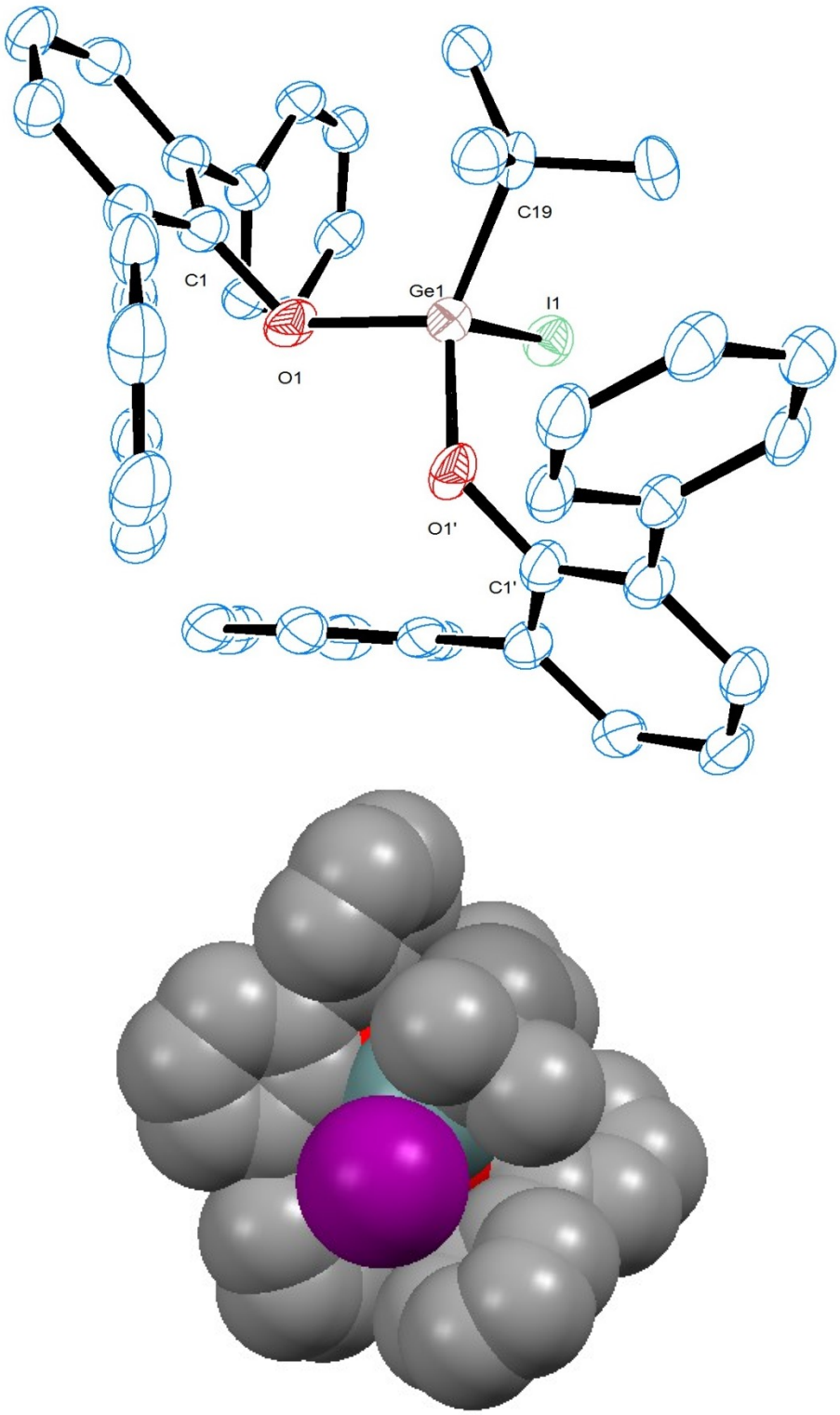

Figure 3.3: X-ray crystal structure (top) and space-filling model (bottom) (I = purple, Ge = green, O = red, C = grey) of $[Ge(OC_6H_3Ph_2\text{-}2,6)_2(Bu^t)(I)]$ (**2**).[11]

Table 3.2: Selected bond distances (Å) and angles (deg) for [Ge($OC_6H_3Ph_2$-2,6)$_2$(Bu^t)(I)] (**2**).[11]

Bond Lengths	Å	Bond Angles	°
Ge(1) - O(1)	1.763(3)	O(1) - Ge(1) - O(1')	96.2(3)
Ge(1) – I(1)	2.641(1)	O(1) - Ge(1) – I(1)	107.8(1)
Ge(1) - C(19)	1.920(1)	O(1) - Ge(1) - C(19)	128.5(3)
O(1) - C(1)	1.391(7)	I(1) - Ge(1) - C(19)	103.0(3)

The Ge-O bond distance for **2** is 1.763(3) Å and is typical for a germanium(IV)-O bond length and it is shorter than a typical germanium(II)-O bond distance which is expected due to the tetravalent oxidation state of germanium in **2**. The Ge-I bond length is 2.641(1) Å and while compounds with a Ge-I bond are rare, this bond distance is consistent with other compounds containing a germanium-iodine bond.[12-16] In comparison, the average Ge-I bond distance in the structure of the triphenylphosphine diiodogermylene Ph_3PGeI_2 is 2.636(2) Å.[12] This Ge-I bond distance is about the same as that for **2** even though the Ge-I bond distance would be expected to be shorter in **2** based on the higher oxidation state (+4) of germanium in **2**. This can be attributed to the steric bulk of the *tert*-butyl group that prevents the iodide atom from approaching closer to the germanium center in **2**. The bipyridine complex $GeI_4 \cdot 3[C_{12}H_9N_2] \cdot 3I$ contains an average Ge-I bond distance of 2.5335(6) Å[13]. This distance is about 0.11 Å shorter than that of **2** and this difference can be attributed to the lack of bulky groups around the germanium atom in the bipyridine complex since this complex and **2** are of the same oxidation state at germanium. Even though there is disorder in **2**, the Ge-C bond length is normal for a germanium(IV)-carbon bond distance and measures 1.920(1)Å. The O(1)-Ge(1)-O(1') bond angle measures only 96.2(3)°, and is more obtuse than that of the O-Ge-O bond angle of Ge($OC_6H_3Ph_2$-2,6)$_2$ (**1**) which is 92.10(5)°. This difference can be attributed to presence of a lone pair of electrons present on the divalent germanium atom in **1**, which by electron repulsions pushes the two aryloxide ligands closer

together, thus resulting in a more acute angle than that of $Ge(OC_6H_3Ph_2\text{-}2,6)_2(Bu^t)(I)$ (**2**). The O(1)-Ge(1)-I(1) and O(1')-Ge(1)-I(1) bond angles are 107.8(1)° and 102.3(1)°, respectively, and approach the idealized tetrahedral angle, while the I(1)-Ge(1)-C(19) bond angle measures 103.0(3)°.

The compound $[Ge(OC_6H_3Ph_2\text{-}2,6)_2]$ (**1**) reacts with iodomethane to yield $[Ge(OC_6H_3Ph_2\text{-}2,6)_2(Me)(I)]$ (**3**) in 86% yield (**Scheme 3.10** above). In order to effectively synthesize **3**, the iodomethane was meticulously dried over magnesium sulfate and activated molecular sieves immediately before use to prevent hydrolysis and the subsequent reaction of **3** with the now unbound 2,6-diphenylphenol (*vide infra*). The ^1H NMR spectrum of **3** contains a singlet at δ -0.49 ppm corresponding to the protons of the methyl group bound directly to the germanium atom. This indicates that the protons of the methyl group are highly shielded and this is likely due to both the electron donating abilities of the aryloxide ligands and the presence of the large iodide ligand placing more electron density around the methyl protons. Several attempts were made to crystallize compound **3**; however, these were unsuccessful. Despite this, the composition of **3** was further confirmed by elemental analysis and mass spectrometry. The mass spectrum of **3** contains a peak at *m/z* = 706 amu with the expected isotope pattern, as well as peaks corresponding to fragmentation of the molecule at *m/z* = 579 amu (M^+-I) and *m/z* = 461 amu (M^+-$OC_6H_3Ph_2$).

Compound **3** can be converted to the triaryloxo- species $[Ge(OC_6H_3Ph_2\text{-}2,6)_3(Me)]$ (**4**) upon reaction with an additional equivalent of 2,6-diphenylphenol (**Scheme 3.11**).

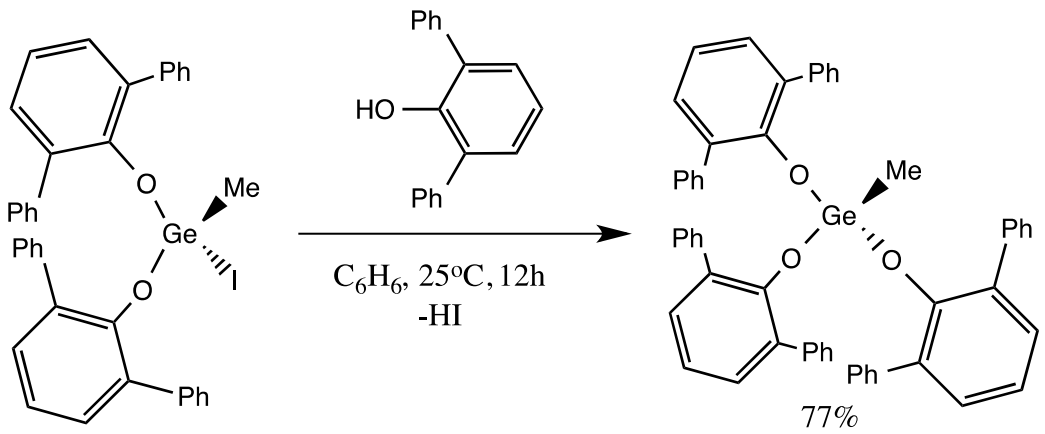

Scheme 3.11: Synthesis of [Ge($OC_6H_3Ph_2$-2,6)$_3$(Me)] (**4**) using [Ge($OC_6H_3Ph_2$-2,6)$_2$(Me)(I)] (**3**) and one equivalent of 2,6-diphenylphenol.

The formation of Ge($OC_6H_3Ph_2$-2,6)$_3$(Me) (**4**) was initially discovered serendipitously upon reaction of Ge($OC_6H_3Ph_2$-2,6)$_2$(Me)(I) (**3**) with 2,6-diphenyphenol that formed by hydrolysis of **3** by water present in the iodomethane reagent when attempting to prepare only compound **3**. The formation of **4** from compound **3** indicates that the iodide ligand present in **3** is labile enough to react with the acidic phenolic proton of 2,6-diphenylphenol. Compound **4** was then prepared directly by reacting compound **3** with an additional equivalent of 2,6-diphenylphenol. The ^{1}H NMR of **4** exhibits a resonance for the methyl group at δ -0.12 ppm that is shifted downfield from the corresponding methyl resonance in compound **3** (δ -0.49 ppm) due to the presence of an additional Ge-O bond.

Crystals that were of X-ray quality were obtained for compound **4** from the slow cooling of a hot dilute benzene solution of **4**, and the crystal structure is shown below as an ORTEP diagram in **Figure 3.4** with selected bond distances and angles listed in **Table 3.3** and the crystallographic data is provided in **Table 3.4**.

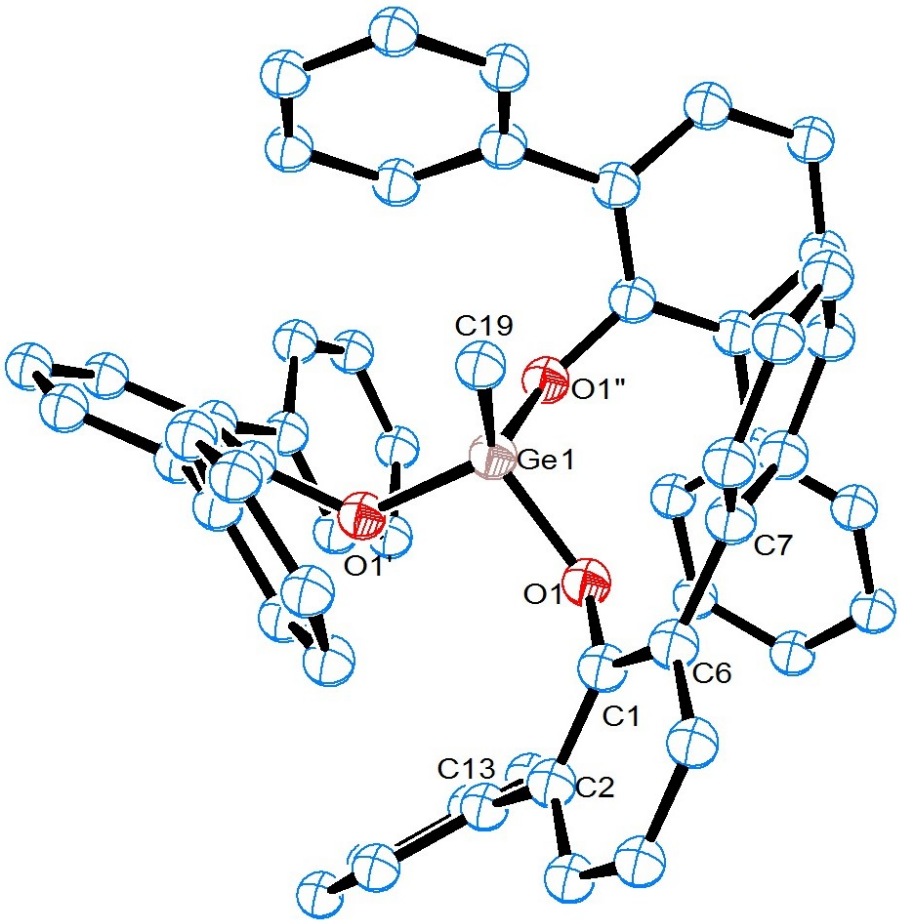

Figure 3.4: X-ray crystal structure of $[Ge(OC_6H_3Ph_2\text{-}2,6)_3(Me)]\bullet C_6H_6$ (**4**$\bullet C_6H_6$).

Table 3.3: Selected bond distances (Å) and angles (deg) for $[Ge(OC_6H_3Ph_2\text{-}2,6)_3(Me)]\bullet C_6H_6$ (**4**$\bullet C_6H_6$).

Bond Lengths	Å	Bond Angles	°
Ge(1) - O(1)	1.770(3)	O(1) - Ge(1) - O(1')	100.8(1)
Ge(1) - C(19)	1.914(6)	O(1) - Ge(1) - C(19)	117.2(2)
O(1) - C(1)	1.374(3)		

There is a C_3-axis of symmetry present in $Ge(OC_6H_3Ph_2\text{-}2,6)_3(Me)$ (**4**) located along the Ge(1)-C(19) bond which renders all three of the aryloxo ligands equivalent. The three Ge-O bonds of **4** have a bond length of 1.770(3) Å, which is similar to the Ge-O bond distance of **2** (1.763(3) Å), while the Ge(1)-C(19) bond length is 1.914(6) Å. The three O-Ge-O bond angles measure 100.8(1)° while the three O-Ge(1)-C(19) bond angles each measure 117.2(2)°. The *ortho*-phenyl rings in **4** are each rotated about the C-C bonds C(6)-C(7) and C(2)-C(13) relative to the plane of the phenolic phenyl ring due to steric effects that arise from there being three bulky 2,6-diphenylphenolate ligands bound to the germanium center. The angle at which the *ortho*-rings are rotated is 48.5(1)° about the C(2)-C(13) bond, and 42.0(1)° about the C(6)-C(7) bond. Therefore, the 2,6-diphenylphenolate ligands interlock in a gear-like fashion in the structure of **4**.

Interestingly, when the same reaction was attempted with $Ge(OC_6H_3Ph_2\text{-}2,6)_2(Bu^t)(I)$ (**2**) and an additional equivalent of 2,6-diphenylphenol, it did not provide the desired tri(aryloxo)-compound $[Ge(OC_6H_3Ph_2\text{-}2,6)_3(Bu^t)]$. Even though it was expected that the iodide ligand in **2** would also be labile enough to react with the acidic phenolic proton of the phenol via protonolysis, no evidence for the formation of $[Ge(OC_6H_3Ph_2\text{-}2,6)_3(Bu^t)]$ was observed even when the reaction mixture was heated for seven days at 85 °C. Therefore, the formation of $Ge(OC_6H_3Ph_2\text{-}2,6)_3(Me)$ (**4**) from $Ge(OC_6H_3Ph_2\text{-}2,6)_2(Me)(I)$ (**3**) seems to be possible due to the presence of the less sterically hindering methyl group in **3** versus the large *tert*-butyl group in **2**. This result is to be expected upon observation of the space-filling model of **2** above in **Figure 3.3**. It can be seen that the *tert*-butyl group is sterically hindering the germanium atom preventing any further reaction.

Table 3.4: Crystallographic data for compounds **2** and **4**.

	2[11]	**4**·C_6H_6
Compound	$[Ge(OC_6H_3Ph_2\text{-}2,6)_2(Bu^t)(I)]$	$[Ge(OC_6H_3Ph_22,6)_3(Me)]\cdot C_6H_6$
Empirical Formula	$C_{40}H_{35}GeIO_2$	$C_{40}H_{35}GeIO_2$
Formula Weight	747.17	899.57
Temperature (K)	100(2)	100(2)
Wavelength (Å)	0.71073 (Mo Kα)	0.71073 (Mo Kα)
Crystal System	Monoclinic	Rhombohedral
Space Group	C2/c	R3
a, Å	14.466(4)	15.8640(5)
b, Å	13.592(4)	15.8640(5)
c, Å	17.452(6)	15.736(1)
α, °	90	90
β, °	100.712(7)	90
γ, °	90	120
V, $Å^3$	3372(2)	3429.6(3)
Z	4	3
ρ (g cm^{-3})	1.472	1.307
Absorption coefficient (mm^{-1})	1.857	0.718
F(000)	1504	1404
Crystal Size (mm)	0.36 x 0.31 x 0.31	0.44 x 0.36 x 0.30
Theta range for data collection	2.07 to 28.18°	1.97 to 25.32°
Index ranges		
	$-18 \le h \le 19$	$-18 \le h \le 18$
	$-13 \le k \le 17$	$-19 \le k \le 19$
	$-22 \le l \le 22$	$-18 \le l \le 16$
Reflections collected	14144	8305
Independent reflections	3800	2492
	(R_{int} = 0.0497)	(R_{int} = 0.0293)
Completeness to θ = 25.00°	97.3%	100.0%
Absorption correction	Multi-scan (SADABS)	Multi-scan (SADABS)
Max. and Min. transmission	0.5967 and 0.5544	0.8134 and 0.7429
Refinement method	Full-matrix least -squares on F^2	Full-matrix least -squares on F^2
Data/restraints/parameters	3800/0/213	2492/1/199
Goodness-of-fit on F^2	1.187	1.052
Final *R* indices (I < 2σ(I))		
R_1	0.0697	0.0407
wR_2	0.1557	0.1090
Final R indices (all data)		
R_1	0.0892	0.0415
wR_2	0.1630	0.1099
Largest diff. peak and hole (e $Å^{-3}$)	0..677 and -1.363	1.189 and -0.299
CCDC deposition number	774958	774959

3.3 Conclusions

The germylene [$Ge(OC_6H_3Ph_2\text{-}2,6)_2$] (**1**) has been shown to react with iodomethane and 2-iodo-2-methylpropane (Bu^tI) to yield the germanium(IV) complexes [$Ge(OC_6H_3Ph_2\text{-}2,6)_2(Bu^t)(I)$] (**2**) and [$Ge(OC_6H_3Ph_2\text{-}2,6)_2(Me)(I)$] (**3**). The X-ray structure of **2** was determined, and compound **3** was found to react with one equivalent of 2,6-diphenylphenol to yield the tri(aryloxo)-species [$Ge(OC_6H_3Ph_2\text{-}2,6)_3(Me)$] (**4**). However, similar reactivity was not observed for compound **2**. The structure of **4** contains a C_3-axis of rotation about the central Ge-CH_3 bond and the three aryloxide ligands in **4** are arranged in an interlocking gear-like fashion about the central germanium atom.

3.4 Experimental

General Considerations

All manipulations were carried out using standard Schlenk, syringe, and glovebox techniques.[17] Solvents were purified using a Glass Contour solvent purification system. The reagents 2,6-diphenylphenol, iodomethane, and 2-iodo-2-methylpropane (Bu^tI) were purchased from Aldrich and the iodo compounds were dried over anhydrous $MgSO_4$ followed by the use of activated molecular sieves immediately prior to use. Proton NMR spectra were run at 25 °C in benzene-d_6 on a Varian Gemini 2000 spectrometer at 300 MHz and were referenced to residual protio solvent. Carbon-13 NMR spectra were not obtained due to the low solubility of these compounds in benzene-d_6 and their instability in more polar solvents including chloroform-*d* and acetonitrile-d_3. Mass spectra were acquired via direct injection using a Shimadzu LCMS-2010 equipped with an ACPI ionization source. Elemental analyses were conducted by Desert Analytics (Tucson, AZ).

Synthesis of [Ge(OC$_6$H$_3$Ph$_2$-2,6)$_2$(Bu^t)(I)][11] ***(2)***

To a solution of **1** (0.100 g, 0.178 mmol) in benzene (10 mL) was added a solution of Bu^{t}I (0.040 g, 0.218 mmol) in benzene (5 mL). The reaction mixture was stirred at room temperature for 8 h and the volatiles were removed *in vacuo* to yield **2** (0.045 g, 34%) as colorless crystals. ^{1}H NMR: δ 7.43 (d, J = 8.1 Hz, 4H, *m*-C$_6$*H*$_3$Ph$_2$), 7.24-7.13 (m, 20H, *o*- and *p*-C$_6$H$_3$(C-$_6$*H*$_5$)$_2$), 6.89 (t, J = 8.1 Hz, 2H, *p*-C$_6$*H*$_3$Ph$_2$), 0.32 (s, 9H, -C(C*H*$_3$)$_3$) ppm. *Anal.* Calcd. for C$_{40}$H$_{35}$GeIO$_2$: C, 64.27; H, 4.72. Found: C, 64.11; H, 4.59.

*Synthesis of [Ge(OC$_6$H$_3$Ph$_2$-2,6)$_2$(Me)(I)] (**3**)*

To a solution of **2** (0.383 g, 0.680 mmol) in benzene (25 mL) was added neat MeI (0.105 g, 0.740 mmol). The reaction mixture was stirred at room temperature for 8 h and the volatiles were removed *in vacuo* to yield **3** (0.412 g, 86%) as a colorless powder. ^{1}H NMR: δ 7.48 (d, J = 7.5 Hz, 4H, *m*-C$_6$*H*$_3$Ph$_2$), 7.28-7.10 (m, 20H, -C$_6$H$_3$(C$_6$*H*$_5$)$_2$), 6.92 (t, J = 7.5 Hz, 2H, *p*-C$_6$*H*$_3$Ph$_2$), -0.49 (s, 3H, -C*H*$_3$) ppm. MS: *m/z* = 706 amu (M$^+$), 579 (M$^+$-I), 461 (M$^+$-OC$_6$H$_3$Ph$_2$) amu. *Anal.* Calcd. For C$_{37}$H$_{29}$GeIO$_2$: C, 63.00; H, 4.15. Found: C, 62.87; H, 4.27.

*Synthesis of [Ge(OC$_6$H$_3$Ph$_2$-2,6)$_3$(Me)] (**4**)*

To a solution of **3** (0.292 g, 0.414 mmol) in benzene (25 mL) was added a solution of 2,6-diphenylphenol (0.102 g, 0.414 mmol) in benzene (10 mL). The reaction mixture was stirred at room temperature for 12 h after which time a white precipitate had formed. The reaction mixture was filtered, washed with benzene (3 x 5 mL) and hexane (3 x 5 mL) and the solid was dried *in vacuo* to yield **4** (0.262 g, 77%) as a colorless powder. This compound was crystallized upon slow cooling of a hot benzene solution of **4**. ^{1}H NMR: δ 7.64 (d, J = 7.7 Hz, 6H, *m*-C$_6$*H*$_3$Ph$_2$),

7.40-7.28 (m, 24H, *o*- and *m*- $C_6H_3(C_6H_5)_2$), 7.07 (t, J = 7.7 Hz, 3H, *p*-$C_6H_3Ph_2$), 7.00 (t, J = 7.5 Hz, 6H, *p*-$C_6H_3(C_6H_5)_2$), -0.12 (s, 3H, -CH_3) ppm. *Anal.* Calcd. For $C_{61}H_{48}GeO_3$ (**4**·C_6H_6): C, 81.24; H, 5.37. Found: C, 81.52; H 5.31.

X-ray crystal structure analysis

Samples were mounted on a Cryoloop with Paratone-N oil under a stream of nitrogen gas at -173°C. Data was collected on APEX2 CCD system and then processed using the APEX2 software for preliminary determination of the unit cell. Diffraction intensity data were collected with a Siemens P4/CCD diffractometer. Crystallographic data and details are provided in **Table 3.4** above. Absorption corrections were applied for all data using SADABS. The structures were solved using direct methods, completed by difference Fourier syntheses, and refined on full-matrix least-squares procedures on F^2. All ordered non-hydrogen atoms were refined with anisotropic displacement coefficients and hydrogen atoms were treated as idealized contributions. All software and sources of scattering factors are contained in the SHEXTL (5.10) program package (G. Sheldrick, Bruker XRD, Madison, WI). The CCDC deposition numbers shown in **Table 3.4** contain the supplementary crystallographic data for this chapter. These data can be obtained free of charge from the Cambridge Crystallographic Data Centre via www.ccdc.ac.uk/data_request/cif.

3.5 References

1. Gehrhus, B.; Hitchcock, P. B.; Lappert, M. F., *Angew. Chem. Int. Edit.* **1997,** *36* (22), 2514-2516.

2. Dickie, D. A.; MacIntosh, I. S.; Ino, D. D.; He, Q.; Labeodan, J. A.; Jennings, M. C.; Schatte, G.; Walsby, C. J.; Clyburne, J. A. C., *Can. J. Chem.* **2008,** *86* (1), 20-31.

3. Glidewell, C.; Lloyd, D.; Lumbard, K. W., *J. Chem. Soc. Dalton* **1987,** (3), 501-508.

4. Hitchcock, P. B.; Jasim, H. A.; Lappert, M. F.; Leung, W. P.; Rai, A. K.; Taylor, R. E., *Polyhedron* **1991,** *10* (11), 1203-1213.

5. Cetinkaya, B.; Gumrukcu, I.; Lappert, M. F.; Atwood, J. L.; Rogers, R. D.; Zaworotko, M. J., *J. Am. Chem. Soc.* **1980,** *102* (6), 2088-2089.

6. Weinert, C. S.; Fenwick, A. E.; Fanwick, P. E.; Rothwell, I. P., *Dalton Trans.* **2003,** (4), 532-539.

7. Green, R. A.; Moore, C.; Rheingold, A. L.; Weinert, C. S., *Inorg. Chem.* **2009,** *48* (16), 7510-2.

8. Boyle, T. J.; Tribby, L. J.; Ottley, L. A. M.; Han, S. M., *Eur. J. Inorg. Chem.* **2009,** (36), 5550-5560.

9. Gerung, H.; Boyle, T. J.; Tribby, L. J.; Bunge, S. D.; Brinker, C. J.; Han, S. M., *J. Am. Chem.Soc.* **2006,** *128* (15), 5244-5250.

10. Stobart, S. R.; Churchill, M. R.; Hollander, F. J.; Youngs, W. J., *J. Chem. Soc. Chem. Comm.* **1979,** (20), 911-912.

11. Wetherby, A. E.; Samanamu, C. R.; Schrick, A. C.; DiPasquale, A.; Golen, J. A.; Rheingold, A. L.; Weinert, C. S., *Inorg. Chim. Acta* **2010,** *364* (1), 89-95.

12. Inoguchi, Y.; Okui, S.; Mochida, K.; Itai, A., *Bull. Chem. Soc. Jpn.* **1985,** *58* (3), 974-977.

13. Cheng, F.; Davis, M. F.; Hector, A. L.; Levason, W.; Reid, G.; Webster, M.; Zhang, W., *Eur. J. Inorg. Chem.* **2007,** (31), 4897-4905.

14. Avent, A. G.; Cloke, F. G. N.; Francis, M. D.; Hitchcock, P. B.; Nixon, J. F., *Chem. Commun.* **2000,** (10), 879-880.

15. Sekiguchi, A.; Ishida, Y.; Fukaya, N.; Ichinohe, M.; Takagi, N.; Nagase, S., *J. Am. Chem. Soc.* **2002,** *124* (7), 1158-1159.

16. Drager, M.; Simon, D., *Z Anorg. Allg. Chem.* **1981,** *472* (1), 120-128.

17. D. F. Shriver, M. A. Drezdzon., *The Manipulation of Air Sensitive Compounds*. John Wiley and Sons, New York: 1986.

CHAPTER IV

POLYFUNCTIONAL PHENOLS FOR THE SYNTHESIS AND CHARACTERIZATION OF A DIVALENT GERMANIUM COMPLEX OF CALIX[5]ARENE, A FULLY SILYLATED CALIX[6]ARENE, AND A BINAPHTHOXOGERMANIUM(II) COMPLEX

4.1 Introduction

Polyfunctional phenols have been utilized as ligands for germanium aryloxides in addition to the phenols described in Chapter 3 of this dissertation. Some of the polyfunctional phenols that have been used are calix[*n*]arenes and 3,3'-disubstituted-1,1'-bi-2,2'-naphthols.

Calix[*n*]arenes are an important class of macrocycles that can be considered to be polyfunctional phenols because they contain four or more phenol moieties that are bound together by methylene bridges at the carbon atoms located *ortho*- to the phenolic group. Variation of the number of phenols present in the macrocycle provides control over the cavity size, which has a profound effect on the properties and reactivity of the calixarene. Calix[*n*]arenes have applications in several areas including catalysis, molecular or ionic recognition, self-assembly, sensors, and enzyme mimics.[1-3]

An example of the basic structure of calix[*n*]arenes is provided below **Figure 4.1**. The calix[*n*]arenes are broken up into two main groups, the "major" calix[*n*]arenes (n = 4,6, or 8) and the "minor" calix[*n*]arenes (n = 5,7, or 9). Alkyl groups may also be present on the calixarene.

The most common group is the *tert*-butyl group; it enhances the structural rigidity of the calixarene when compared to the unsubstituted derivatives. Calix[*n*]arenes, like all molecules, exist in three dimensional space and the actual structure of these macrocycles is depicted by **Figure 4.2**[4] where the upper rim contains the *para*- alkyl substituents and the lower rim contains the phenolic moieties.

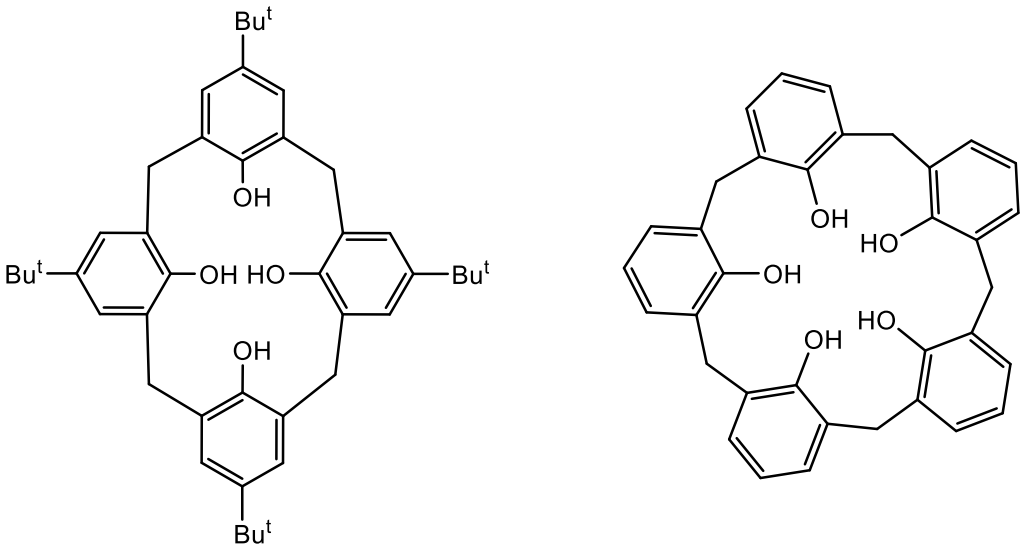

Figure 4.1: *p-tert*-butylcalix[4]arene (left) and calix[5]arene (right).

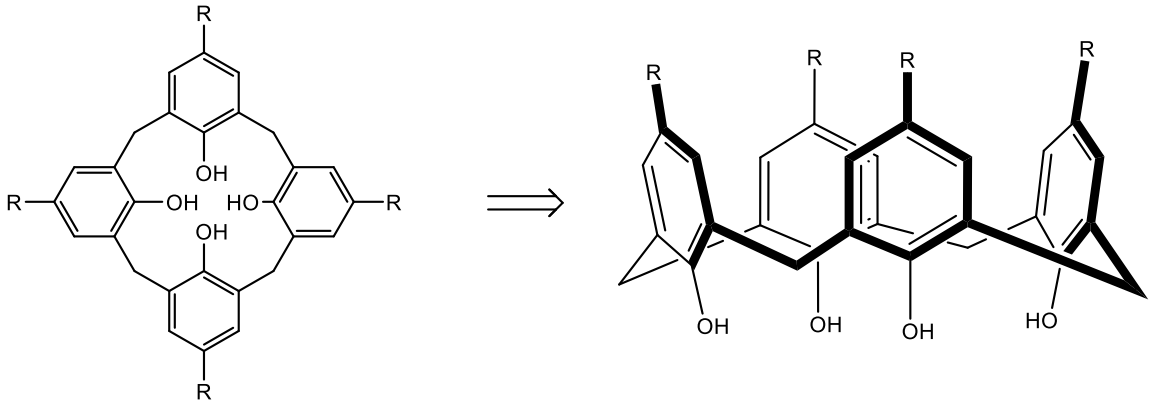

Figure 4.2: Conformational depiction of a *para*- substituted calix[4]arene.[4]

Calix[*n*]arenes have also been shown to serve as platforms for the support of single or multiple transition metals or some of the main group elements. An example of a transition metal complex of a calix[*n*]arene is W(*p-tert*-butylcalix[4]arene)Cl_2 (**Figure 4.3**).[5] Calix[*n*]arene complexes containing main group elements include bismuth[6] (**Figure 4.4**) silicon[7-10] (**Figure 4.5**), phosphorus,[7, 11-17] and some of the heavier group 15 elements[6, 18-20] are known (**Figure 4.6**).

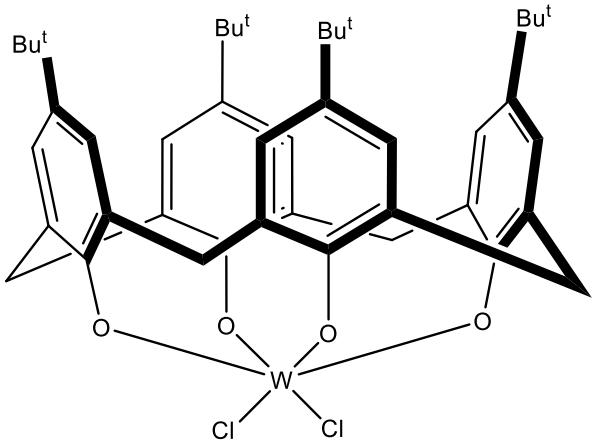

Figure 4.3: Structure of W(*p-tert*-butylcalix[4]arene)Cl_2.[5]

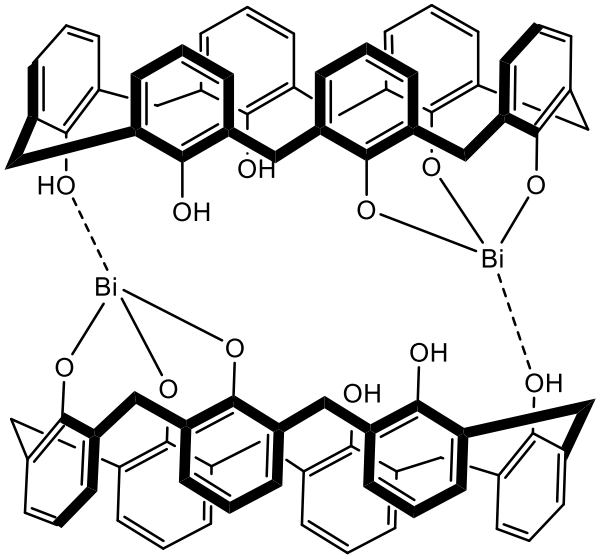

Figure 4.4: Structure of $[Bi\{calix[6]arene\}(OH)_3]_2$.[6]

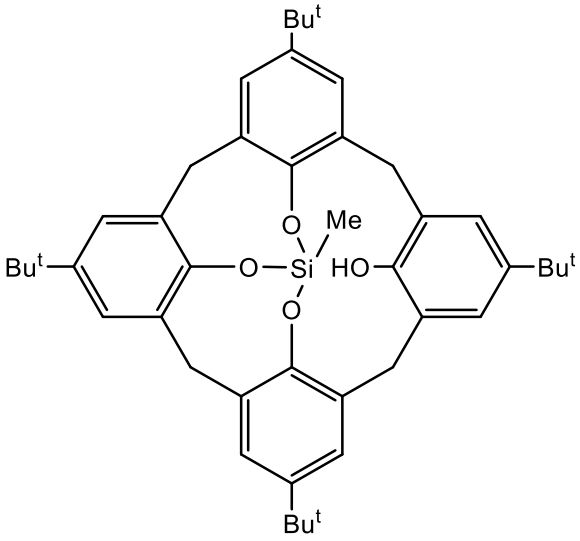

Figure 4.5: Structure of a silicon containing *p-tert*-butyl calix[4]arene.[9]

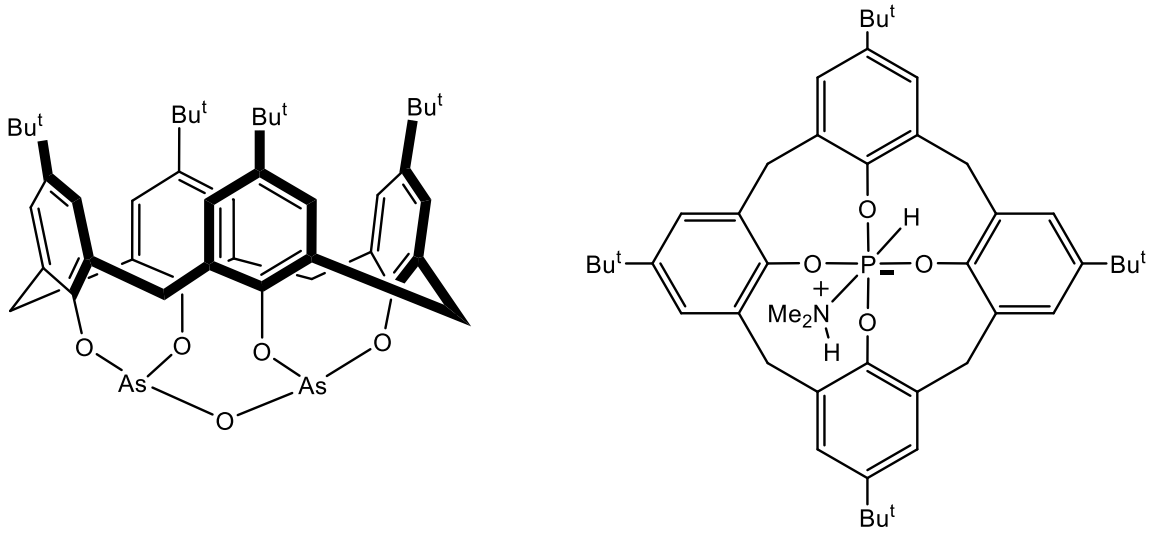

Figure 4.6: Structures of an arsenic[21] (left) and phosphorus[12] (right) containing Bu^{t}calix[4]arene.

Although calix[*n*]arene complexes of the group 14 elements have received considerably less attention when compared to other groups of the periodic table, several germanium-,[22-27] and tin-containing[22-24] species have been reported. However, all of the group 14 complexes involve the "major" calixarenes and no group 14 complexes of the "minor" calixarenes have been reported. Before our investigation with calix[5]arene, there had only been five divalent germanium calix[*n*]arene complexes reported.[23, 25-27] These consisted of {*p*-Bu$^t_4$-calix[4]arene}Ge_2 (**1**) (**Figure 4.7**),[23] {calix[4]arene}Ge_2 (**2**) (**Figure 4.7**),[25] {calix[8]arene}Ge_4 (**3**) (**Figure 4.8**),[25] {*p*-Bu$^t_8$-calix[8]arene}Ge_4 (**4**) (**Figure 4.8**),[27] as well as the unusual complex $[(C_6H_3)_6(CH_2)_6O_3Ge_2(NH_2)(OSiMe_3)\{OSi(H)(NH_2)_2\}_2]$ (**5**) (**Figure 4.9**).[26] All of these complexes were obtained via the protonolysis reaction between $Ge[N(SiMe_3)_2]_2$[28-30] and the corresponding calix[*n*]arene.

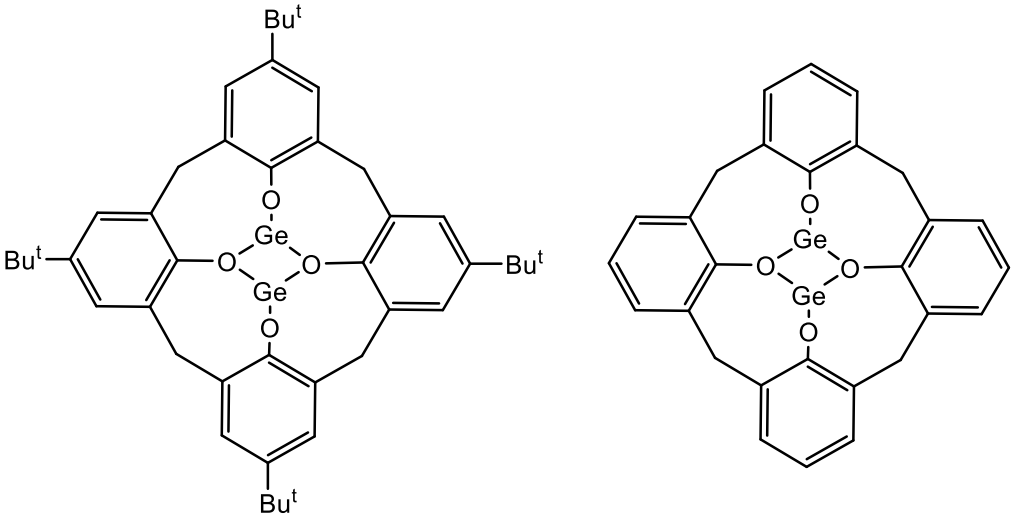

Figure 4.7: Structures of {*p*-Bu^t_4-calix[4]arene}Ge_2 (**1**)[23] (left) and {calix[4]arene}Ge_2 (**2**)[25] (right).

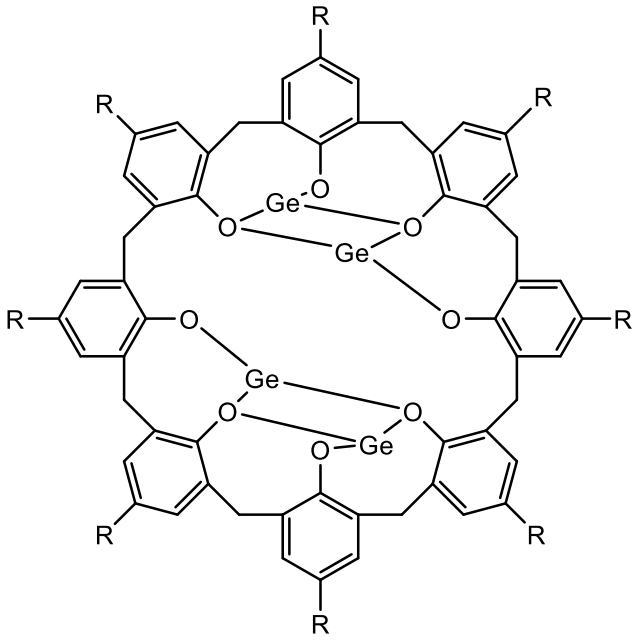

Figure 4.8: R = H {calix[8]arene}Ge_4 (**3**)[25] and R = Bu^t {*p*-Bu^t_8-calix[8]arene}Ge_4 (**4**).[27]

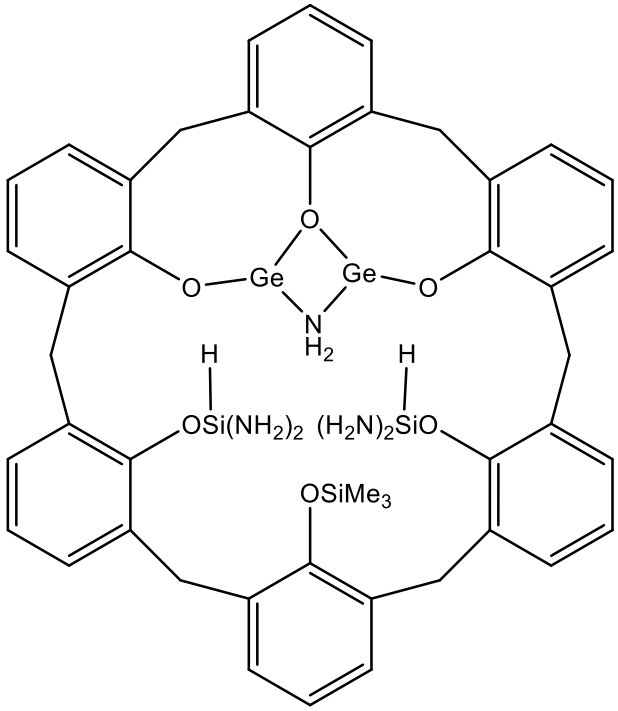

Figure 4.9: Structure of $[(C_6H_3)_6(CH_2)_6O_3Ge_2(NH_2)(OSiMe_3)\{OSi(H)(NH_2)_2\}_2]$ (**5**).[26]

The complex {calix[4]arene}Ge_2 (**2**) contains a Ge_2O_2 rhombus in the center of the calix[4] macrocycle where the Ge-$O_{rhombus}$ bond distances average 1.988(2) Å, while the Ge-O bond distance for the oxygen atom not contained in the rhombus is 1.845(1) Å. In comparison, the calix[6]arene complex **5** contains a Ge_2NO rhombus in the center of the macrocycle where the Ge-$O_{rhombus}$ bond distance is 1.992(3) Å and the Ge-O distance for the oxygen atom not within the rhombus is 1.860(3) Å. In both of these complexes the Ge-$O_{rhombus}$ bond distance is longer than the Ge-O bond distance for the oxygen not in the rhombus by at least 0.13 Å. This is likely due to the oxygen atoms within the rhombus being more strained in a four-membered ring preventing closer approach to the germanium atoms and the $O_{rhombus}$ atoms are interacting with two germanium atoms. One of the Ge-$O_{rhombus}$ interactions is covalent in nature while the other interaction is dative in nature with the electrons coming only from the oxygen atom. The Ge-N bond distance in **5** is 2.011 Å. The angles within the rhombus of **2** average 72.11(4)^o at the germanium atoms and 107.89(6)^o at the oxygen atoms while the angles within the rhombus of **5**

average 77.3(1)° at the germanium atoms and are 103.0(1)° and 102.3(2)° at the oxygen and nitrogen atoms, respectively.[25]

The structures of {*p*-Bu^t_4-calix[4]arene}Ge_2 (**1**) and {calix[4]arene}Ge_2 (**2**) contain a single Ge_2O_2 rhombus in the center of the macrocyclic cavity while {calix[8]arene}Ge_4 (**3**) and {*p*-Bu^t_8-calix[8]arene}Ge_4 (**4**) each contain two Ge_2O_2 rhombi contained within the cavity of the calix[8]arene. The calix[6]arene complex **5** contains a Ge_2NO rhombus in the center of the macrocyclic cavity rather than a Ge_2O_2 moiety, resulting from the desilylation of the $–N(SiMe_3)_2$ groups present during the course of the reaction.

The 3,3'-disubstituted-1,1'-bi-2,2'-naphthols are polyfunctional phenols that have also been used as ligands in germanium aryloxide complexes via the protonolysis reaction with $Ge[N(SiMe_3)_2]_2$.[31-32] Those that have been synthesized and structurally characterized include (*R*,*R*)-[Ge{$OC_{20}H_{10}(OSiMe_3)$-2'-$(SiMe_3)_2$-3,3'}$_2$] (**6**) (**Scheme 4.1**),[31] (*R*)-Ge{$O_2C_{20}H_{10}(SiMe_2Ph)_2$-3,3'}{$NH_3$} (**7**) (**Scheme 4.2**),[31] and (*S*)-Ge{$O_2C_{20}H_{10}(SiMe_2Ph)_2$-3,3'}{$NH_3$} (**8**) (**Scheme 4.2**).[32] The X-ray crystal structures of these compounds are also given below in **Figure 4.10** (**6**), and **Figure 4.11** (**8**) with their corresponding bond distances and angles in **Tables 4.1** and **4.2** for **6** and **8** respectively. The structure of **7** differs from **8** only by the handedness of the binaphthol ring.

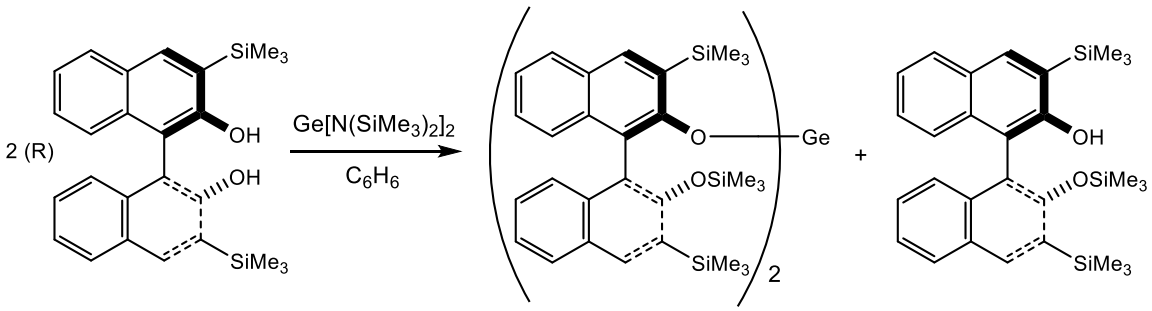

Scheme 4.1: Synthesis of (*R*,*R*)-[Ge{$OC_{20}H_{10}(OSiMe_3)$-2'-$(SiMe_3)_2$-3,3'}$_2$] (**6**).[31]

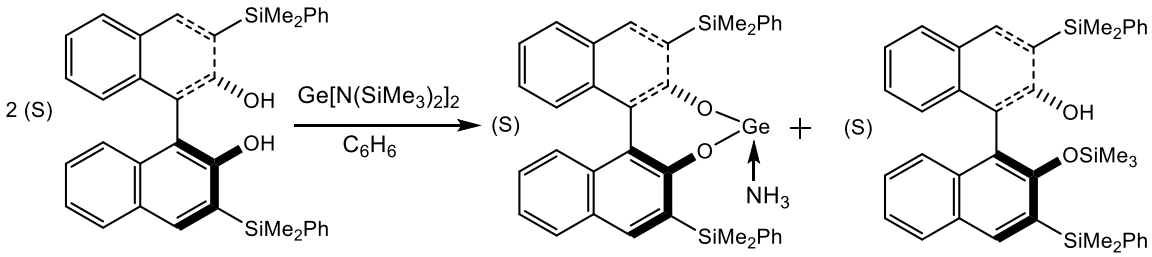

Scheme 4.2: Synthesis of (*S*)-Ge{$O_2C_{20}H_{10}(SiMe_2Ph)_2$-3,3'}{$NH_3$} (**8**). The synthesis of (*R*)-Ge{$O_2C_{20}H_{10}(SiMe_2Ph)_2$-3,3'}{$NH_3$} (**7**) is achieved with two equivalents of the starting binaphthol in the "R" form.[31-32]

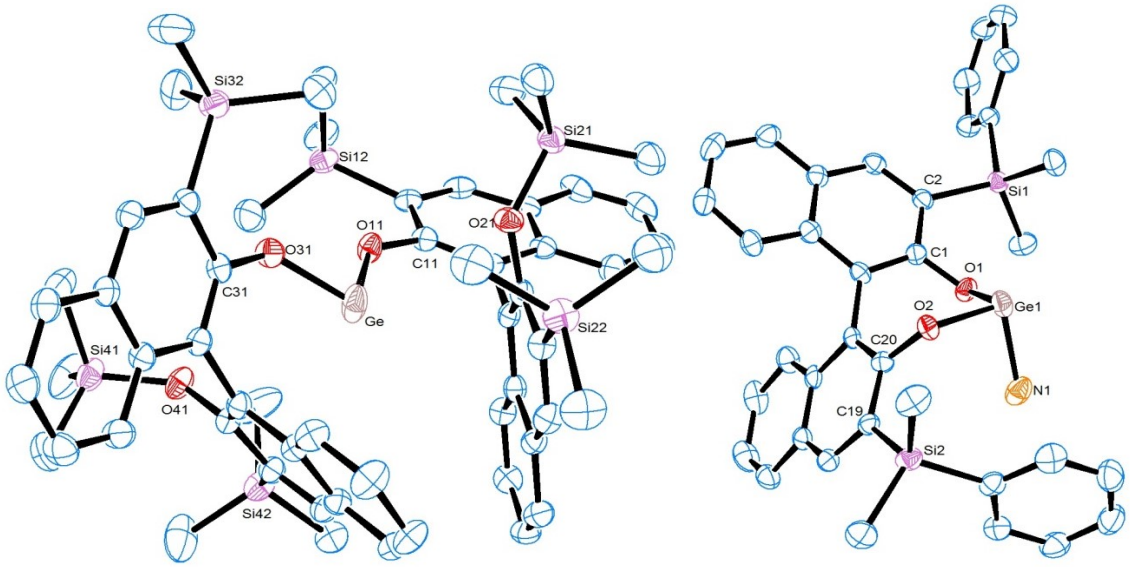

Figure 4.10: X-ray crystal structures of (*R*,*R*)-[Ge{$OC_{20}H_{10}(OSiMe_3)$-2'-$(SiMe_3)_2$-3,3'}$_2$] (**6**)[31] (left) and (S)-Ge{$O_2C_{20}H_{10}(SiMe_2Ph)_2$-3,3'}{$NH_3$} (**8**)[32] (right).

Table 4.1: Selected bond distances (Å) and angles (deg) for (*R*,*R*)-[Ge{$OC_{20}H_{10}(OSiMe_3)$-2'-$(SiMe_3)_2$-3,3'}$_2$] (**6**).[31]

Bond Lengths	Å	Bond Angles	deg
Ge - O(11)	1.809(2)	O(11) - Ge - O(31)	89.40(8)
Ge - O(31)	1.820(2)	Ge - O(11) - C(11)	133.9(1)
O(11) - C(11)	1.363(3)	Ge - O(31) - C(31)	124.0(1)
O(31) - C(31)	1.378(2)		
Si(21) - O(21)	1.674(2)		
Si(41) - O(41)	1.676(2)		

Table 4.2: Selected bond distances (Å) and angles (deg) for (S)-Ge{$O_2C_{20}H_{10}(SiMe_2Ph)_2$-3,3'}{$NH_3$} (**8**).[32]

Bond Length	Å	Bond Angle	deg
Ge(1) - O(1)	1.886(2)	O(1) - Ge(1) - O(2)	97.9(1)
Ge(1) - O(2)	1.863(3)	O(1) - Ge(1) - N(1)	81.6(1)
Ge(1) - N(1)	2.107(4)	O(2) - Ge(1) - N(1)	90.2(1)
O(1) - C(1)	1.363(5)		
O(2) - C(20)	1.364(5)		
C(10) - C(11)	1.501(6)		

The germanium(II) calix[5]arene complex {calix[5]arene}$_2Ge_2(OSiMe_3)_4(OH)_2$, the calix[6]arene complex [$(C_6H_3)_6(CH_2)_6(OSiMe_2Ph)_6$], and the binaphthoxogermanium(II) complex (*S*,*S*)-[Ge{$OC_{20}H_{10}(OSiMe_2Ph)$-2'-$(SiMe_3)_2$-3,3'}$_2$] were prepared in order to determine the effects of having an odd number of phenolic groups in the calixarene, and the effects of a more bulky amido group on the germanium precursor on the reactivity of these systems. It was found that changing these factors has a significant impact on the nature of the products obtained. All three of these complexes have been structurally characterized.

4.2 Results and Discussion

The reaction of $Ge[N(SiMe_3)_2]_2$ with one equivalent of *para*-unsubstituted calix[5]arene did not yield a structure similar to that seen for compounds **1-5**, but rather $\{calix[5]arene\}_2Ge_2(OSiMe_3)_4(OH)_2$ (**9**) was formed in 69% yield (**Scheme 4.3**).

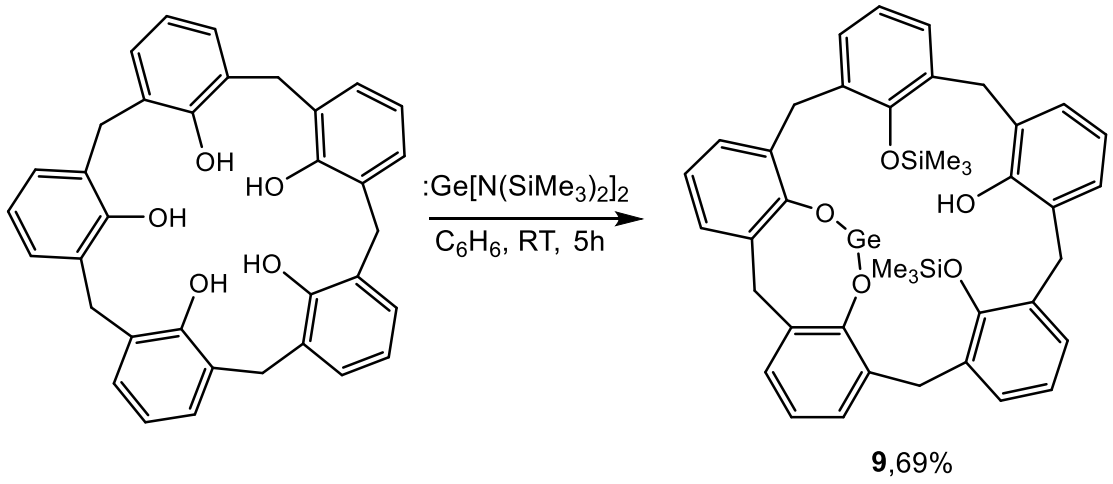

9,69%

Scheme 4.3: Synthesis of $\{calix[5]arene\}_2Ge_2(OSiMe_3)_4(OH)_2$ (**9**).

The X-ray structure of **9** was obtained and an ORTEP diagram is shown below along with the asymmetric unit in **Figure 4.11**, with selected bond distances and angles provided in **Table 4.3**. This structure is unique among the other germanium calixarene complexes, for comparison the structures of $\{calix[4]arene\}Ge_2$ (**2**) and $[(C_6H_3)_6(CH_2)_6O_3Ge_2(NH_2)(OSiMe_3)\{OSi(H)(NH_2)_2\}_2]$ (**5**) are provided below in **Figure 4.12** with their corresponding selected bond distances and angles in **Tables 4.4** and **4.5**.

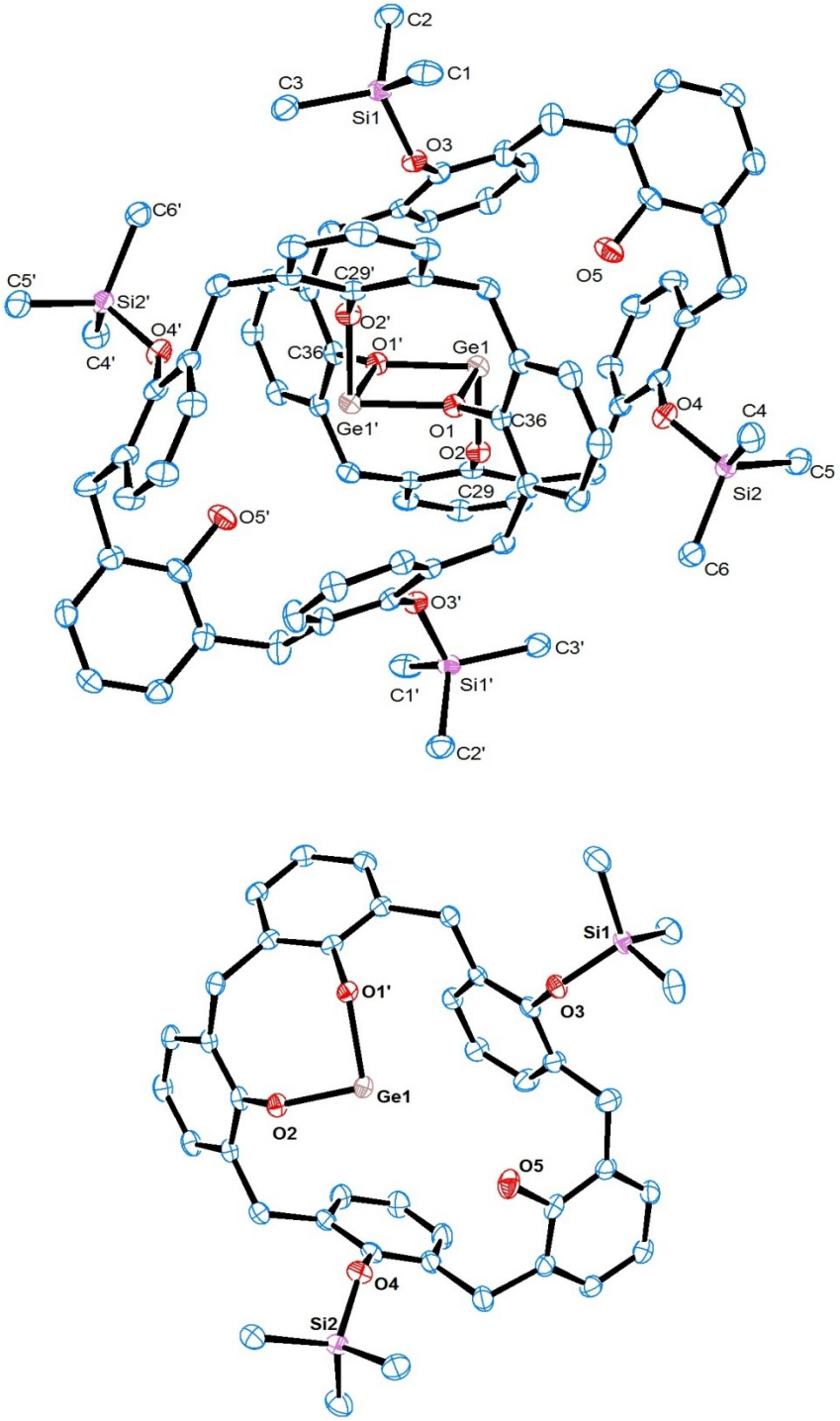

Figure 4.11: X-ray crystal structure of {calix[5]arene}$_2$Ge$_2$(OSiMe$_3$)$_4$(OH)$_2$ (**9**) including the asymmetric unit (below).

Table 4.3: Selected bond distances and angles for {calix[5]arene}$_2$Ge$_2$(OSiMe$_3$)$_4$(OH)$_2$ (**9**).

Bond Lengths	(Å)	Bond Angles	(°)
Ge(1) - O(1)	2.021(1)	Ge(1) - O(1) - Ge(1')	106.39(6)
Ge(1) – O(1')	1.980(1)	O(1) - Ge(1) - O(2)	93.17(5)
Ge(1) - O(2)	1.828(1)	O(1) - Ge(1) - O(1')	73.61(5)
O(1) - C(36)	1.391(2)	Ge(1) - O(1) - C(36)	126.8(1)
O(2) - C(29)	1.362(3)	Ge(1) - O(2) - C(29)	127.8(1)
Si(1) - O(3)	1.658(2)		
Si(2) - O(4)	1.659(1)		

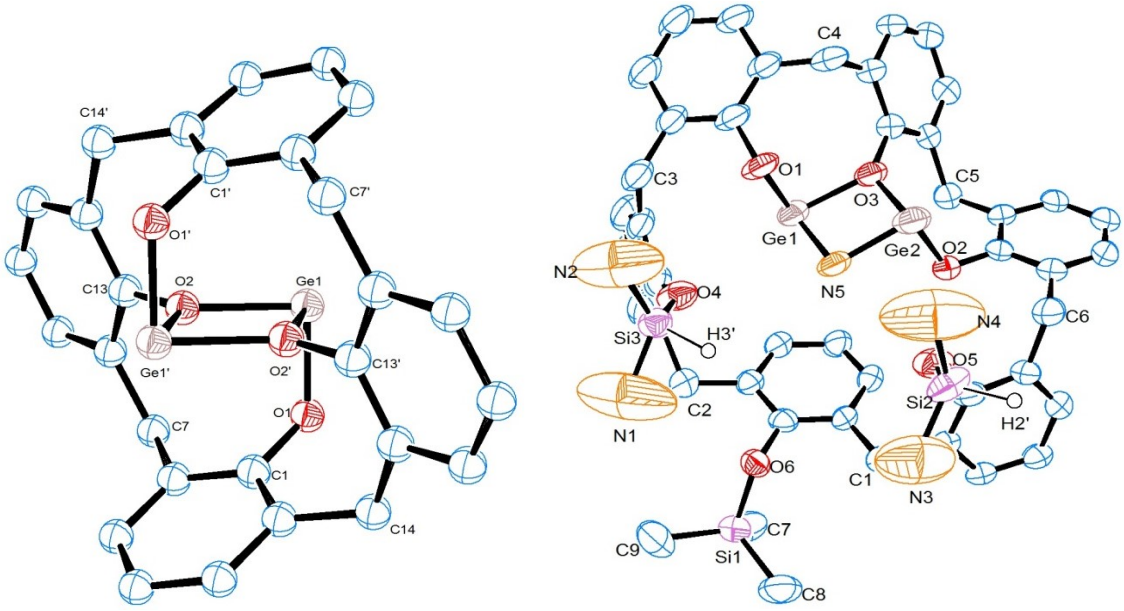

Figure 4.12: X-ray structure of {calix[4]arene}Ge$_2$ (**2**)[25] (left) and [(C$_6$H$_3$)$_6$(CH$_2$)$_6$O$_3$Ge$_2$(NH$_2$)(OSiMe$_3$){OSi(H)(NH$_2$)$_2$}$_2$] (**5**)[26] (right).

Table 4.4: Selected bond distances and angles for {calix[4]arene}Ge_2 (**2**)[25]

Bond Lengths	(Å)	Bond Angles	(°)
Ge(1) - O(1)	1.845(1)	Ge(1) - O(2) - Ge(1')	107.89(6)
Ge(1) - O(2)	1.989(1)	O(1) - Ge(1) - O(2)	91.72(6)
Ge(1) - O(2')	1.987(3)	O(2) - Ge(1) - O(2')	72.11(4)
C(1) - O(1)	1.373(3)	Ge(1) - O(1) - C(1)	117.9(1)
C(13) - O(2)	1.385(2)	Ge(1) - O(2) - C(13)	126.5(1)

Table 4.5: Selected bond distances and angles for

$[(C_6H_3)_6(CH_2)_6O_3Ge_2(NH_2)(OSiMe_3)\{OSi(H)(NH_2)_2\}_2]$ (**5**)[26]

Bond Lengths	(Å)	Bond Angles	(°)
Ge(1)–O(1)	1.860(3)	O(1)–Ge(1)–O(3)	91.4(1)
Ge(1)–O(3)	1.992(3)	O(1)–Ge(1)–N(5)	89.7(1)
Ge(1)–N(5)	2.011(4)	O(2)–Ge(2)–O(3)	91.6(1)
Ge(2)–O(2)	1.835(3)	O(2)–Ge(2)–N(5)	91.4(1)
Ge(2)–O(3)	1.993(3)	O(3)–Ge(1)–N(5)	77.1(1)
Ge(2)–N(5)	1.995(4)	O(3)–Ge(2)–N(5)	77.4(1)
Si(1)–O(6)	1.664(3)	Ge(1)–O(3)–Ge(2)	103.0(1)
Si(2)–O(5)	1.696(5)	Ge(1)–N(5)–Ge(2)	102.3(2)
Si(2)–N(3)	1.816(8)	O(5)–Si(2)–N(3)	111.6(3)
Si(2)–N(4)	1.715(8)	O(5)–Si(2)–N(4)	108.2(3)
Si(3)–O(4)	1.712(4)	N(3)–Si(2)–N(4)	122.8(5)
Si(3)–N(1)	1.700(8)	O(4)–Si(3)–N(1)	112.4(4)
Si(3)–N(2)	1.806(9)	O(4)–Si(3)–N(2)	108.8(4)
		N(1)–Si(3)–N(2)	119.6(4)

The calix[5] complex {calix[5]arene}$_2Ge_2(OSiMe_3)_4(OH)_2$ (**9**) co-crystallizes with two toluene molecules in the unit cell per germanium atom. The structure of **9** is dimeric and containes two calix[5]arene moieties held together by a planar Ge_2O_2 rhombus. The Ge-$O_{terminal}$ bond distances in **9** are similar to those in the major calix[*n*]arene complexes **1-4** which range from 1.831-1.844 Å[23, 25, 27] and measures 1.828(1) Å, while the Ge-$O_{bridging}$ bond distances in **9** average 2.001 Å and are similar to those in **1-4** which range from 1.970-2.036 Å.[23, 25, 27] However, the Ge_2O_2

rhombus in **9** is unsymmetric, in that the Ge(1)-$O(1)_{bridging}$ bond distance of 2.021 Å is longer that the other Ge(1)-$O(1')_{br}$ distance by 0.041(1) Å. The analogous rhombi in **1-4** each have one Ge-O_{br} distance that is longer than the other, but the largest difference is only 0.030(3) Å, which was found in the structure of {calix[8]arene}Ge_4 (**3**).[25] The structure of {calix[5]arene}$_2Ge_2(OSiMe_3)_4(OH)_2$ (**9**) can be compared to that of the bismuth(III) calix[5]arene complex {Bu^t_5calix[5]areneH_2}Bi (**10**) that also adopts a centrosymmetric dimeric structure in the solid state and contains a planar Bi_2O_2 rhombus.[19] The Bi-$O_{bridging}$ bond distances in **10** measure 2.142(5) and 2.733(5) Å, where the longer Bi-$O_{bridging}$ distance is between bismuth and the oxygen atom within the same calix[5]arene macrocycle. This was observed in **9** as well, where the longer of the two Ge-$O_{bridging}$ distances is between germanium and an oxygen atom in the same macrocycle.

Of the ten oxygen atoms present among each of the two calix[5]arene macrocycles in the dimeric structure of **9**, four are involved in bonding in the Ge_2O_2 rhombus, and two of them remain protonated as hydroxyl groups. The remaining four oxygen atoms in the macrocycles have been incorporated into –$OSiMe_3$ groups, and these groups are located immediately adjacent to the two oxygen atoms incorporated in the Ge_2O_2 rhombus (O(3), O(3'),O(4), and O(4')), while the remaining –OH groups (O(5) and O(5')) are located on opposite sides of each of the macrocycles. The two trimethylsiloxy groups containing O(3) and O(4) are directed toward the divalent germanium center, but the Ge-O contacts are very long (4.50 and 3.85Å, respectively). The long Ge-O bond distances indicates there is likely no interaction between Ge(1) and O(3) or O(4).

The conversion taking place in these reactions is the conversion of –OH to –$OSiR_3$ groups during the reaction of $Ge[N(SiR_3)_2]_2$ with aryloxide substrates. This interconversion involves the shift of a –SiR_3 group from nitrogen to oxygen (**Scheme 4.4**). The success of the silyl group transfer depends on the proximity of the O-M-$N(SiR_3)_2$ moiety to the –OH group which is to be converted to the silyl ether.

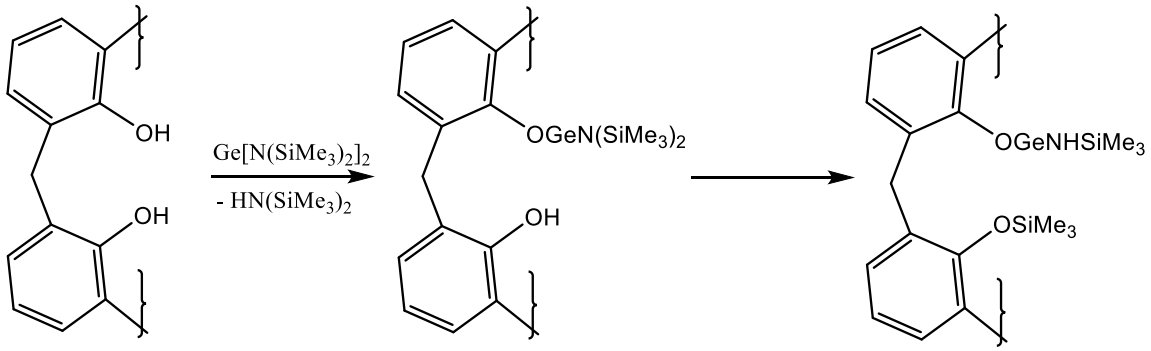

Scheme 4.4: Silyl group transfer in reactions of germanium aryloxides with $Ge[N(SiMe_3)_2]_2$.

The ^{1}H NMR spectrum of $\{calix[5]arene\}_2Ge_2(OSiMe_3)_4(OH)_2$ (**9**) (**Figure 4.13**) in benzene-d_6 indicates that the structural rigidity of this molecule is maintained in solution. There are eight distinct AB spin patterns and two unresolved doublets observed in the range of δ 5.21-3.09 ppm for the methylene protons in **9**, which indicates that the protons of the –CH_2- fragments are diastereotopic, since one of these protons is directed inward toward the cavity of the calix[5]arene macrocycle and one is directed away. The 10 doublets with their corresponding coupling constants are as follows: 5.21 (J = 16.2 Hz), 4.90 (J = 14.7 Hz), 4.79 (J = 15.0Hz), 4.64 (J = 12.3 Hz), 4.21 (J = 13.5 Hz), 3.95 (J = 16.2 Hz), 3.89 (J = 15.0 Hz), 3.71 (J = 14.7 Hz), 3.33 (J = 13.5 Hz), 3.09 (J = 12.3 Hz). The observed coupling constants are consistent with the coupling constants reported for other calix[n]arene complexes.[7, 19, 33] The proton of each pair that is directed toward the cavity is shifted downfield and the proton of each pair that is pointed away from the cavity is shifted upfield where the shielding or deshielding is due to anisotropic effects. Similar structural and spectral features were observed for the major calix[n]arene complexes **1**-**5**.[23, 25, 27, 26] Resonances for the aromatic protons of **9** were observed between δ 7.63-6.07 ppm with a significant amount of overlap of several of the resonances, and two signals corresponding to the –$OSiMe_3$ groups were observed at δ 0.29 and 0.01 ppm. The ^{13}C NMR spectrum of **9**

contains five resonances for the methylene carbon atoms in the range of δ 35.1-32.4 ppm, as well as two signals at δ 1.3 and 0.3 ppm corresponding to the carbon atoms of the –$OSiMe_3$ groups.

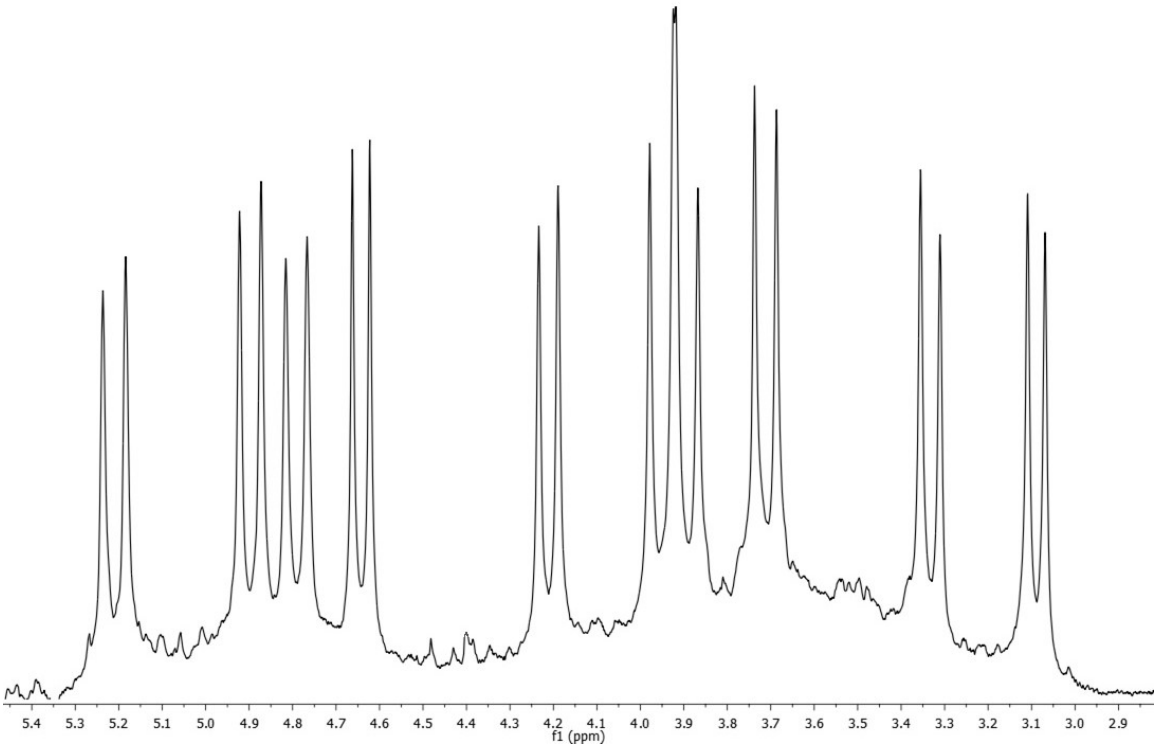

Figure 4.13: ^{1}H NMR spectrum of $\{calix[5]arene\}_2Ge_2(OSiMe_3)_4(OH)_2$ (**9**) showing range δ 5.21 – 3.09 ppm.

The reaction of *para*-unsubstituted calix[6]arene with 3 equivalents of the new germylene $Ge[N(SiMe_2Ph)_2]_2$ did not yield a product similar to the identical reaction using $Ge[N(SiMe_3)_2]_2$ ($[(C_6H_3)_6(CH_2)_6O_3Ge_2(NH_2)(OSiMe_3)\{OSi(H)(NH_2)_2\}_2]$ (**5**)), but instead yielded the completely silylated calix[6]arene complex $[(C_6H_3)_6(CH_2)_6(OSiMe_2Ph)_6]$ (**11**) (**Scheme 4.5**). The crystal structure of complex **11** was obtained and is shown as an ORTEP diagram below in **Figure 4.14** with selected bond distances and angles provided in **Table 4.6**.

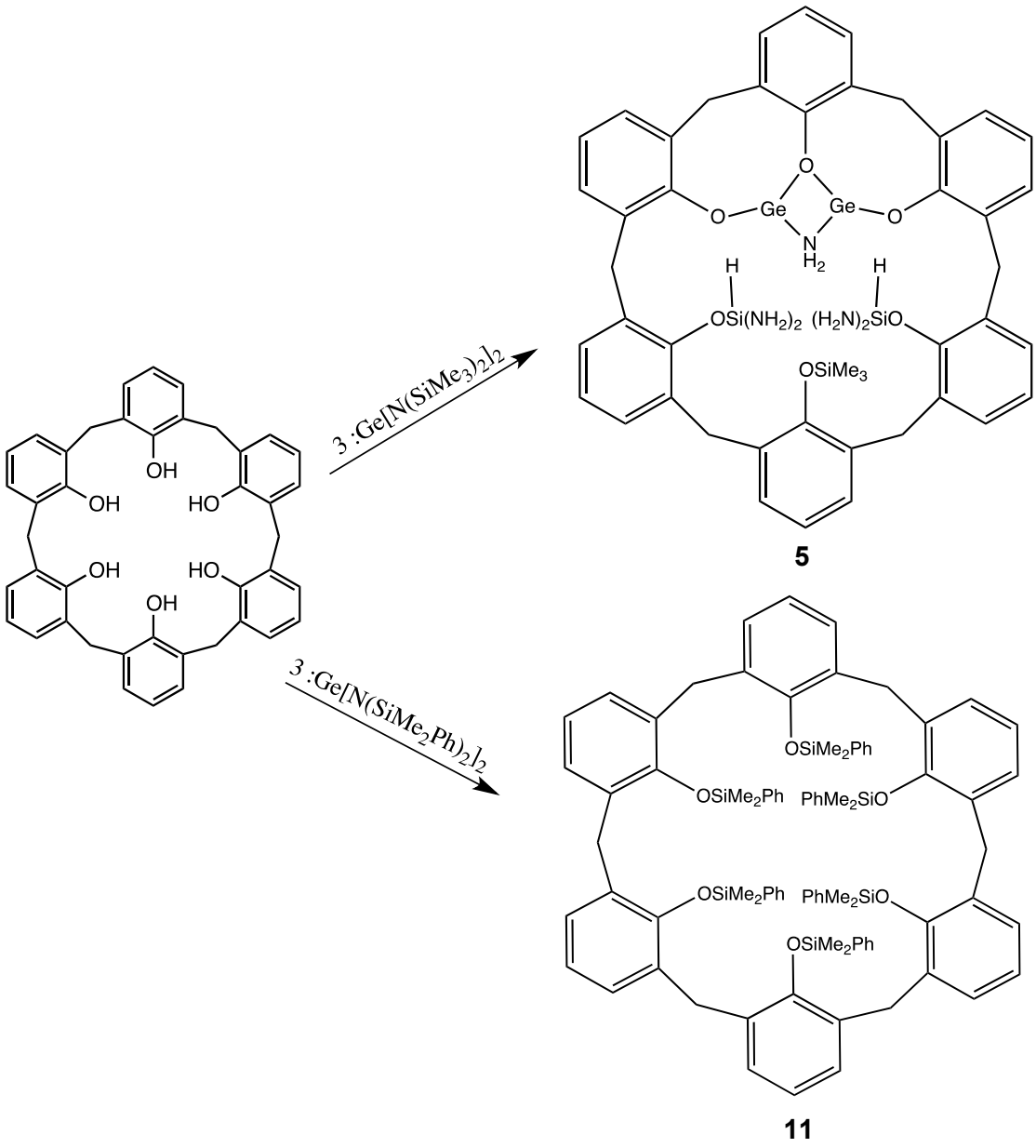

Scheme 4.5: The reaction of calix[6]arene with three equivalents of $Ge[N(SiMe_3)_2]_2$ (top)[26] or with three equivalents of $Ge[N(SiMe_2Ph)_2]_2$ (bottom).

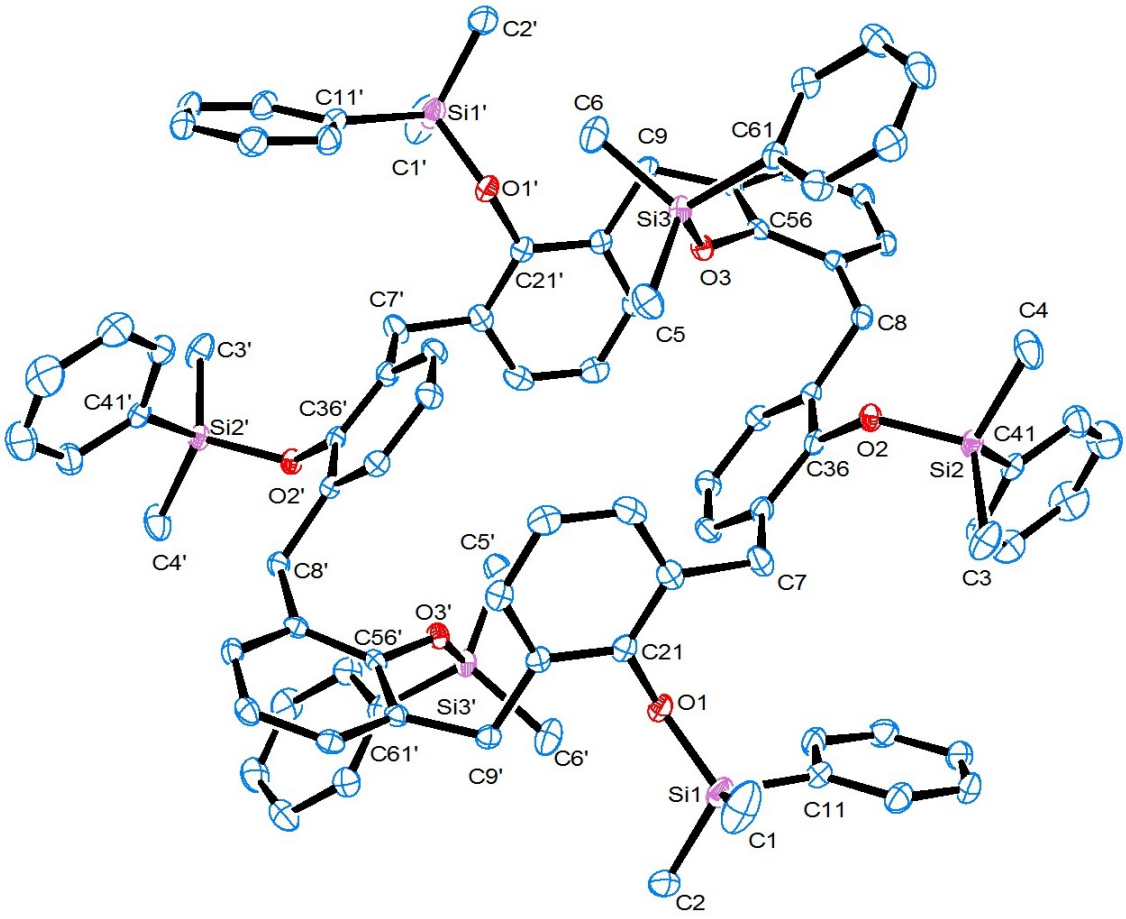

Figure 4.14: X-ray crystal structure of $[(C_6H_3)_6(CH_2)_6(OSiMe_2Ph)_6]$ (**11**).

Table 4.6: Selected bond distances (Å) and angles (°) for **11**.

Bond Lengths	(Å)	Bond Angles	(°)
Si(1) - O(1)	1.657(1)	Si(1) - O(1) - C(21)	131.3(1)
Si(2) - O(2)	1.657(1)	Si(2) - O(2) - C(36)	126.92(9)
Si(3) - O(3)	1.652(1)	Si(3) - O(3) - C(56)	134.1(1)
O(1) - C(21)	1.377(2)	O(1) - Si(1) - C(1)	110.61(8)
O(2) - C(36)	1.392(2)	O(1) - Si(1) - C(2)	106.71(7)
O(3) - C(56)	1.370(2)	O(1) - Si(1) - C(11)	106.07(7)
		C(1) - Si(1) - C(2)	113.08(9)
		C(1) - Si(1) - C(11)	111.13(9)
		C(2) - Si(1) - C(11)	108.91(8)

This reaction demonstrates that the chemistry of germanium bisamides can differ significantly simply by changing the identity of one of the alkyl groups contained in the silyl groups of germylenes with the structure $Ge[N(SiR_3)_2]_2$. As shown above, the reaction of calix[6]arene with three equivalents of $Ge[N(SiMe_3)_2]_2$ yields a significantly different product than the reaction of calix[6]arene with three equivalents of $Ge[N(SiMe_2Ph)_2]_2$. This suggests that $Ge[N(SiMe_2Ph)_2]_2$ is a stronger silylating reagent than $Ge[N(SiMe_3)_2]_2$. The average bond enthalpy of a Si-O bond (466 kJ/mol)[34] is higher than that of a Ge-O bond (350 kJ/mol)[34] and thus it is more favorable for a silicon-oxygen bond to be formed versus a germanium-oxygen bond. The sterics of the dimethylphenyl silyl group are increased in comparison to the trimethylsilyl group which typically makes it more difficult to silylate a hydroxyl group however this also makes the resulting silyl ether more robust with respect to hydrolysis back to the hydroxyl group.

All six of the hydroxyl groups of the calix[6]arene have been converted to $–OSiMe_2Ph$ groups. There is an inversion center in the center of the crystal structure which yields three crystallographically unique $–OSiMe_2Ph$ groups. The O-Si bond distances average 1.655(1) Å and the O-C bond lengths average 1.380(2) Å and the bond angles present are typical for the atoms present. The ^{1}H NMR spectrum of $[(C_6H_3)_6(CH_2)_6(OSiMe_2Ph)_6]$ (**11**) in benzene-d_6 indicates that the structural rigidity of this molecule is maintained in solution. The ^{1}H NMR of **11** contains a significant amount of overlapping peaks in the methylene proton range which appears in the range of δ 4.74-2.85 ppm. All of the methylene hydrogens are non-equivalent and diastereotopic however, there are two distinct doublets that appear at δ 4.27 (J = 15.9 Hz) and 4.11 (J = 13.2 Hz) ppm. Resonances for the aromatic protons of **11** were observed between δ 7.84-6.70 ppm with a significant amount of overlap of several of the resonances, and one signal corresponding to the methyl groups of the silyl ether groups $–OSiMe_2Ph$ was observed at δ 0.25 ppm.

The reaction of two equivalents of the 3,3'-disubstituted-1,1'-bi-2,2'-naphthol (*S*)-$[C_{20}H_{10}(OH)_2$-2,2'-$(SiMe_3)_2$-3,3'] with the germanium bisamide $Ge[N(SiMe_2Ph)_2]_2$ yielded the

binaphthoxogermanium(II) complex (*S*, *S*)-[Ge{$OC_{20}H_{10}(OSiMe_2Ph)$-2'-$(SiMe_3)_2$-3,3'}$_2$] (**12**) (**Scheme 4.6**) which has been structurally characterized. The X-ray crystal structure is provided below as an ORTEP diagram in **Figure 4.15** with selected bond distances and angles given in **Table 4.7**.

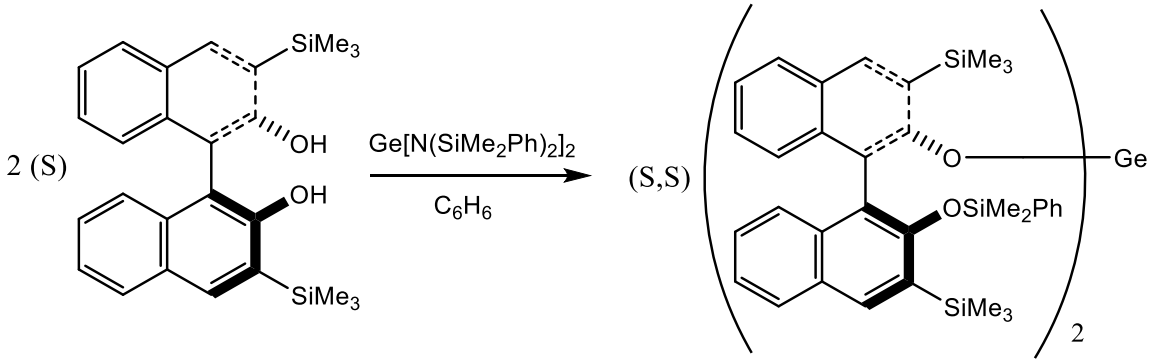

Scheme 4.6: Synthesis of (*S*, *S*)-[Ge{$OC_{20}H_{10}(OSiMe_2Ph)$-2'-$(SiMe_3)_2$-3,3'}$_2$] (**12**).

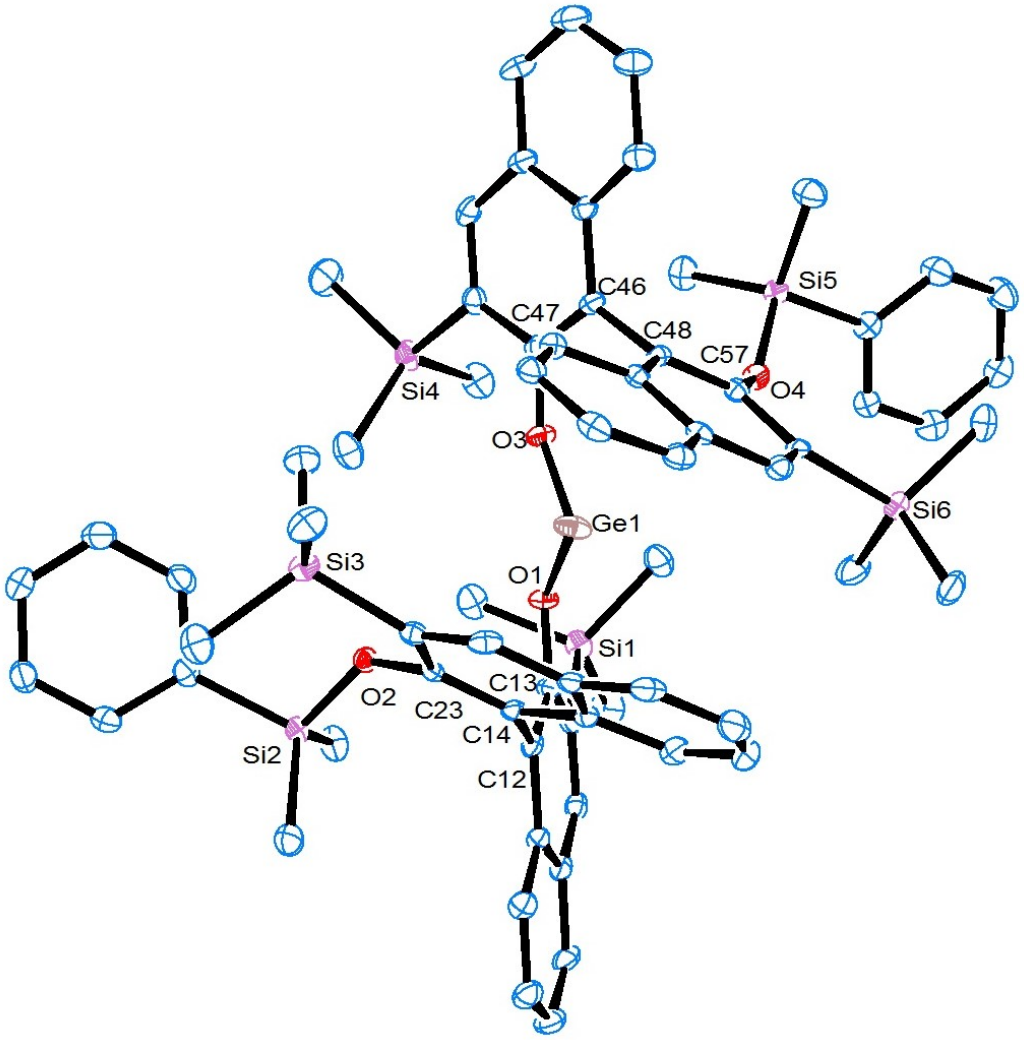

Figure 4.15: X-ray crystal structure of (*S*, *S*)-[Ge{$OC_{20}H_{10}(OSiMe_2Ph)$-2'-$(SiMe_3)_2$-3,3'}$_2$] (**12**).

Table 4.7: Selected bond distances (Å), angles, and torsion angles* (°) for **12**.

Bond Lengths	(Å)	Bond Angles	(°)
Ge(1) - O(1)	1.815(2)	O(1) - Ge(1) - O(3)	87.77(8)
Ge(1) - O(3)	1.816(2)	C(23) - O(2) - Si(2)	133.9(2)
O(1) - C(13)	1.367(3)	C(57) - O(4) - Si(5)	136.5(2)
O(3) - C(47)	1.378(3)	C(13) - C(12) - C(14) - C(23)*	75.2(3)
O(2) - C(23)	1.377(3)	C(47) - C(46) - C(48) - C(57)*	75.6(3)
O(4) - C(57)	1.372(3)		
O(2) - Si(2)	1.672(2)		
O(4) - Si(5)	1.666(2)		

The structure of (*S*, *S*)-[Ge{$OC_{20}H_{10}(OSiMe_2Ph)$-2'-$(SiMe_3)_2$-3,3'}$_2$] (**12**) is nearly identical to the structure of (*R*,*R*)-[Ge{$OC_{20}H_{10}(OSiMe_3)$-2'-$(SiMe_3)_2$-3,3'}$_2$] (**6**).[31] The incorporation of the $–OSiMe_2Ph$ groups instead of $–OSiMe_3$ groups at the 3,3' positions is the only main difference. The O(1)-Ge(1)-O(3) bond angle of **12** measures 87.77(8)^o and is slightly more acute than the corresponding O-Ge-O angle of **6**. This is likely due to the incorporation of the larger $–OSiMe_2Ph$ groups. All of the Ge-O and O-C bond distances in **12** are as expected when compared to **6**. The average Si-O bond distance in **12** is 1.669(2) Å which is slightly smaller than the average Si-O bond distance of **6** which is 1.675(2) Å. When compound **6** was first synthesized, there was some doubt that the $–OSiMe_3$ groups may not have come from the germylene, $Ge[N(SiMe_3)_2]_2$, but were perhaps attached during the synthesis of the binaphthol (R)-$[C_{20}H_{10}(OH)_2$-2,2'-$(SiMe_3)_2$-3,3']. This reaction (**Scheme 4.6**) clearly shows that the silyl ether groups ($-OSiMe_2Ph$) present in **12** must come directly from silyl group transfer of the germylene, $Ge[N(SiMe_2Ph)_2]_2$. Since the reactions were performed in an identical fashion, we can now say that the silyl ether groups ($-OSiMe_3$) in **6** must also come directly via silyl group transfer from the corresponding germylene $Ge[N(SiMe_3)_2]_2$.

The ^{1}H NMR of **12** (**Figure 4.16**) contains a singlet at δ 8.16 ppm corresponding to the 4, 4' hydrogens, and there are two doublets that appear at δ 7.69 (J = 8.1 Hz) and 7.46 (J = 8.1 Hz) ppm which correspond to the 6, 6' and 9, 9' hydrogens respectively. There is a singlet at δ 0.80 ppm which corresponds to one of the trimethylsilyl groups, and another singlet at δ 0.19 ppm which corresponds to the other trimethylsilyl group. The methyl groups of the $–OSi(CH_3)_2Ph$ group are non-equivalent and one appears at δ -0.02 ppm and the other at δ -0.20 ppm. The peaks and J-values observed for **12** are consistent with those reported for the germanium(II) binaphthoxo complex (*R*,*R*)-[Ge{$OC_{20}H_{10}(OSiMe_3)$-2'-$(SiMe_3)_2$-3,3'}$_2$] (**6**).[31]

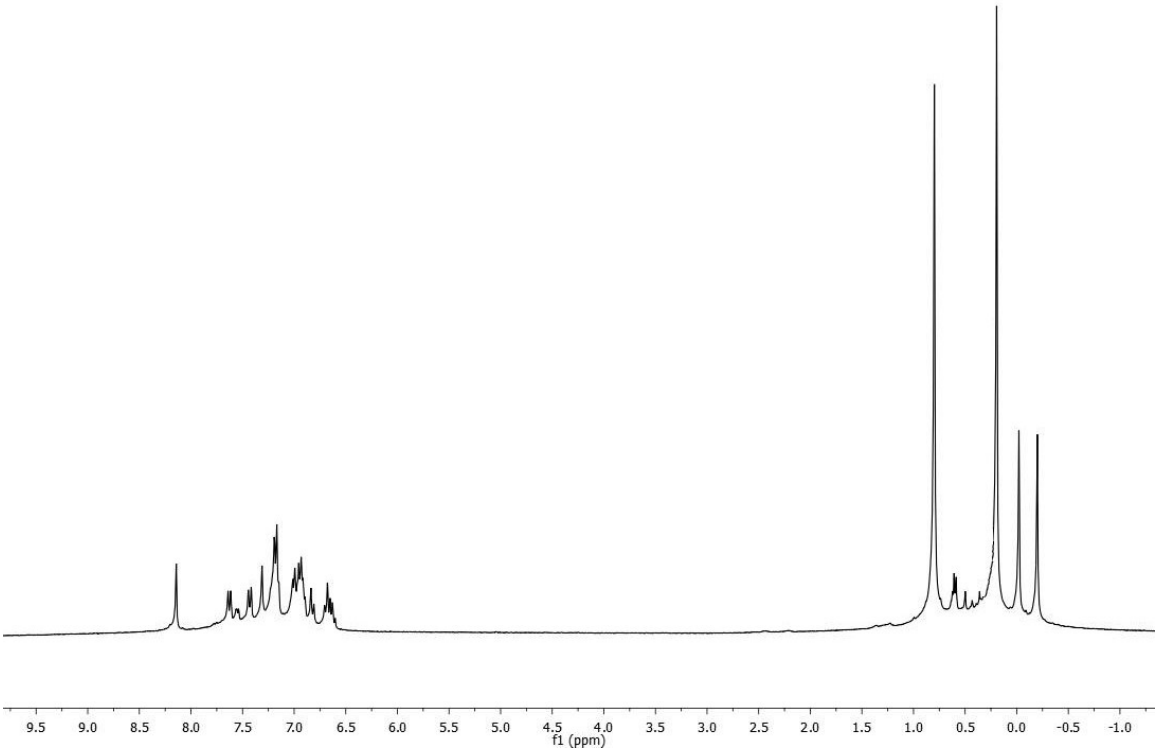

Figure 4.16: ^{1}H NMR spectrum of (*S*, *S*)-[Ge{$OC_{20}H_{10}(OSiMe_2Ph)$-2'-$(SiMe_3)_2$-3,3'}$_2$] (**12**) in d_6-benzene.

4.3 Conclusion

Calix[5]arene has been shown to react with the germylene $Ge[N(SiMe_3)_2]_2$ to yield the germanium(II)calix[5]arene complex {calix[5]arene}$_2Ge_2(OSiMe_3)_4(OH)_2$ (**9**), and the X-ray crystal structure of **9** was obtained and indicates that the complex is dimeric in the solid state. The NMR spectrum of **9** indicates that the structural rigidity of complex **9** is maintained in solution. The reaction of three equivalents of the germylene $Ge[N(SiMe_2Ph)_2]_2$ with calix[6]arene yielded the complex $[(C_6H_3)_6(CH_2)_6(OSiMe_2Ph)_6]$ (**11**) and the X-ray crystal structure of **11** was obtained. This reaction demonstrates that the reactivity of the $Ge[N(SiMe_2Ph)_2]_2$ is significantly different

than the reactivity of the well-known germylene $Ge[N(SiMe_3)_2]_2$ simply by changing one of the methyl groups to a phenyl group. The reaction of two equivalents of the 3,3'-disubstituted-1,1'-bi-2,2'-naphthol (*S*)-$[C_{20}H_{10}(OH)_2$-2,2'-$(SiMe_3)_2$-3,3'] with the germanium bisamide $Ge[N(SiMe_2Ph)_2]_2$ yielded the binaphthoxogermanium(II) complex (*S*,*S*)-$[Ge\{OC_{20}H_{10}(OSiMe_2Ph)$-2'-$(SiMe_3)_2$-3,3'$\}_2]$ (**12**). The X-ray crystal structure of **12** was obtained and the structure indicates that the silyl ether group is a direct result of silylation via the germylene present in the reaction. The crystallographic data for **9**, **11**, and **12** are provided below in **Tables 4.8** and **4.9**.

Table 4.8: Crystallographic data for compounds **9** and **11**.

	9	**11**
Compound	*{calix[5]arene}$_2$Ge$_2$(OSiMe$_3$)$_4$(OH)$_2$*	*[(C$_6$H$_3$)$_6$(CH$_2$)$_6$(OSiMe$_2$Ph)$_6$]*
Empirical Formula	$C_{100}H_{120}Ge_2O_{10}Si_4$	$C_{45}H_{48}O_3Si_3$
Formula Weight	1859.60	721.10
Temperature (K)	100(2)	100(2)
Wavelength (Å)	1.54178 (Mo Kα)	0.71073 (Mo Kα)
Crystal System	Triclinic	Monoclinic
Space Group	P-1	P2(1)/n
a, Å	13.6684(9)	8.8796(8)
b, Å	14.1898(18)	26.572(3)
c, Å	14.3933(10)	17.2903(17)
α, °	96.451(5)	90
β, °	117.150(3)	97.786(5)
γ, °	99.266(5)	90
V, Å^3	2399.6(4)	4042.1(7)
Z	1	4
ρ (g cm^{-3})	1.287	1.185
Absorption coefficient (mm^{-1})	1.720	0.156
F(000)	980	1536
Crystal Size (mm)	0.30 x 0.20 x 0.10	0.33 x 0.30 x 0.27
Theta range for data collection	3.74 to 65.16°	1.53 to 26.48°
Index ranges		
	$-16 \le h \le 14$	$-11 \le h \le 11$
	$-16 \le k \le 16$	$-33 \le k \le 31$
	$-16 \le l \le 16$	$-21 \le l \le 21$
Reflections collected	27572	59619
Independent reflections	7961	8318
	(R_{int} = 0.0236)	(R_{int} = 0.0469)
Completeness to θ = 25.00°	97.3%	100.0%
Absorption correction	Multi-scan (SADABS)	Multi-scan (SADABS)
Max. and Min. transmission	0.8468 and 0.6265	0.8334 and 0.8189
Refinement method	Full-matrix least-squares on F^2	Full-matrix least-squares on F^2
Data/restraints/parameters	7961 / 0 / 568	8318/0/466
Goodness-of-fit on F^2	1.147	0.996
Final *R* indices (I < 2σ(I))		
R_1	0.0282	0.0365
wR_2	0.0722	0.0904
Final R indices (all data)		
R_1	0.0307	0.0508
wR_2	0.0736	0.0989
Largest diff. peak and hole	0.359 and -0.366 e Å^{-3}	0.332 and -0.300 e Å^{-3}

Table 4.9: Crystallographic data for compounds **12**.

	12
Compound	*(S,S)-[Ge{$OC_{20}H_{10}$($OSiMe_2Ph$)-2'-($SiMe_3$)$_2$-3,3'}$_2$]*
Empirical Formula	$C_{68}H_{78}GeO_4Si_6$
Formula Weight	1200.43
Temperature (K)	100(2)
Wavelength (Å)	0.71073 (Mo Kα)
Crystal System	Monoclinic
Space Group	P2(1)
a, Å	12.6376(4)
b, Å	14.3935(5)
c, Å	17.7907(6)
α, °	90
β, °	90.249(2)
γ, °	90
V, Å^3	3236.09(19)
Z	2
ρ (g cm^{-3})	1.232
Absorption coefficient (mm)	0.630
F(000)	1268
Crystal Size (mm)	0.33 x 0.31 x 0.30
Theta range for data collection	1.82 to 28.31°
Index ranges	
	$-16 \leq h \leq 16$
	$-19 \leq k \leq 19$
	$-23 \leq l \leq 23$
Reflections collected	46499
Independent reflections	15701
	(R_{int} = 0.0801)
Completeness to θ = 25.00°	99.7%
Absorption correction	Multi-scan (SADABS)
Max. and Min. transmission	0.8334 and 0.8189
Refinement method	Full-matrix least -squares on F^2
Data/restraints/parameters	15701/1/728
Goodness-of-fit on F^2	0.999
Final *R* indices (I < 2σ(I))	
R_1	0.0466
wR_2	0.0965
Final R indices (all data)	
R_1	0.0592
wR_2	0.1020
Largest diff. peak and hole (e Å^{-3})	0.632 and -0.464

4.4 Experimental

General Remarks

All manipulations were carried out under an inert atmosphere of nitrogen using standard Schlenk, syringe, and glovebox techniques.[35] Solvents were dried using a Glass Contour solvent purification system. We are grateful to Professor Michael Lattman (Southern Methodist University) for a generous gift of calix[5]arene. The reagents $Ge[N(SiMe_3)_2]_2$ (**1**) and (*S*)-$[C_{20}H_{10}(OH)_2$-2,2'-$(SiMe_3)_2$-3,3'] were prepared following literature procedures.[30, 36] The germylene $Ge[N(SiMe_2Ph)_2]_2$ was prepared as before (Chapter 2). Calix[6]arene was purchased from Aldrich and dried under vacuum in a 50 °C water bath before use. ^1H and ^{13}C NMR were recorded on a Inova Gemini 2000 spectrometer at 300.0 and 75.5 MHz respectively and were referenced to the solvent. Elemental analyses were conducted by Galbraith Laboratories (Knoxville, TN).

*Synthesis of $[(C_6H_5)_5(CH_2)_5O_2Ge(OSiMe_3)_2(OH)]$ (**9**)*

To a solution of calix[5]arene (0.100 g, 0.189 mmol) in benzene (10 mL) was added to a solution of $Ge[N(SiMe_3)_2]_2$ (0.074 g, 0.19 mmol) in benzene (5 mL). The reaction mixture was stirred for 5 h at room temperature and the volatiles were removed *in vacuo* to yield a white solid which was recrystallized via slow evaporation of a toluene solution (3 mL) to yield 0.097 g (69%) of **9** as colorless crystals. ^1H NMR (C_6D_6, 23 °C): δ 7.63 (d, J = 6.6 Hz, 2H, *m*-C_6H_3), 7.45-6.81 (m, 14H, *m*-C_6H_3 and *p*-C_6H_3), 6.66-6.54 (m, 6H, *m*-C_6H_3 and *p*-C_6H_3), 6.38 (d, J = 7.2 Hz, 2H, *m*-C_6H_3), 6.30 (t, J = 7.8 Hz, 2H, *p*-C_6H_3), 6.17 (d, J = 7.8 Hz, 2H, *m*-C_6H_3), 6.11 (d, J = 7.2 Hz, 2H, *m*-C_6H_3), 6.07 (d, J = 7.2 Hz, 2H, *m*-C_6H_3), 5.21 (d, J = 16.2 Hz, 2H, -CH_2-), 4.90 (d, J = 14.7 Hz, 2H, -CH_2-), 4.79 (d, J = 14.7Hz, 2H, -CH_2-), 4.64 (d, J = 12.3 Hz, 2H, -CH_2-), 4.21 (d, J = 13.5 Hz, 2H, -CH_2-), 3.95 (d, J = 16.2 Hz, 2H, -CH_2-), 3.89 (d, J = 15.0 Hz, 2H, -CH_2-), 3.71

(d, J = 15.0 Hz, 2H, -CH_2-), 3.33 (d, J = 13.5 Hz, 2H, -CH_2-), 3.09 (d, J = 12.3 Hz, 2H, -CH_2-), 0.29 (s, 6H, -Si(CH_3)$_3$), 0.15 (s, 6H, -Si(CH_3)$_3$), 0.13 (s, 6H, -Si(CH_3)$_3$), 0.01 (s, 6H, -Si(CH_3)$_3$) ppm. *Anal.* Calcd. For $C_{41}H_{44}GeO_5Si_2$: C, 66.05; H, 5.95. Found: C, 65.74; H, 5.76.

Synthesis of [$(C_6H_3)_6(CH_2)_6(OSiMe_2Ph)_6$] ***(11)***

To a solution of calix[6]arene (0.100 g, 0.157 mmol) in benzene (10 mL) was added a solution of Ge[N(SiMe$_2$Ph)$_2$]$_2$ (0.302 g, 0.471 mmol) in benzene (5 mL). The reaction mixture was stirred for 5 h and the volatiles were removed *in vacuo* to yield a light yellow solid which was recrystallized from the slow evaporation of a benzene solution (5 mL) to yield 0.164 g (73%) of **11** as colorless crystals. ^{1}H NMR (C_6D_6, 23 $^\circ$C): δ 7.84-6.70 (m, 48H, aromatic protons), δ 4.74-4.44 (m, 5H, methylene protons), 4.27 (d, 1H, J = 15.9 Hz, -CH_2-), 4.11 (d, 1H, J = 13.2 Hz, -CH_2-), 3.29-2.86 (m, 5H, methylene protons), 0.25 (s, 36H, -OSi(CH_3)$_2$Ph) ppm.

*Synthesis of (S,S)-[Ge{$OC_{20}H_{10}$(OSiMe$_2$Ph)-2'-(SiMe$_3$)$_2$-3,3'}$_2$] (**12**)*

To a solution of the binaphthol [$C_{20}H_{10}$(OH)$_2$-2,2'-(SiMe$_3$)$_2$-3,3'] (0.671g, 1.560 mmol) in benzene (15mL) was added a solution of Ge[N(SiMe$_2$Ph)$_2$]$_2$ (0.500g, 0.779 mmol) in benzene (5mL). The reaction mixture was stirred for 5h and the volatiles were removed *in vacuo* to yield a thick yellow liquid. After one week colorless crystals began to form in the liquid and were isolated to yield 0.340g (36%) as colorless crystals. ^{1}H NMR (C_6D_6, 23°C): δ 8.14 (s, 4H, 4,4' hydrogens), 7.63 (d, 4H, J = 8.1 Hz, 6,6' hydrogens), 7.43 (d, 4H, J = 8.1 Hz, 8,8' hydrogens), 7.19-6.60 (m, 18H, aromatics), 0.80 (s, 18H, -Si(CH_3)$_3$), 0.19 (s, 18H, -Si(CH_3)$_3$), -0.02 (s, 6H, -OSi(CH_3)$_2$Ph), -0.20 (s, 6H, -OSi(CH_3)$_2$Ph) ppm.

4.5 References

1. Gutsche, C. D.; Gutsche, C. D.; Royal Society of Chemistry (Great Britain), *Calixarenes : An Introduction*. 2nd ed.; RSC Publishing: Cambridge, 2008; p xiii, 276 p.

2. Gutsche, C. D., *Calixarenes revisited*. Royal Society of Chemistry: Cambridge, 1998; p xii, 233 p.

3. Asfari, Z., *Calixarenes 2001*. Kluwer Academic Publishers: Dordrecht; Boston, 2001; p x, 683 p.

4. Cotton, F. A.; Daniels, L. M.; Lin, C.; Murillo, C. A., *Inorg. Chim. Acta* **2003,** *347*, 1-8.

5. Brown, M.; Jablonski, C., *Can. J. Chem.* **2001,** *79* (5-6), 463-471.

6. Mendoza-Espinosa, D.; Rheingold, A. L.; Hanna, T. A., *Dalton Trans.* **2009,** (26), 5226-5238.

7. Fan, M. M.; Shevchenko, I. V.; Voorhies, R. H.; Eckert, S. F.; Zhang, H. M.; Lattman, M., *Inorg. Chem.* **2000,** *39* (21), 4704-4712.

8. Fan, M. M.; Zhang, H. M.; Lattman, M., *Organometallics* **1996,** *15* (24), 5216-5219.

9. Shang, S.; Khasnis, D. V.; Burton, J. M.; Santini, C. J.; Fan, M. M.; Small, A. C.; Lattman, M., *Organometallics* **1994,** *13* (12), 5157-5159.

10. Sood, P.; Zhang, H. M.; Lattman, M., *Organometallics* **2002,** *21* (21), 4442-4447.

11. Khasnis, D. V.; Burton, J. M.; Lattman, M.; Zhang, H. M., *J. Chem. Soc. Chem. Comm.* **1991,** (8), 562-563.

12. Khasnis, D. V.; Lattman, M.; Gutsche, C. D., *J. Am. Chem. Soc.* **1990,** *112* (25), 9422-9423.

13. Fan, M. M.; Zhang, H. M.; Lattman, M., *Chem. Commun.* **1998,** (1), 99-100.

14. Fan, M. M.; Zhang, H. M.; Lattman, M., *Phosphorus, Sulfur, and Silicon* **1999,** *146*, 257-260.

15. Fan, M. M.; Zhang, H. M.; Lattman, M., *Phosphorus, Sulfur, and Silicon* **2002,** *177* (6-7), 1549-1551.

16. Khasnis, D. V.; Burton, J. M.; Mcneil, J. D.; Santini, C. J.; Zhang, H. M.; Lattman, M., *Inorg. Chem.* **1994,** *33* (12), 2657-2662.

17. Sood, P.; Koutha, M.; Fan, M. M.; Klichko, Y.; Zhang, H. M.; Lattman, M., *Inorg. Chem.* **2004,** *43* (9), 2975-2980.

18. Liu, L. H.; Zakharov, L. N.; Rheingold, A. L.; Hanna, T. A., *Chem. Commun.* **2004,** (13), 1472-1473.

19. Mendoza-Espinosa, D.; Hanna, T. A., *Dalton Trans.* **2009,** (26), 5211-5225.

20. Mendoza-Espinosa, D.; Hanna, T. A., *Inorg. Chem.* **2009,** *48* (21), 10312-10325.

21. Shang, S.; Khasnis, D. V.; Zhang, H. M.; Small, A. C.; Fan, M. M.; Lattman, M., *Inorg. Chem.* **1995,** *34* (14), 3610-3615.

22. Hascall, T.; Pang, K.; Parkin, G., *Tetrahedron* **2007,** *63* (44), 10826-10833.

23. McBurnett, B. G.; Cowley, A. H., *Chem. Commun.* **1999,** (1), 17-18.

24. Hascall, T.; Rheingold, A. L.; Guzei, I.; Parkin, G., *Chem. Commun.* **1998,** (1), 101-102.

25. Wetherby, A. E.; Goeller, L. R.; DiPasquale, A. G.; Rheingold, A. L.; Weinert, C. S., *Inorg. Chem.* **2007,** *46* (18), 7579-7586.

26. Wetherby, A. E.; Rheingold, A. L.; Feasley, C. L.; Weinert, C. S., *Polyhedron* **2008,** *27* (7), 1841-1847.

27. Green, R. A.; Rheingold, A. L.; Weinert, C. S., *Inorg. Chim. Acta* **2009,** *362* (9), 3159-3164.

28. Harris, D. H. L., M. F., *J.C.S. Chem. Comm.* **1974**, 895-896.

29. Gynane, M. J. S.; Harris, D. H.; Lappert, M. F.; Power, P. P.; Riviere, P.; Rivierebaudet, M., *J. Chem. Soc. Dalton* **1977,** (20), 2004-2009.

30. Zhu, Q. F., K. L.; Roskamp, E. J., *Heteroatom Chem.* **1992,** *3*, 647-649.

31. Weinert, C. S.; Fanwick, P. E.; Rothwell, I. P., *J. Chem. Soc. Dalton* **2002,** (15), 2948-2950.

32. Wetherby, A. E.; Goeller, L. R.; DiPasquale, A. G.; Rheingold, A. L.; Weinert, C. S., *Inorg. Chem.* **2008,** *47* (6), 2162-2170.

33. Durr, S.; Bechlars, B.; Radius, U., *Inorg. Chim. Acta* **2006,** *359* (13), 4215-4226.

34. Atkins, P. W.; Shriver, D. F., *Inorganic Chemistry* 4th ed.; W.H. Freeman: New York, 2006; p xxi, 822 p.

35. D. F. Shriver, M. A. Drezdzon., *The Manipulation of Air Sensitive Compounds*. John Wiley and Sons, New York: 1986.

36. Buisman, G. J. H.; Vanderveen, L. A.; Klootwijk, A.; deLange, W. G. J.; Kamer, P. C. J.; vanLeeuwen, P. W. N. M.; Vogt, D., *Organometallics* **1997,** *16* (13), 2929-2939.

CHAPTER V

OLIGOGERMANES AS MOLECULAR PRECURSORS FOR GERMANIUM(0) NANOPARTICLES: SIZE CONTROL AND SIZE-DEPENDENT FLUORESCENCE

5.1 Introduction

Semiconductor nanoparticles exhibit photoluminescence and optical absorption that is dependent on particle size. These properties arise from quantum confinement which is the result of the confinement of charge carriers within nanoparticles whose dimensions are smaller than the Bohr radius of an electrostatically bound electron-hole pair (exciton) in the bulk material.[1] Quantum dots from compound semiconductors such as CdS, CdSe, InP, and GaAs have all been made with well-defined size, morphology, and surface chemistry.[2-4] These semiconductor materials are all direct bandgap semiconductors and are well understood. However, the usefulness of these materials may be diminished by the inherent electrochemical instability present in III-V and II-VI semiconductors.[1] Unlike these materials, silicon and germanium are indirect band gap semiconductors in the bulk and they are electrochemically stable.[5] Even though bulk germanium is an indirect band gap material, germanium nanocrystals have been found to behave as a direct band gap material.[6-7]

There has recently been an increased interest in the preparation of germanium nanoparticles since the limitations of silicon-based materials are being approached and germanium could possibly be used as a replacement material for silicon in various applications

such as transistors, [8-10] photovoltaic devices,[11-13] and biological imaging.[14-15] This material change stems from the fact that the useful electronic properties of these germanium-based materials are enhanced relative to those of silicon due to the fact that germanium has a smaller band gap (0.66 eV at 291K) [16] than silicon (1.11 eV at 291K),[16] a higher electron and hole mobility (Ge: 3900 cm^2/Vs, Si: $\leq$ 1400 cm^2/Vs),[17] and a more pronounced quantum confinement effect due to the larger Bohr exciton radius of germanium.[18-20]

In the preparation of germanium nanoparticles, size control is paramount since the physical properties of these materials are dependent on their size and morphology. Germanium nanocrystals with diameters on the order of 4-10 nm deposited into SiO_2 films have been prepared by germanium ion implantation using a molecular beam[21] or by sputtering techniques.[22] Solution methods have also been developed for the preparation of germanium nanoparticles. These methods involve the direct reduction of tetravalent germanium precursors; however, several of these techniques result in the formation of unwanted byproducts that are difficult to remove from the germanium nanoparticles.[1, 23-26]

Recently it was demonstrated by the Boyle group that the germanium(II) precursors $Ge[N(SiMe_3)_2]_2$ [27] and $Ge(OC_6H_3Bu^t_2\text{-}2,6)_2$ [28] were effective starting materials for the preparation of germanium(0) nanomaterials using a solution based synthesis method. They also showed that changing the ligands among several germanium(II) alkoxide $Ge(OR)_2$ precursors gave nanoparticles with different morphologies, thus demonstrating a morphology dependence of the germanium(0) nanoparticles on the precursor.[29]

We have prepared a series of three oligogermanes including a digermane, a trigermane, and a branched neopentyl germane where the formal oxidation states at germanium vary from +3 to +2 and zero depending on the number of germanium-germanium single bonds present at a given germanium atom. We have found that these oligogermanes can be used as precursors for

the preparation of germanium(0) nanomaterials, and that the size of the resulting nanoparticles correlates with the number of catenated germanium atoms in the precursor compounds. These nanoparticles are fluorescent and the position of the emission maximum is red shifted as the size of the particles increases.

5.2 Results and Discussion

For these initial investigations, we selected the three oligogermanes $Bu^n_3GeGePh_3$ (**1**),[30] $Bu^n_3GeGePh_2GeBu^n_3$ (**2**), and $Ge(GeMe_3)_4$ (**3**)[31] as potential precursors (**Figure 5.1**). These oligogermanes were chosen because of the alkyl ligands present on the terminal germanium atoms. The preparation of the nanomaterials using these precursors entails using oleylamine and 1-octadecene solvents. In order for the synthesis of the germanium nanoparticles to be successful, the starting precursor materials must be soluble in oleylamine and 1-octadecene. Perphenylated oligogermanes such as the digermane $Ph_3GeGePh_3$ or the trigermane $Ph_3GeGePh_2GePh_3$ are not soluble in aliphatic hydrocarbon solvents, however using terminal butyl or methyl groups on the germanium atoms in place of phenyl substituents allows for the material to be dissolved in hydrocarbon solvents. As mentioned before, the formal oxidation states at germanium in these compounds are either +3, +2, or zero. Both of the germanium atoms in **1** and all of the terminal germanium atoms in the other two compounds have a formal oxidation state of +3. The central germanium atom in **2** has a formal oxidation state of +2, and the central germanium atom in **3** has a formal oxidation state of zero since it is bound to four other germanium atoms.

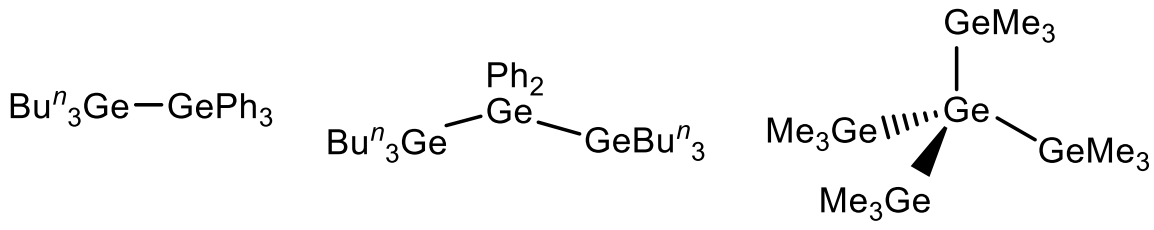

1 **2** **3**

Figure 5.1: Structures of the $Bu^n_3GeGePh_3$ (**1**), $Bu^n_3GeGePh_2GeBu^n_3$ (**2**), and $Ge(GeMe_3)_4$ (**3**) oligogermane precursors for germanium nanoparticle synthesis.

A sample of 0.500 g of each of these compounds was dissolved in 4 mL of oleylamine and the resulting solution was injected into 4 mL of refluxing 1-octadecene held at a temperature of 315 ^oC and the temperature of the resulting solution decreased by about 15 ^oC followed by a return to reflux after 3-5 minutes. Because 0.500 g of each precursor was used, the concentrations of the samples were similar, measuring 0.114 M, 0.087 M, and 0.115 M for **1**, **2**, and **3** respectively. After refluxing the mixture for 1 h, the solution was cooled to room temperature and the nanoparticles were precipitated from the solution by dissolving an aliquot in chloroform followed by the addition of methanol in a layered fashion. The methanol layer was pipetted into a vial and the methanol was removed *in vacuo* to yield the nanoparticles. The germanium materials obtained by this method were colorless and also appeared to be amorphous.

The size and morphology of the three different germanium(0) nanoparticles were initially assessed using transmission electron microscopy (TEM) and the images are provided below in **Figure 5.2**. The TEM images were acquired by pipetting a drop of germanium nanoparticles suspended in chloroform, that had been sonicated for 30 minutes, onto a copper TEM grid.

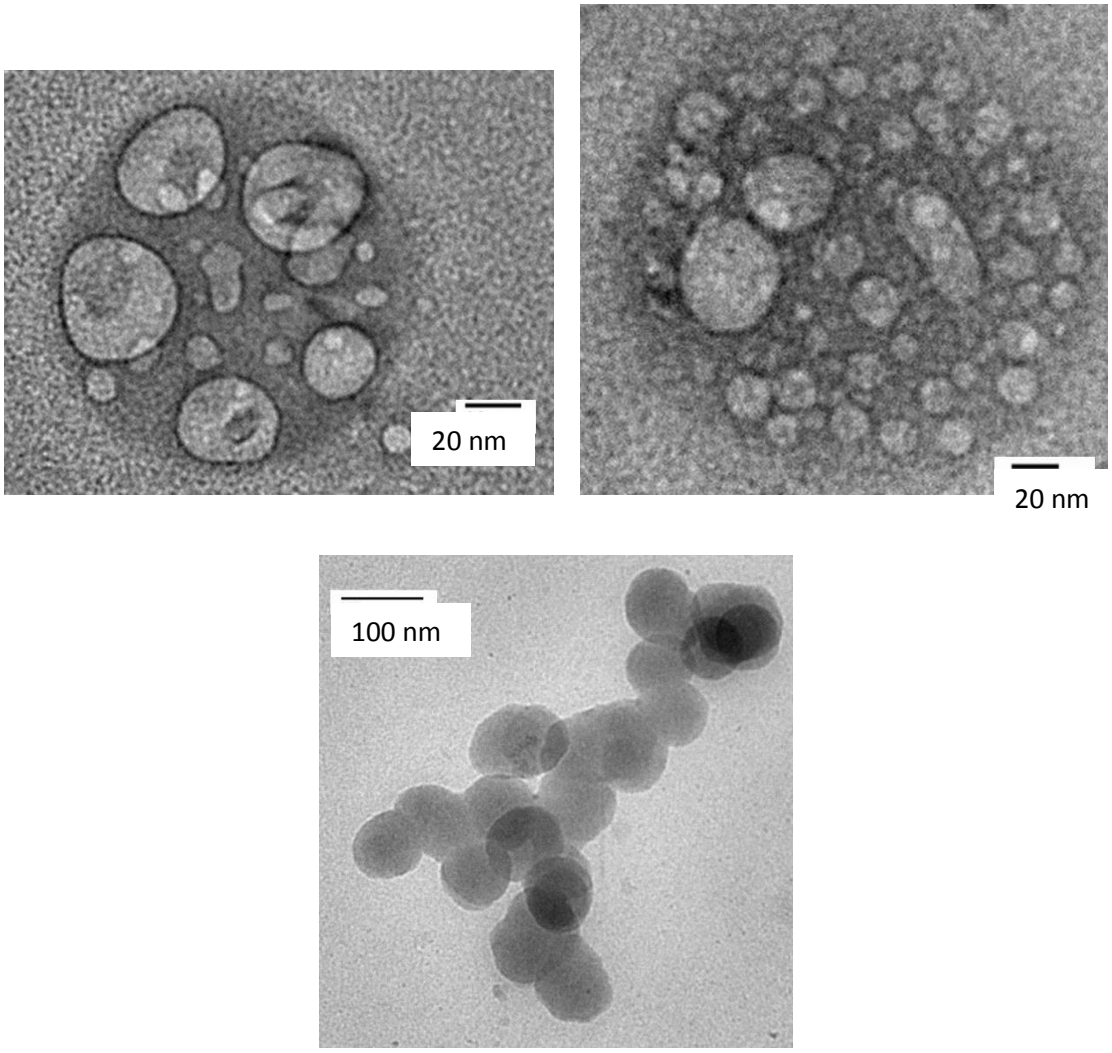

Figure 5.2: TEM images of Ge nanoparticles from precursors $Bu^n_3GeGePh_3$ (**1**) (top left), $Bu^n_3GeGePh_2GeBu^n_3$ (**2**) (top right), and $Ge(GeMe_3)_4$ (**3**) (bottom).

From the TEM images it can be seen that the particles are somewhat aggregated and could not be effectively separated even after prolonged sonication, and this is likely due to their amorphous nature. However, it can be seen that there is a correlation between the size of the germanium nanoparticles and the number of catenated germanium atoms present in the oligogermane precursors. In order to analyze this further, the size distribution of the particles were obtained

using dynamic light scattering with the particles suspended in chloroform, after sonication for 30 minutes. These results are provided below in **Figure 5.3**. The average particle size for the material from $Bu^n_3GeGePh_3$ (**1**) is 13 ± 3 nm, from $Bu^n_3GeGePh_2GeBu^n_3$ (**2**) is 28 ± 5 nm, and the particles from $Ge(GeMe_3)_4$ (**3**) have a larger particle size distribution with an average size of 44 ± 12 nm. The particle size distributions below in **Figure 5.3** clearly indicate that there is a correlation between precursor catenation and particle size.

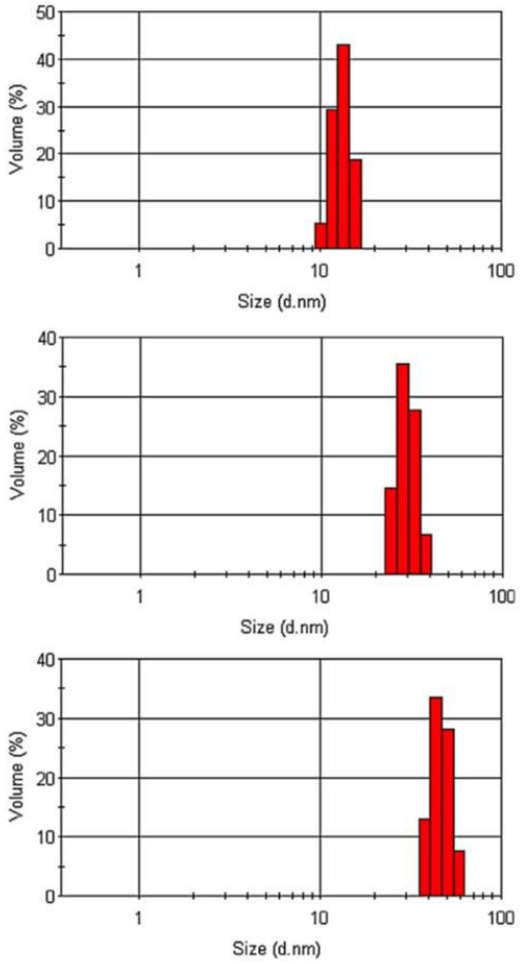

Figure 5.3: Particle size distributions of Ge nanoparticles from precursors $Bu^n_3GeGePh_3$ (**1**) (top), $Bu^n_3GeGePh_2GeBu^n_3$ (**2**) (middle), and $Ge(GeMe_3)_4$ (**3**) (bottom).

In an attempt to ascertain if oleylamine was passivating the surface of the germanium nanoparticles, the FTIR spectra of the three samples were obtained. The nanoparticles were washed with methanol three times to remove any remaining free oleylamine that might still be present prior to acquiring the FTIR spectra. The FTIR spectra of all three samples indicate that oleylamine is attached to the surface of the particles (**Figure 5.4**).[32-35] The characteristic IR peaks for the material made from $Bu^{n}_{3}GeGePh_3$ (**1**) for the C-H stretching modes appear at 2854 cm^{-1}, 2925 cm^{-1}, and 2957 cm^{-1}, two N-H stretches appear at 3330 cm^{-1} and 3400 cm^{-1}, and the N-H scissor mode appears at 1565 cm^{-1}, and the C-H bending mode appears at 1465 cm^{-1}. In addition, the C-N stretching mode appears at 1050 cm^{-1} and the NH_2 bending modes are found at 991 cm^{-1}, 966 cm^{-1}, and 909 cm^{-1}.[36-37] Therefore, the C-N bond as well as the N-H bonds of oleylamine remain intact. The FTIR of the particles made from **2** and **3** are essentially identical to that of the particles made from **1** indicating that the surface of all three samples are passivated with the oleylamine.

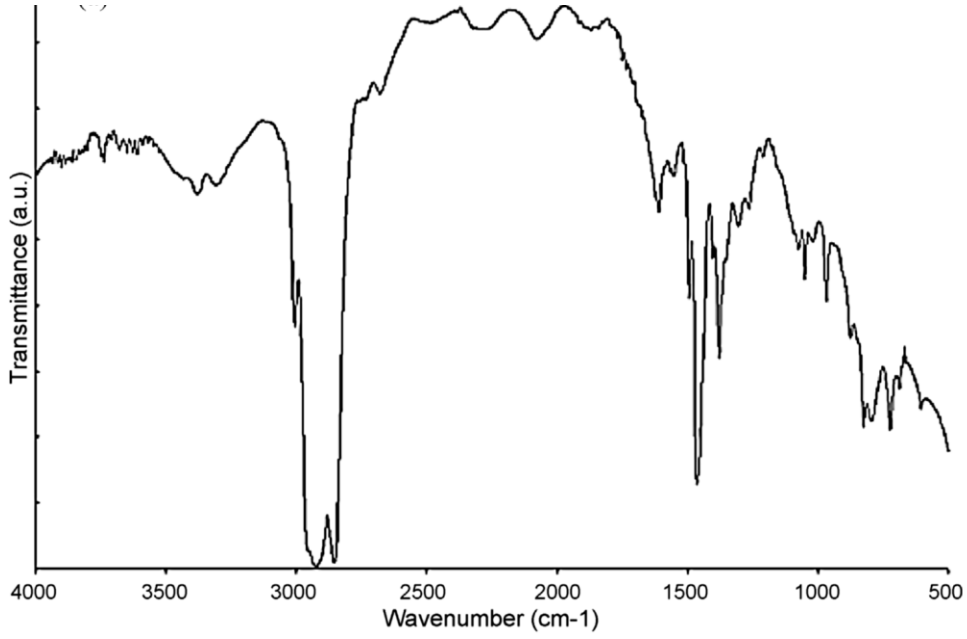

Figure 5.4: FTIR spectrum of germanium nanoparticles from $Bu^{n}_{3}GeGePh_3$ (**1**).

As expected from visual inspection and the TEM images, powder X-ray diffraction (XRD) confirmed that the germanium nanomaterials were amorphous rather than crystalline (**Figure 5.5**).The diffraction pattern of each of the samples lack the peaks expected for crystalline germanium (111, 220, 311, 400, 331) in all three cases.[38-39] However, the presence of germanium in each of the samples was confirmed by both energy dispersive X-ray spectroscopy (EDS) and X-ray photoelectron spectroscopy (XPS). The EDS spectrum of the nanoparticles from $Bu^{n}_{3}GeGePh_3$ (**1**) contains peaks that correspond to germanium at 1.18 keV, 9.83 keV, and 10.99 keV. The EDS spectra for the particles from **2** and **3** are nearly identical to those of **1** and all three of these spectra are provided below in **Figure 5.6**.

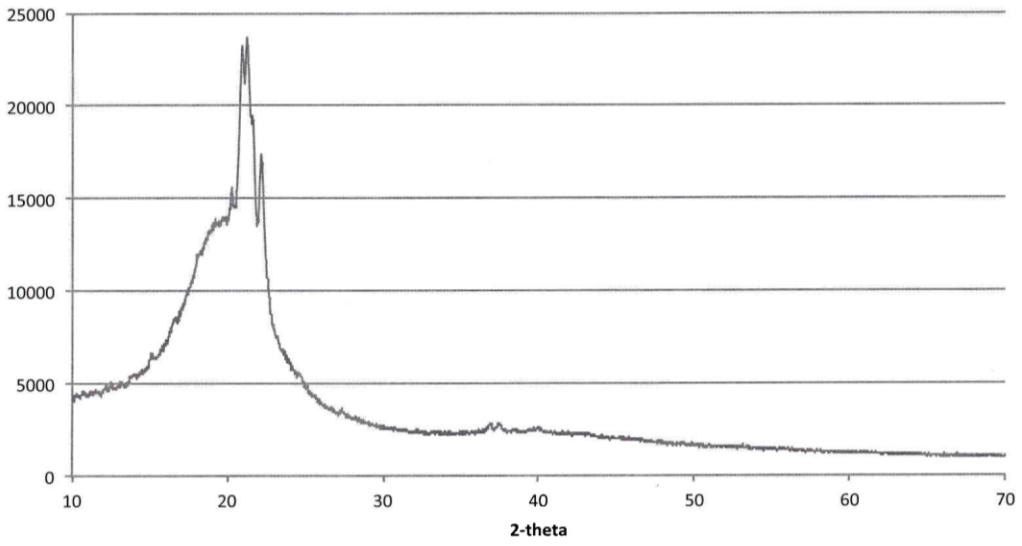

Figure 5.5: Powder XRD of Ge nanoparticles from $Bu^{n}_{3}GeGePh_3$ (**1**).

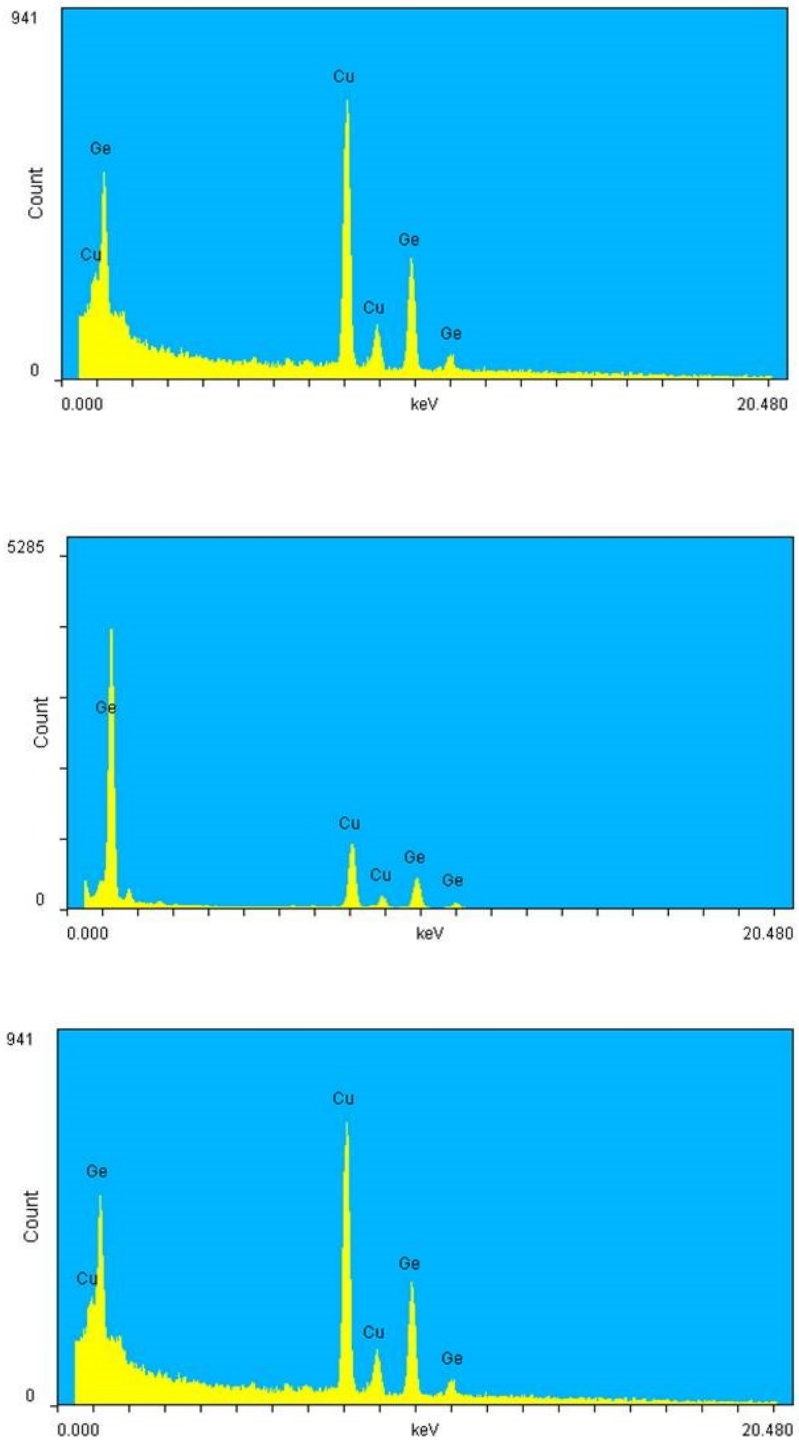

Figure 5.6: EDS spectra of Ge nanoparticles from $Bu^n_3GeGePh_3$ (**1**) (top), $Bu^n_3GeGePh_2GeBu^n_3$ (**2**) (middle), and $Ge(GeMe_3)_4$ (**3**) (bottom).

The germanium 3d electrons appear at 29.0 eV in the XPS spectrum of all three samples. This indicates that the germanium present is germanium(0) since the electrons do not appear at 32.0 eV which is the expected value for germanium(IV) in GeO_2.[40-43] Additionally, all three samples are missing a FTIR stretch at 850 cm^{-1} that corresponds to the Ge-O stretching mode of GeO_2.[44]

The fluorescence spectra of all three samples were obtained in chloroform at an excitation wavelength of 360 nm (**Figure 5.7**). The emission maxima were observed at 420 nm for $Bu^n_3GeGePh_3$ (**1**), 435 nm for $Bu^n_3GeGePh_2GeBu^n_3$ (**2**), and 456 nm for $Ge(GeMe_3)_4$ (**3**). This indicates that the larger nanoparticles emit at a larger wavelength (lower energy) than the smaller nanoparticles, which is consistent with other findings.[18, 45-48] The emission spectra are also broadened which is expected for samples having a variable particle size distribution. Additionally, the appearance of the spectra remain the same when 330 nm or 430 nm wavelengths are used as the excitation wavelength.

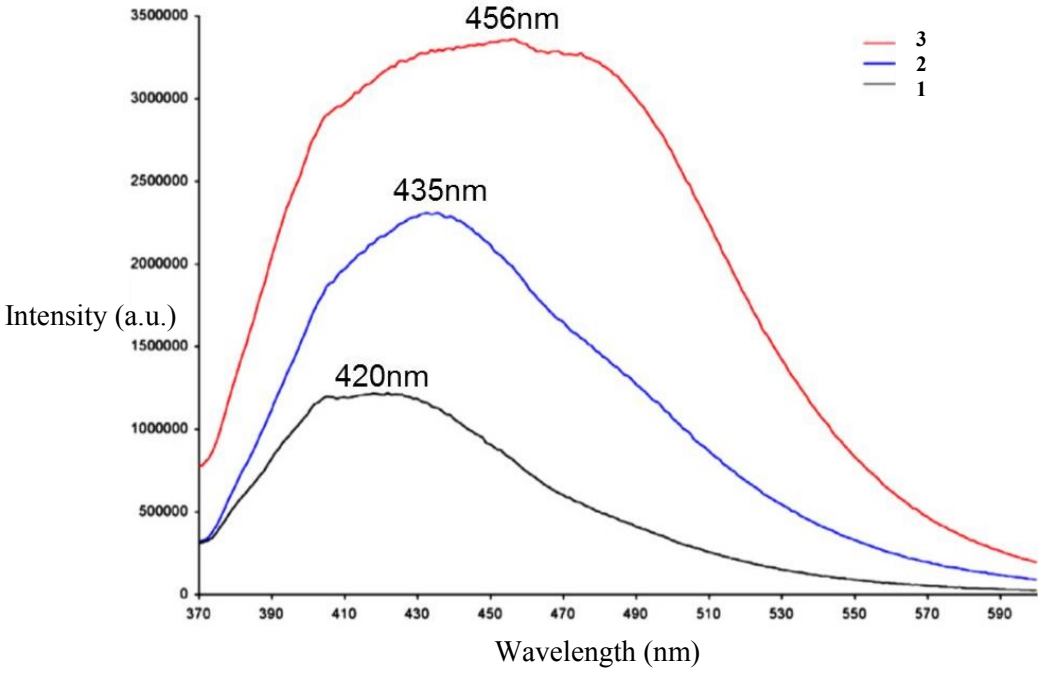

Figure 5.7: Fluorescence spectra of germanium nanoparticles dispersed in chloroform. Excitation wavelength = 360 nm, slit width = 3 mm.

5.3 Conclusion

We have utilized oligogermanes containing two, three, or five catenated germanium atoms as precursors for the preparation of germanium nanoparticles by a solution synthesis method. We have seen a reasonable correlation between precursor catenation and particle size, where larger germanium nanoparticles are obtained from oligogermanes with a higher degree of catenation. The nanoparticles range in size from 13 ± 3 nm to 44 ± 12 nm, and this type of molecular precursor/ nanoparticle relationship has not been previously investigated. The particle surfaces are passivated with oleylamine and all three samples obtained were found to be amorphous. The samples also exhibit the expected size-dependent emission spectra where the smaller particles emit at a higher energy than the larger particles. Therefore, we have demonstrated the potential to control the emissive properties of the germanium nanoparticles by varying the oligogermane precursor utilized in their preparation. It is anticipated that using other oligogermanes (linear, branched, and cyclic) will provide germanium(0) nanomaterials having an array or particle sizes. Furthermore, the amorphous nanoparticles we have obtained can likely be converted to crystalline materials by high-temperature annealing followed by the generation of hydride-passivated particles followed by hydrogermylation to yield particles with different solubilities.[26, 38-39, 45, 49-51]

5.4 Experimental

General Considerations

The reagent Ph_2GeH_2 was purchased from Gelest Inc. and $Bu^n_3GeNMe_2$ was synthesized according to the literature procedure.[30] Solvents were dried using a GlassCol solvent purification system and all manipulations of reagents were carried out using standard Schlenk, syringe, and glovebox techniques under a dry nitrogen atmosphere. NMR (^1H and ^{13}C) spectra were recorded

using a INOVA Gemini 2000 spectrometer and FTIR spectra were acquired in Nujol using a Hewlett-Packard FTIR spectrometer. Elemental analysis was carried out by Galbraith Laboratories (Knoxville, TN).

Synthesis of $Bu^n_3GeGePh_2GeBu^n_3$

To a solution of $Bu^n_3GeNMe_2$ (1.385 g, 4.810 mmol) in acetonitrile (15 mL) was added a solution of Ph_2GeH_2 (0.500 g, 2.18 mmol) in acetonitrile (10 mL) under an atmosphere of nitrogen. The reaction mixture was sealed in a Schlenk tube under nitrogen and stirred for 48 h at 85 °C. The acetonitrile was removed *in vacuo* and the resulting oil was vacuum distilled in a Kugelrohr oven (125 °C, 0.10 torr) to yield $Bu^n_3GeGePh_2GeBu^n_3$ (0.992 g, 63.5%) as a colorless oil. ^{1}H NMR (C_6D_6, 23°C): δ 7.73 (d, J = 8.4 Hz, 6H, *o*-H), 7.22 (m, 6H, *m*-H), 7.14 (d, J = 7.8 Hz, 3H, *p*-H), 1.49 (m, 6H, -$CH_2CH_2CH_2CH_3$), 1.34 (q, J = 7.8 Hz, 6H, -$CH_2CH_2CH_2CH_3$), 1.19 (m, 6H, -$CH_2CH_2CH_2CH_3$), 0.90 (t, J = 7.2 Hz, 9H, -$CH_2CH_2CH_2CH_3$) ppm. ^{13}C NMR δ 140.7 (*ipso*-C), 136.1 (*o*-C), 128.3 (*p*-C), 128.1 (*m*-C), 28.8 (-$CH_2CH_2CH_2CH_3$), 27.1 (-$CH_2CH_2CH_2CH_3$), 15.0 (-$CH_2CH_2CH_2CH_3$), 13.9 (-$CH_2CH_2CH_2CH_3$) ppm. *Anal.* Calcd. For $C_{36}H_{64}Ge_3$: C, 60.47; H, 9.03. Found: C, 60.35; H, 9.11.

General solution synthesis of germanium nanoparticles

A 0.500 g sample of oligogermane was dissolved in oleylamine (4 mL) under an atmosphere of N_2. 4 mL of 1-octadecene was brought to reflux under nitrogen at 315 °C in a round bottom flask equipped with a water-cooled condenser. The oleylamine solution was injected into the refluxing 1-octadecene via syringe through the top of the condenser, and the temperature of the resulting solution decreased followed by a return to reflux after 3-5 minutes.

The resulting solution was then allowed to reflux for 90 minutes and was then allowed to cool to room temperature. The entire solution was then poured into approximately 20-25 mL of chloroform and then methanol was layered on top of this solution to precipitate the nanomaterial. The methanol layer, which contained the germanium nanomaterial, was removed and additional chloroform was added to re-dissolve the nanoparticles. Methanol was then layered on this mixture to precipitate the nanomaterial again. The mixture was centrifuged at 3100 rpm for 10 minutes and the liquid phase was decanted from the germanium nanoparticles.

Methods of characterization

TEM images were acquired by pipetting an aliquot of germanium nanoparticles suspended in chloroform onto a copper TEM grid. After evaporation of the chloroform, the sample was analyzed using a JEOL JEM-2100 equipped with an Evex EDS analyzer. Powder XRD patterns were acquired using a Bruker D8-A25-ADVANCE diffractometer. Sample sizes were obtained using a Malvern HPP5001 dynamic light scattering particle sizing apparatus, FTIR were obtained using a Perkin-Elmer 1720 infrared spectrometer, and fluorescence spectra were acquired using a Horbia Fluorolog 3 spectrometer. All XPS experiments were carried out using an instrument constructed in-house at Oklahoma State University.

5.5 References

1. Fok, E.; Shih, M. L.; Meldrum, A.; Veinot, J. G. C., *Chem. Commun.* **2004,** (4), 386-387.

2. Trindade, T.; O'Brien, P.; Pickett, N. L., *Chem. Mater.* **2001,** *13* (11), 3843-3858.

3. Manna, L.; Scher, E. C.; Alivisatos, A. P., *J. Am. Chem. Soc.* **2000,** *122* (51), 12700-12706.

4. Dabbousi, B. O.; RodriguezViejo, J.; Mikulec, F. V.; Heine, J. R.; Mattoussi, H.; Ober, R.; Jensen, K. F.; Bawendi, M. G., *J. Phys. Chem. B* **1997,** *101* (46), 9463-9475.

5. Ding, Z. F.; Quinn, B. M.; Haram, S. K.; Pell, L. E.; Korgel, B. A.; Bard, A. J., *Science* **2002,** *296* (5571), 1293-1297.

6. Rossetti, R.; Hull, R.; Gibson, J. M.; Brus, L. E., *J. Chem. Phys.* **1985,** *83* (3), 1406-1410.

7. Kanemitsu, Y.; Uto, H.; Masumoto, Y.; Maeda, Y., *Appl. Phys. Lett.* **1992,** *61* (18), 2187-2189.

8. An, X.; Huang, R.; Zhang, X.; Wang, Y. Y., *Semicond. Sci. Tech.* **2005,** *20* (10), 1034-1038.

9. Khakifirooz, A.; Antoniadis, D. A., *Ieee Electr. Device L* **2004,** *25* (2), 80-82.

10. Lauhon, L. J.; Gudiksen, M. S.; Wang, C. L.; Lieber, C. M., *Nature* **2002,** *420* (6911), 57-61.

11. Wang, R.; Guo, Z. L.; Wang, G. P., *Sol. Energ. Mat. Sol. C* **2006,** *90* (7-8), 1052-1057.

12. Deshmukh, M. P.; Nagaraju, J., *Sol. Energ. Mat. Sol. C* **2005,** *89* (4), 403-408.

13. Du Pasquier, A.; Mastrogiovanni, D. D. T.; Klein, L. A.; Wang, T.; Garfunkel, E., *Appl. Phys. Lett.* **2007,** *91* (18).

14. Lambert, T. N.; Andrews, N. L.; Gerung, H.; Boyle, T. J.; Oliver, J. M.; Wilson, B. S.; Han, S. M., *Small* **2007,** *3* (4), 691-699.

15. Hernandez-Sanchez, B. A.; Boyle, T. J.; Lambert, T. N.; Daniel-Taylor, S. D.; Oliver, J. M.; Wilson, B. S.; Lidke, D. S.; Andrews, N. L., *Ieee T. Nanobiosci.* **2006,** *5* (4), 222-230.

16. Kanoun, M.; Busseret, C.; Poncet, A.; Souifi, A.; Baron, T.; Gautier, E., *Solid State Electron* **2006,** *50* (7-8), 1310-1314.

17. Sze, S. M., *Physics of semiconductor devices*. 2nd ed.; Wiley: New York, 1981; p xii, 868 p.

18. Takagahara, T.; Takeda, K., *Phys. Rev. B* **1992,** *46* (23), 15578-15581.

19. Melnikov, D. V.; Chelikowsky, J. R., *Solid State Commun.* **2003,** *127* (5), 361-365.

20. Warner, J. H.; Tilley, R. D., *Nanotechnology* **2006,** *17* (15), 3745-3749.

21. Guha, S.; Wall, M.; Chase, L. L., *Nucl. Instrum. Meth. B* **1999,** *147* (1-4), 367-372.

22. Maeda, Y.; Tsukamoto, N.; Yazawa, Y.; Kanemitsu, Y.; Masumoto, Y., *Appl. Phys. Lett.* **1991,** *59* (24), 3168-3170.

23. Wilcoxon, J. P.; Provencio, P. P.; Samara, G. A., *Phys. Rev. B* **2001,** *64* (3).

24. Gerion, D.; Zaitseva, N.; Saw, C.; Casula, M. F.; Fakra, S.; Van Buuren, T.; Galli, G., *Nano Lett.* **2004,** *4* (4), 597-602.

25. Lu, X. M.; Ziegler, K. J.; Ghezelbash, A.; Johnston, K. P.; Korgel, B. A., *Nano Lett.* **2004,** *4* (5), 969-974.

26. Kornowski, A.; Giersig, M.; Vogel, R.; Chemseddine, A.; Weller, H., *Adv. Mater.* **1993,** *5* (9), 634-636.

27. Gerung, H.; Bunge, S. D.; Boyle, T. J.; Brinker, C. J.; Han, S. M., *Chem. Commun.* **2005,** (14), 1914-1916.

28. Gerung, H.; Boyle, T. J.; Tribby, L. J.; Bunge, S. D.; Brinker, C. J.; Han, S. M., *J. Am. Chem. Soc.* **2006,** *128* (15), 5244-5250.

29. Boyle, T. J.; Tribby, L. J.; Ottley, L. A. M.; Han, S. M., *Eur. J. Inorg. Chem.* **2009,** (36), 5550-5560.

30. Subashi, E.; Rheingold, A. L.; Weinert, C. S., *Organometallics* **2006,** *25* (13), 3211-3219.

31. Hlina, J.; Baumgartner, J.; Marschner, C., *Organometallics* **2010,** *29* (21), 5289-5295.

32. Bhattacharjee, C. R.; Purkayastha, D. D.; Das, N., *Mater. Lett.* **2013,** *90*, 111-114.

33. Davar, F.; Salavati-Niasari, M.; Mir, N.; Saberyan, K.; Monemzadeh, M.; Ahmadi, E., *Polyhedron* **2010,** *29* (7), 1747-1753.

34. Nguyen, T. D.; Dinh, C. T.; Nguyen, D. T.; Do, T. O., *J. Phys. Chem. C* **2009,** *113* (43), 18584-18595.

35. Salavati-Niasari, M.; Dadkhah, M.; Davar, F., *Polyhedron* **2009,** *28* (14), 3005-3009.

36. Gerung, H.; Boyle, T. J.; Tribby, L. J.; Bunge, S. D.; Brinker, C. J.; Han, S. M., *J. Am. Chem. Soc.* **2006,** *128* (15), 5244-5250.

37. Polavarapu, L.; Xu, Q. H., *Nanotechnology* **2009,** *20* (18).

38. Ma, X. C.; Wu, F. Y.; Kauzlarich, S. M., *J. Solid State Chem.* **2008,** *181* (7), 1628-1633.

39. Chiu, H. W.; Chervin, C. N.; Kauzlarich, S. M., *Chem. Mater.* **2005,** *17* (19), 4858-4864.

40. Bearden, J. A.; Burr, A. F., *Rev. Mod. Phys.* **1967,** *39* (1), 125.

41. Cardona, M.; Ley, L., *Photoemission in solids*. Springer-Verlag: Berlin ; New York, 1978; p v.

42. Fuggle, J. C.; Martensson, N., *J. Electron Spectrosc.* **1980,** *21* (3), 275-281.

43. Manna, S.; Prtljaga, N.; Das, S.; Daldosso, N.; Ray, S. K.; Pavesi, L., *Nanotechnology* **2012,** *23* (6).

44. Galeener, F. L.; Leadbetter, A. J.; Stringfellow, M. W., *Phys. Rev. B* **1983,** *27* (2), 1052-1078.

45. Taylor, B. R.; Kauzlarich, S. M.; Delgado, G. R.; Lee, H. W. H., *Chem. Mater.* **1999,** *11* (9), 2493-2500.

46. Taylor, B. R.; Kauzlarich, S. M.; Lee, H. W. H.; Delgado, G. R., *Chem. Mater.* **1998,** *10* (1), 22-24.

47. Brus, L., *J. Phys. Chem.* **1986,** *90* (12), 2555-2560.

48. Zunger, A.; Wang, L. W., *Appl. Surf. Sci.* **1996,** *102*, 350-359.

49. Chou, N. H.; Oyler, K. D.; Motl, N. E.; Schaak, R. E., *Chem. Mater.* **2009,** *21* (18), 4105-4107.

50. Chiu, H. W.; Kauzlarich, S. M., *Chem. Mater.* **2006,** *18* (4), 1023-1028.

51. Hanrath, T.; Korgel, B. A., *J. Am. Chem. Soc.* **2004,** *126* (47), 15466-15472.

CHAPTER VI

SYNTHESIS, CHARACTERIZATION, AND PHOTOCHEMISTRY OF OLIGOGERMANES $R_3GeGePh_3$ AND $R_3Ge(GePh_2)_nGeR_3$ (n = 1, 2; R = *n*-butyl, ethyl)

6.1 Introduction

Catenated heavy group 14 element compounds exhibit σ-delocalization that results in interesting optical and electronic properties in these molecules. The electrons in the HOMO are delocalized across the element-element backbone rather than being localized in a formal two-center, two-electron bond.[1-3] The highest occupied molecular orbital (HOMO) of the heavy group 14 catenates is σ-bonding in nature due to the overlap of the diffuse sp^3 orbitals when they are configured in a *trans co-planar* conformation (**Figure 6.1**)[3] The σ-delocalization imparts properties to oligomeric germanium compounds having Ge-Ge single bonds that resemble those of conjugated unsaturated hydrocarbons even though they are structurally analogous to saturated hydrocarbons.[1-5]

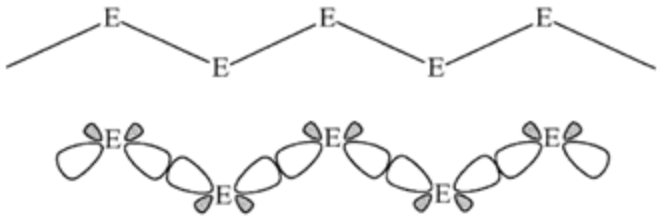

Figure 6.1: The σ-bonding HOMO in oligomeric group 14 compounds exhibited upon sequential *trans co-planar* conformations along the element-element backbone.[3]

The heavy group 14 catenates require the presence of organic side groups to stabilize the element-element bonds while their carbon-based congeners do not. Compounds with the general formula E_nH_{2n+2} (E = Si, Ge, Sn, Pb), which are the direct analogues of the alkanes, are generally highly reactive and often pyrophoric. The degree of σ-delocalization in these group 14 oligomers are directly related to their structure, where varying the number of catenated atoms or changing the organic side groups can have a detectable effect on their physical attributes. The HOMO/LUMO energy levels for catenated germanium compounds can be "coarse-tuned" by altering the length of the germanium-germanium backbone or they can be "fine-tuned" by altering the organic substituents bound to the germanium atoms. The germanium oligomers typically exhibit absorption maxima in the ultraviolet region and are electrochemically intriguing in that they display one or more irreversible oxidation waves in their cyclic voltammograms.[6-13]

The synthesis, properties, and chemistry of the heavy group 14 catenates containing silicon[14-22] and tin[23-39] are well developed, but those of the germanium[4-5, 40-44] analogues are much less understood. While discrete oligomeric compounds containing germanium-germanium single bonds have been known since 1925,[4-13, 45] detailed investigations of their properties and reactivity have been hampered due to the available synthetic methods being complicated by low yields and/or the formation of product mixtures. These mixtures are difficult to separate because the

oligogermanes are air and moisture sensitive, and thus the separation must be conducted under an inert atmosphere of nitrogen or argon.

The most common methods for the preparation of oligogermanes include the Wurtz-type coupling of organogermanium halides using alkali metals,[46] the mercuration and demercuration of germyl mercury compounds,[47-48] nucleophilic substitution reactions involving a triorganogermanium anion and an organogermanium halide,[49] and the action of Grignard reagents on germanium(IV) halides[50] (**Scheme 6.1**). The formation of triorganogermanium anions used in nucleophilic substitution reactions is unique to germanium chemistry because metallation by organolithium reagents can be achieved by the removal of a hydrogen atom from triorganogermanes to yield triorganogermanum anions, and this does not occur for silicon or tin compounds.[51]

I) Wurtz-type coupling:[46]

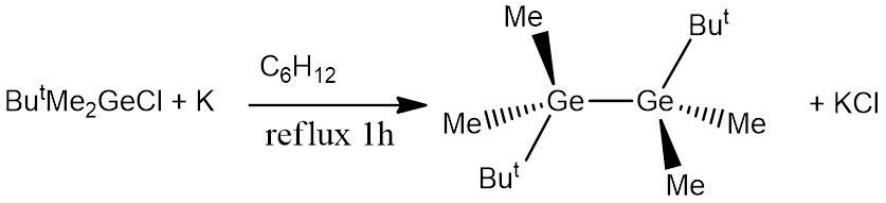

II) Mercuration/demercuration of germyl mercury compounds:[47-48]

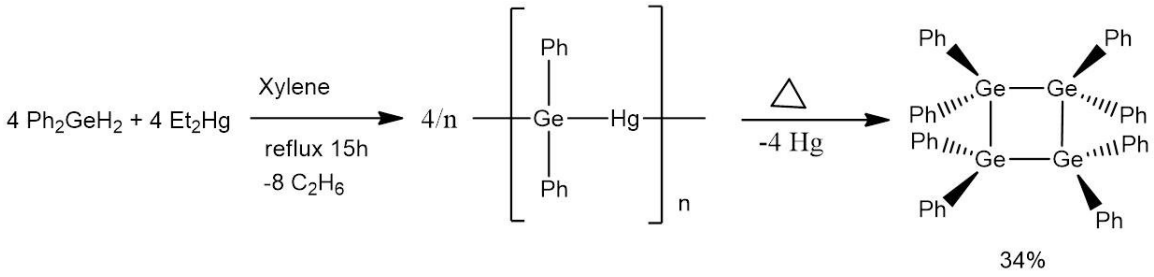

III) Nucleophilic reactions of germyl anions:[49, 51]

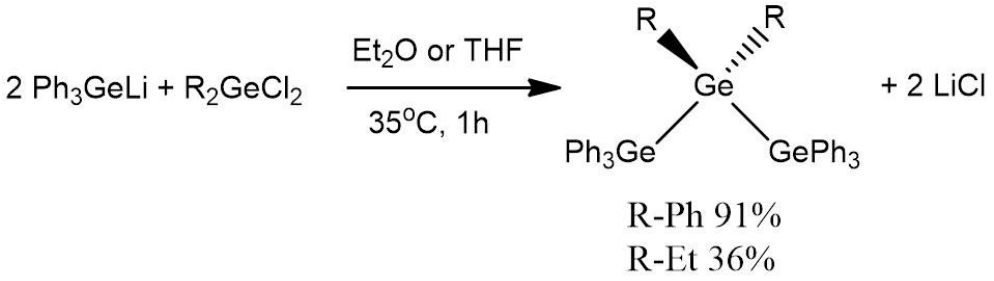

IV) Action of Grignard reagents on germanium (IV) halides:[50]

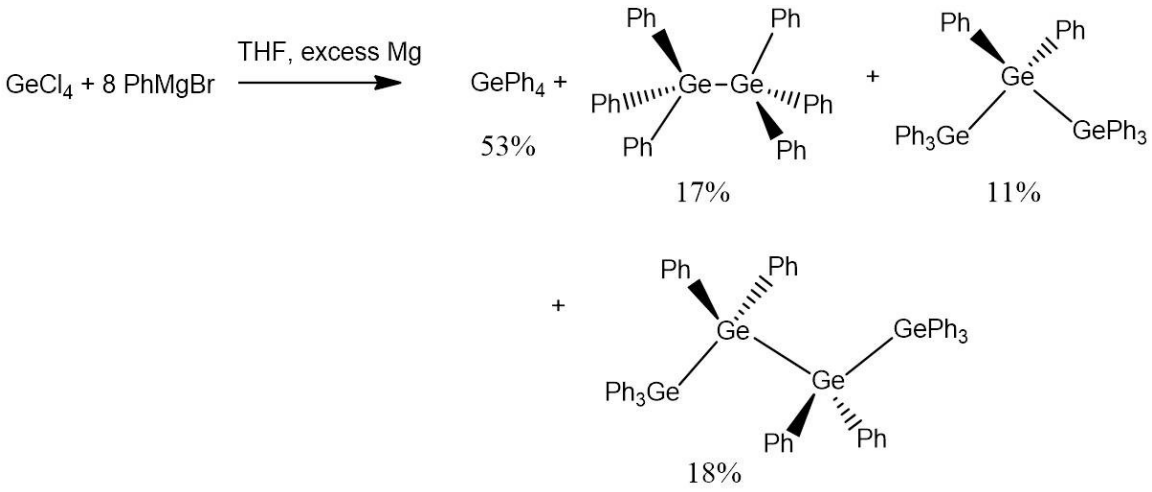

Scheme 6.1: Reaction schemes of the most common preparative methods for oligogermanes.

The most in depth investigations utilizing these methods for the synthesis of oligogermanes having single germanium-germanium bonds were reported in the 1980s by Dräger and co-workers in a series of nineteen publications in which they described the reactivity, spectra, and structures of several germanium catenates having between two and six germanium atoms in the germanium-germanium backbone.[50, 52-69] In 1995 it was reported that using samarium(II)

iodide as a mild one electron reducing agent could produce discrete oligogermanes in good to excellent yields (**Table 6.1**).[70-71]

Table 6.1: Reaction scheme for synthesis of oligogermanes using SmI_2 and experimental data.[71]

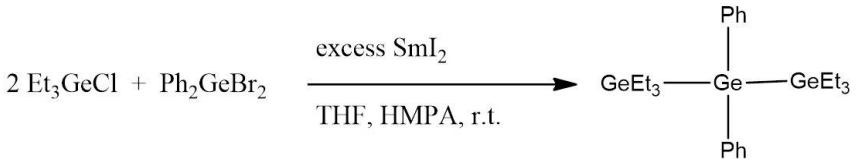

Product	Conditions[a]	Yield(%)	Product	Conditions[a]	Yield(%)
$Et_3GeGePh_2GeEt_3$	A	94	$Me_3GeGePh_2GeMe_3$	A	87
$Et_3GeGePh_2GeEt_3$	B	90	$^{n}Bu_3GeGePh_2Ge^{n}Bu_3$	B	87
$Et_3GeGePh_2GeEt_3$	C	89	$^{i}Pr_3GeGePh_2Ge^{i}Pr_3$	A	30
$Et_3GeGePh_2GeEt_3$	D	83	$Et_3GeGeMePhGeEt_3$	A	70
$Et_3GeGePh_2GeEt_3$	E	74			

[a] A, THF solutions of substrates were reacted for 3 h at rt., c= 0.6 mmol dm^{-3}, B, c = 3 mmol dm^{-3}, C, c = 15 mmol dm^{-3}, D, THF solutions of substrates were reacted for 1 h. E, reaction carried out at 0 ^{o}C.

The hydrogermolysis reaction is the reaction of a germanium amide and a germanium hydride to yield germanium-germanium bonds. Previously this reaction was thought to only proceed with the use of an "activated" germanium hydride such as $(C_6F_5)_3GeH$ (**Scheme 6.2**).[72]

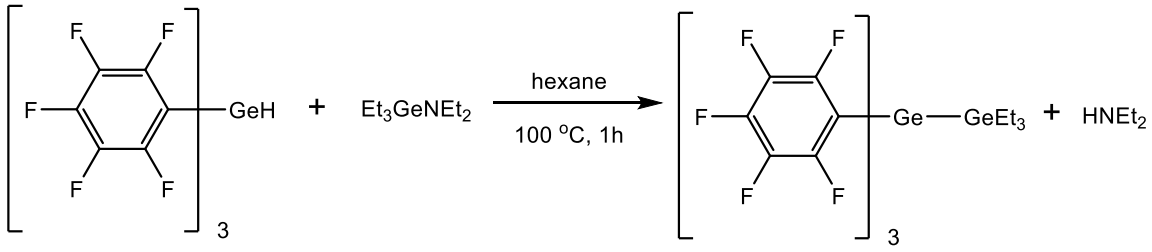

Scheme 6.2: Hydrogermolysis reaction using an "activated" germanium hydride and a germanium amide.[72]

Later in 2006, Weinert and co-workers began investigating the hydrogermolysis reaction to determine its potential to form germanium-germanium bonds.[73] Initial studies directed at using the hydrogermolysis reaction for germanium-germanium bond formation began by reacting $^{n}Bu_3GeNMe_2$ with Ph_3GeH in an equimolar ratio using benzene as the solvent at room temperature but there was not any formation of the digermane $^{n}Bu_3GeGePh_3$ detected. Other attempts were made with the same amide and hydride using refluxing benzene or toluene for up to one week still with no product formation. It wasn't until refluxing acetonitrile was used as the solvent that the digermane $^{n}Bu_3GeGePh_3$ was obtained in 83% yield with a reaction time of 48 hours. Germanium amides were shown to react with acetonitrile to give an α-germyl nitrile R_3GeCH_2CN that contains a reactive Ge-C bond **Scheme 6.3**.[74-76] Bisgermylnitriles $(R_3Ge)_2CHCN$ can also be formed, and the generation of these germylnitriles can be catalyzed by the addition of small amounts of Lewis acids such as $ZnCl_2$ to the reaction mixture. In order to determine if an intermediate such as an α-germyl nitrile plays a role in the formation of germanium-germanium bonds, the hydrogermolysis reaction was repeated using $^{n}Bu_3GeNMe_2$ and Ph_3GeH in acetonitrile-d_3 solvent and monitored by ^{1}H NMR spectroscopy. The observed pathway is shown below in **Scheme 6.4**.[73]

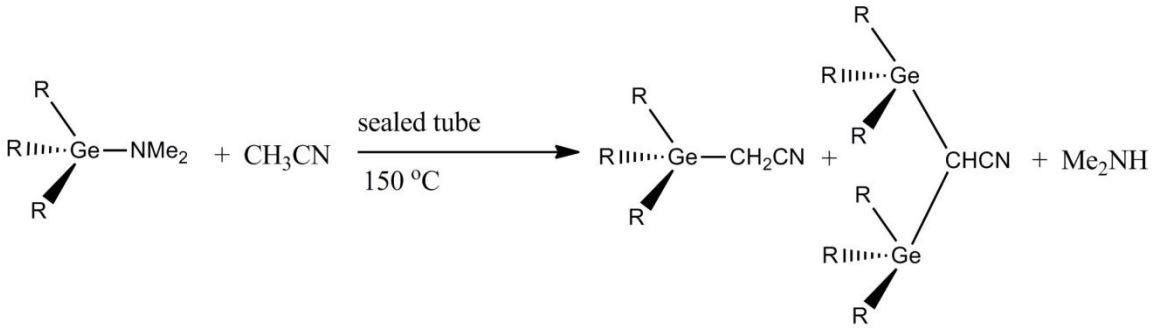

Scheme 6.3: Formation of an α-germyl nitrile R_3GeCH_2CN from the reaction of R_3GeNMe_2 with acetonitrile.[74]

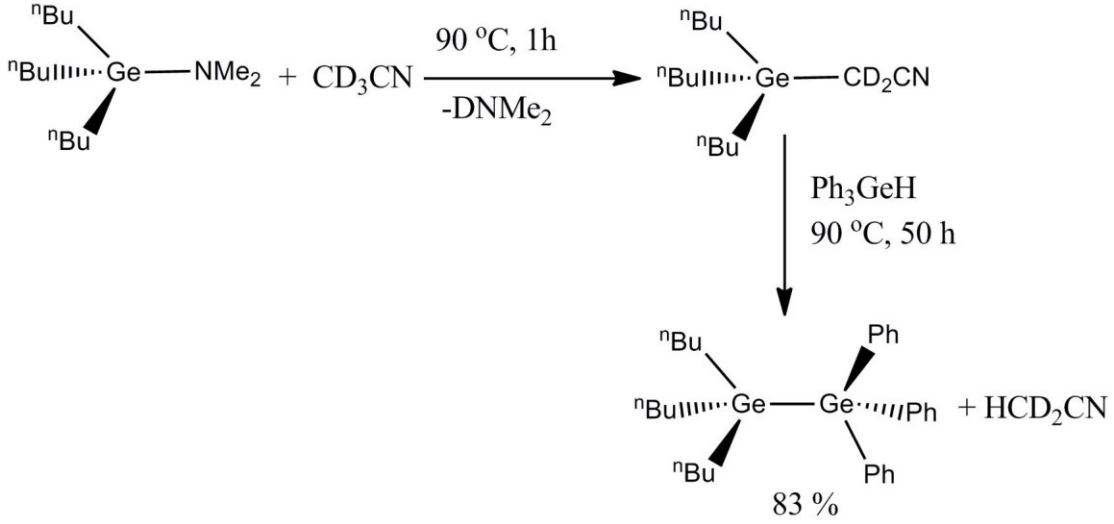

Scheme 6.4: Observed pathway of the hydrogermolysis reaction of $^{n}Bu_3GeNMe_2$ with Ph_3GeH in CD_3CN.[73]

The reaction was monitored by ^{1}H and ^{13}C NMR spectroscopy, which clearly showed the formation of tributyl α-germyl nitrile $Bu^{n}{}_3GeCH_2CN$ and then its disappearance upon addition of Ph_3GeH. The formation of HCD_2CN was also confirmed spectroscopically.[73]

In order to fully ascertain if an α-germyl nitrile is a crucial intermediate in the germanium-germanium bond forming process, the α-nitrile $^{n}Bu_3GeCH_2CN$ was synthesized directly. In order to do this, acetonitrile was first lithiated using $LiN^{i}Pr_2$ to which $^{n}Bu_3GeCl$ was added to form $^{n}Bu_3GeCH_2CN$ (**Scheme 6.5**).[73]

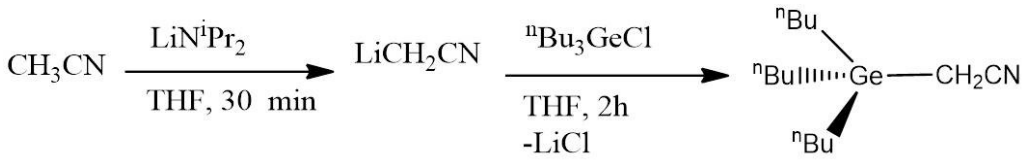

Scheme 6.5: Direct synthesis of the α-germylated nitrile $^{n}Bu_3GeCH_2CN$.[73]

The α-germyl nitrile $^{n}Bu_3GeCH_2CN$ was then added directly to one equivalent of Ph_3GeH in CD_3CN and the reaction was monitored by ^{1}H and ^{13}C NMR spectroscopy. Signals for the formation of $^{n}Bu_3GeGePh_3$ were clearly visible in the ^{1}H and ^{13} C NMR spectra after only ten minutes. Upon heating the sample at 90 ^{o}C there was complete consumption of Ph_3GeH and quantitative formation of $^{n}Bu_3GeGePh_3$ in 50 minutes. The product was obtained on a preparative scale under the same conditions and was isolated in 89 % yield (**Scheme 6.6**).[73] It was found that acetonitrile is essential for this reaction to proceed since the $^{n}Bu_3GeCH_2CN$ did not react with Ph_3GeH in toluene even with the addition of a catalytic amount of acetonitrile. This indicates that the acetonitrile is not only playing the role of solvent but it is also a reagent that reacts with the germanium amide to form the α-germyl nitrile. The α-germyl nitrile is the key component to the success of the germanium-germanium bond forming process. [73]

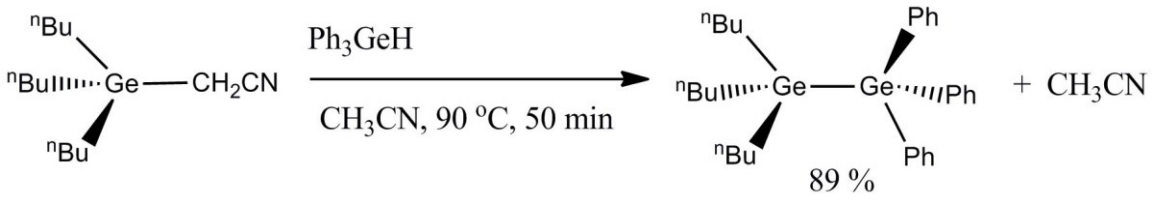

Scheme 6.6: Hydrogermolysis reaction of $^{n}Bu_3CH_2CN$ with Ph_3GeH in CH_3CN to form the digermane $^{n}Bu_3GeGePh_3$.[73]

The hydrogermolysis reaction offers several advantages over previously employed methods including generally improved yields, the formation of discrete compounds rather than unwanted product mixtures, and when combined with a hydride protection/deprotection strategy, the germanium atoms can be added step-wise to the chain one at a time offering direct control over the possible organic side group substituent pattern. Therefore, the hydrogermolysis reaction allows for the preparation of germanium oligomers with varying chain lengths and a diverse range of substitution patterns, where the latter allows for the fine-tuning of molecules that can exhibit certain desired optical and electronic properties.

Previously, it has been shown that the optical and electronic properties of oligogermanes can be tuned by altering the germanium-germanium chain length and/or by changing the organic substituents bound to the germanium atoms.[5-6, 77] To observe these changes UV/visible spectroscopy is utilized to monitor the absorbance maxima of these compounds and differential pulse voltammetry (DPV) is utilized to monitor the oxidation potentials in these systems. The electronic transition occurring in the UV/visible spectra of the oligogermanes is typically the promotion of an electron from the HOMO to the LUMO which is a σ-σ^* electronic transition. It was previously observed that increasing the amount of germanium-germanium catenation results in a red shift in the UV/visible spectrum and having more electron donating organic substituents

on the germanium atoms leads to a decrease in the oxidation potentials of these compounds.[6] This indicates that the HOMO/LUMO gap is decreasing with an increase in catenation and an increase in electron donating ability of the organic groups.

Initially, cyclic voltammetry (CV) was utilized in lieu of DPV, but the voltammograms that were obtained lacked distinct peaks unless a high concentration of germane is used. DPV was used since it has a higher sensitivity, which leads to voltammograms having well-defined peaks and allows for the use of smaller sample sizes. DPV has a higher sensitivity than CV because the charging current is suppressed. Both methods produce two forms of current when voltage is applied. These are the charging current and the faradaic current which is the current generated by the oxidation of the sample, and the faradaic current can more easily be observed with suppression of the charging current. CV applies a continuous changing potential while at the same time continually measuring the current without the suppression of the charging current. In contrast, DPV applies a rectangular pulse potential where the current is measured only before the pulse and after the pulse. Therefore, since the current measurement is made only during the last part of the pulse, the charging current has an opportunity to decay to zero and the only current that is measured is a result of the faradaic current.[78] This allows the detection limit for DPV to be 10^{-8} M which is three orders of magnitude higher than the 10^{-5} M detection limit for CV.

Sections **6.2-6.3** of this chapter will focus on the properties of the two previously known digermanes $Et_3GeGePh_3$ and $^nBu_3GeGePh_3$, the synthesis of the two new trigermanes $Et_3GeGePh_2GeEt_3$ and $^nBu_3GeGePh_2Ge^nBu_3$, and the two new tetragermanes $Et_3Ge(GePh_2)_2GeEt_3$ and $^nBu_3Ge(GePh_2)_2Ge^nBu_3$ along with an analysis of their structures, optical and electronic properties which were probed using UV/visible spectroscopy and differential pulse voltammetry where the values provided for the DPVs are an average of four independent scans. Sections **6.4.1-6.4.3** of this chapter will introduce and discuss the photolysis of the six oligogermanes listed above.

6.2 Results and Discussion

In order to effectively synthesize the tetragermanes $Et_3Ge(GePh_2)_2GeEt_3$ and $^nBu_3Ge(GePh_2)_2Ge^nBu_3$, an efficient method for the preparation of starting materials was necessary. One of the starting materials is 1,2-dichloro-1,1,2,2-tetraphenyl digermane $ClPh_2GeGePh_2Cl$ (**1**). Compound **1** has been previously synthesized with some preparative complications resulting in an isolation step following each subsequent reaction.[8] By altering some of the literature methods, it can be synthesized in a pure and facile fashion with good yields. It was prepared by using hexaphenyldigermane $Ph_3GeGePh_3$ and adding four equivalents of trichloroacetic acid Cl_3COOH in toluene and heating at 110 ^oC for four days followed by the direct addition of two equivalents of ethereal hydrochloric acid $HCl_{(ether)}$ to the toluene solution and then stirring for an additional 18 hours in a sealed tube. The volatiles are then removed *in vacuo* and the re-formed Cl_3CCOOH and other impurities are removed by washing with hexane three times and then removing any volatiles *in vacuo* to yield $ClPh_2GeGePh_2Cl$ in 53% yield (**Scheme 6.7**). By utilizing this method it is no longer necessary to isolate $Cl_3CCOOPh_2Ge$-$GePh_2OOCCCl_3$ which results in a higher overall yield for the reaction and it is no longer necessary to perform the washing and filtration steps after each step.

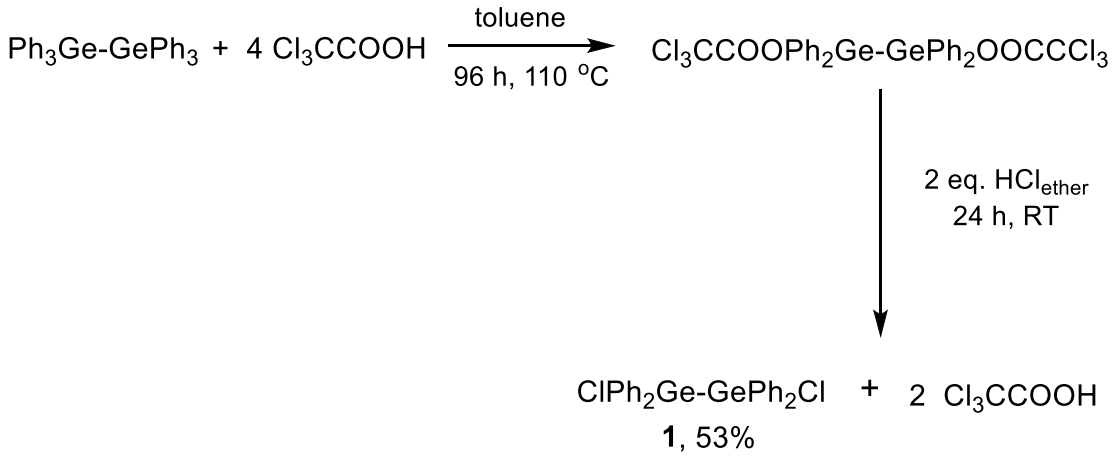

Scheme 6.7: Synthesis of $ClPh_2GeGePh_2Cl$ (**1**).

The ^{1}H NMR spectrum of $ClPh_2GeGePh_2Cl$ (**1**) taken in benzene-d_6 contains only multiplets in the aromatic region. There is a multiplet at δ 7.77-7.73 ppm which corresponds to the eight *meta*-C_6H_5 protons and a multiplet at δ 7.03-6.99 ppm corresponding to the 8 *meta*- and 4 *para*-C_6H_5 protons. The ^{13}C NMR spectrum contains all four phenyl carbon resonances at δ 135.8, 134.1, 130.8, and 129.1 corresponding to the *ipso*-, *ortho*-, *meta*-, and *para*- carbons of the phenyl groups respectively. The X-ray crystal structure of $ClPh_2GeGePh_2Cl$ (**1**) was obtained (**Figure 6.2**). The structure contains two unique molecules in the unit cell where Molecule 1 is not disordered while in Molecule 2 the two germanium atoms and the two chlorine atoms are disordered over two sites each with 50 % occupancy. Selected bond distances and angles are provided below in **Table 6.2**. The Ge-Ge bond distance is 2.4269(9) Å for Molecule 1 and 2.409(5) Å for Molecule 2. Since Molecule 1 is not disordered, its Ge-Ge bond distance will be used for comparisons. The Ge-Ge bond length of $ClPh_2GeGePh_2Cl$ (**1**) is typical for Ge-Ge bond distances in oligogermanes. Hexaphenyldigermane Ph_3Ge-$GePh_3$ has a Ge-Ge bond distance of 2.446(1) Å which is slightly longer than that of $ClPh_2GeGePh_2Cl$ (**1**) which is to be expected upon the substitution of two phenyl groups for two electronegative and smaller chlorine atoms. This is due to electron density being pulled away from the two germanium atoms by the electronegative chlorine atoms and because they are less sterically hindering than the phenyl groups, the germanium atoms can come closer together.

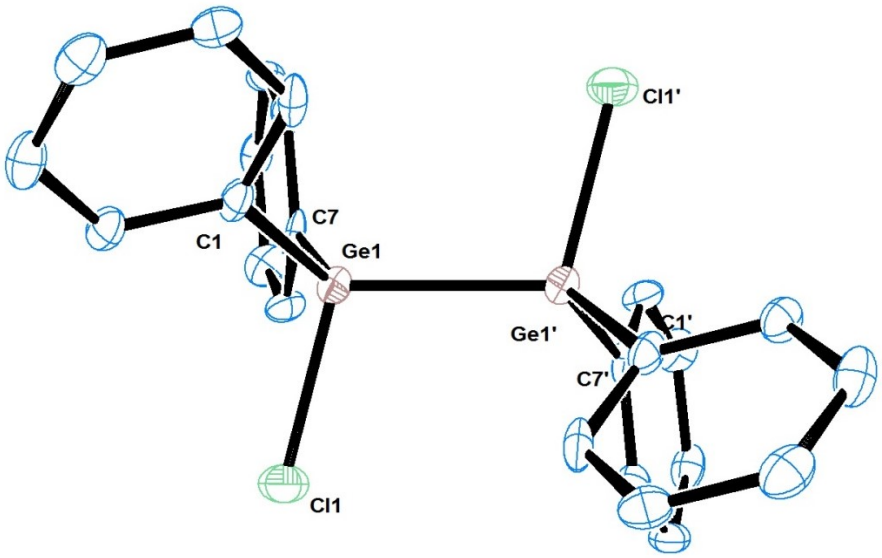

Molecule 1

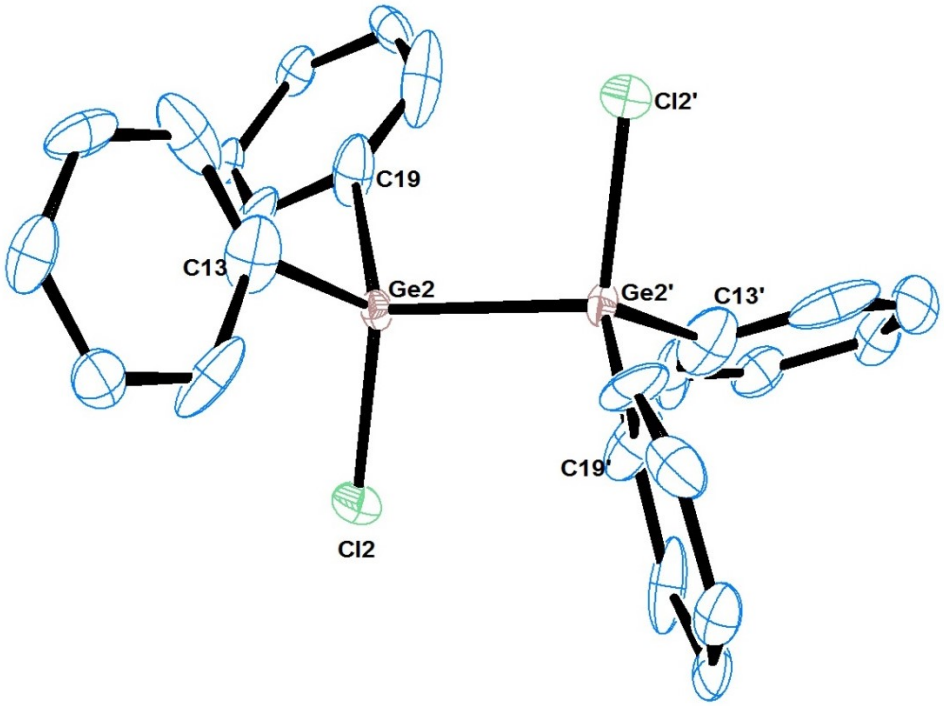

Molecule 2

Figure 6.2: X-ray crystal structure of $ClPh_2GeGePh_2Cl$ (**1**): Molecule 1 (top) and Molecule 2 (bottom).

Molecule 1

Bond Lengths	Å	Bond Angles	°
Ge(1) - Ge(1')	2.4269(9)	Ge(1') - Ge(1) - Cl(1)	104.64(6)
Ge(1) - Cl(1)	2.190(2)	Ge(1') - Ge(1) - C(1)	117.0(3)
Ge(1) - C(1)	1.923(8)	Ge(1') - Ge(1) - C(7)	108.0(3)
Ge(1) - C(7)	1.970(8)	Cl(1) - Ge(1) - C(1)	107.3(3)
		Cl(1) - Ge(1) - C(7)	105.2(3)

Molecule 2

Bond Lengths	Å	Bond Angles	°
Ge(2) - Ge(2')	2.409(5)	Ge(2') - Ge(2) - Cl(2)	102.9(3)
Ge(2) - Cl(2)	2.176(4)	Ge(2') - Ge(2) - C(13)	121.9(3)
Ge(2) - C(13)	2.06(1)	Ge(2') - Ge(2) - C(19)	122.0(3)
Ge(2) - C(19)	2.057(9)	Cl(2) - Ge(2) - C(13)	116.3(3)
		Cl(2) - Ge(2) - C(19)	116.5(3)

Table 6.2: Selected bond distances and angles for $ClPh_2GeGePh_2Cl$ (**1**): Molecule 1 (top), Molecule 2 (bottom).

The dichloride $ClPh_2GeGePh_2Cl$ (**1**) can be converted into the 1,2-dihydride $HPh_2GeGePh_2H$ (**2**) by adding two equivalents of $LiAlH_4$ to **1** in THF. The reaction is allowed to stir overnight and since the digermane product contains a moisture sensitive germanium-germanium bond, the typical work-up with water cannot be carried out. Instead, the solvent is removed *in vacuo* and then benzene is added to the product to dissolve **2**. The benzene solution is heated to 60 °C in a warm water bath and then cannulated through a fritted filter containing celite that removes the byproducts. Compound **2** is then isolated after the removal of volatiles *in vacuo* (**Scheme 6.8**).

$$ClPh_2Ge\text{-}GePh_2Cl + 2\ LiAlH_4 \xrightarrow[24h,\ 25^oC]{THF} HPh_2Ge\text{-}GePh_2H$$
2

Scheme 6.8: Synthesis of $HPh_2GeGePh_2H$ (**2**).

The ^{1}H NMR spectrum of $HPh_2GeGePh_2H$ (**2**) in benzene-d_6 contains a singlet at δ 5.57 ppm corresponding to the two germanium bound hydrogen atoms. The aromatic protons appear as two multiplets. There is a multiplet at δ 7.52-7.49 ppm which corresponds to the eight *meta*-C_6H_5 protons and a multiplet at δ 7.07-7.04 ppm corresponding to the 12 *ortho*- and *para*-C_6H_5 protons (**Figure 6.3**). The *meta*- protons are shifted upfield from their counterparts in $ClPh_2GeGePh_2Cl$ (**1**), and this is expected since the two chloride atoms have been replaced with two less electronegative hydrogen atoms. The ^{13}C NMR spectrum is lacking a signal for the *ipso*- carbon but the other phenyl carbon resonances appear at δ 135.7, 129.1, and 128.7 corresponding to the *ortho*-, *meta*-, and *para*- carbons of the phenyl groups respectively (**Figure 6.3**).

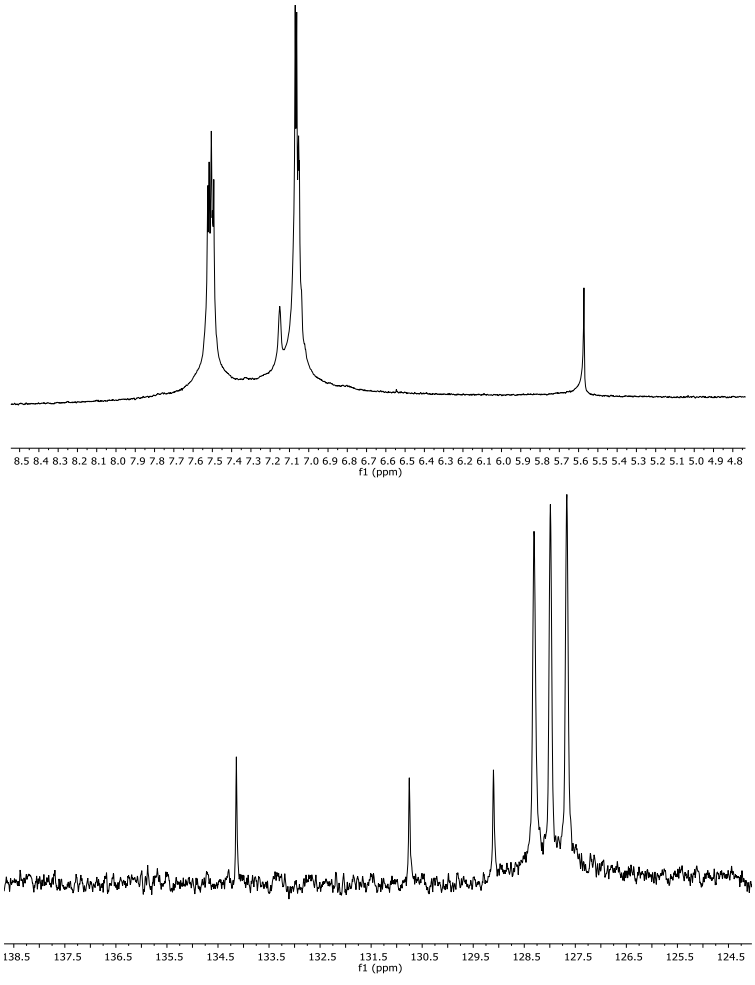

Figure 6.3: ^{1}H (top) and ^{13}C (bottom) NMR spectra in benzene-d_6 for $HPh_2GeGePh_2H$ (**2**).

In the process of synthesizing $ClPh_2GeGePh_2Cl$ (**1**), if the first step is not allowed to proceed for a full four days, a mixture of chlorides is obtained, where both the mono-chloride $ClPh_2GeGePh_3$ and **1** are formed. This is most easily observed in the ^1H NMR spectrum of the product after the chlorides have been converted to the hydrides which results in the mono-hydride $HPh_2GeGePh_3$ (**3**) as a minor product and the 1,2-dihydride **2**. In the ^1H NMR spectrum of the mixture of **2** and **3** the hydride peak for **3** appears at δ 5.72 ppm (**Figure 6.4**). This peak appears downfield from the hydride peak for the dihydride **2** which is to be expected since one of the hydrogen atoms attached to a germanium atom in **2** is replaced with a more electron withdrawing phenyl group. The X-ray crystal structure of **3** (**Figure 6.5**) was obtained during attempts to try and separate the two hydrides by crystallization methods. Selected bond distances and angles are provided below in **Table 6.3**. There were two crystals of **3** that were analyzed via X-ray crystallography. One crystal contained one molecule that has one germanium atom disordered over two positions with occupancies of 97% and 3%. The second crystal contained three unique molecules in the unit cell which each contained a similar disordered orientation, but with less than three percent occupancy for the germanium atoms, but is omitted for clarity. Several attempts were made to synthesize **3** in pure form but these were unsuccessful.[49]

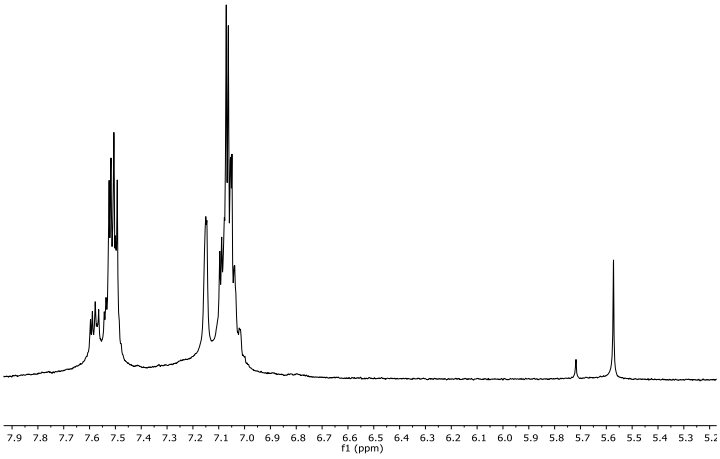

Figure 6.4: ^1H NMR spectra in benzene-d_6 of the mixture of $HPh_2GeGePh_2H$ (**2**) and $HPh_2GeGePh_3$ (**3**).

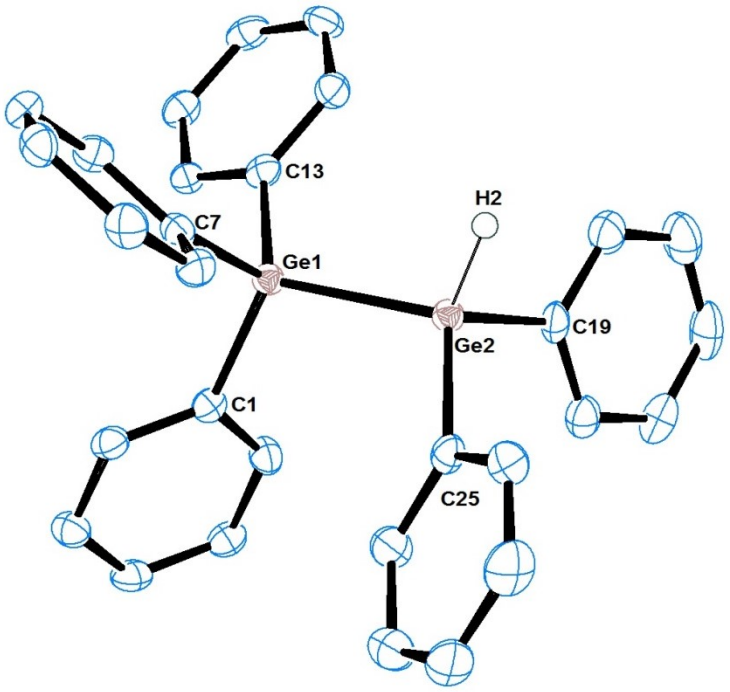

Crystal 1

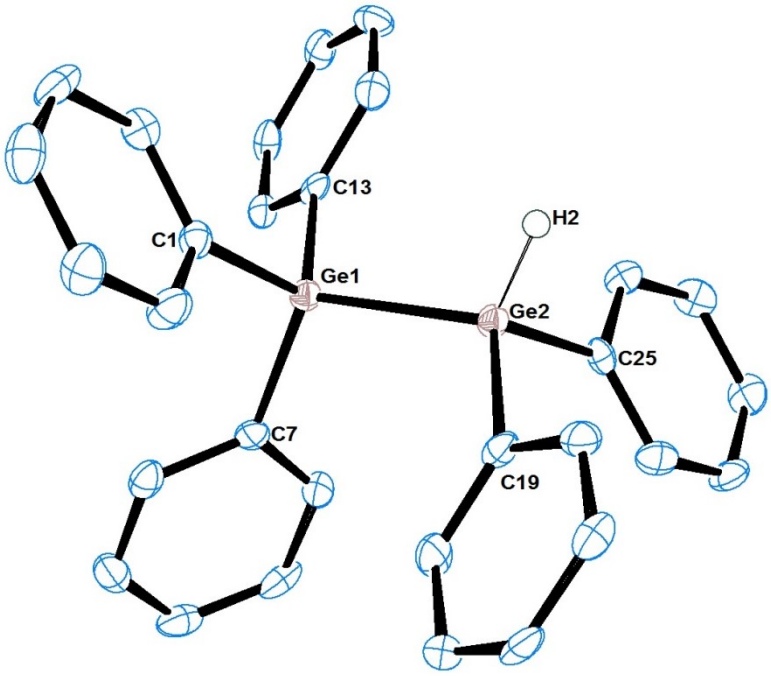

Crystal 2 Molecule 1

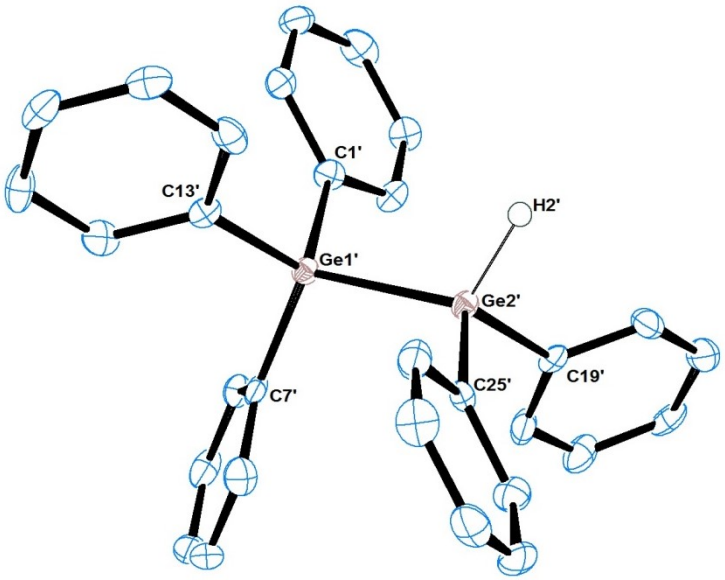

Crystal 2 Molecule 2

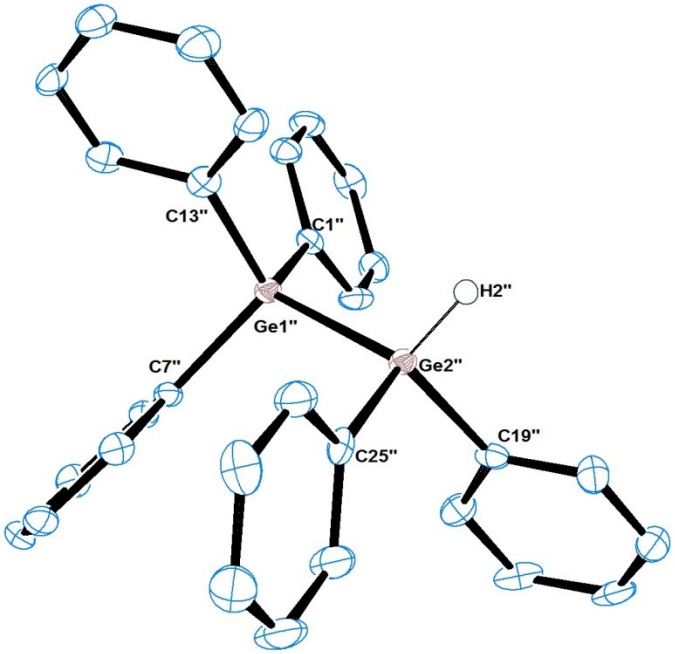

Crystal 2 Molecule 3

Figure 6.5: X-ray crystal structure of $HPh_2GeGePh_3$ (**3**) generated from CIF files of two individual crystals: Crystal 1 (top) Crystal 2 (bottom three molecules).

Table 6.3: Selected bond distances and angles (averaged for Crystal 2) for $HPh_2GeGePh_3$ (**3**): Crystal 1 (top) Crystal 2 (bottom).

Crystal 1

Bond Lengths	Å	Bond Angles	°
Ge(1) - Ge(2)	2.4213(6)	C(1) - Ge(1) - Ge(2)	110.3(1)
Ge(1) - C(1)	1.958(4)	C(1) - Ge(1) - C(7)	110.5(1)
Ge(1) - C(7)	1.951(4)	C(1) - Ge(1) - C(13)	107.1(2)
Ge(1) - C(13)	1.953(3)	Ge(1) - Ge(2) - H(2)	109(2)
Ge(2) - C(19)	1.956(4)	Ge(1) - Ge(2) - C(19)	115.9(1)
Ge(2) - C(25)	1.954(4)	Ge(1) - Ge(2) - C(25)	108.9(1)
Ge(2) - H(2)	1.49(4)	C(19) - Ge(2) - H(2)	106(2)
		C(19) - Ge(2) - C(25)	106(2)

Crystal 2

Bond Lengths	Å	Bond Angles	°
Ge(1) - Ge(2)	2.4234(7)	C(1) - Ge(1) - Ge(2)	110.0(1)
Ge(1) - C(1)	1.949(4)	C(1) - Ge(1) - C(7)	108.9(2)
Ge(1) - C(7)	1.958(4)	C(1) - Ge(1) - C(13)	109.5(2)
Ge(1) - C(13)	1.958(4)	Ge(1) - Ge(2) - H(2)	115.1(2)
Ge(2) - C(19)	1.967(4)	Ge(1) - Ge(2) - C(19)	113.2(1)
Ge(2) - C(25)	1.953(4)	Ge(1) - Ge(2) - C(25)	111.4(1)
Ge(2) - H(2)	1.38(4)	C(19) - Ge(2) - H(2)	103.6(2)
		C(19) - Ge(2) - C(25)	108.4(2)

Since $HPh_2GeGePh_2H$ (**2**) can now be easily prepared, we could proceed with the synthesis of the tetragermanes $Et_3Ge(GePh_2)_2GeEt_3$ and $^nBu_3Ge(GePh_2)_2Ge^nBu_3$.

The series of oligogermanes that were prepared for this investigation includes a total of six oligogermanes. These include the digermanes $Et_3GeGePh_3$ (**4**) and $^nBu_3GeGePh_3$ (**5**), the two trigermanes $Et_3GeGePh_2GeEt_3$ (**6**) and $^nBu_3GeGePh_2Ge^nBu_3$ (**7**), and the two new tetragermanes $Et_3Ge(GePh_2)_2GeEt_3$ (**8**) and $^nBu_3Ge(GePh_2)_2Ge^nBu_3$ (**9**). All six of these compounds were synthesized using the hydrogermolysis reaction.

1,1,1-triethyl-2,2,2-triphenyl digermane - $Et_3GeGePh_3$ (4) and

1,1,1-tri-n-butyl-2,2,2-triphenyl digermane – $Bu^n{}_3GeGePh_3$ (5)

The digermanes **4** and **5** were synthesized following literature methods.[73] Both of these digermanes were synthesized using the corresponding germanium amide R_3GeNMe_2 (R = Et or ^{n}Bu) and triphenylgermanium hydride Ph_3GeH via the hydrogermolysis reaction in acetonitrile solvent (**Scheme 6.9**).[73] Their reported absorption maxima, oxidation potentials and germanium-germanium bond lengths are provided below in **Table 6.4**.[73] An interesting structural feature of the digermanes $Et_3GeGePh_3$ (**4**) and $Me_3GeGePh_3$ is that the alkyl groups and the phenyl groups are eclipsed rather than the expected staggered geometry, and this results in a longer than expected germanium-germanium bond length.

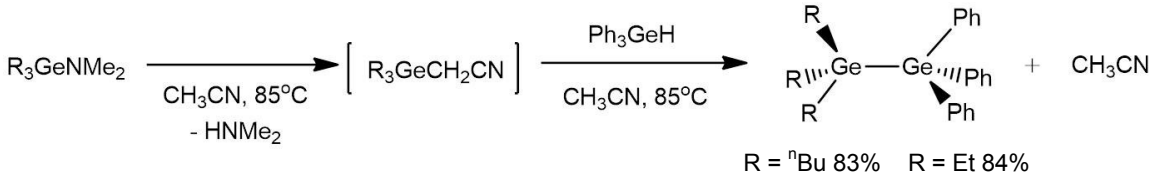

Scheme 6.9: Synthesis of the digermanes $Et_3GeGePh_3$ (**4**) and $^nBu_3GeGePh_3$ (**5**) via the hydrogermolysis reaction.[73]

Digermane	λ_{max}	E_{ox} (mV)	d(Ge-Ge) Å
Et_3Ge-$GePh_3$ (**4**)	231 nm	1587 ± 17	2.4253(7)
$Bu^n{}_3Ge$-$GePh_3$ (**5**)	232 nm	1588 ± 11	2.4212(8)

Table 6.4: Absorption maxima, oxidation potentials, and germanium-germanium bond lengths for digermanes $Et_3GeGePh_3$ (**4**) and $^nBu_3GeGePh_3$ (**5**).[73]

1,1,1,3,3,3-hexaethyl-2,2-diphenyl trigermane - Et_3Ge-$GePh_2$-$GeEt_3$ (6)

The synthesis of $Et_3GeGePh_2GeEt_3$ (**6**) has been previously described using samarium(II) iodide as the reductant,[70-71] however we synthesized **6** using the hydrogermolysis reaction. The trigermane $Et_3GeGePh_2GeEt_3$ (**6**) was synthesized by adding one equivalent of $LiNMe_2$ to Et_3GeCl in THF to yield Et_3GeNMe_2. The triethyl amide is volatile and so the THF was removed by distillation under an atmosphere of nitrogen. Hexane was added to the remaining product and it was then filtered through a frit with celite to remove LiCl from the product mixture. The remaining hexane was then removed via distillation to yield the Et_3GeNMe_2. Next, two equivalents of the Et_3GeNMe_2 were added to one equivalent of diphenylgermanium dihydride Ph_2GeH_2 in acetonitrile and the solution was heated in a sealed tube at 85 ^oC for 48 hours. The volatiles were removed *in vacuo* to yield $Et_3GeGePh_2GeEt_3$ (**6**) in 82% yield as a clear liquid (**Scheme 6.10**). The NMR data obtained was consistent with the original synthesis.[71] Compound **6** was also characterized using UV/visible spectroscopy and DPV, and the results are provided below in **Figures 6.6** and **6.7** respectively. The λ_{max} observed for **6** is at 247 nm which is red-shifted when compared to the digermanes $Et_3GeGePh_3$ (**4**) and $^nBu_3GeGePh_3$ (**5**). There are two oxidation waves in the DPV corresponding to irreversible oxidation processes, and this corresponds to the expected n-1 pattern where n is the number of germanium atoms. This is observed for other oligogermanes as well, and it has been postulated that either germylene extrusion and/or radical formation are occurring as competing processes.[8, 79-80] The two oxidation waves observed for $Et_3GeGePh_2GeEt_3$ (**6**) in the DPV are at 1350 mV and 1535 mV, where the first oxidation potential is lower than the oxidation potential for $Et_3GeGePh_3$ (**4**) indicating that the trigermane is easier to oxidize, which is expected as the degree of catenation increases.

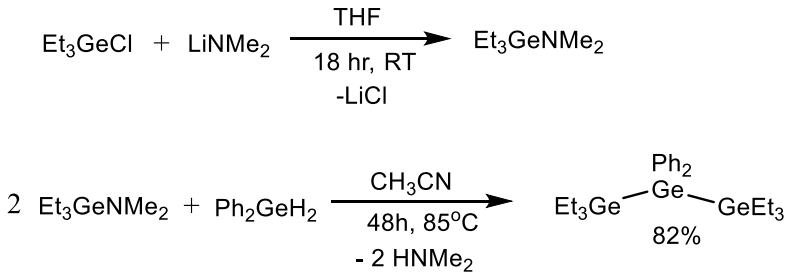

Scheme 6.10: Synthesis of $Et_3Ge\text{-}GePh_2\text{-}GeEt_3$ (**6**) via the hydrogermolysis reaction.

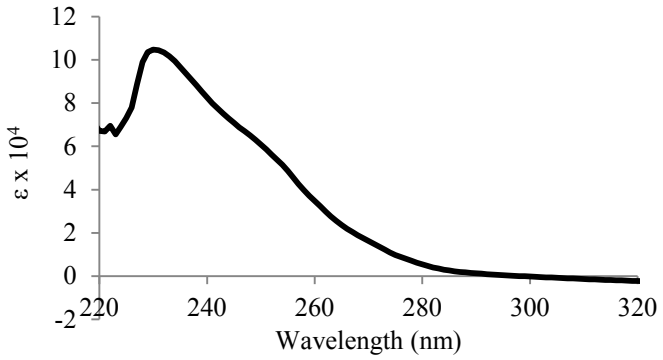

Figure 6.6: UV/visible spectrum of $Et_3GeGePh_2GeEt_3$ (**6**) in hexane. (λ_{max} = 247 nm, c = 4.995 x 10^{-6} M, and ε = 6.70 x 10^4 $M^{-1}cm^{-1}$)

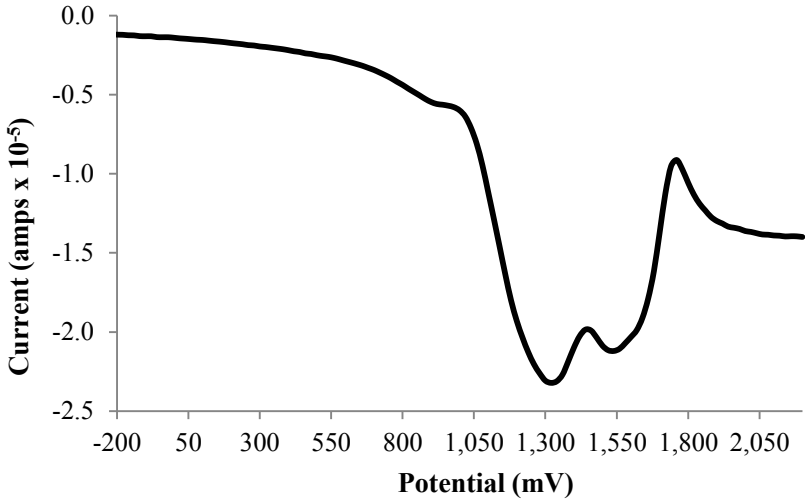

Figure 6.7: DPV of $Et_3GeGePh_2GeEt_3$ (**6**) in CH_2Cl_2. (E_{ox} = 1350 ± 12 mV and 1535 ± 10 mV)

1,1,1,3,3,3-hexa-n-butyl-2,2-diphenyl trigermane - Bu^n_3Ge-$GePh_2$-$GeBu^n_3$ (7)

The synthesis of Bu^n_3Ge-$GePh_2$-$GeBu^n_3$ (**7**) has been previously described using samarium(II) iodide as the reductant,[71] however **7** could also be synthesized using the hydrogermolysis reaction. The trigermane **7** was prepared by adding one equivalent of $LiNMe_2$ to Bu^n_3GeCl in benzene. The resulting solution was then filtered through a frit with celite to remove LiCl from the product mixture. The volatiles were then removed *in vacuo* to yield $Bu^n_3GeNMe_2$. Next, two equivalents of $Bu^n_3GeNMe_2$ were added to one equivalent of diphenylgermanium dihydride Ph_2GeH_2 in acetonitrile and it was heated in a sealed tube at 85 °C for 48 hours. The volatiles were then removed *in vacuo* and the product was purified by Kugelrohr distillation to remove unreacted Ph_2GeH_2 to yield $Bu^n_3GeGePh_2GeBu^n_3$ in 89% yield as a clear liquid (**Scheme 6.11**). The NMR data obtained is consistent with the original synthesis.[71] The trigermane Bu^n_3Ge-$GePh_2$-$GeBu^n_3$ (**7**) was also characterized using UV/visible spectroscopy and DPV. The UV/visible spectrum and differential pulse voltammogram are provided below in **Figure 6.8** and **6.9** respectively.

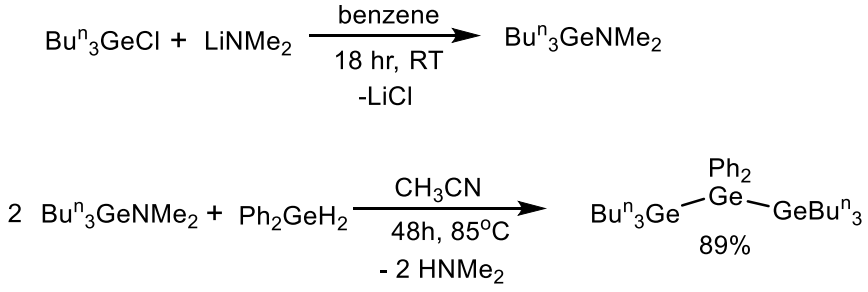

Scheme 6.11: Synthesis of $Bu^n_3GeGePh_2$-$GeBu^n_3$ (**7**) via the hydrogermolysis reaction.

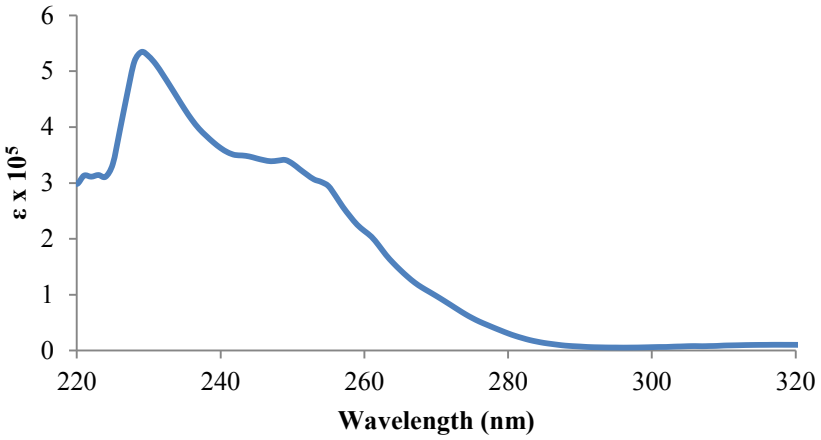

Figure 6.8: UV/visible spectrum of $Bu^n_3GeGePh_2GeBu^n_3$ (**7**) in hexane. (λ_{max} = 248 nm, c = 1.252 x10^{-5} M, and ε = 3.40 x 10^5 $M^{-1}cm^{-1}$)

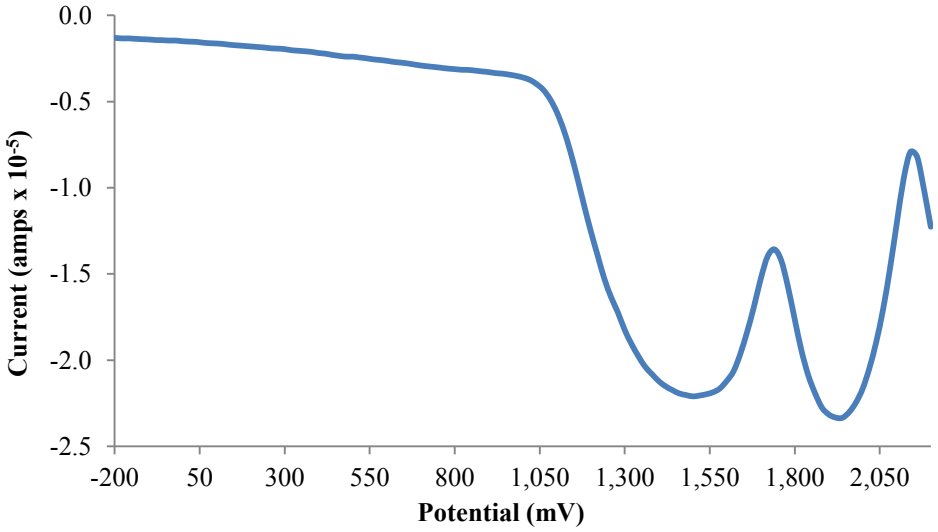

Figure 6.9: DPV of $Bu^n_3GeGePh_2GeBu^n_3$ (**7**) in CH_2Cl_2. (E_{ox} = 1525 ± 30 mV and 1925 ± 19 mV)

The λ_{max} observed for $Bu^n_3GeGePh_2GeBu^n_3$ (**7**) is at 248 nm which is slightly red-shifted when compared to the absorbance maximum for $Et_3GeGePh_2GeEt_3$ (**6**), and the two oxidation waves

observed for $Bu^n_3GeGePh_2GeBu^n_3$ (**7**) in the DPV are at 1525 mV and 1925 mV. The first oxidation potential is more negative than the oxidation potential for $^nBu_3GeGePh_3$ (**5**) indicating that the trigermane is easier to oxidize, as expected due to the higher degree of catenation in **7**.

1,1,1,4,4,4-hexaethyl-2,2,3,3-tetraphenyl tetragermane - Et_3Ge-$GePh_2$-$GePh_2$-$GeEt_3$ (8)

The synthesis of Et_3Ge-$GePh_2$-$GePh_2$-$GeEt_3$ (**8**) was detected by NMR[70] using the samarium(II) iodide method but has not been previously isolated as a pure product before. The tetragermane **8** was synthesized utilizing the hydrogermolysis reaction starting with $HPh_2GeGePh_2H$ (**2**) and two equivalents of Et_3GeNMe_2 in acetonitrile solvent (**Scheme 6.12**). The synthesis was performed in a sealed tube under a nitrogen atmosphere for 48 hours at 85 °C. The volatiles were then removed *in vacuo* and the product was purified via distillation of unreacted starting materials in a Kugelrohr oven to yield **8** (61%) as a thick yellow-green liquid.

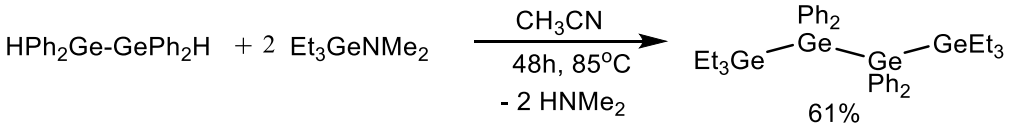

Scheme 6.12: Synthesis of Et_3Ge-$GePh_2$-$GePh_2$-$GeEt_3$ (**8**) via the hydrogermolysis reaction.

The ^1H NMR spectrum of **8** contains aromatic resonances in the ranges δ 7.72-7.56 ppm corresponding to the *meta*- protons and δ 7.22-6.88 ppm corresponding to the *ortho*- and *para*- protons of the four phenyl substituents. The NMR spectrum also contains an unresolved quartet at δ 1.05 ppm and a multiplet in the range δ 0.97-0.91 ppm corresponding to the 30 ethyl protons.

The ^{13}C NMR spectrum contains three aromatic resonances at δ 137.1, 136.5, and 136.0 ppm corresponding to the *meta*-, *ortho*-, and *para*- carbon atoms of the phenyl substituents respectively. It also contains two resonances at δ 10.3 and 6.6 ppm corresponding to the β-carbon and α-carbon atoms of the ethyl groups, respectively (**Figure 6.10**). The X-ray crystal structure of Et_3Ge-$GePh_2$-$GePh_2$-$GeEt_3$ (**8**) was obtained and an ORTEP diagram is provided below (**Figure 6.11**) with selected bond distances and angles listed in **Table 6.5**. Compound **8** crystallizes with two independent molecules in the unit cell. **Molecule 1** contains thermal disorder in the ethyl groups, and therefore **Molecule 1** is shown with the carbon atoms represented as spheres rather than thermal ellipsoids at 50% probability. The average germanium-germanium bond distance for **8** is 2.4386(6) Å which is typical for oligogermanes. In comparison, the following linear tetragermanes have average germanium-germanium bond distances of 2.455(3) Å for Tol_3Ge-$(GePh_2)_2$-$GeTol_3$,[8] 2.462(2) Å for Ph_3Ge-$(GePh_2)_2$-$GePh_3$,[50] 2.450(4) Å for $ClPh_2Ge$-$(GePh_2)_2$-$GePh_2Cl$,[66] and 2.451(1) Å for IPh_2Ge-$(GePh_2)_2$-$GePh_2I$.[57] The average germanium-germanium bond length of **8** is the shortest among these and this is likely due to the smaller size of the ethyl groups allowing the germanium atoms to come closer together while the other four tetragermanes contain at least two larger aryl groups on their terminal germanium atoms. The tetragermane Et_3Ge-$GePh_2$-$GePh_2$-$GeEt_3$ (**8**) was also characterized using UV/visible spectroscopy and DPV. The UV/visible spectrum and differential pulse voltammogram are provided below in **Figure 6.12** and **6.13** respectively.

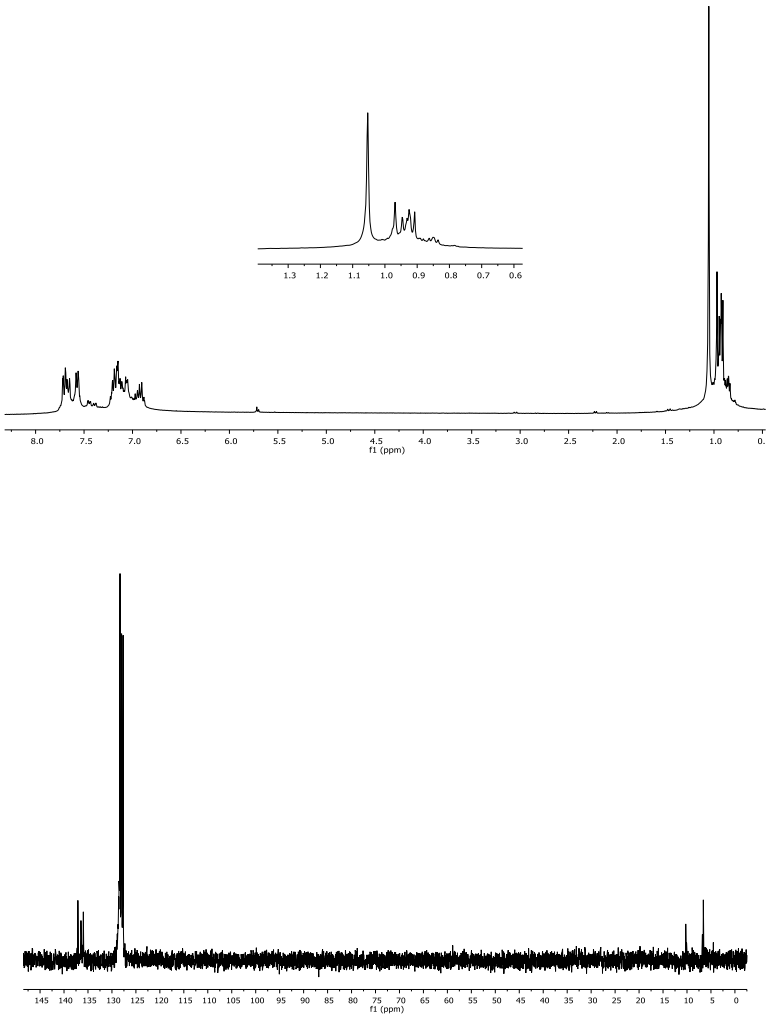

Figure 6.10: ^{1}H (top) and ^{13}C (bottom) NMR spectra (benzene-d_6) of the tetragermane $Et_3Ge\text{-}GePh_2\text{-}GePh_2\text{-}GeEt_3$ (**8**)

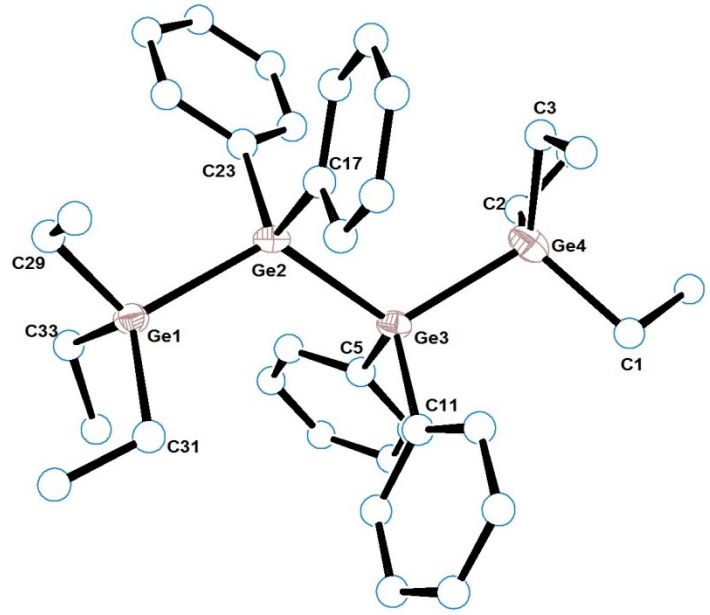

Molecule 1

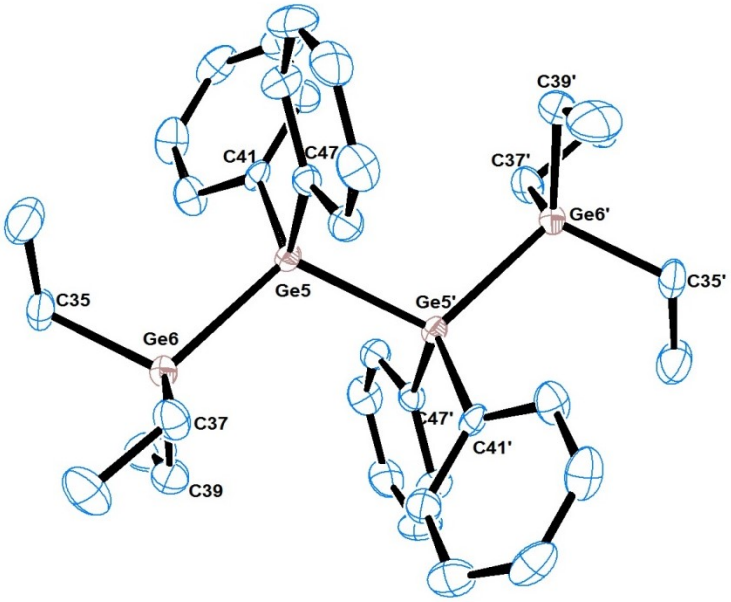

Molecule 2

Figure 6.11: X-ray crystal structure of Et_3Ge-$GePh_2$-$GePh_2$-$GeEt_3$ (**8**): Molecule 1 (top), Molecule 2 (bottom).

Table 6.5: Selected bond distances and angles for Et_3Ge-$GePh_2$-$GePh_2$-$GeEt_3$ (**8**): Molecule 1 (top), Molecule 2 (bottom).

Molecule 1

Bond Lengths	Å	Bond Angles	°
Ge(1) - Ge(2)	2.4437(6)	C(29) - Ge(1) - Ge(2)	108.5(2)
Ge(2) - Ge(3)	2.4385(6)	Ge(1) - Ge(2) - Ge(3)	118.46(2)
Ge(3) - Ge(4)	2.4437(7)	Ge(2) - Ge(3) - Ge(4)	115.35(2)
Ge(1) - C(29)	1.974(5)	Ge(1) - Ge(2) - C(17)	106.8(1)
Ge(1) - C(31)	1.967(4)	Ge(2) - Ge(3) - C(5)	110.9(1)
Ge(1) - C(33)	1.966(6)	Ge(3) - Ge(4) - C(1)	105.6(5)
Ge(2) - C(17)	1.964(4)	C(29) - Ge(1) - C(31)	108.2(2)
Ge(2) - C(23)	1.972(4)	C(17) - Ge(2) - C(23)	107.7(2)
Ge(3) - C(5)	1.972(4)	C(15) - Ge(3) - C(11)	105.6(2)
Ge(3) - C(11)	1.967(4)	C(1) - Ge(4) - C(2)	109.4(5)
Ge(4) - C(1)	2.06(2)		
Ge(4) - C(2)	1.975(8)		
Ge(4) - C(3)	1.951(8)		

Molecule 2

Bond Lengths	Å	Bond Angles	°
Ge(5) - Ge(6)	2.4352(6)	C(35) - Ge(6) - Ge(5)	109.4(1)
Ge(5) - Ge(5')	2.4319(5)	Ge(6) - Ge(5) - Ge(5')	112.76(2)
Ge(5) - C(41)	1.965(4)	Ge(6) - Ge(5) - C(41)	112.7(1)
Ge(5) - C(47)	1.970(4)	C(41) - Ge(5) - C(47)	108.6(2)
Ge(6) - C(35)	1.962(4)	C(35) - Ge(6) - C(37)	107.9(2)
Ge(6) - C(37)	1.969(4)		
Ge(6) - C(39)	1.961(4)		

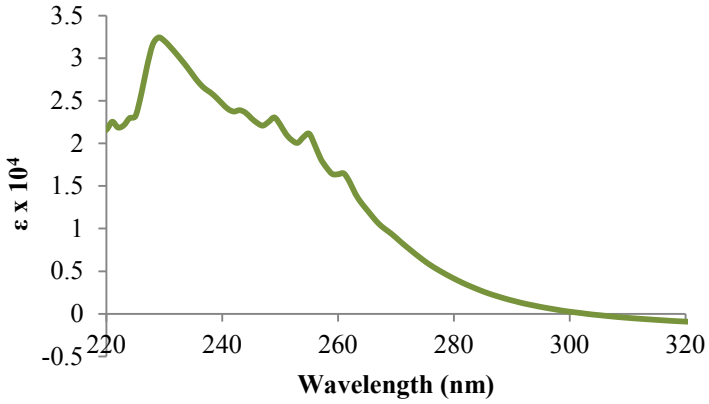

Figure 6.12: UV/visible spectrum of Et_3Ge-$GePh_2$-$GePh_2$-$GeEt_3$ (**8**) in hexane. (λ_{max} = 253 nm, c = 1.294 x10^{-5} M, and ε = 2.01 x 10^4 $M^{-1}cm^{-1}$)

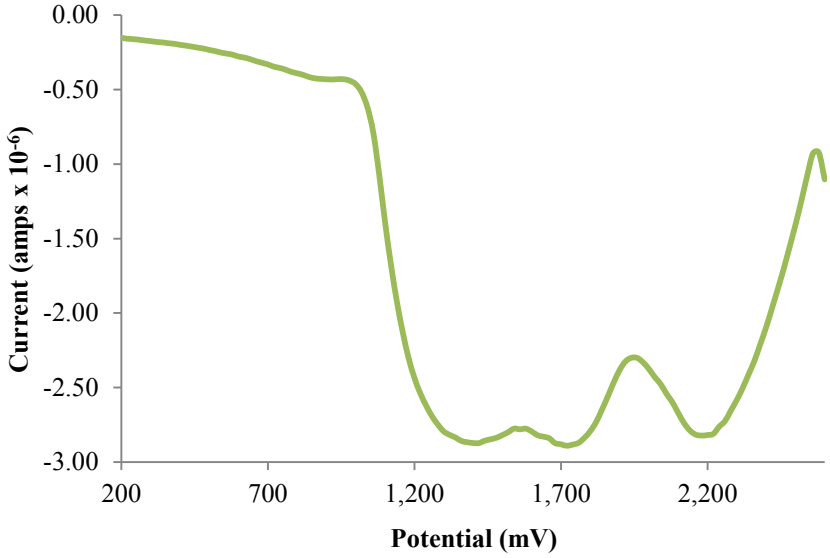

Figure 6.13: DPV of Et_3Ge-$GePh_2$-$GePh_2$-$GeEt_3$ (**8**) in CH_2Cl_2. (E_{ox} = 1413 ± 10 mV, 1695 ± 25 mV, and 2145 ± 19 mV)

The absorption maximum for **8** appears at 253 nm, but there are a total of four defined peaks in the UV/visible spectrum of **8** that appear at 242, 248, 253, and 259 nm. These are likely due to transitions between different nearly-degenerate energy levels such as HOMO to LUMO, HOMO

to LUMO+1, etc. Similar transitions have been calculated for other oligogermanes and the absorbances have a similar energy separation.[79] As expected, when considering the DPVs of other oligogermanes, there are three oxidation waves in the DPV of **8** corresponding to an n-1 pattern, and they appear at 1413, 1695, and 2145 mV, where the first oxidation potential is lower than the oxidation potential for the digermanes $Et_3GeGePh_3$ (**4**) and $^nBu_3GeGePh_3$ (**5**) indicating that the tetragermane is easier to oxidize and it is also lower than the first oxidation potential of the trigermane $Bu^n_3GeGePh_2GeBu^n_3$ (**7**) which appears at 1525 mV.

1,1,1,4,4,4-hexa-n-butyl-2,2,3,3-tetraphenyl tetragermane - Bu^n_3Ge-$GePh_2$-$GePh_2$-$GeBu^n_3$ (9)

The tetragermane Bu^n_3Ge-$GePh_2$-$GePh_2$-$GeBu^n_3$ (**9**) was synthesized utilizing the hydrogermolysis reaction starting with $HPh_2GeGePh_2H$ (**2**) and two equivalents of $Bu^n_3GeNMe_2$ in acetonitrile solvent (**Scheme 6.13**). The synthesis was performed in a sealed tube under a nitrogen atmosphere for 48 hours at 85 °C. The volatiles were then removed *in vacuo* and the product was purified via distillation in a Kugelrohr oven to yield **9** (67%) as a thick yellow liquid.

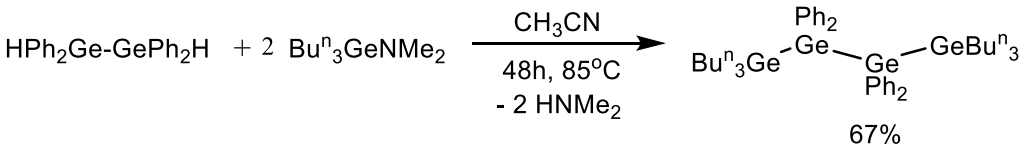

Scheme 6.13: Synthesis of Bu^n_3Ge-$GePh_2$-$GePh_2$-$GeBu^n_3$ (**9**) via the hydrogermolysis reaction.

The ^1H NMR spectrum of **9** contains aromatic resonances in the ranges δ 7.75-7.64 ppm for the *meta*- protons and δ 7.25-7.10 ppm corresponding to the *ortho*- and *para*- protons. The protons

for the six *n*-butyl groups appear in the range δ 1.51-0.82 ppm (**Figure 6.14**). The ^{13}C NMR spectrum contains three resonances at δ 137.1, 136.5, and 136.0 ppm corresponding to the *ortho*-, *para*-, and *meta*- aromatic carbons, respectively, and resonances at 28.9, 26.5, 14.0, and 12.2 ppm corresponding to the δ-, γ-, β-, and α-carbon atoms of the *n*-butyl groups, respectively. The tetragermane $Bu^n_3Ge\text{-}GePh_2\text{-}GePh_2\text{-}GeBu^n_3$ (**9**) was also characterized using UV/visible spectroscopy and DPV, and the UV/visible spectrum and differential pulse voltammogram are shown in **Figure 6.15** and **6.16**, respectively. The absorption maximum for **9** appears at 254 nm and is red-shifted compared to the other five oligogermanes **4**-**8**, which is expected since it contains the longest germanium-germanium backbone with four catenated germanium atoms and the butyl groups are more inductively donating than the ethyl groups in **8**. There is only one oxidation wave in the DPV of **9** and it appears as a very broad peak with a current minimum at 1355 mV. As expected, the oxidation potential of $Bu^n_3Ge\text{-}GePh_2\text{-}GePh_2\text{-}GeBu^n_3$ (**9**) is lower than that of the *n*-butyl terminated digermane **5** and trigermane **7**. The expected n-1 pattern was not observed for **9**, and this is likely due to the presence of the terminal *n*-butyl groups. This has been observed in other oligogermanes including the tetragermane $Ph_3Ge(GeBu^n_2)_3CH_2CH_2OEt$.[6]

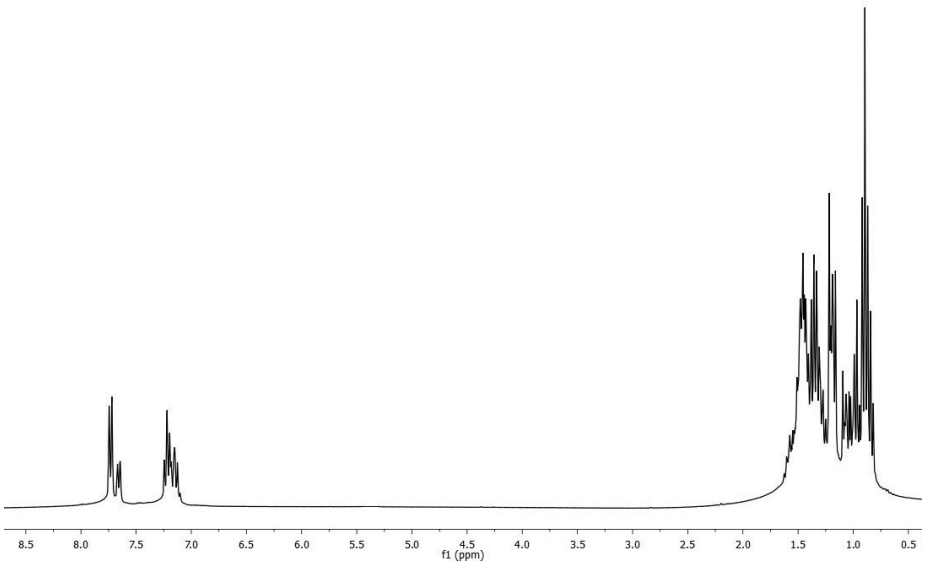

Figure 6.14: ^1H NMR spectra in d_6-benzene for $Bu^n_3Ge\text{-}GePh_2\text{-}GePh_2\text{-}GeBu^n_3$ (**9**).

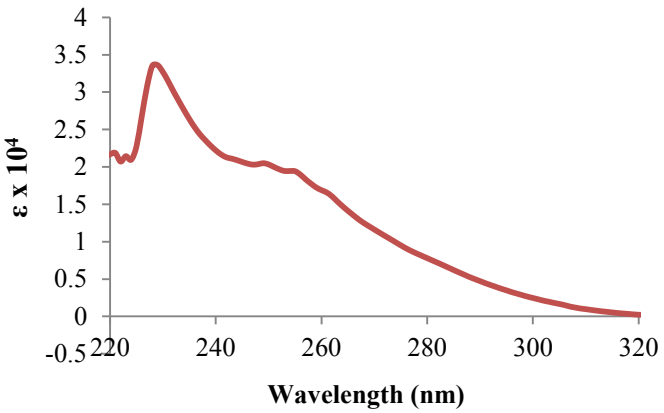

Figure 6.15: UV/visible spectrum of $Bu^n_3Ge\text{-}GePh_2\text{-}GePh_2\text{-}GeBu^n_3$ (**9**) in hexane. (λ_{max} = 254 nm, c = 1.311 x10^{-5} M, ε = 1.95 x10^4 $M^{-1}cm^{-1}$)

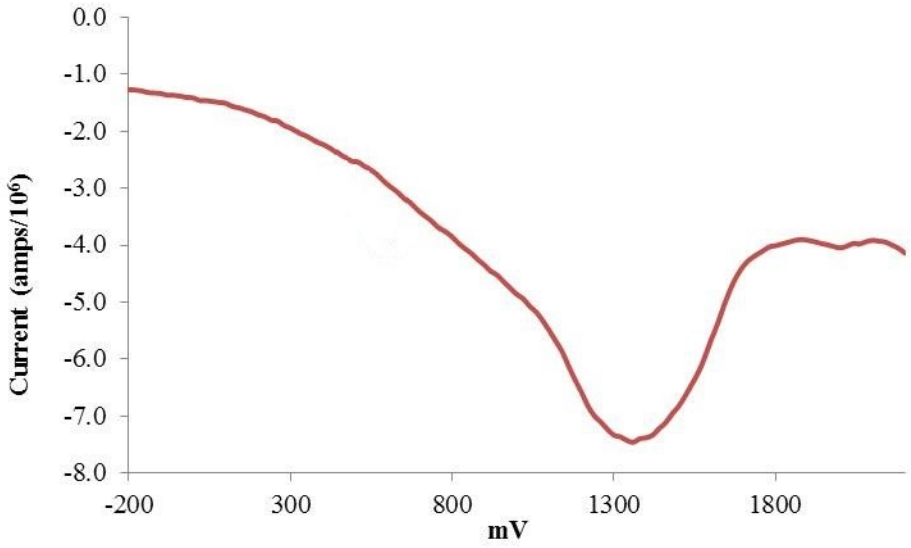

Figure 6.16: DPV of $Bu^n_3Ge\text{-}GePh_2\text{-}GePh_2\text{-}GeBu^n_3$ (**9**) in CH_2Cl_2. (E_{ox} = 1355 ± 10 mV)

All six of the oligogermanes **4-9** have been characterized using UV/visible spectroscopy and differential pulse voltammetry. The following section compares and discusses all of these results, with the UV/visible spectra discussed first followed by the DPV voltammograms. All of

the absorbance maxima for compounds **4-9** are collected in **Table 6.6** and all of the of the oxidation potentials for compounds **4-9** are collected in **Table 6.7**.

Table 6.6: UV/visible absorption maxima for **4-5** (**Table 6.4**)[73] and **6-9**.

Compound	**4**	**5**	**6**	**7**	**8**	**9**
λ_{max} (nm)	231	232	247	248	253	254

As can be seen from **Table 6.6**, when comparing the ethyl terminated oligogermanes **4**, **6**, and **8** there is a red-shift in the absorbtion maxima going from the digermane $Et_3GeGePh_3$ (**4**) to the tetragermane $Et_3Ge(GePh_2)_2GeEt_3$ (**8**). This trend is also evident in the *n*-butyl terminated series **5**, **7**, and **9**. This transition, which corresponds to a σ to σ* electronic transition or a transition between another set of nearly degenerate orbitals, is shifting to a lower energy due to a decrease in the HOMO-LUMO gap as the germanium-germanium backbone increases in length. This trend has been observed with other series of oligogermanes.[4-5, 8, 80] When directly comparing the ethyl terminated series to the *n*-butyl terminated series, there is a slight red-shift in the oligogermane pairs (ex. $Et_3GeGePh_3$ vs. $Bu^n_3GeGePh_3$); however, the change is not significantly different. This has also been observed in larger explorations on the substituent effects in oligogermanes.[6, 79] Thus, the oligogermane with the most blue-shifted absorption maximum is the digermane $Et_3GeGePh_3$ (**4**) and the oligogermane with the most red-shifted absorption maximum is the tetragermane $Bu^n_3Ge\text{-}GePh_2\text{-}GePh_2\text{-}GeBu^n_3$ (**9**).

Table 6.7: Oxidation potentials for **4-5** (**Table 6.3**)[73] and **6-9**. Values are an average of four separate runs.

Compound	**4**	**5**	**6**	**7**	**8**	**9**
Oxidation Potentials (mV)	1587 ± 17	1588 ± 11	1350 ± 12 1535 ± 10	1525 ± 30 1925 ± 19	1413 ± 10 1695 ± 25 2145 ± 19	1355 ± 10

As can be seen from **Table 6.7**, the oxidation potentials of the *n*-butyl terminated series **5**, **7**, and **9** indicate that the compounds become easier to oxidize as the degree of catenation increases. The oxidation potentials are a function of the energy of the HOMO.[4-8, 81-82] When directly comparing the ethyl terminated series to the *n*-butyl terminated series, the *n*-butyl derivative in all cases is easier to oxidize than the ethyl derivative in the oligogermane pairs (ex. $Et_3GeGePh_3$ vs. $Bu^n{}_3GeGePh_3$). This relationship is due to the HOMO energy level being destabilized as the electron donating ability of the alkyl groups increases (*n*-butyl > ethyl) thus rendering the oligogermanes with *n*-butyl groups easier to oxidize. This demonstrates the fine tuning of the electronic properties of oligogermanes that is possible by variation of the organic substituents.

Additionally, when attempting other hydrogermolysis reactions to prepare perphenylated oligogermanes $Ph_3Ge\text{-}(GePh_2)_n\text{-}GePh_3$ (n = 1 or 2) triphenylgermanium amide Ph_3GeNMe_2 was used as the amide source in the hydrogermolysis reaction. During efforts to crystallize several perphenylated oligogermanes, the triphenyl α-germylated nitrile Ph_3GeCH_2CN (**10**) crystallized out of solution. The X-ray crystal structure of **10** was obtained and is provided below as an ORTEP diagram in **Figure 6.17** with selected bond distances and angles provided in **Table 6.8**. All of the bond distances and angles are typical for a germanium(IV) center. The environment

around the germanium atom approaches the idealized tetrahedral geometry with the C(13) -Ge(1)-C(35) angle being the most distorted from the ideal value of 109.5° with an angle of 102.4(2)°. The Ge−C_α bond distance is 1.982(4) Å and is similar to those in two other crystallographically characterized α-germyl nitriles, [Mes*P=C]GeBu^t(Tip)CH_2CN[83] (**11**) and $[(Me_3Si)_2CH]_2Ge(H)CH_2CN$[84] (**12**) that measure 2.004(2) and 1.911(9) Å, respectively. The $-CH_2CN$ ligand is nearly linear, as shown by the C(19)−C(20)−N(1) bond angle, which is 178.9(5)° and the Ge(1)−C(19)−C(20) bond angle is 116.6(3)°, which is similar to the disposition of the $-CH_2CN$ ligand in the germanium complexes **11** and **12**. In these compounds, the C−C−N bond angles are 179.4(2)° (**11**) and 117(1)° (**12**), while the Ge−C−C bond angles are 113.5(1)° (**11**)and 115.2(7)° (**12**).

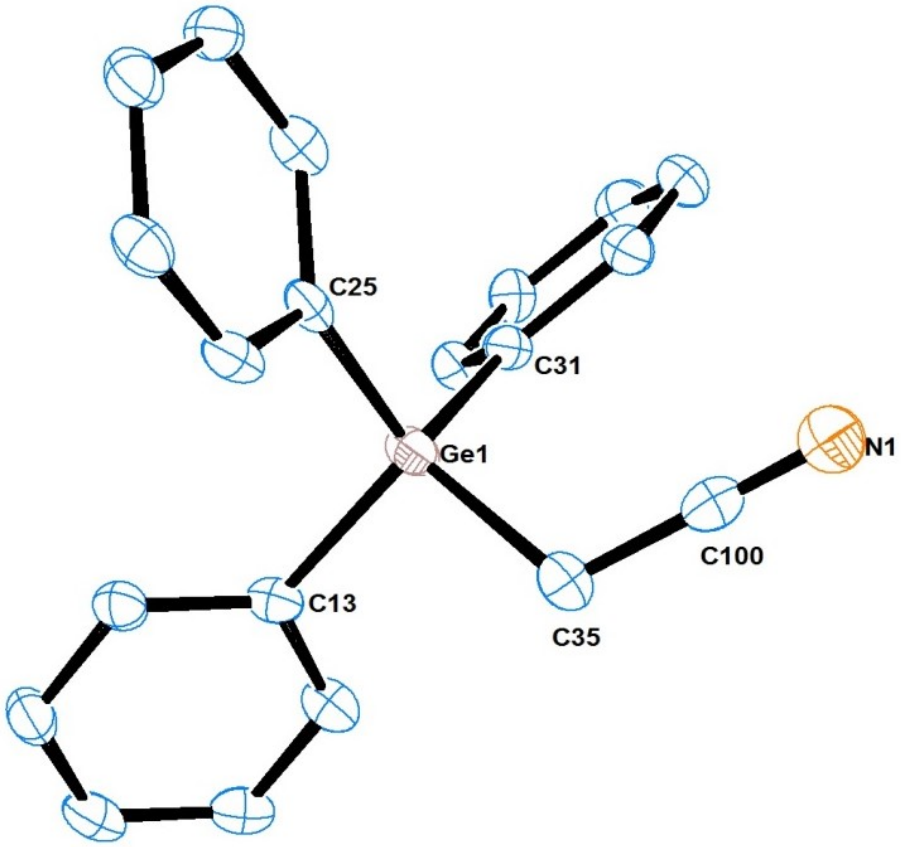

Figure 6.17: X-ray crystal structure of Ph_3GeCH_2CN (**10**).

Table 6.8: Selected bond distances and angles for **10**.

Bond Lengths	Å	Bond Angles	°
Ge(1) - C(13)	1.940(4)	C(13) - Ge(1) - C(25)	111.9(2)
Ge(1) - C(25)	1.929(4)	C(13) - Ge(1) - C(31)	110.5(2)
Ge(1) - C(31)	1.943(4)	C(13) - Ge(1) - C(35)	102.4(2)
Ge(1) - C(35)	1.983(5)	C(25) - Ge(1) - C(31)	111.5(2)
C(35) - C(100)	1.449(6)	C(25) - Ge(1) - C(35)	108.9(2)
C(100) - N(1)	1.149(6)	Ge(1) - C(35) - C(100)	116.6(3)
		C(35) - C(100) - N(1)	178.9(5)

6.3 Conclusion

The oligogermane precursor compounds $ClPh_2Ge$-$GePh_2Cl$ and HPh_2Ge-$GePh_2H$ were synthesized in good yields in order to serve as precursors for the tetragermanes $Et_3Ge(GePh_2)_2GeEt_3$ and $^nBu_3Ge(GePh_2)_2Ge^nBu_3$, which are part of a series of six related oligogermanes $Et_3GeGePh_3$, $^nBu_3GeGePh_3$, $Et_3GeGePh_2GeEt_3$, $^nBu_3GeGePh_2Ge^nBu_3$, $Et_3Ge(GePh_2)_2GeEt_3$, and $^nBu_3Ge(GePh_2)_2Ge^nBu_3$ prepared via the hydrogermolysis reaction. The X-ray crystal structure for the digermane $ClPh_2Ge$-$GePh_2Cl$ and the tetragermane $Et_3Ge(GePh_2)_2GeEt_3$ were obtained as well as the structure for the monohydride Ph_3Ge-$GePh_2H$, which is formed as a byproduct in the synthesis of $HPh_2GeGePh_2H$, and the triphenyl alpha-germylated nitrile Ph_3GeCH_2CN. All six of the oligogermanes in the series were characterized by NMR spectroscopy to verify their successful synthesis, and their electronic properties were investigated via UV/visible spectroscopy and differential pulse voltammetry. The UV/visible absorption maxima and the oxidation potentials observed for the series are consistent with previous findings related to oligogermanes of this nature.[4-6, 8, 79] It was observed that as the catentation increases there is a distinct red-shift in the absorption maxima of these compounds

due to a decrease in the HOMO-LUMO gap. The DPVs of these six oligogermanes demonstrated that as precursor catenation increased, the oxidation of these compounds became more facile since the HOMO increases in energy as a function of catenation, and there are n-1 irreversible oxidation waves (n = number of catenated germanium atoms) observed in all cases except for compound **9**. The oligogermanes in the *n*-butyl terminated series are easier to oxidize than those in the ethyl terminated series due to the higher electron donating ability of the *n*-butyl groups in comparison the ethyl groups. Crystallographic datum for compounds **1**, **3**, **8**, and **10** are collected below in **Tables 6.9-6.11**.

6.4.1 Introduction

All of the oxidation waves that we have observed thus far are irreversible, but all of the observed oxidation waves can be correlated with both the degree of catenation along the germanium-germanium backbone and the electron donating or withdrawing nature of the organic substituents bound to the germanium atoms.[4-6, 8, 13, 79-81] The irreversibility of these waves is likely due to one of three possible reactions that occur after the oxidation event takes place. These possibilities include **i)** the extrusion of a germylene with concomitant chain contraction, **ii)** the homolytic scission of a germanium-germanium bond to generate germyl radicals, or **iii)** the stepwise extrusion of a germylene with formation of two germyl radicals that then re-combine to gernerate a new oligogermane chain (**Scheme 6.14**).

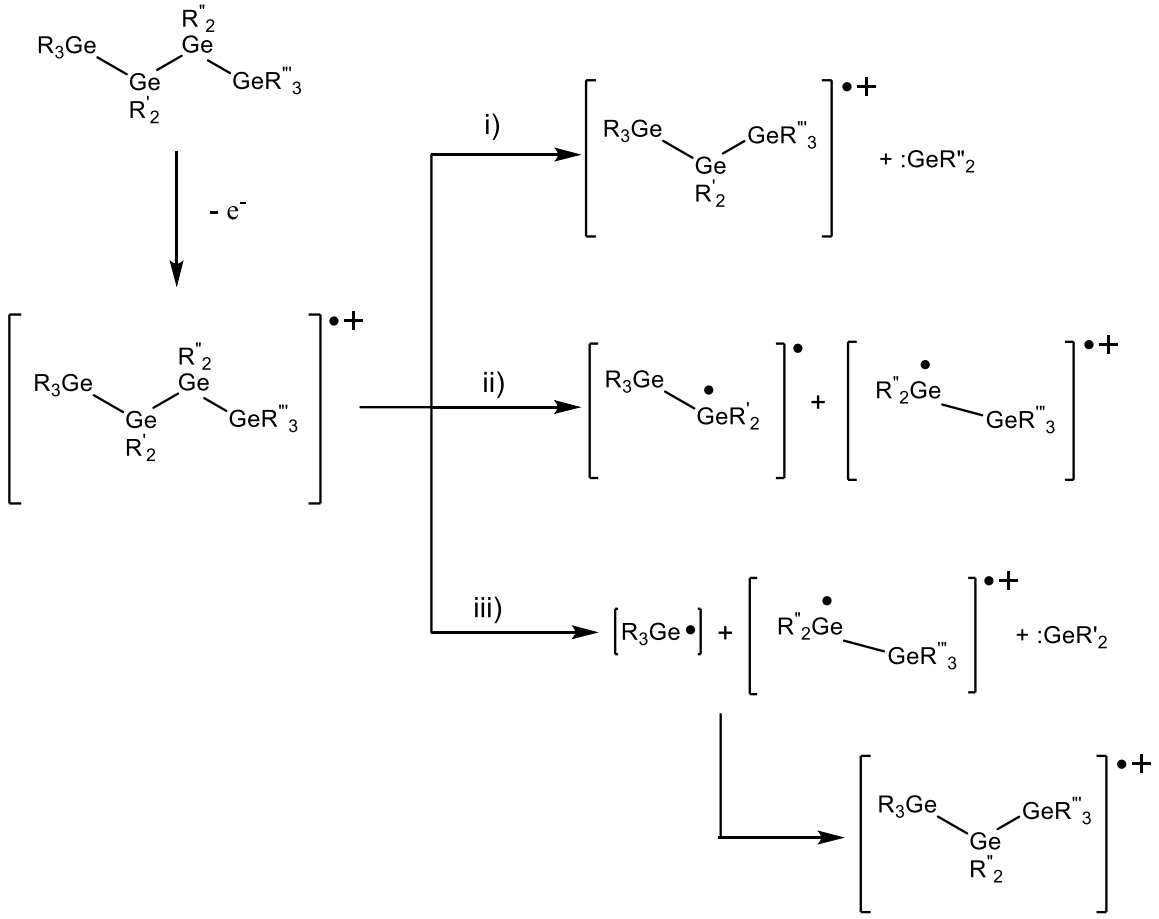

Scheme 6.14: Proposed decomposition pathways for the oxidation of oligogermanes.

All three of these processes have been observed in photolytic studies[85-86] and we anticipate that one or more of these are occurring after oxidation of the oligogermanes leading to the observed irreversibility. Linear oligogermanes that have aryl groups on at least one germanium atom in the chain exhibit n-1 oxidation waves in their CVs and DPVs, where n is the number of catenated germanium atoms.[5, 79-80] These results suggest that several successive decomposition processes are occurring during the course of the sweep. However, it has been observed that peralkyl substituted oligogermanes Ge_nR_{2n+2} exhibit only one irreversible oxidation

wave,[12] and this was also observed for the series of oligogermanes Ge_nMe_{2n+2}, for example. This is also true for the branched oligogermanes which all exhibit only one irreversible oxidation wave. [5, 13, 80-81] The aryl- and alkyl-substituted oligogermanes are not overly different thus the decomposition pathways for oligogermanes having both types of substituent patterns are expected to be similar. If germylene extrusion is occurring accompanied by simultaneous chain contraction, the same number of oxidation waves should be observed for oligogermanes of the type Ge_nR_{2n+2} (R = alkyl) and Ge_nAr_{2n+2} (Ar = aryl). Similarly, if homolytic bond scission or germylene extrusion accompanied by radical formation is occurring, the same number of oxidation waves would also be expected for each type of substituent pattern. For linear oligogermanes, the internal (non-terminal) germanium atoms can be regarded as having some Ge^{2+} character that is absent in the branched oligogermanes we have characterized by electrochemical methods. This difference could explain the presence of only one irreversible oxidation wave in the CVs and DPVs of the branched systems. However, we are uncertain if the argument that the divalent nature of the internal germanium atoms in linear compounds results in solely germylene extrusion. Thus, the observed electrochemical behavior of these systems is not fully understood and further investigations are necessary.

An investigation of the products formed upon photolysis of three linear phenylated trigermanes $(PhMe_2Ge)_2GeMe_2$, $(Me_3Ge)_2GeMePh$, and $(Me_3Ge)_2GePh_2$ has been performed.[86] Laser flash-photolysis, matrix isolation techniques, and trapping experiments of the phenylated trigermanes indicated both the simple extrusion of germylenes (**i**) and the formation of germyl radicals and digermyl radicals (**iii**).[86] It was found that by using 2,3-dimethyl-1,3-butadiene (DMB) as a trapping agent, the germylenes R_2Ge: (R = Me or Ph) could be trapped with 18-32% conversion with the concomitant formation of digermanes (**Figure 6.18**).[86]

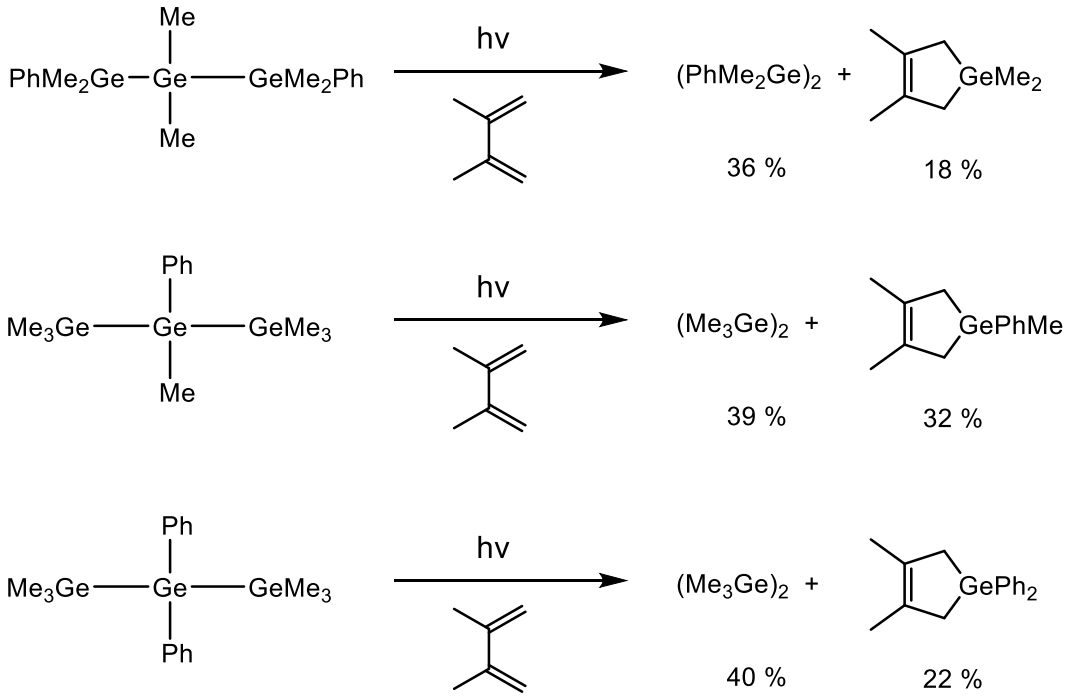

Figure 6.18: Photolysis of three linear phenylated trigermanes with trapping agent DMB.[86]

The formation of the digermanes $(PhMe_2Ge)_2$, and $(Me_3Ge)_2$ from the photolysis indicates the formation of germyl radicals which subsequently combine together to yield the digermanes, and the formation of the germacyclopentenes clearly indicates the extrusion of germylenes. These trigermanes were also photolyzed in the presence of CCl_4 (**Figure 6.19**).[86]

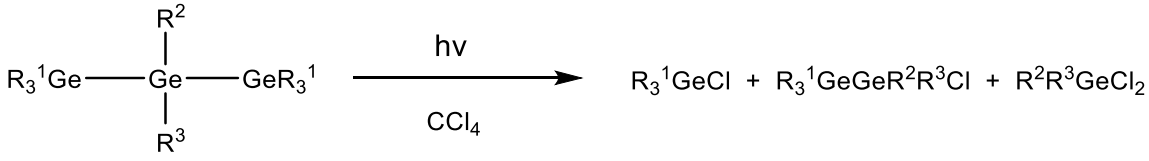

Figure 6.19: Photolysis of three linear phenylated trigermanes in the presence of CCl_4.[86]

This provides further evidence for the formation of both a germyl radical and a digermyl radical generated by germanium-germanium bond homolysis of the trigermanes which then abstract a chlorine atom from CCl_4. The formation of dichlorogermanes (R_2GeCl_2) indicates that germylenes are formed and then insert into the C-Cl bond of CCl_4 to yield trichloromethylchlorogermane (Cl_3CGeR_2Cl) which is thermally unstable and decomposes to dichlorogermane and dichlorocarbene.[86]

Another study was performed on the chemistry of :GeH_2 in solution where dihydro-3-methyl-4-phenyl-1-germacyclopent-3-ene was photolyzed via laser flash photolysis methods in cyclohexane-d_{12} with the goal of detecting the parent germylene :GeH_2 and studying its reactivity in solution using acetic acid (AcOH) as a germylene trapping agent. This reaction was monitored by ^{1}H NMR spectroscopy and demonstrates the formation of 2-methyl-3-phenyl-1,3-butadiene and the O-H insertion products $AcOGeHL_2$ (L = H or D) indicating that AcOH can be used as a germylene trapping agent (**Figure 6.20**).[87]

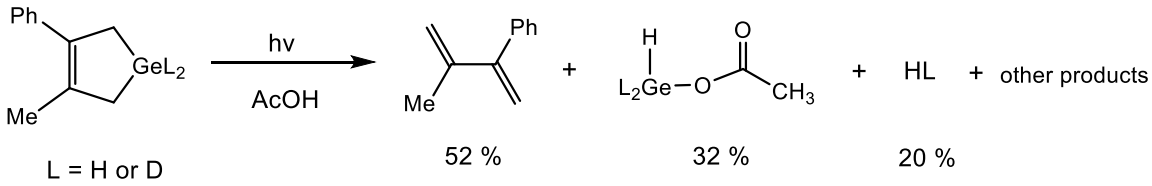

Figure 6.20: Photolysis of dihydro-3-methyl-4-phenyl-1-germacyclopent-3-ene in the presence of AcOH and the products observed by ^{1}H NMR.[87]

In this investigation we endeavored to determine if germylene extrusion is occurring as the main pathway in the decomposition or if radical formation is a competing process in the

photolysis of oligogermanes. We have used the digermanes $Et_3GeGePh_3$ (**4**) and $Bu^n{}_3GeGePh_3$ (**5**), the trigermanes $Et_3GeGePh_2GeEt_3$ (**6**) and $^nBu_3GeGePh_2Ge^nBu_3$ (**7**), and the tetragermanes $Et_3Ge(GePh_2)_2GeEt_3$ (**8**) and $^nBu_3Ge(GePh_2)_2Ge^nBu_3$ (**9**). We have chosen these compounds to study because the trigermanes and tetragermanes each contain internal $GePh_2$ fragments and terminal GeR_3 fragments where R is *n*-butyl or ethyl. These compounds were each photolyzed using UV-C light (280-100 nm) in the presence of acetic acid as a germylene trapping agent. If germylenes $:GeR_2$ are formed, they should be trapped to yield $R_2Ge(H)OAc$.[87] The species formed were characterized by NMR (^1H and ^{13}C), infrared spectroscopy (FTIR), and gas-chromatography mass spectroscopy (GC/MS).

6.4.2 Results and Discussion

Initially, all six of the oligogermanes were analyzed by using a large excess of acetic acid in THF. The oligogermane (300-500 mg) was dissolved in THF (15 mL) in a 100 mL quartz flask and the flask was closed with a septum and copper wire under an inert atmosphere of nitrogen. The flask was removed and connected to a schlenk line under blowing nitrogen and glacial acetic acid (30 mol equivalents) was directly injected into the THF solution. The solution was irradiated with UV-C light for 18 hours, and the THF was then removed *in vacuo.* The remaining thick liquid was dissolved in benzene (10 mL), the excess acetic acid was extracted using water (3 x 5 mL), and the volatiles from the benzene layer were removed *in vacuo* to yield the photolysis products. The products obtained were analyzed by ^1H NMR, FTIR, and GC/MS. The ^1H and ^{13}C NMR spectra obtained for the photolysis and trapping by acetic acid of the trigermane $^nBu_3GeGePh_2Ge^nBu_3$ (**7**) are shown below (**Figure 6.21**) and are representative of the spectra obtained for the other oligogermanes.

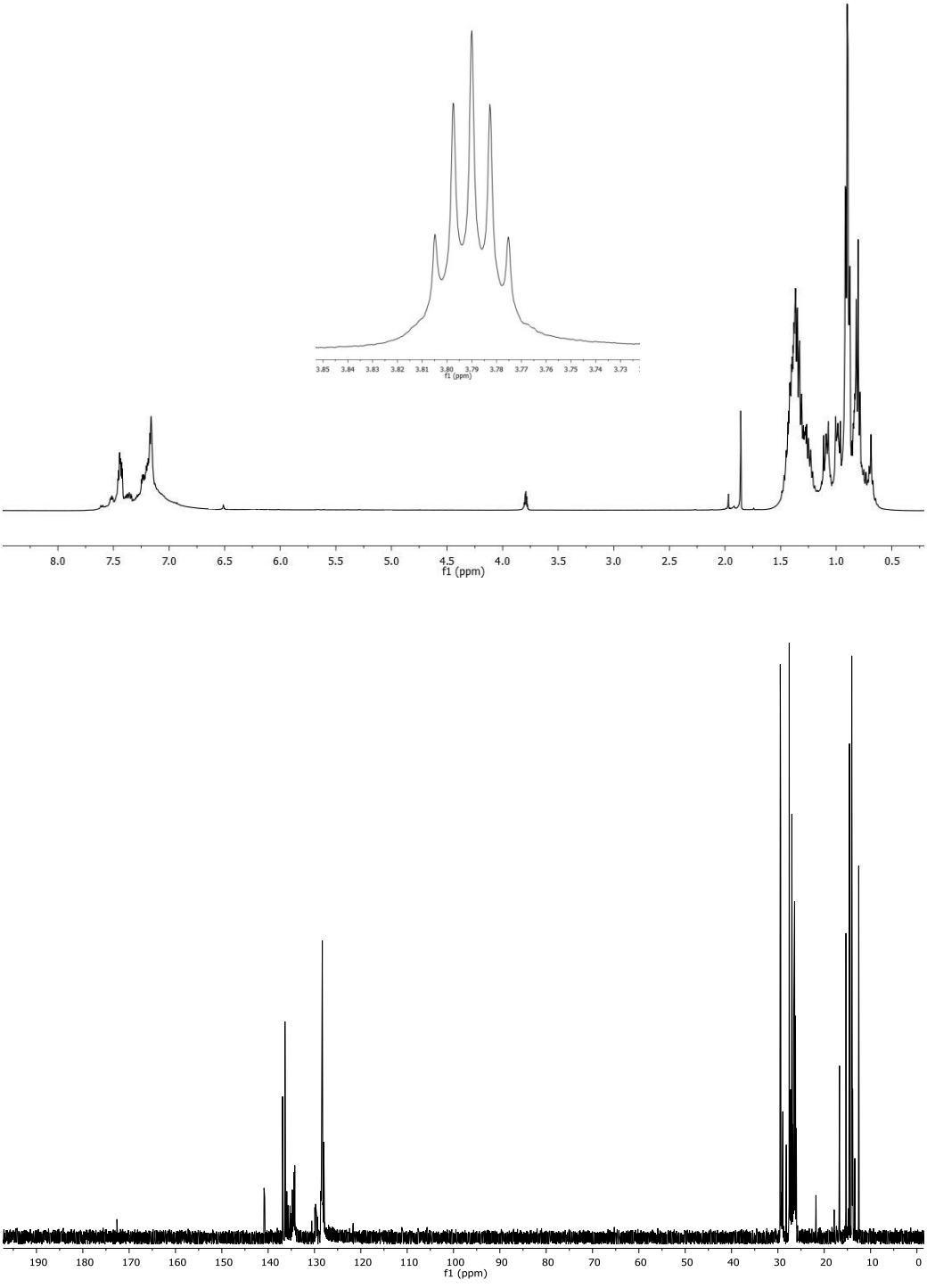

Figure 6.21: ^{1}H (top) and ^{13}C (bottom) NMR spectrum in cyclohexane-d_{12} of the trapping product of $^{n}Bu_3GeGePh_2Ge^{n}Bu_3$ (**7**) with AcOH.

The ^{1}H NMR spectrum for the trapping product of $^{n}Bu_3GeGePh_2Ge^{n}Bu_3$ (**7**) with AcOH contains resonances with substantial overlap in the range of δ 7.81-7.09 ppm that correspond to the aromatic protons of the products and resonances in the range of δ 1.57-0.78 ppm which indicate that the *n*-butyl protons are still present, which is not surprising since those peaks also appear in the ^{1}H NMR spectrum of the starting trigermane $^{n}Bu_3GeGePh_2Ge^{n}Bu_3$ (**7**). However, there are two distinct resonances that appeared that do not correspond to either compound **7** or acetic acid. There is a pentet that appears at δ 3.79 ppm (J = 2.8 Hz) in cyclohexane-d_{12} that corresponds to a germanium bound hydrogen, where two *n*-butyl groups are also bound to the germanium atom, resulting in the Ge-H proton coupling with the α-CH_2 protons of the *n*-butyl groups. The observed coupling constant of 2.8 Hz is consistent with the coupling constants observed for other dibutyl germanes. The other new resonance appears as a singlet at 1.87 ppm which corresponds to the –CH_3 group of the acetyl group which is now bound to the germanium atom. The ^{1}H NMR indicates that the major product formed is acetoxydibutyl germane (**11**) (**Figure 6.22**). There are also two other singlets that appear at δ 6.52 and 1.97 ppm which correspond to the Ge-H and the –CH_3 group of an acetyl group of acetoxydiphenyl germane (**12**) respectively (**Figure 6.22**). This indicates that both the dibutyl germylene and the diphenyl germylene are being extruded in the photolysis of the oligogermanes, where it appears the dibutylgermylene is formed first, and also that formation of Bu_2Ge: is favored due to the higher yield of $Bu^{n}_2Ge(H)OAc$ (**11**) versus $Ph_2Ge(H)OAc$ (**12**). The ^{13}C NMR spectrum of the trapping product of $^{n}Bu_3GeGePh_2Ge^{n}Bu_3$ (**7**) with AcOH clearly demonstrates that there is a product mixture upon the photolysis of the oligogermanes with several observed peaks in the range of δ 34.9-11.6 ppm which correspond to the *n*-butyl carbon atoms. There is a distinct peak at δ 172.6 ppm corresponding to the carbonyl carbon of the acetoxy group verifying its presence further.

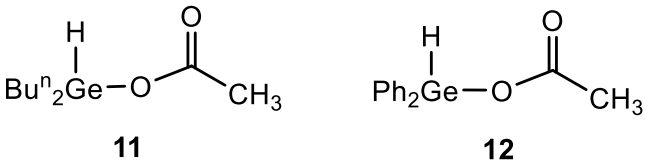

11 **12**

Figure 6.22: Structures of $Bu^n_2Ge(H)OAc$ (**11**) (left) and $Ph_2Ge(H)OAc$ (**12**) (right).

In order to further verify the presence of the Ge-H bond and the carbonyl group, the FTIR spectrum of the trapping product of $^nBu_3GeGePh_2Ge^nBu_3$ (**7**) with AcOH was obtained and is provided below in **Figure 6.23**.

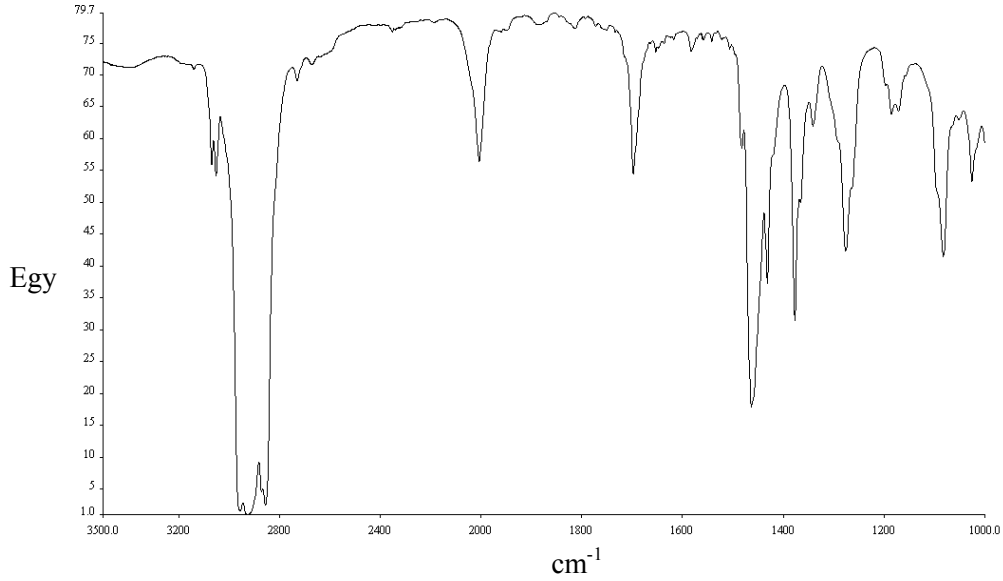

Figure 6.23: FTIR spectrum of the trapping product of $^nBu_3GeGePh_2Ge^nBu_3$ (**7**) with AcOH.

The FTIR spectrum clearly indicates the presence of a Ge-H bond and a carbonyl group with characteristic peaks that appear at 2006 cm^{-1} corresponding to the Ge-H stretch and 1698 cm^{-1} corresponding to the carbonyl stretch of the acetoxy ligand.

In an attempt to try and separate and further characterize the product(s) formed individually, GC/MS was used and the chromatogram and mass spectrum obtained for the largest peak are provided below in **Figure 6.24**. The GC indicates that there are five main components in the product mixture. The largest peak which has a retention time of 10.95 minutes has a mass spectrum that corresponds to fragments from $Bu^n_2Ge(H)OAc$ (**11**). The ionization technique used is electron impact, which is a hard ionization technique and we therefore do not expect a peak for the M^+ ion to be present, but rather fragments from the main compound should appear.

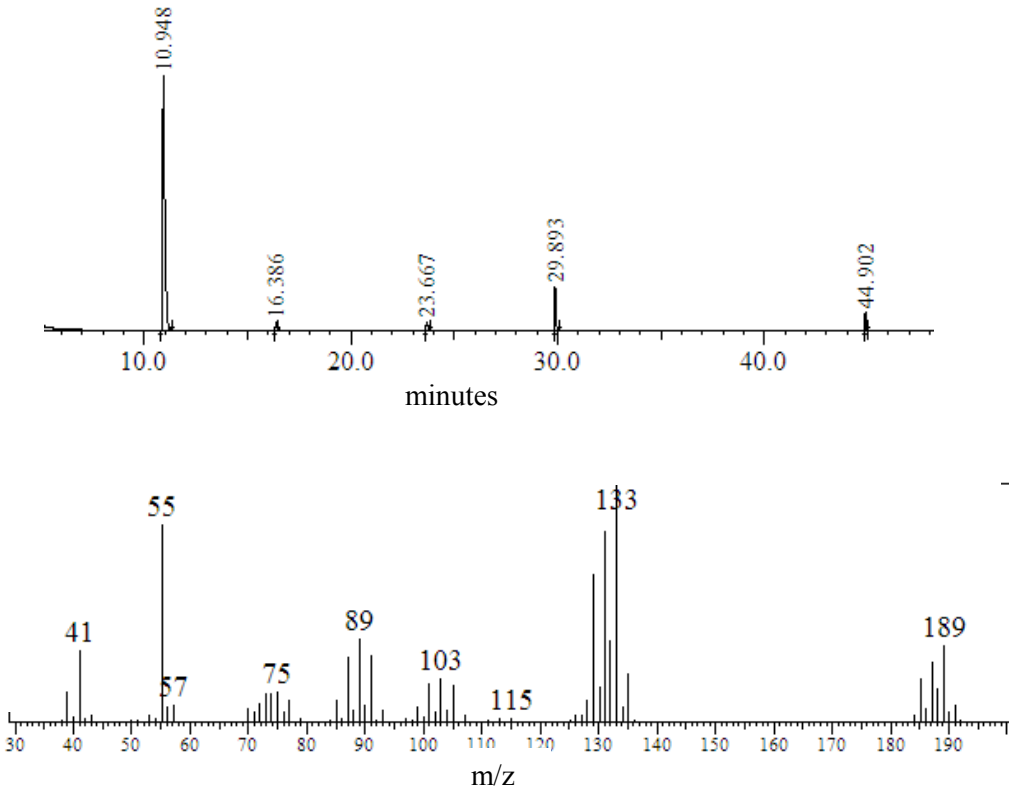

Figure 6.24: GC (top) and MS of the 10.45 min peak (bottom) of the trapping product of $^nBu_3GeGePh_2Ge^nBu_3$ (**7**) with AcOH.

The main peaks and their assignments that contain germanium in the MS for the species with a retention time of 10.95 minutes are as follows: *m/z* = 189 (-OC(O)CH_3), 133 (-C_4H_8), 103 (-C_2H_6), 89 (-CH_2), and 75 (-CH_2) amu. The isotope pattern observed in the MS peaks at *m/z* = 189, 133, 103, 103, 89, and 75 amu indicate that germanium is present in the detected fragments. Germanium has five naturally occurring isotopes (^{70}Ge, ^{72}Ge, ^{73}Ge, ^{74}Ge, and ^{76}Ge) which results in an isotope pattern consistent with that observed in the MS of the trapping product of $^{n}Bu_3GeGePh_2Ge^{n}Bu_3$ (**7**) with AcOH. The second most abundant component of the product mixture eluted off of the column at 29.89 minutes and the MS for that peak corresponds with an 84 % similarity to hexabutyldigermane Bu^{n}_3Ge-$GeBu^{n}_3$ (**Figure 6.25**) indicating that $Bu^{n}_3Ge^{\bullet}$ radicals are being formed in the photolysis as well as germylenes and are recombining to form hexabutyldigermane. This indicates that process **iii** in **Scheme 6.14** is occurring predominantly since there is germylene formation followed by trapping with AcOH, and the recombination of germyl radicals which results in chain contraction. The main peaks that contain germanium in the MS of the 29.9 minute peak are as follows: *m/z* = 431 (-C_4H_9), 375 (-C_4H_8), 319 (-C_4H_8), 263 (-C_4H_8), 207 (-C_4H_8), 189 (-Ge), 149 (-C_4H_{10}), 133 (-CH_4), 103 (-C_2H_6), 89 (-CH_2) amu. The *m/z* peaks 431, 375, 319, 263, and 207 amu appear to contain two germanium atoms based on the isotope pattern and the *m/z* peaks 189, 149, 133, 103, and 89 amu indicate that one germanium atom is present in those fragments.

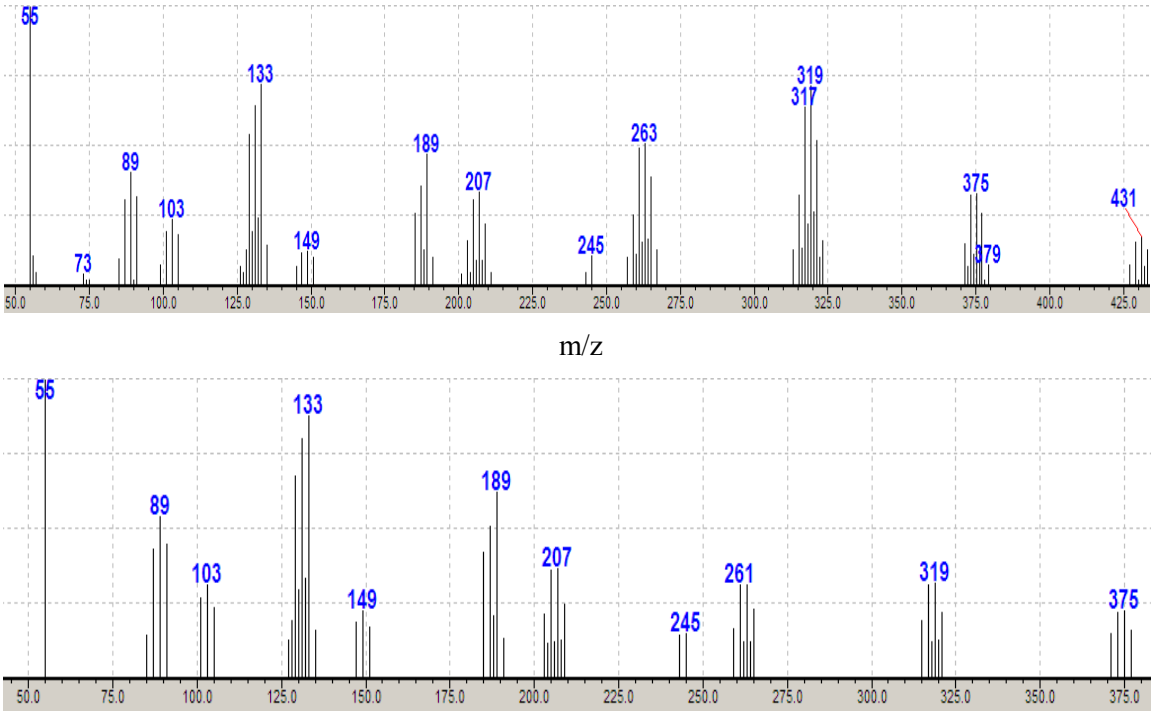

Figure 6.25: MS of the 29.89 min peak (top) of the trapping product of $^{n}Bu_3GeGePh_2Ge^{n}Bu_3$ (**7**) with AcOH, and the library MS for hexabutyldigermane $Bu^{n}_3Ge\text{-}GeBu^{n}_3$ (bottom).

There were three minor components in the product mixture that had retention times of 16.4, 23.7, and 44.9 min. corresponding to the digermanes $Bu^{n}PhMeGe\text{-}GeMePhBu^{n}$ (**13**), $Bu^{n}_2PhGe\text{-}GePhBu^{n}_2$ (**14**), and $Bu^{n}_2PhGe\text{-}GeBu^{n}_3$ (**15**) that result from ligand scrambling. The mass spectrum of the first of these three materials (t = 16.4 min), which is also the least abundant, contained a peak at *m*/*z* = 223 that corresponds to a $Bu^{n}PhMeGe^{+}$ fragment. This fragment arises from cleavage of the Ge – Ge bond in the digermane **13** that was in turn generated by loss of a C_2H_6 fragment from each germanium atom of $Bu^{n}_3Ge\text{-}GeBu^{n}_3$ during the photolysis reaction.

The mass spectrum of the second species eluted (t =23.7 min) contained a peak at *m*/*z* = 265 that is assigned to the fragment $PhBu^{n}_2Ge^{+}$ resulting from the cleavage of the Ge – Ge bond in the digermane **14**. Digermane **14** was likely generated by the coversion of $Bu^{n}_3Ge\text{-}GePh_2\text{-}GeBu^{n}_3$ (**7**) to germyl radicals such as $Bu^{n}_3GeGePh_2\cdot$ that undergo ligand scrambling followed by

a second homolytic cleavage to generate $PhBu^{n}_{2}Ge\cdot$, and these radicals then combine to generate the digermane $Bu^{n}_{2}PhGe\text{-}GePhBu^{n}_{2}$ (**14**).

The mass spectrum of the last minor product to be eluted (t = 44.9 min) contained a peak at *m*/*z* = 394 that is assigned to the fragment $PhBu^{n}_{3}Ge_{2}^{+}$ that results from the loss of two *n*-butyl ligands from the digermane $PhBu^{n}_{2}Ge\text{-}GeBu^{n}_{3}$ (**15**)**.** This digermane likely is generated from the combination of the two radical fragments $PhBu^{n}_{2}Ge\cdot$ and $Bu^{n}_{3}Ge\cdot$ that are formed during the photolysis of $Bu^{n}_{3}Ge\text{-}GePh_{2}\text{-}GeBu^{n}_{3}$ (**7**). The mass spectrum of **15** contains a complex fragmentation pattern that contains $Ph_{3}Ge^{+}$ and its subsequent decomposition products. Thus, five products were identified in the product mixture resulting from photolysis of $Bu^{n}_{3}Ge\text{-}GePh_{2}\text{-}GeBu^{n}_{3}$ (**7**)**.** There was no GC/MS evidence for the formation of $Ph_{2}Ge(H)OAc$ (**12**) in this experiment, however, the prolonged irradiation time of 18 h and the high temperature used on the GC column may have decomposed **12**.

The NMR, FTIR, and GC/MS spectra of the trapping product of $Bu^{n}_{3}Ge\text{-}GePh_{2}\text{-}GeBu^{n}_{3}$ (**7**) with AcOH all indicate that $Bu^{n}_{2}Ge(H)OAc$ (**11**) is being formed as the major trapping product, and the ^{1}H NMR spectrum indicates that $Ph_{2}Ge(H)OAc$ (**12**) is also being formed in the photolysis and trapping process. The GC/MS data also indicates the presence of hexabutyldigermane which is the result of radical formation followed by combination of those radicals which leads to chain contraction of the original oligogermane. In order to investigate further, we performed a timed NMR experiment in cyclohexane-d_{12} where instead of using a large excess of AcOH, only 2 molar equivalents were used. The experiment was performed using concentrations of 0.05 M $Bu^{n}_{3}Ge\text{-}GePh_{2}\text{-}GeBu^{n}_{3}$ (**7**) and 0.1 M AcOH in 0.5 mL of cyclohexane-d_{12} in a quartz NMR tube. This experiment was performed by photolyzing the sample for specific time intervals and then immediately taking the ^{1}H NMR. The experiment appeared to be complete after three hours of exposure to UV light. The sequential ^{1}H NMR spectra for this experiment are provided below in **Figure 6.26(a-h)**.

a) t = 0

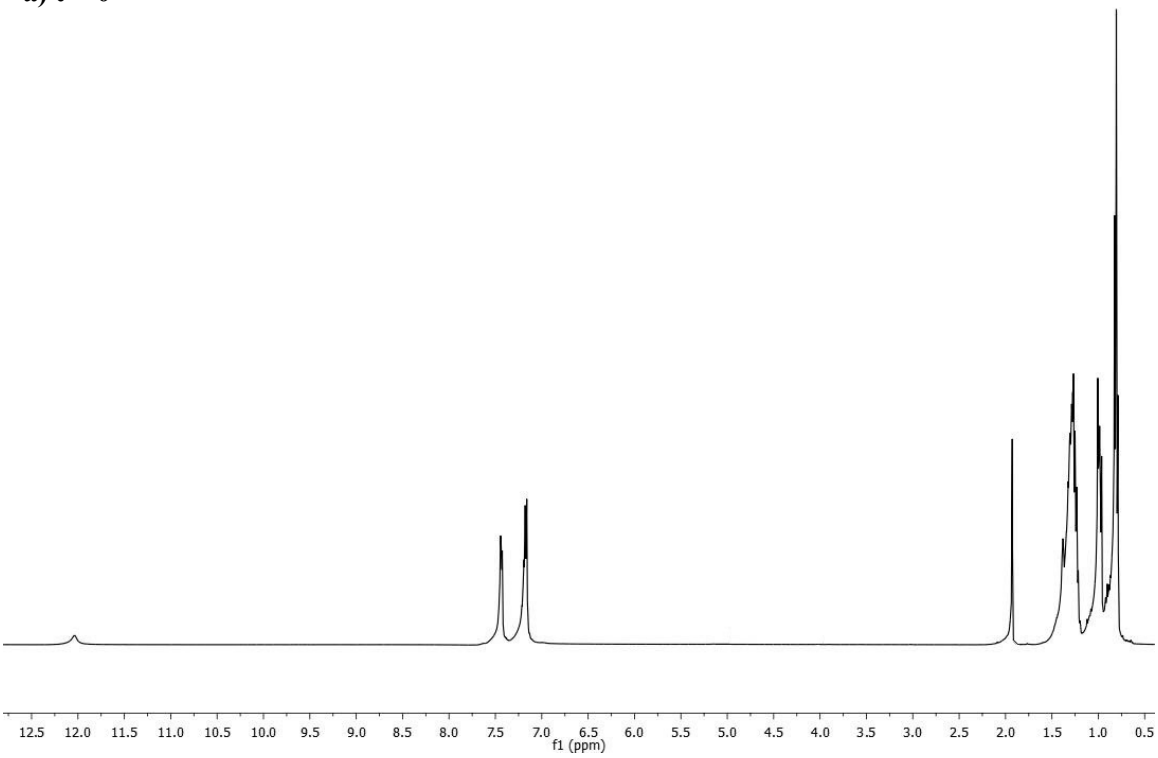
12.5 12.0 11.5 11.0 10.5 10.0 9.5 9.0 8.5 8.0 7.5 7.0 6.5 6.0 5.5 5.0 4.5 4.0 3.5 3.0 2.5 2.0 1.5 1.0 0.5
f1 (ppm)

b) t = 3 min

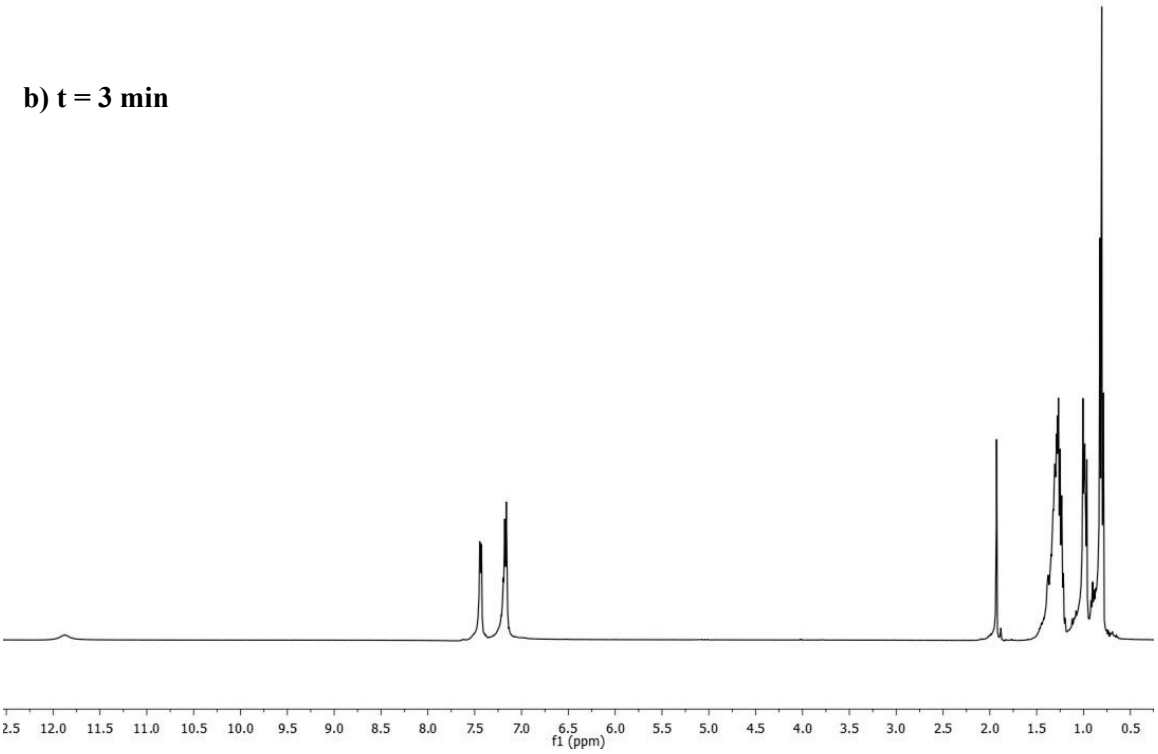
2.5 12.0 11.5 11.0 10.5 10.0 9.5 9.0 8.5 8.0 7.5 7.0 6.5 6.0 5.5 5.0 4.5 4.0 3.5 3.0 2.5 2.0 1.5 1.0 0.5
f1 (ppm)

c) t = 15 min

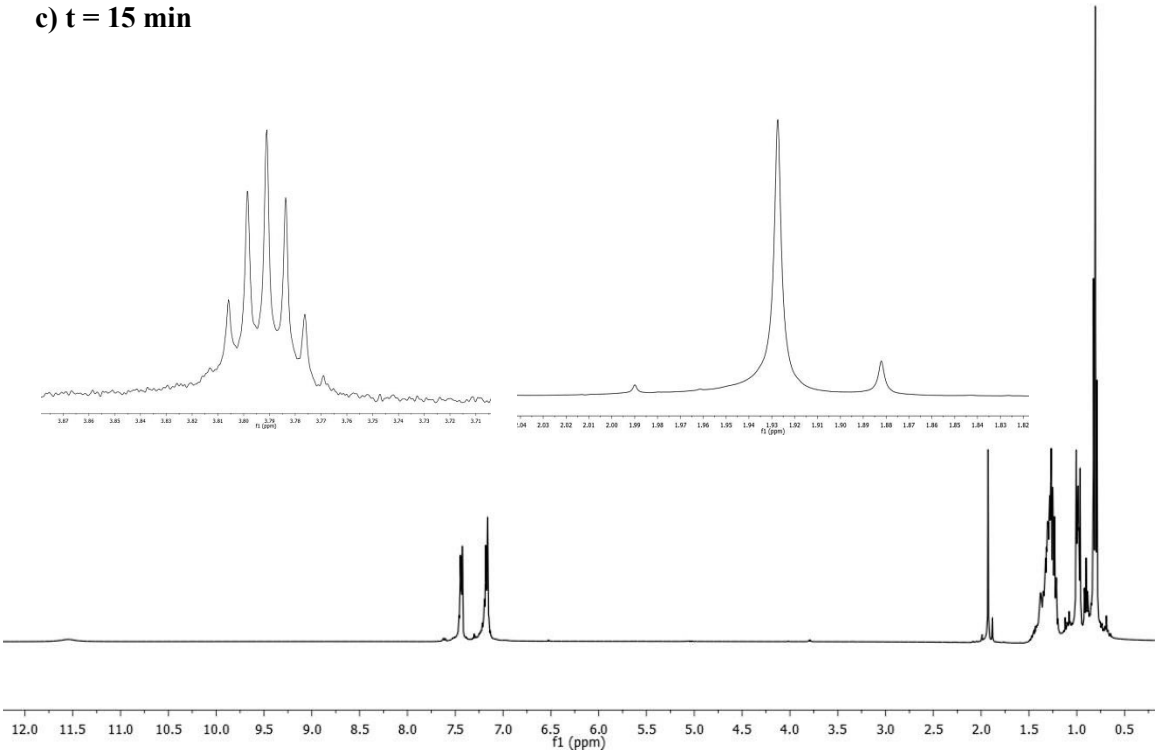

d) t = 30 min

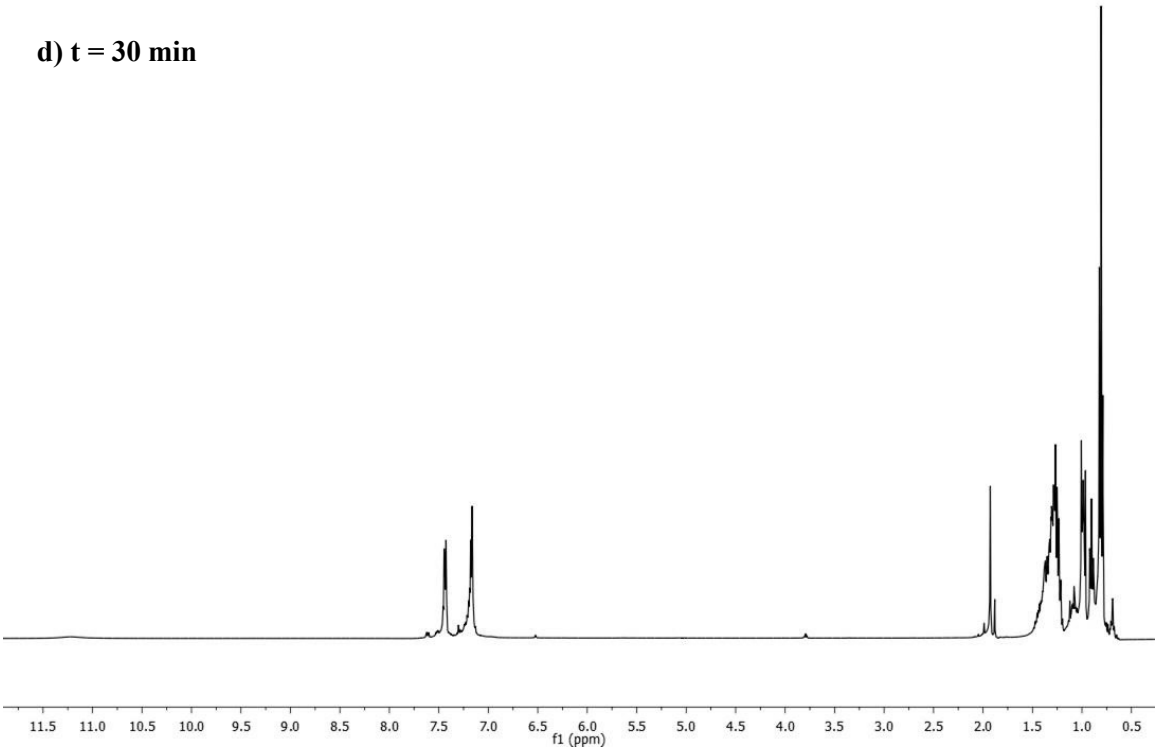

e) t = 1 hour

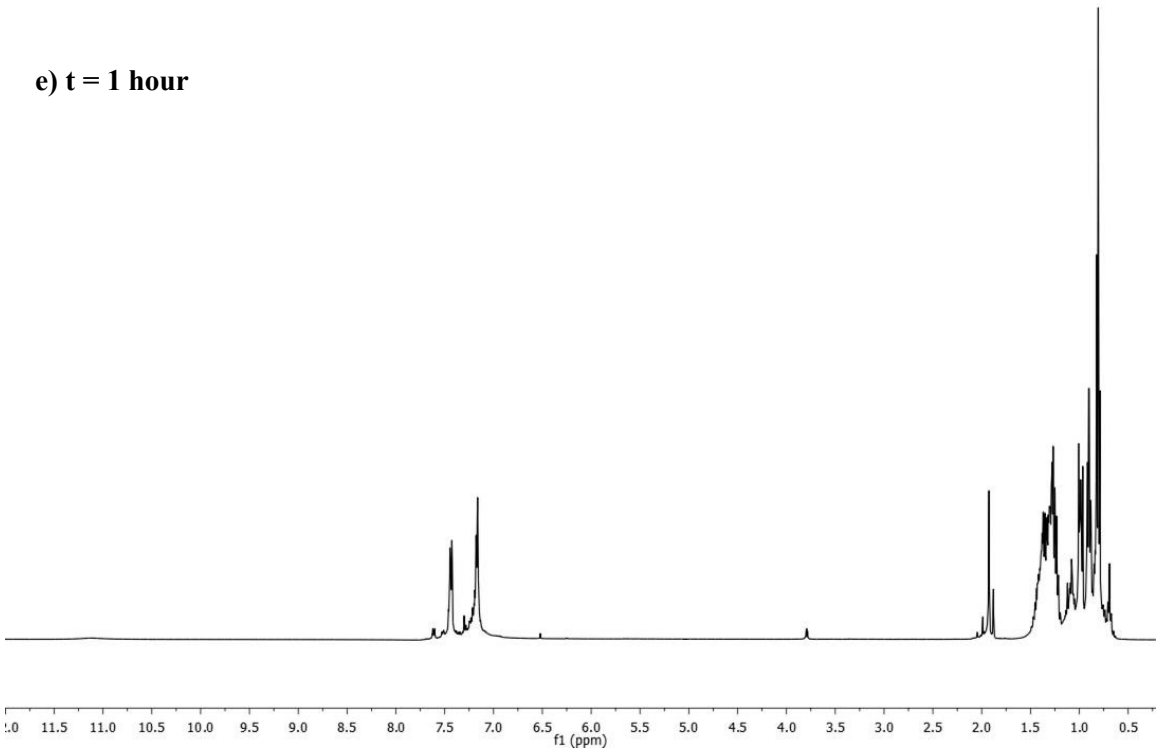

f) t = 1 hr 30 min

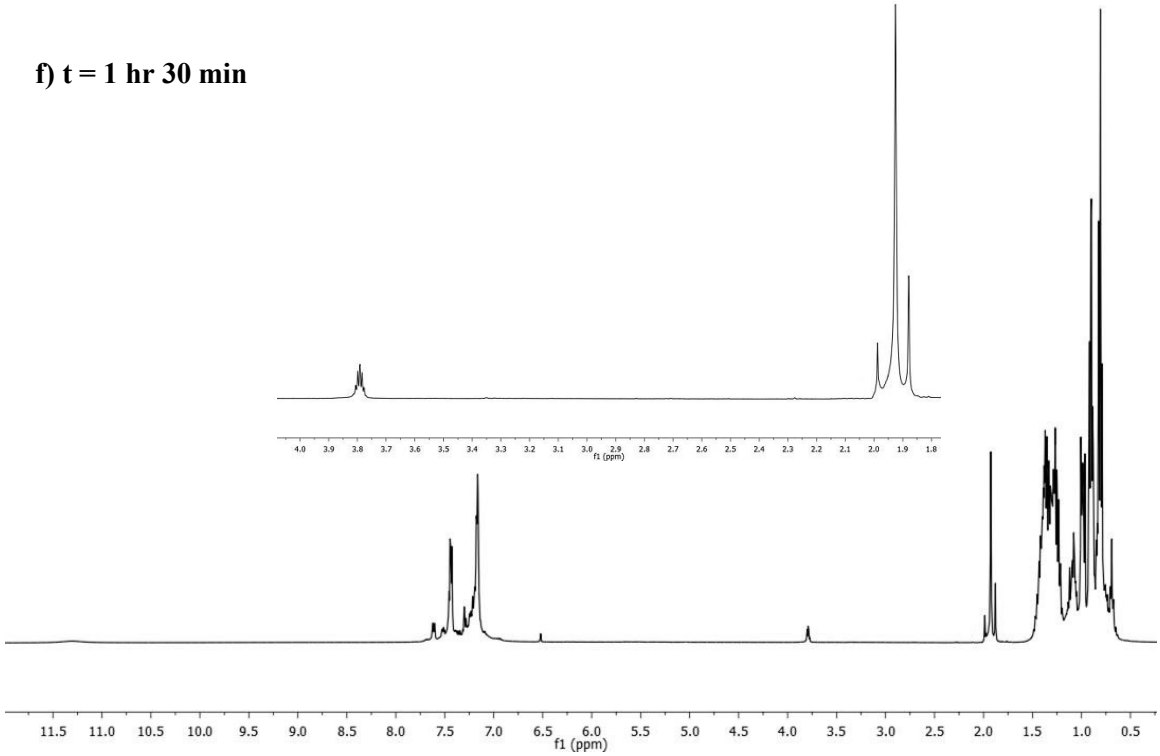

g) t = 2 hours

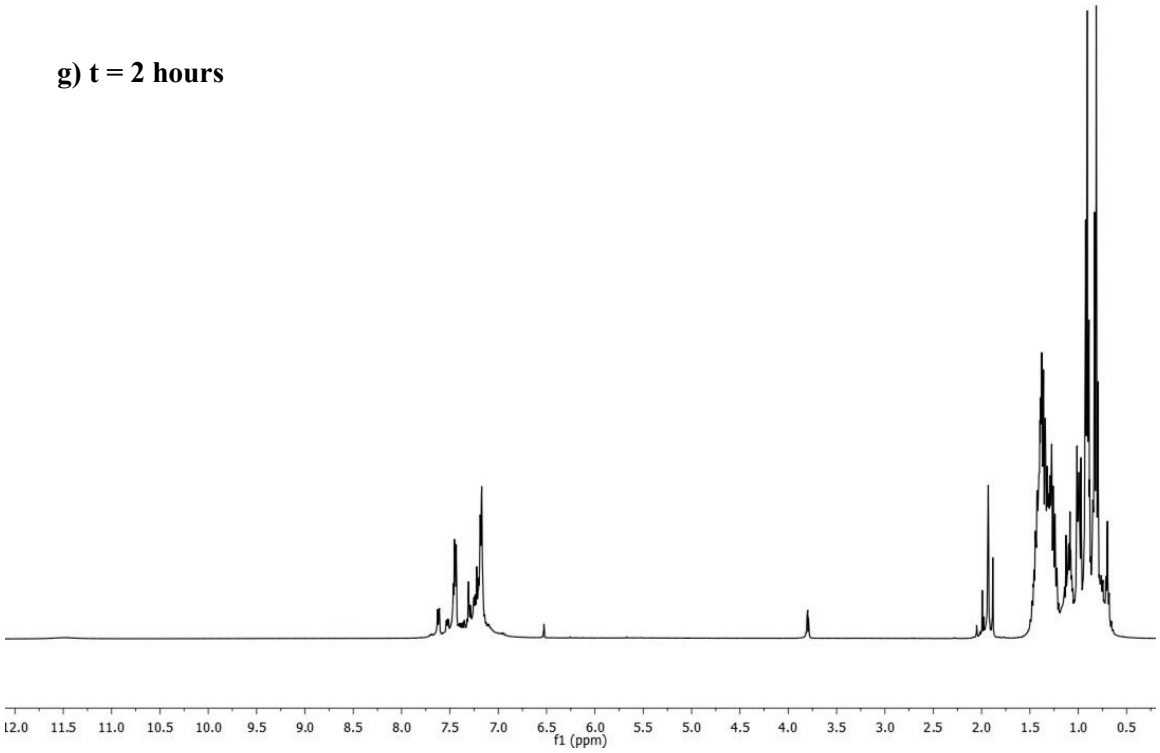

h) t = 3 hr 15min

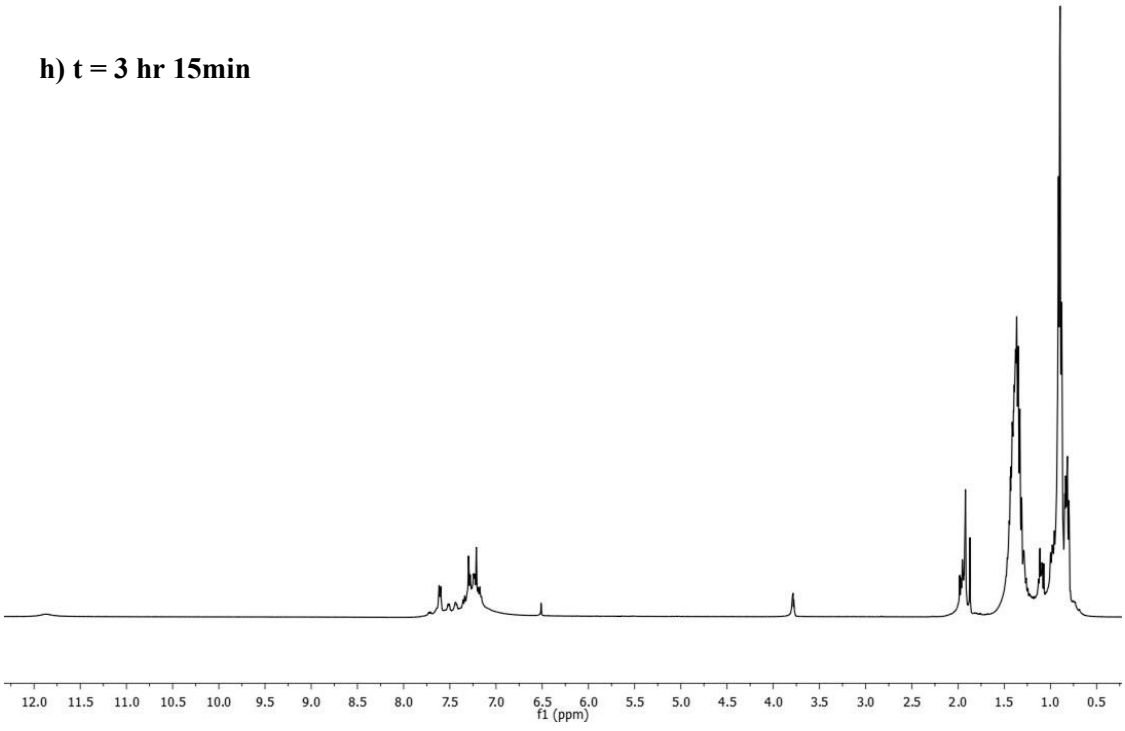

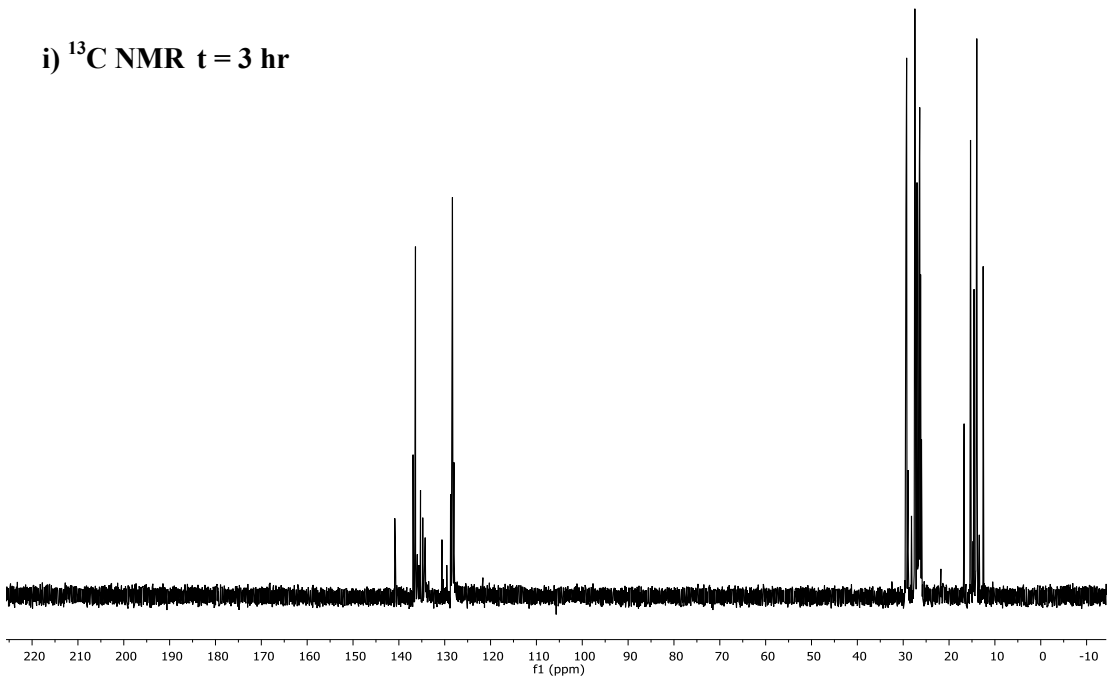

Figure 6.26: Timed NMR experiment ^{1}H (**a-h**) and ^{13}C (**i**) of 0.05 M $^{n}Bu_3GeGePh_2Ge^{n}Bu_3$ (**7**) and 0.1 M AcOH in cyclohexane-d_{12}.

At t = 0 the ^{1}H NMR spectrum contained only peaks for the phenyl and *n*-butyl groups of Bu^{n}_3Ge-$GePh_2$-$GeBu^{n}_3$ (**7**) and the –OH group and methyl group of the acetic acid. The hydroxyl group of the acetic acid appeared as a broad singlet at δ 12.03 ppm and the $–CH_3$ group appeared as a sharp singlet at δ 1.93 ppm. After three minutes of exposure to the UV-C light there was the appearance of a small singlet at δ 1.88 ppm corresponding to the formation of another compound containing a methyl group with a similar chemical environment as the methyl group in acetic acid. The signals for the *n*-butyl groups also began to decrease slightly in intensity. After 15 total minutes of UV-C exposure the hydroxyl group from the acetic acid and the *n*-butyl groups from the trigermane **7** continued to decrease in intensity. The singlet that appeared at δ 1.88 ppm continued to increase in intensity and there was also the appearance of another singlet at δ 1.99

ppm corresponding to the formation of yet another compound containing a methyl group with a similar chemical environment as the methyl group in acetic acid. The alkyl region became increasingly complex and there was also the appearance of new small peaks in the phenyl region, as well as the first noticeable appearance of the pentet at δ 3.79 ppm as well as another small singlet at δ 6.52 ppm of which both were in the range for a Ge-H proton. This was the first instance of the formation of $Bu^n_2Ge(H)OAc$ (**11**) and $Ph_2Ge(H)OAc$ (**12**). As time progressed, there was a steady increase in the intensity of the pentet at δ 3.79 ppm and singlet at δ 6.52 ppm with a concomitant increase of the methyl peaks at δ 1.88 ppm and δ 1.99 ppm. However, the intensity of the pentet and the singlet at δ 1.88 was higher than those of the singlets at δ 6.52 and 1.99 ppm. This indicated that the formation of $Bu^n_2Ge(H)OAc$ (**11**) is favored versus the formation of $Ph_2Ge(H)OAc$ (**12**). After about three hours, the NMR spectra were largely unchanged and thus the reaction was completed. Throughout the experiment as time progressed, the *n*-butyl region became more complex and thus it was likely that hexabutyldigermane is being formed at this point as well, but it was difficult to tell based on the spectrum. The ^{13}C NMR (**Figure 6.26i**) was obtained at the ending time (3 hours and 15 minutes) and was not highly informative. The alkyl region contained a large number of peaks with significant overlap in the ranges of δ 29.5 – 26.9 and 16.7 – 12.6 ppm and the phenyl region contained a large number of peaks with significant overlap in the range of δ 140.9 – 128.0 ppm indicating the possibility of the formation of other oligogermanes in this process that arose via the formation of and reaction between germyl radicals.

6.4.3 Conclusion

The oligogermanes **4-9** have been photolyzed with UV-C light in the presence of AcOH as a germylene trapping agent. The ^1H and ^{13}C NMR spectra demonstrate the formation of the

trapped germylenes $Bu^n_2Ge(H)OAc$ (**11**) and $Ph_2Ge(H)OAc$ (**12**). The FTIR spectrum of these compounds clearly indicates the presence of a Ge-H bond and a carbonyl bond. The GC/MS of the photolysis product also shows the presence of $Bu^n_2Ge(H)OAc$ (**11**) as well as hexabutyldigermane $Bu^n_3Ge\text{-}GeBu^n_3$. These preliminary results clearly demonstrate that this photolysis is a complex process in that germylenes are being extruded from the oligogermanes, but it is not solely $:GePh_2$ which was initially expected due to the internal $\text{-}GePh_2\text{-}$ fragments having Ge(II) character. Trialkylgermyl radicals $Bu^n_3Ge^{\bullet}$ are also being formed in the photolytic process which then recombine to form the hexabutyldigermane. It is also expected that butylphenylgermylenes BuPhGe: are being extruded upon photolysis but are not evident in the spectroscopic techniques utilized. We currently have a collaboration underway with Dr. Willie Leigh at McMaster University to perform laser flash photolysis experiments on all six of the oligogermanes **4-9** to try and gain more insight into the oxidation products of these systems.

The mass spectra for all five components of the product mixture in the GC (**Figure 6.24**) as well as the NMR spectra for the other photolysis products for compounds **4-6** and **8-9** with AcOH can be found in the appendix of this dissertation.

Table 6.9: Crystallographic data for compounds **1** and **8**.

	1	**8**
Compound	*$ClPh_2Ge$-$GePh_2Cl$*	*$Et_3Ge(GePh_2)_2GeEt_3$*
Empirical Formula	$C_{24}H_{20}Cl_2Ge_2$	$C_{36}H_{50}Ge_4$
Formula Weight	524.48	773.12
Temperature (K)	100(2)	100(2)
Wavelength (Å)	0.71073 (Mo Kα)	0.71073 (Mo Kα)
Crystal System	Monoclinic	Monoclinic
Space Group	C2	P2(1)/c
a, Å	15.012(3)	27.1925(10)
b, Å	11.818(2)	10.6491(4)
c, Å	13.164(2)	18.6622(8)
α, °	90	90
β, °	108.381(4)	90.853(2)
γ, °	90	90
V, Å^3	2216.3(7)	5403.5(4)
Z	4	6, 1.5
ρ (g cm^{-3})	1.572	1.426
Absorption coefficient (mm^{-1})	2.961	3.327
F(000)	1048	2364
Crystal Size (mm)	0.20 x 0.12 x 0.10	0.30 x 0.10 x 0.10
Theta range for data collection	1.63 to 26.39°	1.50 to 26.42°
Index ranges		
	$-18 \le h \le 17$	$-33 \le h \le 32$
	$0 \le k \le 14$	$-13 \le k \le 13$
	$0 \le l \le 16$	$-23 \le l \le 23$
Reflections collected	2966	77117
Independent reflections	2969	11066
	(R_{int} = 0.0000)	(R_{int} = 0.0588)
Completeness to θ = 25.00°	99.8%	99.8%
Absorption correction	Multi-scan (SADABS)	Multi-scan (SADABS)
Max. and Min. transmission	0.7562 and 0.5889	0.8334 and 0.8189
Refinement method	Full-matrix least-squares on F^2	Full-matrix least-squares on F^2
Data/restraints/parameters	2969 / 15 / 273	11066/1/548
Goodness-of-fit on F^2	1.088	1.027
Final *R* indices (I < 2σ(I))		
R_1	0.0489	0.0421
wR_2	0.0959	0.0879
Final R indices (all data)		
R_1	0.0660	0.0650
wR_2	0.1026	0.0964
Largest diff. peak and hole	0.727 and -0.578 e Å^{-3}	1.0488 and -0.818 e Å^{-3}

Table 6.10: Crystallographic data for compound **3** (both CIF files).

	3-1	**3-2**
Compound	*Ph_3Ge-$GePh_2H$*	*Ph_3Ge-$GePh_2H$ ($C_{30}H_{26}Ge_{1.96}$, 0.02(Ge2)*
Empirical Formula	$C_{30}H_{26}Ge_2$	$C_{30}H_{26}Ge_2$
Formula Weight	531.69	531.69
Temperature (K)	100	100
Wavelength (Å)	0.71073 (Mo Kα)	0.71073 (Mo Kα)
Crystal System	Triclinic	Triclinic
Space Group	P-1	P-1
a, Å	9.4057(6)	10.0843(10)
b, Å	9.8810(6)	13.8993(14)
c, Å	13.8179(9)	27.553(3)
α, °	96.726(2)	93.627(3)
β, °	105.752(2)	98.798(3)
γ, °	95.146(2)	102.790(3)
V, Å^3	1217.51(13)	3702.9(6)
Z	2	6
ρ (g cm^{-3})	1.450	1.431
Absorption coefficient (mm^{-1})	2.484	2.450
F(000)	540	1620
Crystal Size (mm)	0.20 x 0.09 x 0.05	0.3 x 0.12 x 0.11
Theta range for data collection	1.548 to 26.342°	1.503 to 26.376°
Index ranges		
	$-11 \le h \le 11$	$-12 \le h \le 12$
	$-12 \le k \le 12$	$-17 \le k \le 17$
	$-17 \le l \le 14$	$-34 \le l \le 34$
Reflections collected	15686	75897
Independent reflections	4930	15133
	(R_{int} = 0.0468)	(R_{int} = 0.0977)
Completeness to θ = 25.00°	99.7%	99.9%
Absorption correction	Multi-scan (SADABS)	Multi-scan (SADABS)
Max. and Min. transmission	0.0931 and 0.0660	0.0932 and 0.0657
Refinement method	Full-matrix least-squares on F^2	Full-matrix least-squares on F^2
Data/restraints/parameters	4930 / 0 / 294	15133/0/880
Goodness-of-fit on F^2	1.010	1.004
Final *R* indices (I < 2σ(I))		
R_1	0.0396	0..0404
wR_2	0.0712	0.0618
Final R indices (all data)		
R_1	0.0631	0.0921
wR_2	0.0781	0.0860
Largest diff. peak and hole	0.977 and -0.758 e Å^{-3}	0.654 and -0.642 e Å^{-3}

Table 6.11: Crystallographic data for compound **10**.

	10
Compound	Ph_3GeCH_2CN
Empirical Formula	$C_{20}H_{17}GeN$
Formula Weight	343.96
Temperature (K)	100(2)
Wavelength (Å)	0.71073 (Mo Kα)
Crystal System	Triclinic
Space Group	P-1
a, Å	9.4123(19)
b, Å	9.4402(19)
c, Å	9.779(2)
α, °	92.021(3)
β, °	108.696(3)
γ, °	98.341(3)
V, Å^3	811.2(3)
Z	2
ρ (g cm^{-3})	1.408
Absorption coefficient (mm)	1.884
F(000)	352
Crystal Size (mm)	0.18 x 0.15 x 0.10
Theta range for data collection	2.19 to 28.36°
Index ranges	
	$-12 \leq h \leq 12$
	$-12 \leq k \leq 12$
	$-12 \leq l \leq 12$
Reflections collected	9828
Independent reflections	3695
	(R_{int} = 0.0862)
Completeness to θ = 25.00°	99.8%
Absorption correction	Multi-scan (SADABS)
Max. and Min. transmission	0.8340 and 0.7280
Refinement method	Full-matrix least -squares on F^2
Data/restraints/parameters	3695/0/199
Goodness-of-fit on F^2	1.000
Final *R* indices (I < 2σ(I))	
R_1	0.0545
wR_2	0.1102
Final R indices (all data)	
R_1	0.0831
wR_2	0.1249
Largest diff. peak and hole (e Å^{-3})	0.971 and -0.879

6.5 Experimental

General Considerations

UV/visible spectroscopy were obtained using a Hewlett-Packard 8453 diode array spectrometer in hexane solvent. Differential pulse voltammograms were recorded using a DigiIvy DY2112 potentiostat with 0.1 M $[Bu_4N][PF_6]$ in CH_2Cl_2 as the supporting electrolyte, and the reported data are the average of four independent runs. GC/MS were acquired using a Shimadzu QP2010S equipped with an EI ionization source. NMR were recorded using a Varian Unity INOVA 400 operating at 400 MHz (^1H) or 100 MHz (^{13}C) and were referenced to residual protio solvent. Infrared spectra were obtained using a Hewlett-Packard FT-IR spectrometer. Bu^n_3GeCl, Et_3GeCl, Ph_3GeH, Ph_2GeH_2, and $Ph_3GeGePh_3$ were purchased from Gelest. $Cl_3CC(O)OH$, $LiAlH_4$, $LiNMe_2$, and glacial acetic acid were purchased from Aldrich, and $HCl_{(ether)}$ was purchased from ACROS Organics. All of these materials were used as received. ^1H NMR (300 MHz) and ^{13}C NMR spectra (75.4 MHz) were recorded on a Gemini 2000 NMR spectrometer and were referenced to benzene-d_6 solvent. Elemental analyses were conducted by Midwest Microlabs and Galbrath Laboratories.

*Synthesis of $ClPh_2Ge$-$GePh_2Cl$ (**1**)*

To a solution of Ph_3Ge-$GePh_3$ (2.000 g, 3.29 mmol) in 20 mL toluene was added 4.2 equivalents of $Cl_3CC(O)OH$ (2.260 g, 13.8 mmol) directly under blowing nitrogen into a 150 mL schlenk tube. The Ph_3Ge-$GePh_3$ was not dissolved in solution at this point. The reaction mixture was heated at 110 ^oC for 96 hours with shaking of the Schlenk tube after 24 hours to ensure the solubility of all reactants in solution. The reaction mixture was allowed to cool to room temperature and was taken into an inert atmosphere glovebox where 2.5 equivalents of 0.1 N $HCl_{(ether)}$ (8.23 mL, 8.23 mmol) was directly injected in the reaction mixture. The mixture was

sealed again and heated at 50 °C for 18 hours. The reaction mixture was allowed to cool to room temperature and the mixture was transferred to a 100 mL schlenk flask and the volatiles were removed *in vacuo* to yield a brown substance with crystals forming on the walls of the flask ($Cl_3CC(O)OH$). The schlenk flask was taken into the glovebox where the product was isolated in a 20 mL glass vial. The product was then washed with hexane 3 x 15 mL to remove the reformed trichloroacetic acid and any other impurities. The resulting product was then dried *in vacuo* to yield 0.914 g of **1** (53 %) as a white powder. ^{1}H NMR (C_6D_6, 23°C) δ 7.76 - 7.73 (m, 8H, *meta*-C_6H_5), 7.02 – 6.99 (m, 12H, *ortho*- and *para*- C_6H_5) ppm. ^{13}C NMR (C_6D_6, 23°C) δ 135.8 (*ipso*-C_6H_5), 134.1 (*ortho*- C_6H_5), 130.8 (*meta*- C_6H_5), 129.1 (*para*- C_6H_5) ppm.

.

*Synthesis of HPh_2Ge-$GePh_2H$ (**2**)*

To a solution of **1** (0.500 g, 0.95 mmol) in THF (20 mL) was directly added $LiAlH_4$ (0.080 g, 2.10 mmol) in a schlenk flask. The reaction mixture was allowed to stir under blowing nitrogen at room temperature for 18 hours. The volatiles were then removed *in vacuo* and the product was extracted from the mixture using hot benzene (60 °C)(3 x 25mL) which was added directly to the product mixture followed by cannulation into a frit containing celite to filter out any unwanted byproducts. The volatiles were then removed *in vacuo* to yield 0.370 g of **2** (85 %) as a white powder. ^{1}H NMR (C_6D_6, 23°C) δ 7.52-7.49 (m, 8H, *meta*-C_6H_5), 7.07-7.04 (m, 12H, *ortho*- and *para*- C_6H_5), 5.57 (s, 2H, Ge-*H*) ppm. ^{13}C NMR (C_6D_6, 23°C) δ 135.7 (*ortho*- C_6H_5), 129.1 (*meta*- C_6H_5), 128.7 (*para*- C_6H_5) ppm.

Synthesis of Et_3GeNMe_2

To a solution of Et_3GeCl (0.300 g, 1.54 mmol) in THF (10 mL) was added $LiNMe_2$ (0.094 g, 1.84 mmol) in THF (10 mL) in a 100 mL schlenk flask. The reaction was allowed to stir

at room temperature for 18 hours. The THF was then removed via short-path distillation and hexane (25 mL) was added to the remaining product. The solution was then cannulated through a frit containing celite to filter out LiCl. The hexane was then removed via short-path distillation to yield 0.276 g of Et_3GeNMe_2 (88%) as a light-yellow liquid. ^{1}H NMR (C_6D_6, 23°C) δ 2.57 (s, 6H, -N(CH_3)$_2$), 1.04 (t, J = 9 Hz, 9H, -CH_2CH_3), 0.79 (q, J = 9 Hz, 6H, CH_2CH_3) ppm.

Synthesis of $Bu^n_3GeNMe_2$

To a solution of Bu^n_3GeCl (1.000 g, 3.58 mmol) in benzene (10 mL) was added $LiNMe_2$ (0.219 g, 4.29 mmol) in benzene (5 mL) in a 100 mL schlenk flask. The reaction was allowed to stir at room temperature for 18 hours. The solution was then filtered through celite and the volatiles were removed *in vacuo* to yield 0.961 g of $Bu^n_3GeNMe_2$ (93 %) as a colorless liquid. ^{1}H NMR (C_6D_6,25 °C): δ 2.62 (s, 6H, GeN-(CH_3)$_2$), 1.52-1.30 (m, 12H, $GeCH_2CH_2CH_2CH_3$), 0.93 (t, J = 7.2 Hz, 9H, $GeCH_2CH_2CH_2CH_3$), 0.89 (m, 6H, $GeCH_2$) ppm. ^{13}C NMR (C_6D_6,25 °C): δ 41.5 (-N(CH_3)$_2$), 27.4, 26.9, 14.1 (butyl group carbons), 13.2 (-$CH_2CH_2CH_2CH_3$) ppm. *Anal.* Calcd for $C_{14}H_{33}GeN$: C, 58.38; H, 11.55. Found: C, 58.28; H, 11.79.

*Synthesis of $Et_3GeGePh_3$ (**4**)*

Compound **4** was prepared in a similar fashion to the literature.[73] A solution of Et_3GeNMe_2 (0.250 g, 1.23 mmol) in CH_3CN (10 mL) was added a solution of Ph_3GeH (0.374 g, 1.23 mmol) in CH_3CN (10 mL) in a schlenk tube. The reaction mixture was heated at 85 °C for 48 hours. The volatiles were removed *in vacuo* and when more CH_3CN was added to transfer the product from the flask to a vial, clear crystals immediately precipitated out of solution and were

isolated to yield 0.477 g of **4** (84%). ^{1}H NMR (C_6D_6, 25 °C): δ 7.64-7.61 (m, 6H, *meta*-C_6H_5), 7.23-7.16 (m, 9H, *ortho*-C_6H_5 and *para*-C_6H_5), 1.03 (m, 15H, Ge-$(CH_2CH_3)_3$) ppm. ^{13}C NMR (C_6D_6,25 °C): δ 139.2 (*ipso*- C_6H_5), 135.6 (*ortho*- C_6H_5), 128.7 (*para*- C_6H_5), 128.6 (*meta*- C_6H_5), 10.2, 6.1 (ethyl group carbons) ppm. *Anal.* Calcd for $C_{24}H_{30}Ge_2$: C, 62.16; H, 6.52. Found: C, 61.96; H, 6.61.

*Synthesis of $^{n}Bu_3GeGePh_3$ (**5**)*

Compound **5** was prepared in a similar fashion to the literature.[73] A solution of $Bu^{n}{}_3GeNMe_2$ (0.300 g, 1.04 mmol) in CH_3CN (10 mL) was added a solution of Ph_3GeH (0.318 g, 1.04 mmol) in CH_3CN (10 mL) in a schlenk tube. The reaction mixture was heated at 85 °C for 48 hours. The volatiles were removed *in vacuo* to yield 0.474 g of **5** (83%) as a white solid. ^{1}H NMR (C_6D_6, 25 °C): δ 7.72-7.64 (m, 6H, *meta*- C_6H_5), 7.24-7.16 (m, 9H, *ortho*- C_6H_5 and *para*- C_6H_5), 1.52-1.39 (m, 6H, $GeCH_2$), 1.27 (sext, J = 7.8 Hz, 6H, $GeCH_2CH_2CH_2CH_3$), 1.21-1.15 (m, 6H, $GeCH_2CH_2CH_2CH_3$), 0.81 (t, J= 6.9 Hz, 9H, $GeCH_2CH_2CH_2CH_3$) ppm. ^{13}C NMR (C_6D_6, 25 °C): δ 139.7 (*ipso*- C_6H_5), 135.7 (*ortho*- C_6H_5), 128.7 (*para*- C_6H_5), 128.6 (*meta*- C_6H_5), 28.8, 26.8,14.5, 13.8 (butyl group carbons) ppm. *Anal.* Calcd for $C_{30}H_{42}Ge_2$:C, 65.77; H, 7.73. Found: C, 65.74; H, 7.80.

*Synthesis of $Et_3GeGePh_2GeEt_3$ (**6**)*

To a solution of Ph_2GeH_2 (0.500 g, 1.73 mmol) in CH_3CN (10 mL) was added a solution of Et_3GeNMe_2 (0.706 g, 3.46 mmol) in CH_3CN (10 mL) in a schlenk tube. The reaction was heated to 85 °C for 48 hours. The volatiles were then removed *in vacuo* and the product was purified via Kugelrohr distillation to yield 0.775 g of **6** (82%) as a clear liquid. ^{1}H NMR (C_6D_6, 25 °C): δ 7.71-7.64 (m, 4H, *meta*-C_6H_5), 7.26-7.15 (m, 6H, *ortho*-C_6H_5 and *para*-C_6H_5), 1.10-1.08 (m, 30H, ethyl groups) ppm. ^{13}C NMR (C_6D_6,25 °C): δ 134.3 (*ortho*- C_6H_5), 130.0 (*para*- C_6H_5), 128.6 (*meta*- C_6H_5), 10.3, 5.8 (ethyl group carbons) ppm.

*Synthesis of $^nBu_3GeGePh_2Ge^nBu_3$ (**7**)*

To a solution of $Bu^n{}_3GeNMe_2$ (1.385 g, 4.810 mmol) in acetonitrile (15 mL) was added a solution of Ph_2GeH_2 (0.500 g, 2.18 mmol) in acetonitrile (10 mL) under an atmosphere of nitrogen. The reaction mixture was sealed in a Schlenk tube under nitrogen and stirred for 48 hours at 85 °C. The acetonitrile was removed *in vacuo* and the resulting oil was vacuum distilled in a Kugelrohr oven (125 °C, 0.10 torr) to yield $Bu^n{}_3GeGePh_2GeBu^n{}_3$ (0.992 g, 64%) as a colorless oil. ^{1}H NMR (C_6D_6, 23°C): δ 7.73 (d, J = 8.4 Hz, 6H, *o*-H), 7.22 (m, 6H, *m*-H), 7.14 (d, J = 7.8 Hz, 3H, *p*-H), 1.49 (m, 6H, -$CH_2CH_2CH_2CH_3$), 1.34 (q, J = 7.8 Hz, 6H, -$CH_2CH_2CH_2CH_3$), 1.19 (m, 6H, -$CH_2CH_2CH_2CH_3$), 0.90 (t, J = 7.2 Hz, 9H, -$CH_2CH_2CH_2CH_3$) ppm. ^{13}C NMR δ 140.7 (*ipso*-C), 136.1 (*ortho*-C), 128.3 (*para*-C), 128.1 (*meta*-C), 28.8 (-$CH_2CH_2CH_2CH_3$), 27.1 ($CH_2CH_2CH_2CH_3$), 15.0 (-$CH_2CH_2CH_2CH_3$), 13.9 (-$CH_2CH_2CH_2CH_3$) ppm. *Anal.* Calcd. For $C_{36}H_{64}Ge_3$: C, 60.47; H, 9.03. Found: C, 60.35; H, 9.11.

*Synthesis of $Et_3Ge(GePh_2)_2GeEt_3$ (**8**)*

To a solution of **2** (0.250 g, 0.549 mmol) in CH_3CN (15 mL) was added a solution of Et_3GeNMe_2 (0.224 g, 1.10 mmol) in CH_3CN (15 mL) under an atmosphere of nitrogen. The reaction mixture was sealed in a Schlenk tube under nitrogen and stirred for 48 hours at 85 °C. The acetonitrile was removed *in vacuo* and the resulting thick oil was vacuum distilled in a Kugelrohr oven (125 °C, 0.10 torr) to yield $Et_3Ge(GePh_2)_2GeEt_3$ (0.259 g, 61%). ^{1}H NMR (C_6D_6, 25 °C): δ 7.72-7.56 (m, 8H, *meta*-C_6H_5), 7.22-6.88 (m, 12H, *ortho*-C_6H_5 and *para*-C_6H_5), 1.05 (m, 12H, -CH_2CH_3), 0.97-0.91 (m, 18H, -CH_2CH_3) ppm. ^{13}C NMR (C_6D_6,25 °C): δ 137.1 (*ortho*-C_6H_5), 136.5 (*meta*- C_6H_5), 136.0 (*para*- C_6H_5), 10.3, 6.6 (ethyl group carbons) ppm.

*Synthesis of $^nBu_3Ge(GePh_2)_2Ge^nBu_3$ (**9**)*

To a solution of **2** (0.400 g, 0.878 mmol) in CH_3CN (15 mL) was added a solution of $Bu^n{}_3GeNMe_2$ (0.506 g, 1.76 mmol) in CH_3CN (15 mL) under an atmosphere of nitrogen. The reaction mixture was sealed in a Schlenk tube under nitrogen and stirred for 48 hours at 85 °C. The acetonitrile was removed *in vacuo* and the resulting thick oil was vacuum distilled in a Kugelrohr oven (125 °C, 0.10 torr) to yield $^nBu_3Ge(GePh_2)_2Ge^nBu_3$ (0.554 g, 67%). ^{1}H NMR (C_6D_6, 25 °C): δ 7.75-7.64 (m, 8H, *meta*-C_6H_5), 7.25-7.10 (m, 12H, *ortho*-C_6H_5 and *para*-C_6H_5), 1.60-0.82 (m, 54H, butyl group protons) ppm. ^{13}C NMR (C_6D_6,25 °C): δ 137.1 (*ortho*- C_6H_5), 136.5 (*meta*- C_6H_5), 136.0 (*para*- C_6H_5), 28.9, 26.5, 14.0, 12.2 (butyl group carbons) ppm.

General Photolysis Experiment

In each of the initial studies 300 mg of the corresponding germane was dissolved in THF (15 mL) in a 100 mL quartz flask and the flask was closed with a septum and copper wire under an inert atmosphere of nitrogen. The flask was removed and connected to a schlenk line under blowing nitrogen and glacial acetic acid (30 mol equivalents) was directly injected into the THF solution. The solution was then irradiated with UV-C light for 18 hours. The THF was then removed *in vacuo* and the remaining thick liquid was dissolved in benzene (10 mL) and the excess acetic acid was extracted using water (3 x 5 mL) and the volatiles from the benzene layer were then removed *in vacuo* to yield the trapping product (approximately 150 mg) as a colorless oil. The timed ^{1}H NMR experiment was performed using 0.05 M **7** and 0.1 M AcOH in 0.5 mL of cyclohexane-d_{12} in a quartz NMR tube.

6.6 References

1. Abd-El-Aziz, A. S., *Half-century of Metal- and Metalloid-Containing Polymers*. Wiley-Interscience: Hoboken, N.J., 2003; p v.

2. Balaji, V.; Michl, J., *Polyhedron* **1991,** *10* (11), 1265-1284.

3. Miller, R. D.; Michl, J., *Chem. Rev.* **1989,** *89* (6), 1359-1410.

4. Amadoruge, M. L.; Weinert, C. S., *Chem. Rev.* **2008,** *108* (10), 4253-4294.

5. Weinert, C. S., *Dalton Trans.* **2009,** (10), 1691-1699.

6. Amadoruge, M. L.; Gardinier, J. R.; Weinert, C. S., *Organometallics* **2008,** *27* (15), 3753-3760.

7. Amadoruge, M. L.; Golen, J. A.; Rheingold, A. L.; Weinert, C. S., *Organometallics* **2008,** *27* (9), 1979-1984.

8. Amadoruge, M. L.; Short, E. K.; Moore, C.; Rheingold, A. L.; Weinert, C. S., *J Organomet. Chem.* **2010,** *695* (14), 1813-1823.

9. Bulten, E. J.; Noltes, J. G., *J. Organomet. Chem.* **1969,** *16* (1), P8-&.

10. Mochida, K.; Hata, R.; Shimoda, M.; Matsumoto, F.; Kurosu, H.; Kojima, A.; Yoshikawa, M.; Masuda, S.; Harada, Y., *Polyhedron* **1996,** *15* (18), 3027-3032.

11. Mochida, K.; Hodota, C.; Hata, R.; Fukuzumi, S., *Organometallics* **1993,** *12* (2), 586-588.

12. Okano, M.; Mochida, K., *Chem. Lett.* **1990,** (5), 701-704.

13. Samanamu, C. R.; Amadoruge, M. L.; Yoder, C. H.; Golen, J. A.; Moore, C. E.; Rheingold, A. L.; Materer, N. F.; Weinert, C. S., *Organometallics* **2011,** *30* (5), 1046-1058.

14. Zuev, V. V.; Sazanov, Y. N.; Skvortsov, N. K., *Polym. Sci. Ser. B* **2003,** *45* (9-10), 316-318.

15. Shankar, R.; Saxena, A.; Brar, A. S., *J. Organomet. Chem.* **2002,** *650* (1-2), 223-230.

16. Miller, R. D.; Jenkner, P. K., *Macromolecules* **1994,** *27* (20), 5921-5923.

17. Lacavegoffin, B.; Hevesi, L.; Devaux, J., *J. Chem. Soc. Chem. Comm.* **1995,** (7), 769-770.

18. Kimata, Y.; Suzuki, H.; Satoh, S.; Kuriyama, A., *Organometallics* **1995,** *14* (5), 2506-2511.

19. Kashimura, S.; Ishifune, M.; Yamashita, N.; Bu, H. B.; Takebayashi, M.; Kitajima, S.; Yoshiwara, D.; Kataoka, Y.; Nishida, R.; Kawasaki, S.; Murase, H.; Shono, T., *J. Org. Chem.* **1999,** *64* (18), 6615-6621.

20. Jones, R. G.; Benfield, R. E.; Cragg, R. H.; Swain, A. C.; Webb, S. J., *Macromolecules* **1993,** *26* (18), 4878-4887.

21. Bratton, D.; Holder, S. J.; Jones, R. G.; Wong, W. K. C., *J. Organomet. Chem.* **2003,** *685* (1-2), 60-64.

22. Benfield, R. E.; Cragg, R. H.; Jones, R. G.; Swain, A. C., *J. Chem. Soc. Chem. Comm.* **1992,** (14), 1022-1024.

23. Khan, A.; Gossage, R. A.; Foucher, D. A., *Can. J. Chem.* **2010,** *88* (10), 1046-1052.

24. Schittelkopf, K.; Fischer, R. C.; Meyer, S.; Wilfling, P.; Uhlig, F., *Appl. Organomet. Chem.* **2010,** *24* (12), 897-901.

25. Choffat, F.; Kaeser, S.; Wolfer, P.; Schmid, D.; Mezzenga, R.; Smith, P.; Caseri, W., *Macromolecules* **2007,** *40* (22), 7878-7889.

26. Abd-El-Aziz, A. S.; John Wiley & Sons., Group IVA polymers. In *Macromolecules containing metal and metal-like elements v 4* [Online] Wiley-Interscience,: Hoboken, NJ, 2005; pp. xviii, 348 p.

27. Sommer, R.; Schneide.B; Neumann, W. P., *Liebigs Ann. Chem.* **1966,** *692*, 12.

28. Sita, L. R., *Organometallics* **1992,** *11* (4), 1442-1444.

29. Sita, L. R., *Acc. Chem. Res.* **1994,** *27* (7), 191-197.

30. Sita, L. R.; Terry, K. W.; Shibata, K., *J. Am. Chem. Soc.* **1995,** *117* (30), 8049-8050.

31. Okano, M.; Matsumoto, N.; Arakawa, M.; Tsuruta, T.; Hamano, H., *Chem. Commun.* **1998,** (17), 1799-1800.

32. Mochida, K.; Hayakawa, M.; Tsuchikawa, T.; Yokoyama, Y.; Wakasa, M.; Hayashi, H., *Chem. Lett.* **1998,** (1), 91-92.

33. Lu, V.; Tilley, T. D., *Macromolecules* **1996,** *29* (17), 5763-5764.

34. Lu, V. Y.; Tilley, T. D., *Macromolecules* **2000,** *33* (7), 2403-2412.

35. Imori, T.; Lu, V.; Cai, H.; Tilley, T. D., *J. Am. Chem. Soc.* **1995,** *117* (40), 9931-9940.

36. Imori, T.; Tilley, T. D., *J. Chem. Soc. Chem. Comm.* **1993,** (21), 1607-1609.

37. Holder, S. J.; Jones, R. G.; Benfield, R. E.; Went, M. J., *Polymer* **1996,** *37* (15), 3477-3479.

38. Deacon, P. R.; Devylder, N.; Hill, M. S.; Mahon, M. F.; Molloy, K. C.; Price, G. J., *J. Organomet. Chem.* **2003,** *687* (1), 46-56.

39. Choffat, F.; Smith, P.; Caseri, W., *J. Mater. Chem.* **2005,** *15* (18), 1789-1792.

40. Baumgartner, J.; Fischer, R.; Fischer, J.; Wallner, A.; Marschner, C.; Florke, U., *Organometallics* **2005,** *24* (26), 6450-6457.

41. Chaubon, M. A.; Ranaivonjatovo, H.; Escudie, J.; Satge, J., *Main Group Metal Chemistry* **1996,** *19* (3), 145-160.

42. Escudie, J.; Couret, C.; Ranaivonjatovo, H.; Satge, J., *Coordin. Chem. Rev.* **1994,** *130* (1-2), 427-480.

43. Escudie, J.; Ranaivonjatovo, H., *Adv. Organomet. Chem.* **1999,** *44*, 113-174.

44. Power, P. P., *Chem. Rev.* **1999,** *99* (12), 3463-3503.

45. Morgan, G. T.; Drew, H. D. K., *J. Chem. Soc.* **1925,** *127*, 1760-1768.

46. Triplett, K.; Curtis, M. D., *J. Organomet. Chem.* **1976,** *107* (1), 23-32.

47. Neumann, W. P.; Kuhlein, K., *Tetrahedron Lett.* **1963,** (23), 1541-1545.

48. Neumann, W. P.; Kuhlein, K., *Liebigs Ann. Chem.* **1965,** *683*, 1.

49. Castel, A.; Riviere, P.; Saintroch, B.; Satge, J.; Malrieu, J. P., *J. Organomet. Chem.* **1983,** *247* (2), 149-160.

50. Roller, S.; Simon, D.; Drager, M., *J. Organomet. Chem.* **1986,** *301* (1), 27-40.

51. Gilman, H.; Gerow, C. W., *J. Am. Chem. Soc.* **1956,** *78* (20), 5435-5438.

52. Drager, M.; Ross, L., *Z. Anorg. Allg. Chem.* **1980,** *460* (1), 207-216.

53. Drager, M.; Ross, L.; Simon, D., *Z. Anorg. Allg. Chem.* **1980,** *466* (7), 145-156.

54. Ross, L.; Drager, M., *J. Organomet. Chem.* **1980,** *194* (1), 23-32.

55. Drager, M.; Ross, L., *Z. Anorg. Allg. Chem.* **1980,** *469* (10), 115-122.

56. Ross, L.; Drager, M., *Z. Anorg. Allg. Chem.* **1981,** *472* (1), 109-119.

57. Drager, M.; Simon, D., *Z. Anorg. Allg. Chem.* **1981,** *472* (1), 120-128.

58. Drager, M.; Ross, L., *Z. Anorg. Allg. Chem.* **1981,** *476* (5), 95-104.

59. Ross, L.; Drager, M., *J. Organomet. Chem.* **1980,** *199* (2), 195-204.

60. Ross, L.; Drager, M., *Z. Naturforsch B* **1983,** *38* (6), 665-673.

61. Ross, L.; Drager, M., *Z. Anorg. Allg. Chem.* **1984,** *515* (8), 141-146.

62. Simon, D.; Haberle, K.; Drager, M., *J. Organomet. Chem.* **1984,** *267* (2), 133-142.

63. Ross, L.; Drager, M., *Z. Anorg. Allg. Chem.* **1984,** *519* (12), 225-232.

64. Drager, M.; Haberle, K., *J. Organomet. Chem.* **1985,** *280* (2), 183-196.

65. Drager, M.; Simon, D., *J. Organomet. Chem.* **1986,** *306* (2), 183-192.

66. Haberle, K.; Drager, M., *J. Organomet. Chem.* **1986,** *312* (2), 155-165.

67. Roller, S.; Drager, M., *J. Organomet. Chem.* **1986,** *316* (1-2), 57-65.

68. Haberle, K.; Drager, M., *Z. Naturforsch B* **1987,** *42* (3), 323-329.

69. Haberle, K.; Drager, M., *Z. Anorg. Allg. Chem.* **1987,** *551* (8), 116-122.

70. Azemi, T.; Yokoyama, Y.; Mochida, K., *J. Organomet. Chem.* **2005,** *690* (6), 1588-1593.

71. Yokoyama, Y.; Hayakawa, M.; Azemi, T.; Mochida, K., *J. Chem. Soc. Chem. Comm.* **1995,** (22), 2275-2275.

72. Bochkarev, M. N.; Vyazankin, N. S.; Bochkarev, L. N.; Razuvaev, G. A., *J. Organomet. Chem.* **1976,** *110* (2), 149-157.

73. Subashi, E.; Rheingold, A. L.; Weinert, C. S., *Organometallics* **2006,** *25* (13), 3211-3219.

74. Riviere-Baudet, M. R., P., *J. Organomet. Chem.* **1976,** *116*, C49-C52.

75. Riviere-Baudet, M., *Main Group Met. Chem.* **1995,** *18*, 353-385.

76. Lappert, M. F., *Metal and metalloid amides : syntheses, structures, and physical and chemical properties*. E. Horwood ; Halsted Press: Chichester New York, 1980; p 847 p.

77. Amadoruge, M. L.; DiPasquale, A. G.; Rheingold, A. L.; Weinert, C. S., *J. Organomet. Chem.* **2008,** *693* (10), 1771-1778.

78. Burge, D. E., *J. Chem. Educ.* **1970,** *47* (2), A81-&.

79. Schrick, E. K.; Forget, T. J.; Roewe, K. D.; Schrick, A. C.; Moore, C. E.; Golen, J. A.; Rheingold, A. L.; Materer, N. F.; Weinert, C. S., *Organometallics* **2013,** *32* (7), 2245-2256.

80. Samanamu, C. R.; Amadoruge, M. L.; Schrick, A. C.; Chen, C.; Golen, J. A.; Rheingold, A. L.; Materer, N. F.; Weinert, C. S., *Organometallics* **2012,** *31* (11), 4374-4385.

81. Samanamu, C. R.; Amadoruge, M. L.; Weinert, C. S.; Golen, J. A.; Rheingold, A. L., *Phosphorus, Sulfur, and Silicon* **2011,** *186* (6), 1389-1395.

82. Samanamu, C. R.; Amadoruge, M. L.; Yoder, C. H.; Golen, J. A.; Moore, C. E.; Rheingold, A. L.; Materer, N. F.; Weinert, C. S., *Organometallics* **2011,** *30* (5), 1046-1058.

83. Ghereg, D.; Gornitzka, H.; Escudie, J.; Ladeira, S., *Inorg. Chem.* **2010,** *49* (22), 10497-10505.

84. Miller, K. A.; Watson, T. W.; Bender, J. E.; Holl, M. M. B.; Kampf, J. W., *J. Am. Chem. Soc.* **2001,** *123* (5), 982-983.

85. Mochida, K.; Kikkawa, H.; Nakadaira, Y., *Bull. Chem. Soc. Jpn.* **1991,** *64* (9), 2772-2777.

86. Mochida, K.; Yoneda, I.; Wakasa, M., *J. Organomet. Chem.* **1990,** *399* (1-2), 53-62.

87. Billone, P. S.; Beleznay, K.; Harrington, C. R.; Huck, L. A.; Leigh, W. J., *J. Am. Chem. Soc.* **2011,** *133* (27), 10523-10534.

APPENDIX

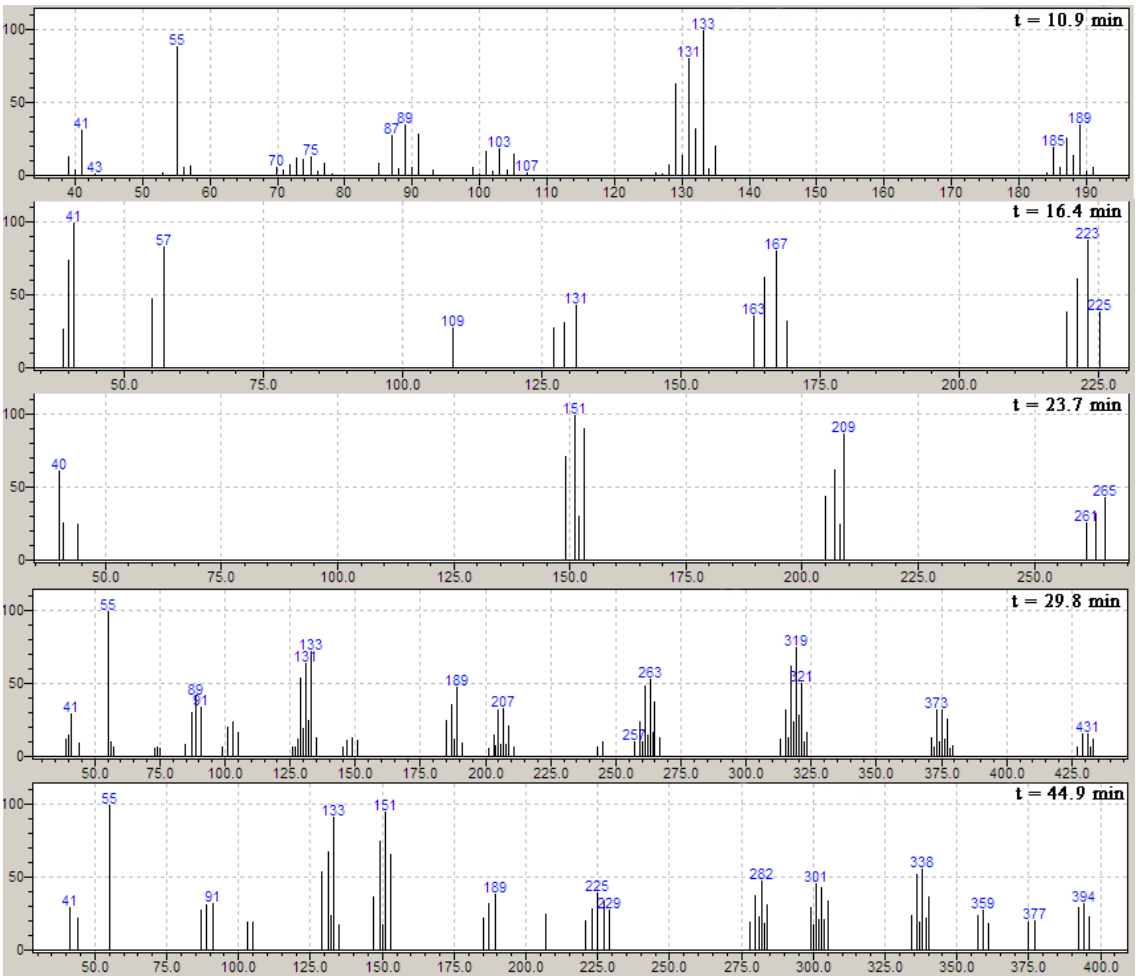

Mass spectra for all five components of GC (**Figure 6.24**) with corresponding retention times.

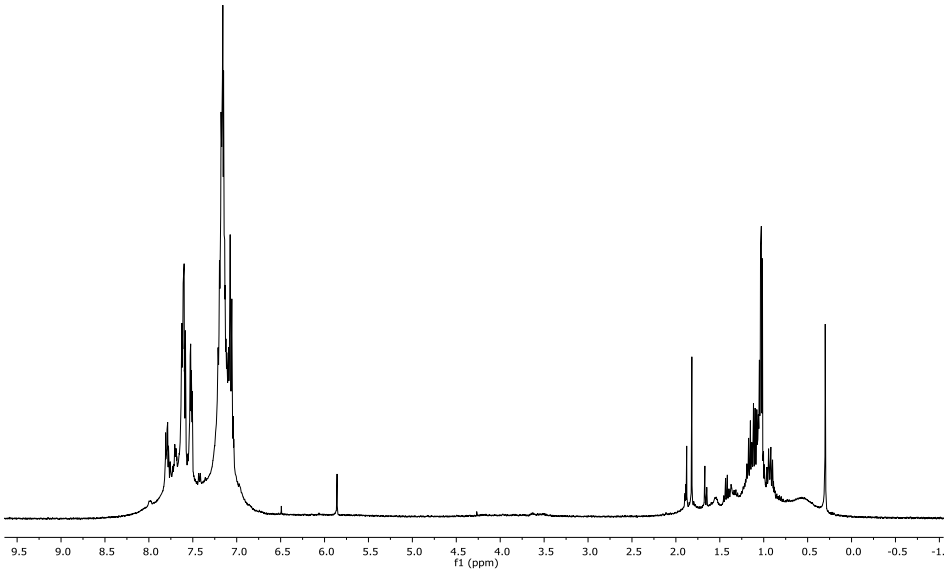

^{1}H NMRspectrum in benzene-d_6 of photolysis product of Et_3Ge-$GePh_3$ (**4**) with AcOH.

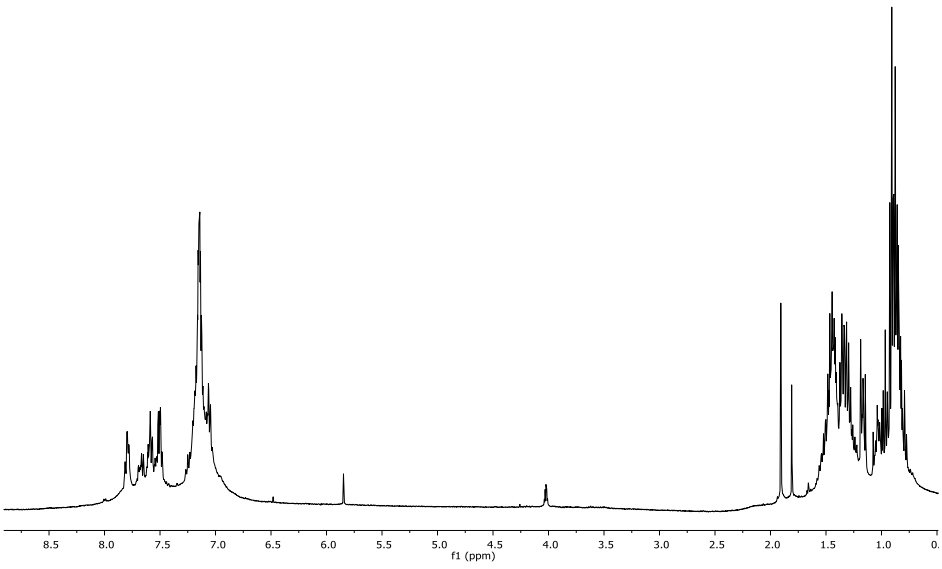

^{1}H NMR spectrum in benzene-d_6 of photolysis product of Bu^n_3Ge-$GePh_3$ (**5**) with AcOH.

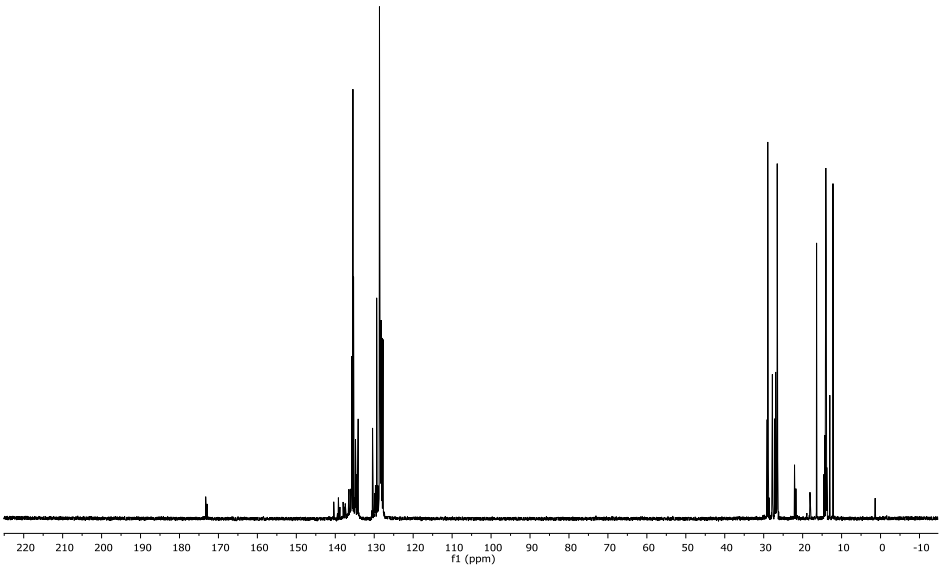

^{13}C NMR spectrum in benzene-d_6 of photolysis product of $Bu^n_3Ge\text{-}GePh_3$ (**5**) with AcOH.

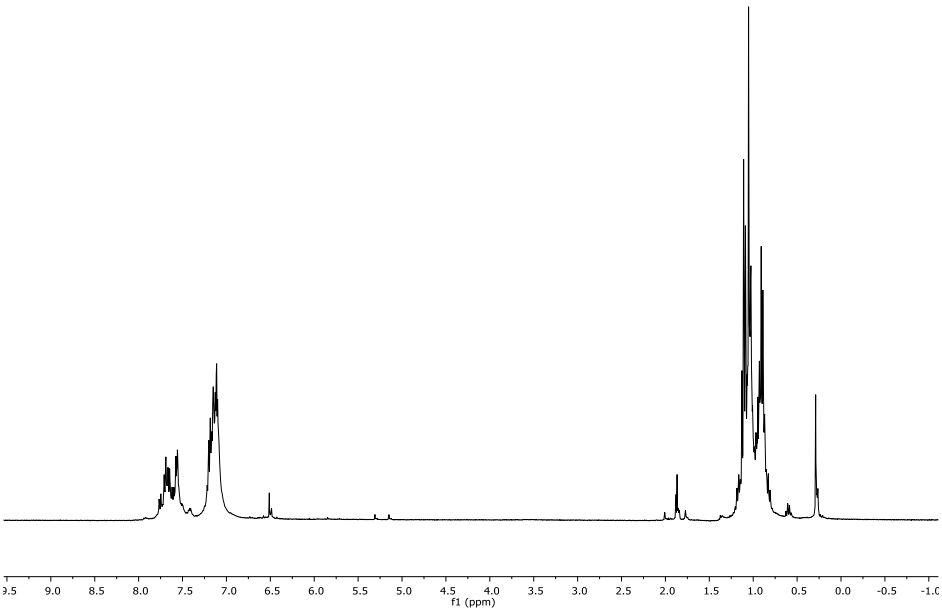

^{1}H NMRspectrum in benzene-d_6 of photolysis product of $Et_3Ge\text{-}GePh_2\text{-}GeEt_3$ (**6**) with AcOH.

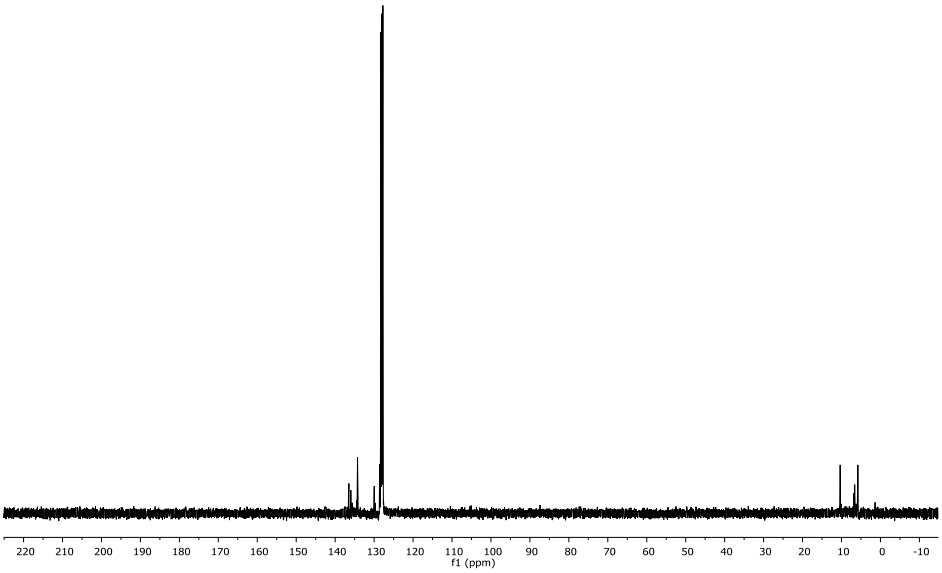

^{13}C NMRspectrum in benzene-d_6 of photolysis product of Et_3Ge-$GePh_2$-$GeEt_3$ (**6**) with AcOH.

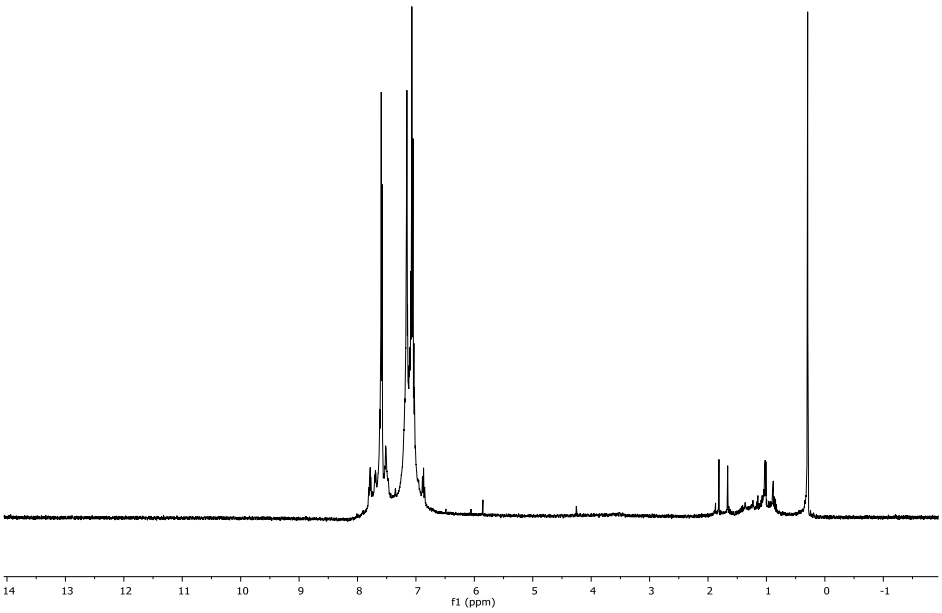

^{1}H NMRspectrum in benzene-d_6 of photolysis product of Et_3Ge-$GePh_2$-$GePh_2$-$GeEt_3$ (**8**) with AcOH.

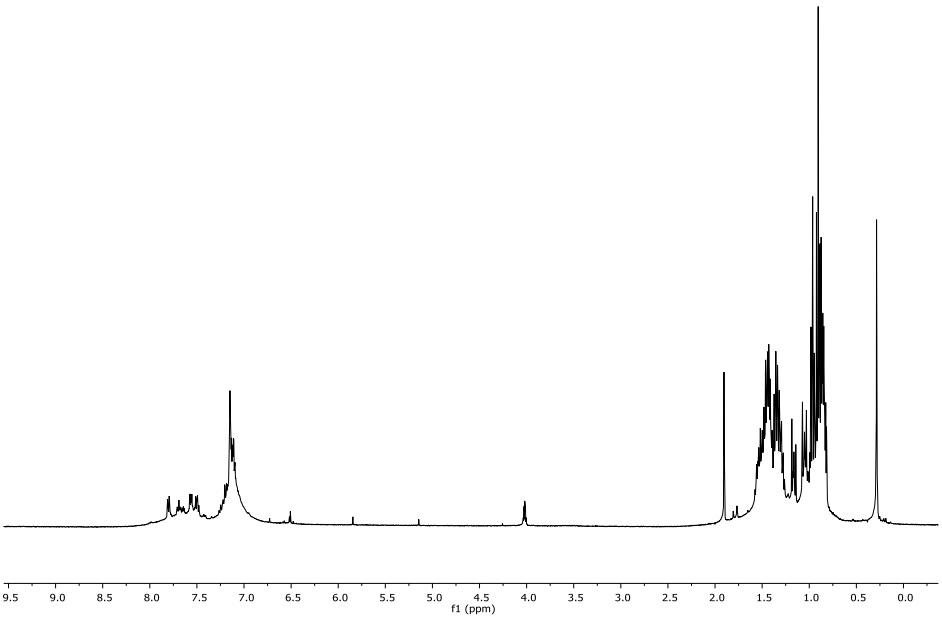

^{1}H NMR spectrum in benzene-d_6 of photolysis product of $Bu^{n}_{3}Ge\text{-}GePh_2\text{-}GePh_2\text{-}GeBu^{n}_{3}$ (**9**) with AcOH.

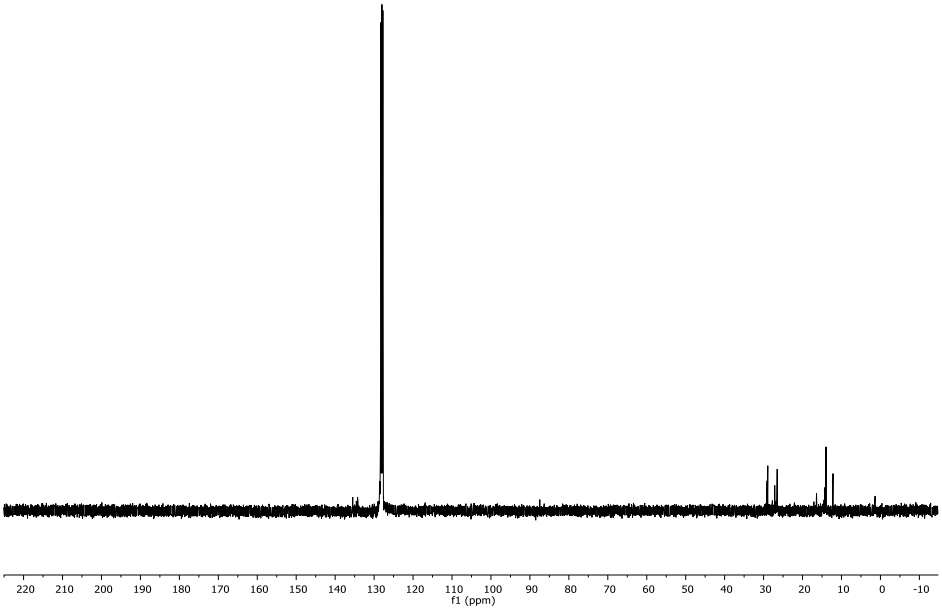

^{13}C NMR spectrum in benzene-d_6 of photolysis product of $Bu^{n}_{3}Ge\text{-}GePh_2\text{-}GePh_2\text{-}GeBu^{n}_{3}$ (**9**) with AcOH.

VITA

Aaron C. Schrick

Candidate for the Degree of

Doctor of Philosophy

Thesis: STRUCTURAL AND PHYSICAL INVESTIGATIONS OF NOVEL GERMANIUM COMPOUNDS: ARYLOXIDES, NANOMATERIALS, AND PHOTOLYSIS OF OLIGOGERMANES

Major Field: Chemistry

Education:

Completed the requirements for the Doctor of Philosophy in Chemistry at Oklahoma State University, Stillwater, Oklahoma in May, 2014.

Completed the requirements for the Bachelor of Science in Chemistry at Midwestern State University, Wichita Falls, Texas in 2009.

Publications:

- Wetherby, A. E.; Samanamu, C. R.; Schrick, A. C.; *et al.*, Synthesis and Structures of Aryloxo- and Binaphthoxogermanium(IV) Alkyl Iodide Complexes. *Inorg. Chim. Acta,* **2010**, *364* (1), 89-95.
- Schrick, A. C.; Rheingold, A. L.; Weinert, C. S., A Divalent Germanium Complex of Calix[5]arene. *Dalton Trans.,* **2011**, *40* (25), 6629-6631.
- Schrick, A. C.; Chen, C.; Rheingold, A. L.; Weinert, C. S., Synthesis of $Ge[N(SiMe_2Ph)_2]_2$ and Crystal Structures of the Benzil Adducts $Ph_2C_2O_2Ge[N(SiMe_2Ph)_2]_2$ and $Ph_2C_2O_2Ge[N(SiMe_3)_2]_2$. *Main Group Chem.,* **2012**, *11* (1), 3-11.
- Samanamu, C. R.; Amadoruge, M. L.; Schrick, A. C.; et al., Synthetic, Structural, and Physical Investigations of the Large Linear and Branched Oligogermanes $Ph_3GeGePh_2GePh_2GePh_2H$, Ge_5Ph_{12}, and $(Ph_3Ge)_4Ge$. *Organometallics,* **2012**, *31* (11), 4374-4385.
- Schrick, E. K.; Forget, T. J.; Roewe, K. D.; Schrick, A. C.; *et al.*, Substituent Effects in Digermanes: Electrochemical, Theoretical, and Structural Investigations. *Organometallics*, **2013**, *32* (7), 2245–2256.
- Schrick, A. C.; Weinert, C. S., Oligogermanes as Molecular Precursors for Germanium(0) Nanoparticles: Size Control and Size Dependent Fluorescence. *Mater. Res. Bull.,* **2013**, *48,* 4390-4394.